A THEORETICAL AND EXPERIMENTAL STUDY OF STRUCTURAL ISOMERISM

by

Willem J. Bouma

A thesis submitted in partial fulfilment of the requirements for the degree of Doctor of Philosophy at the Australian National University.

Research School of Chemistry

June 1979

Oan ús Mem

To my dear Susie

The work described in this thesis is my own, except where otherwise stated, and has not been submitted for any other degree. It was carried out in the Research School of Chemistry at the Australian National University from 1976 to 1979 during the tenure of an A.N.U. Post-Graduate Scholarship.

Willem J. Bouma

ACKNOWLEDGEMENTS

I wish to express my thanks to my supervisors, Drs Leo Radom and John MacLeod, for their guidance and friendship during the past three years. Further thanks are due to Alan Hinde, Ross Nobes, William Rodwell and Mark Vincent for their assistance and their stimulating discussions.

I am grateful to all other members of the Research School of Chemistry who have assisted me, especially Carol Jacob, Greta Pribyl, Martin Chapman, Terry Davies, Byam Wight and Gary Brown.

Part of the work described in Chapters 3 and 4 was carried out with the help of two vacation scholars, Mat Ballard and Paul Adeney, respectively, whom I thank for their contribution. Acknowledgements are due to Mark Vincent for the RHF programme, Dieter Poppinger for the transition state geometry optimization routine, William Rodwell for the use of the ATMOL programme for the 6-31G* calculations, and Geraldine Badham for typing this manuscript.

SUMMARY

In this thesis a study of structural isomerism has been made using two distinct approaches. *Ab initio* molecular orbital theory has been employed for theoretical studies of isomeric ions and neutral systems. Ion cyclotron resonance spectrometry was used to study ion/molecule reactions of isomeric gas-phase ions with various neutral substrates, in order to try to distinguish isomeric ions by differences in their observed ion/molecule reactions.

In Part I of this thesis, the theoretical background and the methods employed in the theoretical studies are presented (Chapter 1), together with a study of three C_2H_4O isomers [acetaldehyde, vinyl alcohol and ethylene oxide (Chapter 2)]. The latter study included the prediction of an experimental structure for vinyl alcohol, based on a systematic correction of the theoretical structures for known deficiencies of the basis sets used. The most stable C_2H_4O isomer is acetaldehyde, which is favoured over the enol, vinyl alcohol, by $\sim$ 50 kJ mol^{-1}. In order to assess the effect of α-substituents on the acetaldehyde/vinyl alcohol energy difference, a study of a large range of relatively simple substituents was made (Chapter 3). It was found that substituents which are π-electron acceptors and σ-electron acceptors, e.g. NO, CHO, N_2^+, reverse the order of stability (the enol being lower in energy than the keto isomer), a result which was rationalized in part in terms of unfavourable geminal interactions between these substituents and the formyl group in the substituted acetaldehyde.

Interconversions of structural isomers by way of 1,3- and 1,5-sigmatropic hydrogen shifts have been studied theoretically and the

results are presented in Part II. In agreement with orbital symmetry considerations, the 1,3-sigmatropic hydrogen shifts in small systems (propene, formic acid, vinyl alcohol and nitrosomethane) were found to be associated with very high activation energies, whereas for 1,5-sigmatropic hydrogen shifts (1,3-pentadiene and β-hydroxyacrolein), lower activation energies were found (Chapter 4). For the nitrosomethane system an alternative rearrangement *via* two successive 1,2-hydrogen shifts was examined, which also was found to be associated with high energy barriers, with formaldonitrone as a relatively low-lying intermediate (Chapter 4). Finally, an asymmetric 1,5-hydrogen shift for the isomerization of nitrosovinyl alcohol to glyoxal monoxime was examined (Chapter 5), and the energy barrier calculated.

In Part III the results of combined theoretical and experimental studies of gas-phase isomeric ion structures are reported. The $CH_2O^{+\cdot}$ isomers were examined theoretically (Chapter 6) and it was found that apart from the well-known formaldehyde radical cation, the hydroxymethylene radical cation might well be an observable isomer. In Chapter 7 a review is given of the previously available experimental information on the $C_2H_4O^{+\cdot}$ isomers. A theoretical study of eleven $C_2H_4O^{+\cdot}$ isomers is presented in Chapter 8. Included are the well-known isomers, the vinyl alcohol, acetaldehyde and ethylene oxide radical cations. A number of potentially stable, identifiable isomers were found, the most promising of which was the C---C ring-opened ethylene oxide radical cation, which previously had been proposed as a reacting species in some experimentally observed ion/molecule reactions. The experimental technique (ICR spectrometry) employed here to study ion/molecule reactions is described in Chapter 9, and the results obtained for the $C_2H_4O^{+\cdot}$ isomers are presented in Chapter 10. For the most stable $C_2H_4O^{+\cdot}$ ion, the

vinyl alcohol radical cation, a substantial number of characteristic ion/molecule reactions were found, the predominant mode of reaction being the addition of the double bond of the ion to carbon-carbon double or triple bonds in the reacting neutral substrates. Based on deuterium labelling experiments, a modification of a previously proposed mechanism for the reaction of the vinyl alcohol radical cation with cyclobutanol is given. A large number of ion-specific reactions were observed for ionized ethylene oxide, almost all involving the transfer of a $CH_2^{+\cdot}$ moiety to suitable substrates. The ion considered to be responsible for these ion/molecule reactions, the C---C ring-opened ethylene oxide ion, was also generated, by electron impact, from 1,3-dioxolane. Deuterium labelling experiments confirmed this, and established the identity of the ion. The two other $C_2H_4O^{+\cdot}$ isomers that were examined, the acetaldehyde and ethylene oxide ions, do not show any unique ion/molecule reactions, but do show differences in their proton transfer reactions to some neutral substrates, e.g. acetaldehyde-d_4, which can be used to distinguish between these two ions. Finally, an extensive theoretical study of the $C_3H_6O^{+\cdot}$ isomers is reported in Chapter II. A number of known isomers has been examined, as well as some which have not as yet been identified experimentally, but on the basis of the theoretical calculations are possibly stable, observable species. For those isomers for which experimental heats of formation are available, good agreement between theoretical and experimental relative energies was found. This lends confidence to the prediction by theoretical calculations of, as yet unknown, low-energy isomers. For two such $C_3H_6O^{+\cdot}$ species, the C---C ring-opened propylene oxide and the C---C ring-opened trimethylene oxide radical cations, preliminary ICR experiments have been carried out, which suggest that these are observable species.

Parts of the work described in this thesis have been published:

Vinyl Alcohol. A Stable Molecule.
Bouma, W.J., Poppinger, D., and Radom, L.,
J. Am. Chem. Soc., 1977, 99, 6443.

The Structure of Vinyl Alcohol.
Bouma, W.J., and Radom, L.,
J. Mol. Struct., 1978, 43, 267.

Keto-Enol Tautomerism. Relative Stabilization of Enol Isomers.
Bouma, W.J., and Radom, L.,
Aust. J. Chem., 1978, 31, 1167.

An *ab initio* Approach to Creating a Simple Stable Enol.
Bouma, W.J., and Radom, L.,
Aust. J. Chem., 1978, 31, 1649.

Theoretical Characterization of an Unusual Isomer of $C_2H_4O^{+\cdot}$:
An Open Ethylene Oxide Cation.
Bouma, W.J., MacLeod, J.K., and Radom, L.,
Nouv. J. Chim., 1978, 2, 439.

Experimental Proof of the Existence of a Fourth Stable Gas Phase $C_2H_4O^{+\cdot}$ Isomer:
the Open Ethylene Oxide Cation.
Bouma, W.J., MacLeod, J.K., and Radom, L.,
J. Chem. Soc., Chem. Commun., 1978, 724.

Ab Initio Molecular Orbital Studies of Sigmatropic Rearrangements.
Bouma, W.J., Vincent, M.A., and Radom, L.,
Int. J. Quant. Chem., 1978, 14, 767.

Nitrosoacetaldehyde and its Enol and Oxime Isomers. A Theoretical Investigation of an Asymmetric 1,5-Sigmatropic Hydrogen Shift.
Bouma, W.J., and Radom, L.,
J. Am. Chem. Soc., in press.

Creation of a Simple Stable Enol. The Stabilizing Properties of the Diazonium Substituent.
Ballard, M.J., Bouma, W.J., Radom, L., and Vincent, M.A.,
Aust. J. Chem., in press.

An *Ab Initio* Molecular Orbital Study of the Structures and Stabilities of the $C_2H_4O^{+\cdot}$ Isomers.
Bouma, W.J., MacLeod, J.K., and Radom, L.,
J. Am. Chem. Soc., in press.

CONTENTS

TABLE OF CONTENTS

IT HEITELAN

Dêr't de dyk it lân omklammet,
Lyk in memme-earm har bern,
Dêr't de wylde sé jamk flammet
Op in hap út Friso's hern,
Dêr't de Stiennen man syn eagen
Stoarje lit oer fjild en strân
Dêr't men eanget fan fjin weagen,
Dêr is't leave Heitelân!

Song of Friesland
by J. Lindeman

PART I

THEORETICAL BACKGROUND AND THERMOCHEMICAL STUDIES OF C_2H_4O AND RELATED SYSTEMS

CHAPTER 1

THEORETICAL BACKGROUND AND METHODS

1.1 INTRODUCTION

In recent years, there has been a vast increase in the use of theoretical approaches for the investigation and the solution of problems in organic chemistry. By the application of quantum mechanical principles to the solution of problems related to physical systems, intrinsic properties of these systems, such as total energies, magnetic and electric properties etc., can be calculated. Such information can then be used to predict geometries of molecules and ions, or to determine the potential energy surface in relation to the relative stability and possible rearrangement of these molecules and ions.

The application of quantum theory is based upon several postulates or assumptions. However, for the theory to be implemented and applied to systems larger than the hydrogen molecule, a number of simplifications (approximations) are necessary. The resulting theoretical methods that have been developed for the investigation of the properties of molecules and ions can be ordered according to the level of approximation applied. They vary from Hückel molecular orbital theory[1], which involves π-electrons only; to extended Hückel theory (EHT), which takes all valence electrons into account[2]; to semi-empirical all valence SCF methods[3], in which experimental data are used to approximate certain parameters, while other simplifying assumptions are made as well, as for example in the CNDO[4,5] (complete neglect of differential overlap), NDDO[4] (neglect of diatomic differential overlap), INDO[6] (intermediate neglect of differential overlap) and MINDO[7-9] (modified INDO) methods; and finally to *ab initio* molecular orbital theory[10-14], in which all electrons are considered, and no experimental data are used (*ab initio* meaning "from the beginning", i.e. from first principles).

With the advent of more sophisticated computers, *ab initio* molecular orbital calculations are rapidly superseding more approximate methods for the study of the properties of an increasing number of polyatomic molecules. In this thesis, *ab initio* molecular orbital theory has been applied to the study of structural isomerism in a number of neutral and ionic systems. Included are studies of intramolecular rearrangements and of the effect of substituents on relative stabilities. This chapter will give an outline of the theoretical methods employed in these studies.

1.2 *AB INITIO* MOLECULAR ORBITAL THEORY

1.2.1 THE SCHRÖDINGER EQUATION

A molecule can be considered as a system of positively charged nuclei together with a number of negatively charged electrons. They move under mutual interaction, dominated by the electrostatic forces between their charges. The motion is determined by the principles of quantum mechanics, most usefully formulated in terms of the Schrödinger wave equation[15]. Within the framework of the Schrödinger method, there are the following postulates:

(i) There exists a function Ψ, the wave function for the system, which determines all measurable quantities of the system. The wave function must be finite, single valued, and continuous throughout all space. It will be a function of the coordinates of the electrons and nuclei in the system.

(ii) With every observable physical property of any dynamical variable, a, in quantum mechanics can be associated an operator A.

(iii) The expected average value of any dynamical variable, $\langle a \rangle$ (the expectation value of a), is given by

$$\langle a \rangle = \frac{\int \Psi^* A \Psi d\tau}{\int \Psi^* \Psi d\tau} = \frac{\langle \Psi | A | \Psi \rangle}{\langle \Psi | \Psi \rangle} \qquad 1.1$$

In classical mechanics, the total energy E of a particle of mass *m* which is moving in an external field described by the potential energy function V(x,y,z) is a sum of the kinetic energy T and the potential energy V,

$$T + V = E \qquad 1.2$$

Thus the energy of a particle can be expressed in terms of its momentum and coordinates. In quantum mechanics, equation 1.2 is replaced by the operator-equivalent of 1.2 giving the one-electron Schrödinger equation:

$$\left\{ -\frac{h^2}{8\pi^2 m} \nabla^2 + V(x,y,z) \right\} \Psi = E\Psi \qquad 1.3$$

where $\nabla^2 = \frac{\partial^2}{\partial x^2} + \frac{\partial^2}{\partial y^2} + \frac{\partial^2}{\partial z^2}$, and h is Planck's constant,

The linear operator in brackets is the quantum mechanical form of the Hamiltonian. In a similar way, the Schrödinger equation for a complete molecule can be written as

$$\hat{H}\Psi = E\Psi \qquad 1.4$$

where $\hat{H}$ is the full Hamiltonian operator, and Ψ is the wave function for all the particles. As with the one-particle wave function, the square magnitude $|\Psi|^2$ may be interpreted as a probability distribution. $|\Psi|^2 \, d\tau_1 \, d\tau_2 \ldots\ldots$ is the probability of particle 1 being in a volume $d\tau_1$, particle 2 in a volume $d\tau_2$ and so on. For a differential equation of this type the energies E, which are the eigenvalues of the operator $\hat{H}$, can be

determined; the corresponding Ψ's are called the eigenfunctions. The Hamiltonian is the sum of kinetic and potential parts (cf. 1.3)

$$\hat{H} = \hat{T} + V \qquad 1.5$$

the kinetic energy operator ($\hat{T}$) being the sum of the kinetic energy operators of all particles, and the potential energy (V) being the sum of the various coulomb interactions (electron-electron, electron-nucleus, and nucleus-nucleus interactions).

1.2.2 THE BORN-OPPENHEIMER APPROXIMATION

Since the mass of an electron is $\sim 5 \times 10^{-4}$ times smaller than the mass of the smallest nucleus, a proton, the motion of the electrons and the motion of the nuclei will be on different timescales. Born and Oppenheimer therefore proposed[16] that equation 1.4 can be separated into two equations, one describing the motion of the electrons within a fixed nuclear framework, leading to the electronic wave function, and the other describing the vibrations and rotations of the nuclei, leading to the nuclear wave function.

Molecular orbital theory is concerned with obtaining the electronic wave function for a fixed nuclear framework

$$\hat{H}^{el}\Psi = \varepsilon^{el}\Psi \qquad 1.6$$

where $\hat{H}^{el}$ is the electronic Hamiltonian operator consisting of the sum of kinetic energy operators for all electrons, the sum of electron-nuclei attraction energies and the sum of electron-electron repulsion energies. This will allow the electronic energy ε^{el} to be determined (cf. 1.1), to which the nuclear repulsion energy ε^{nuc} will have to be added.

$$\varepsilon^{total} = \varepsilon^{el} + \varepsilon^{nuc} \qquad 1.7$$

1.2.3 ORBITAL APPROXIMATION

Hartree proposed[17] that the many-electron wave function, Ψ (1,2,.....n) for n electrons, should be approximated by a simple product of one-electron spin-orbitals ψ_i:

$$\Psi(1,2,....,n) = \psi_1(1)\psi_2(2).....\psi_n(n) \qquad 1.8$$

A spin-orbital ψ_i can be separated into a spatial part χ_i and a spin part η_i such that

$$\psi_i = \chi_i\eta_i \qquad 1.9$$

where η_i can be α or β depending on the spin of the electron (+ ½ or - ½). When the many-electron wave function Ψ is expressed as a determinantal product, rather than a simple product of one-electron functions, the function will satisfy the Pauli principle, i.e. the wave function will be antisymmetric on interchange of two electrons.

$$\Psi(1,2,....,n) = \frac{1}{\sqrt{n!}} \begin{vmatrix} \psi_1(1)\psi_2(1).....\psi_n(1) \\ \psi_1(2).....\psi_n(2) \\ \vdots \qquad\qquad \vdots \\ \psi_1(n).....\psi_n(n) \end{vmatrix} \qquad 1.10$$

Such a determinant is known as a Slater determinant[18]. If the same spatial orbital χ_i is used for describing an electron pair with spins α and β, these are denoted as χ_i and $\bar{\chi}_i$. Thus for a closed-shell system with 2n electrons, n spatial orbitals are needed. Equation 1.10 then becomes (in abbreviated form):

$$\Psi(1,2,....,2n) = |\chi_1\bar{\chi}_1\chi_2\bar{\chi}_2.....\chi_n\bar{\chi}_n| \qquad 1.11$$

Finally, in order to obtain a better approximation to the many-electron wave function for a system, configuration interaction (CI) or multiconfigurational techniques may be used whereby the wave function Ψ is expressed as a linear combination of suitably chosen single determinantal functions ψ_i.

$$\Psi = a\Psi_1 + b\Psi_2 + c\Psi_3 + \ldots\ldots \qquad 1.12$$

An electron in the spatial orbital χ_i experiences a potential due to the nuclei and the instantaneous positions of all other electrons in the system. This problem can be simplified if one takes the average position of the other electrons (which resemble a charge cloud). In order to determine χ_i and the orbital energy ε_i, one has to know the other orbitals χ_j. However, χ_j are dependent on the value of χ_i; such a problem can only be solved by an iterative procedure which is executed until self consistency for the orbitals (and hence the orbital energies) is obtained.

1.2.4 THE SELF-CONSISTENT FIELD METHOD

The aim of the calculations is to find a solution to equation 1.6 and obtain a stationary state for the energy of the system. This means that for a small change $\delta\Psi$ in the wave function, $\delta\varepsilon^{el}$ will be zero. The variational theorem states that for a trial function Ψ' the energy $\varepsilon^{el'}$ (obtained according to equation 1.1) is an upper bound to the true energy ε^{el}. The trial function Ψ' will depend upon one or more parameters which can be optimized so that $\varepsilon^{el'}$ is minimized with respect to these parameters. The wave function thus obtained will be an approximation to the true electronic wave function Ψ, and will depend on the flexibility of Ψ'.

Since it was found that a convenient way to express Ψ is as a determinantal product of spatial orbitals χ_i (equation 1.11), it will

be necessary initially to determine the best set of spatial orbitals which will result in the calculated total energy being as close as possible to the true energy. In order to calculate the total energy, χ_i is needed; to obtain the best set of χ_i, the energy will have to be minimized. This can be solved by an iterative self-consistent procedure. The resulting orbitals, constituting the best single determinantal wave function for the system under consideration, are referred to as the Hartree-Fock or self-consistent field orbitals, after the men who pioneered the development of the method[17,19]. The corresponding energy is known as the Hartree-Fock energy.

1.2.5 LCAO APPROXIMATION

Roothaan[20] suggested that to make the calculations practicable for molecules, the spatial (molecular) orbitals χ_i should be represented by a linear combination of atomic orbitals:

$$\chi_i = \sum_{\mu} c_{\mu i} \phi_{\mu} \qquad 1.13$$

These atomic orbitals, ϕ_{μ}, are known more generally as basis functions. If one chooses a large enough basis set, then no error is introduced by this method. In practice, however, the basis set is truncated, which introduces an error. This approach is known as the linear combination of atomic orbitals (LCAO) approximation.

From this, the Roothaan equations are obtained (1.14) from which the wave function can be determined:

$$FC = SCE \qquad 1.14$$

where F is the Fock matrix, a matrix of one-electron and two-electron

integrals describing the motion of an electron in the field of the nuclei and the average field of the other electrons, and depends on the molecular orbital coefficients, $c_{\mu i}$; C is the matrix of the molecular orbital coefficients $c_{\mu i}$ (describing the wave function); S is the overlap matrix, the elements of which represent the overlap between pairs of basis functions; and E is a diagonal matrix whose elements correspond to the molecular orbital energies ε_i. A total energy calculation for a given system will proceed as follows:

1. Assign coordinates to the atomic nuclei.

2. Choose a suitable set of basis functions.

3. Evaluate the one-electron and two-electron integrals needed for F and S over the atomic basis functions.

4. Obtain an initial set of coefficients, $c_{\mu i}$, from an extended Hückel calculation.

5. Now the Fock matrix can be calculated, and the eigenvalues ε_i for the molecular orbitals χ_i determined. This will lead to a new set of coefficients $c_{\mu i}$.

6. The improved coefficients can be used to get better eigenvalues (i.e. a lower total electronic energy); this process is repeated until an arbitrarily defined convergence limit on the coefficients is reached.

7. Once the SCF orbitals are obtained, the total electronic energy is calculated to which the nuclear repulsion energy is added to give the total energy for the system.

The total energy obtained in this way is a unique energy for the nuclear coordinates that were assumed, for the particular basis

set used. Thus, by varying the nuclear coordinates (i.e. the geometry of the molecule) it will be possible to calculate a new total energy, and in this way construct a potential energy surface.

1.2.6 BASIS SETS

The term basis set designates a set of basis functions which is consistently used to describe the various atoms (e.g. H, C, N, O, F) that constitute the molecules under consideration. The functions most commonly used are either Slater-type orbitals[21] (STO's).

$$f_n(r) = (2\xi)^{n+\frac{1}{2}} [(2n)!]^{-\frac{1}{2}} r^{n-1} e^{-\xi r} \qquad 1.15$$

where n (= 1,2,3.....) is an identifying quantum number and ξ is a constant inversely related to the spatial extension of the function, or gaussian-type orbitals[22] (GTO's) e.g.

$$g_{1s}(x,y,z) = \left(\frac{2\alpha}{\pi}\right)^{3/4} e^{-\alpha r^2}$$

$$g_{2p_x}(x,y,z) = \left(\frac{128\alpha^5}{\pi^3}\right)^{1/4} e^{-\alpha r^2} \qquad 1.16$$

The GTO's are used extensively since the two-electron integral evaluation is a lot simpler compared with using STO's. Finally it is noted that a basis function ϕ_μ need not be a single gaussian function. A more flexible expression is a sum of the type

$$\phi_\mu = \sum_k^K d_{\mu k} g_k(x,y,z) \qquad 1.17$$

where $g_k(x,y,z)$ are a set of gaussians all of the same type (e.g. all 1s) and $d_{\mu k}$ are fixed constants. Such a function is called a contracted gaussian basis function.

Three types of basis set can be distinguished with regard to the size of the basis set:

(a) A minimal basis set. Only the minimum number of basis functions necessary to accommodate all electrons is used, taking care to maintain spherical symmetry.

(b) An extended basis set. More than one basis function is used to describe atomic orbitals. This allows for the coefficients for an "inner" and an "outer" orbital to be determined so that the radial size of the orbital can be adjusted (Fig. 1.1).

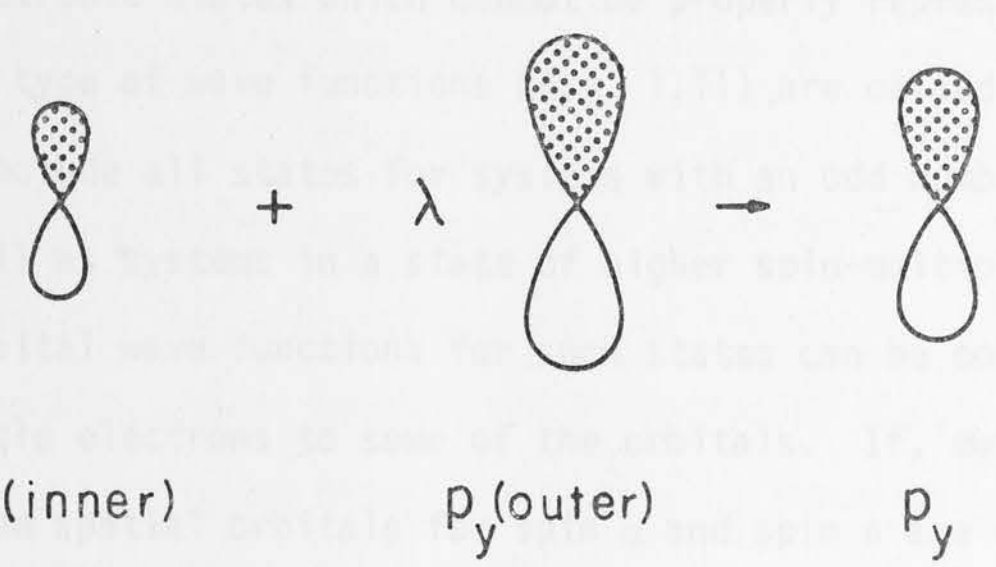

Fig. 1.1 Schematic diagram showing the adjustment in the size of a p_y orbital in an extended basis set.

(c) A polarization basis set. Basis functions of a higher quantum number are allowed to mix into the basis representation (p-type functions on hydrogen and d-type functions on the first-row elements). This allows for small displacements of the centre of electronic charge away from the nuclear positions (Fig. 1.2).

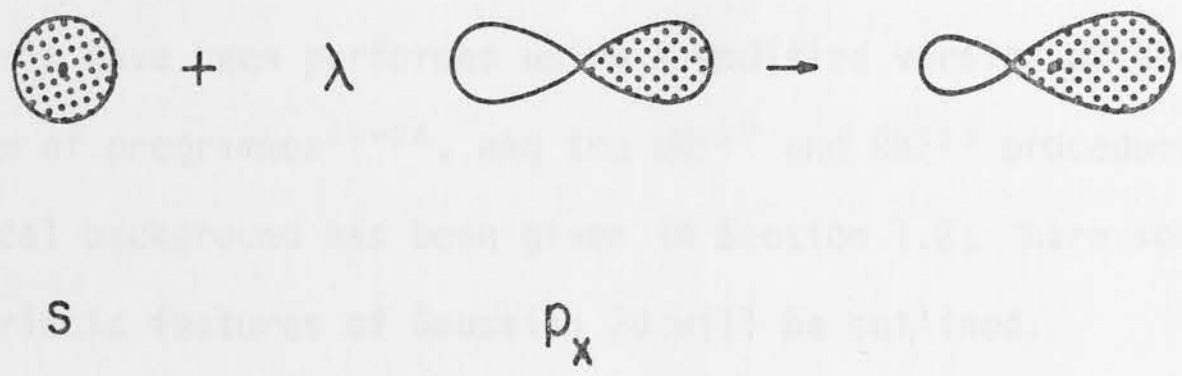

Fig. 1.2 Schematic diagram showing the effect of a polarization function (p_x) on the valence (s) orbital of hydrogen.

1.2.7 UNRESTRICTED AND RESTRICTED HARTREE-FOCK PROCEDURES

Electronic states which cannot be properly represented by the closed-shell type of wave functions (e.g. 1.11) are called open-shell states. These include all states for systems with an odd number of electrons, as well as systems in a state of higher spin-multiplicity. The molecular orbital wave functions for such states can be constructed by assigning single electrons to some of the orbitals. If, during the SCF procedure, the spatial orbitals for spin α and spin β are varied independently, the spin-unrestricted Hartree-Fock (UHF) wave function is obtained. If, however, the spatial orbitals for spin α and spin β are restricted to be the same, the spin-restricted Hartree-Fock (RHF) wave function is obtained. The UHF procedure allows more flexibility for the total electronic wave function, and produces an energy lower than or equal to the RHF procedure. On the other hand, the UHF procedure is known to run occasionally into problems due to contamination from states of higher spin multiplicity.[23]

1.3 IMPLEMENTATION: THE GAUSSIAN 70 SYSTEM OF PROGRAMMES

The *ab initio* molecular orbital calculations reported in this thesis have been performed using a modified version of the Gaussian 70 system of programmes[24-26], and the UHF[27] and RHF[23] procedures. The theoretical background has been given in Section 1.2; here some of the characteristic features of Gaussian 70 will be outlined.

1.3.1 STANDARD BASIS SETS

There are a number of basis sets internal to Gaussian 70. The use of these standard basis sets allows for comparisons of the results of calculations performed with the same basis set among a large set of molecules. As mentioned in Section 1.2.6, the simplest level of *ab initio* molecular orbital theory involves the use of a minimal basis set. Throughout this thesis, all minimal basis set calculations have been carried out using the STO-3G basis set[28] which has a 1s orbital for H and He and a 1s, 2s, $2p_x$, $2p_y$ and $2p_z$ orbital for Li, Be, B, C, N, O and F. The expression STO-3G denotes the expansion of Slater-type orbitals in terms of a fixed linear combination of three gaussian functions (e.g. 1.17, K=3). In order to provide a greater flexibility to the molecular orbitals, an extended basis set can be used. A straightforward procedure would be to double the number of basis functions, so that each atomic orbital is represented by two basis functions. This is called a double-zeta basis set. A simpler solution is to provide flexibility for all valence-shell electrons, since they are important in molecular bonding, but to keep the orbitals for the inner shell the same. This is called a split-valence basis set. The 4-31G basis set[29] is the split-valence basis set used for all atoms studied throughout this thesis,

with the exception of Li and Be, for which the 5-21G basis set[30] was employed (this will be implicit when 4-31G results are discussed). The expression 4-31G denotes the use of a fixed linear combination of four gaussian functions for the inner shell orbitals, and sets of three and one gaussian functions to represent the inner and the outer part of the valence shell.

For some calculations the larger split-valence 6-31G basis set[31] with polarization functions[32] has been used, which is denoted as the 6-31G* basis set.

1.3.2 MOLECULAR GEOMETRY

For any given arrangement of atoms (i.e. molecular geometry), a unique total energy can be calculated, which will depend only on the basis set employed. By varying the nuclear coordinates (i.e. bond lengths, bond angles and dihedral angles in a molecule), and calculating the corresponding total energy for each new geometry, the potential energy surface can be searched for a minimum. Minimization of the energy with respect to each independent geometrical parameter will yield an optimized structure. Not always will such an approach be necessary or feasible.

1.3.2.1 Standard Geometries

A simple approach, when studying a large number of related systems, is the use of standard molecular geometries. A set of standard bond lengths and angles[33-37] for use in systems containing first and second row elements has been obtained by averaging large numbers of experimental, and, in a few cases, the best available theoretical

structural parameters.

1.3.2.2 Optimized Geometries

Two techniques have been used for obtaining optimized geometries. The first is the axial iteration technique (AIT). In this procedure each parameter is varied individually over an interval which can be specified. When, for three values of the parameter, three total energies have been obtained, an optimum value of the parameter is determined by parabolic interpolation. This is done repeatedly for all parameters which are to be optimized. Variation of the geometrical parameters is continued until they are believed to be within 0.001 Å (for bond lengths) or 0.1° (for bond angles) of their limiting values. At this point the total energy is normally stable to 10^{-6} hartrees. The second optimization technique employed is the gradient method. This technique is based on the fact that at a potential energy minimum, the derivative of the total energy with respect to all independent parameters should be zero:

$$\frac{\partial \varepsilon^{\text{total}}}{\partial R_i} = 0 \qquad 1.18$$

When starting an optimization at a geometry which is not at a potential energy minimum, the gradient, $\frac{\partial \varepsilon^{\text{total}}}{\partial R_i}$, can be used for locating the stationary point.[38] In particular for systems with a large number of parameters to be optimized, or for systems where parameters are coupled (i.e. the optimum value of one parameter depends strongly on the optimum value of another parameter, and *vice-versa*), the gradient procedure is found to be superior to the AIT method, both in speed and reliability.

1.3.2.3 Transition State Geometries

Apart from the optimized geometries, which correspond to potential energy minima, there are also stationary points which are not at a minimum. The points of particular interest are transition states, which are situated between two minima on the potential energy surface. A transition state geometry is a structure which corresponds to the lowest maximum energy when going from one minimum to another (a so-called saddle point).

One method of finding a transition state, and thus the barrier for a particular reaction or rearrangement, consists of choosing a suitable parameter as reaction coordinate, and optimizing the intermediate structures for different values of this parameter to determine the reaction profile. This method can fail, since the choice of reaction coordinate is rather arbitrary.

A better method of locating a transition state is based on two properties that a transition state must have. Firstly, it must be a stationary point on the energy surface (equation 1.18). Secondly, it must be a saddle point, i.e. in only one direction of the hypersurface is it a maximum; in all other directions it is a minimum. This corresponds to the matrix of second derivatives of the total energy with respect to all independent parameters (1.19) having only one negative eigenvalue.

$$\frac{\partial^2 \varepsilon^{\text{total}}}{\partial R_i \partial R_j} \qquad 1.19$$

An optimization routine based on these properties is available.[39]

1.3.3 TOTAL ENERGIES

Throughout this thesis the total energies that have been obtained with the various basis sets will be reported in atomic units. According to the basis set and the geometry used, the following notation will indicate the procedure followed: STO-3G//Std denotes the total energy calculated with the STO-3G basis set for a standard geometry; STO-3G//STO-3G denotes the STO-3G energy for an STO-3G optimized geometry. The meaning of other notations such as 4-31G//Std, 4-31G//STO-3G, 4-31G//4-31G and 6-31G*//STO-3G will now be straightforward. In Chapters 6, 8 and 11 where open shell systems are discussed, the notation is expanded to include the Hartree-Fock method used, e.g. RHF/4-31G//RHF/STO-3G means a 4-31G single energy calculation employing the RHF method, of a geometry optimized with the STO-3G basis set, also using the RHF procedure.

1.3.4 MULLIKEN POPULATION ANALYSIS

Organic chemists tend to think of electrons in molecules as being localized on atoms. In order to provide a picture consistent with this idea, a way to distribute the electrons over the basis functions has been designed. The Mulliken population analysis[40] gives the number of electrons in a basis function, or the number of electrons shared between basis functions. The latter is often referred to as the overlap population, and gives a measure of bonding or attraction between atoms. By summation over all basis functions centered on an atom the total number of electrons for that atom will be obtained. Comparison of this total number with the number of electrons in the isolated atom will give the total charge.

1.3.5 CONFIGURATION INTERACTION

In studies of sigmatropic hydrogen shifts (Chapter 4), the effect of configuration interaction (CI) on the total energies of reactants and transition states was of interest, since the transition states are thought not to be well described at the single determinant level[41]. For the systems studied a full CI treatment is currently not feasible, and the 3 x 3 CI procedure has been used.

The 3 x 3 configuration interaction procedure was developed[42] in order to describe loosely bound transition states and diradicals, which are not well described at the single determinant level. The 3 x 3 CI treatment consists of mixing of the closed shell configuration obtained in an SCF calculation with a configuration with one electron in a virtual orbital, and a configuration with two electrons in a virtual orbital. The occupied orbital and virtual orbital involved can be specified, but in general will be the highest occupied molecular orbital (HOMO) and the lowest unoccupied molecular orbital (LUMO).

1.4 PERTURBATION MOLECULAR ORBITAL THEORY

To understand conformational preferences and other properties in molecules, the molecule under consideration can be thought of as being built up from two or more assemblies of atoms (i.e. functional groups). Perturbation molecular orbital (PMO) theory[43,44] describes the orbital interactions between these functional groups, which will result in bonding and antibonding combinations of neighbouring group-orbitals. Two types of molecular orbital interactions arise when both subsystems are in their closed shell ground state. The first is a four-electron interaction

between doubly occupied MO's of each unit, which is destabilizing. The destabilization is proportional to the square of the overlap integral (β), but independent of the energy gap between the two-interacting MO's. The second interaction is a stabilizing two-electron interaction involving a doubly occupied MO on one subsystem and an empty one on the other. The stabilization energy (SE) is proportional to the square of the overlap integral of the combining MO's, and inversely proportional to their energy separation, ΔE (Fig. 1.3).

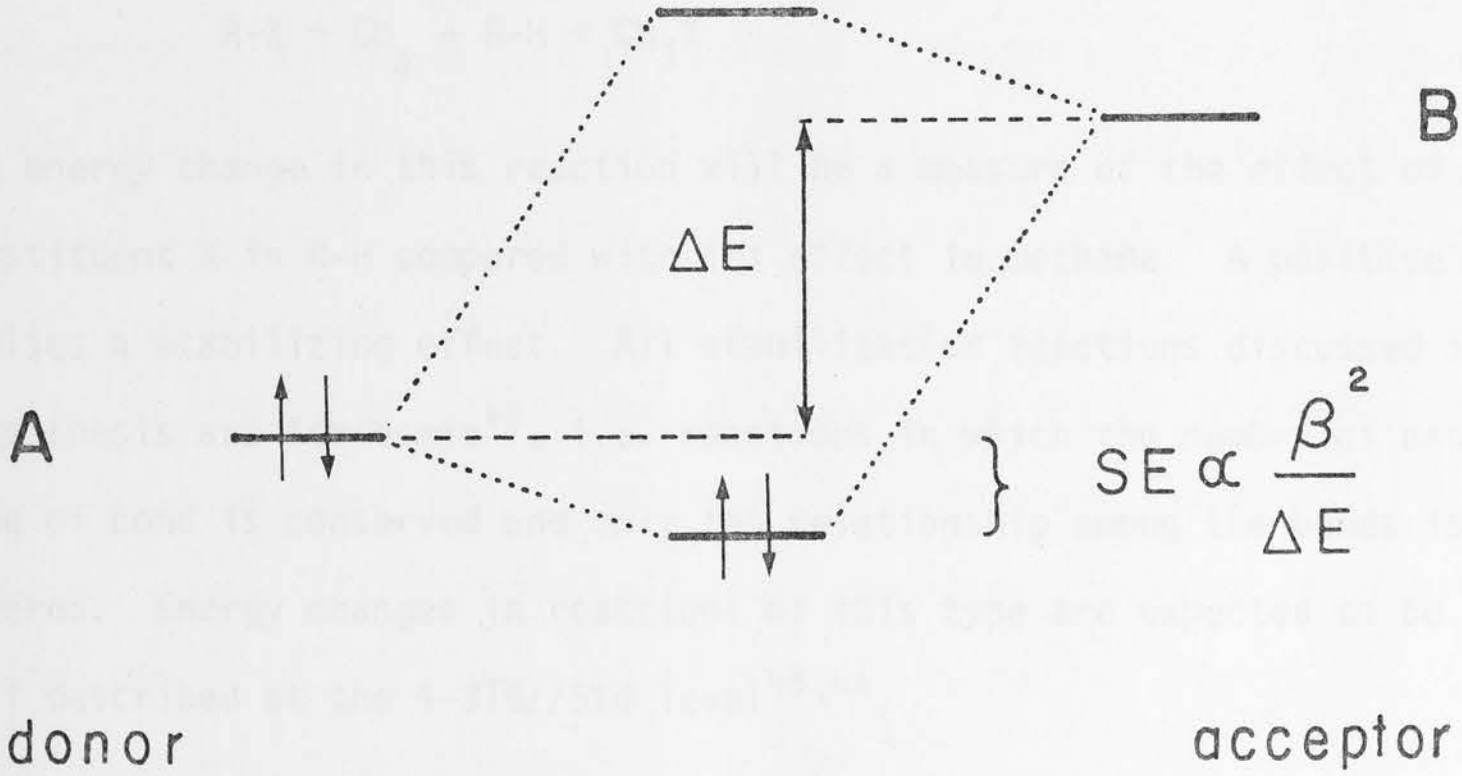

Fig. 1.3 Interaction of a filled orbital of fragment A with an empty orbital of fragment B in A-B.

PMO theory will also make it possible to examine substituent effects, since substitution of molecular fragment A by a fragment C is likely to change the energy level of the doubly occupied MO (Figure 1.3) and thus will change ΔE, which in turn will alter the stabilization energy (SE).

Finally it should be noted that a substituent or a molecular fragment with a high-lying highest occupied molecular orbital (HOMO) can

be classified as an electron donor, while a low-lying lowest unoccupied molecular orbital (LUMO) will be typical of an electron-accepting substituent.

1.5 STABILIZATION REACTIONS

When studying the effect of a substituent X in a particular system R-H, a stabilization energy (E_S) can be derived for X by calculating the energy change in the stabilization reaction:

$$R\text{-}X + CH_4 \rightarrow R\text{-}H + CH_3X \qquad 1.20$$

The energy change in this reaction will be a measure of the effect of the substituent X in R-H compared with its effect in methane. A positive value implies a stabilizing effect. All stabilization reactions discussed in this thesis are isodesmic[45], i.e. reactions in which the number of each type of bond is conserved and only the relationship among the bonds is altered. Energy changes in reactions of this type are expected to be well described at the 4-31G//Std level[45,46].

1.6 ANALYSIS OF ROTATIONAL POTENTIAL SURFACES

When internal rotation around a single bond B-C in a molecule A-B-C-D is studied, the rotational potential function $V(\phi)$ can be analyzed by fitting a number of calculated points to a Fourier series[47,48], where ϕ is the dihedral angle ABCD (equation 1.21).

$$V(\phi) = \tfrac{1}{2}V_1(1-\cos\phi) + \tfrac{1}{2}V_2(1-\cos 2\phi) + \tfrac{1}{2}V_3(1-\cos 3\phi) + \ldots\ldots$$

$$V(\phi) = V_1(\phi) + V_2(\phi) + V_3(\phi) + \ldots\ldots \qquad 1.21$$

The series is usually truncated after the third term, since in several instances the fourth and subsequent terms have been found to be small in comparison with the first three terms.[47] The function is used to predict the stationary points on the rotational potential surface, while the individual terms $V_n(\phi)$ are useful for the understanding of the factors that contribute to the total potential.

1.7 UNITS AND CONVERSION FACTORS

In this thesis the total energies produced by *ab initio* MO calculations are in atomic units (hartrees), and will be given to five decimal places. Relative energies obtained from total energies are expressed in kJ mol^{-1} (1 hartree = 2625.5 kJ mol^{-1}), and will be given to one decimal place. Calculated dipole moments are in debyes (1 debye = 3.336×10^{-30} Cm). In cases where our results are compared with other experimental or theoretical data, which are reported in kcal mol^{-1}, or electron volts (eV), these have been converted to kJ mol^{-1} (1 kcal mol^{-1} = 4.184 kJ mol^{-1}, 1 eV = 96.485 kJ mol^{-1}). Energy conversion factors[49] are summarized in Table 1.1.

Table 1.1 Conversion Factors for Energy Units[a]

	hartree	eV	kcal mol^{-1}	kJ mol^{-1}	cm^{-1}
1 atomic unit =	1	27.212	627.52	2625.5	2.1947×10^{5}
1 electron volt =	3.6749×10^{-2}	1	23.061	96.485	8065.5
1 kcal mol^{-1} =	1.5936×10^{-3}	4.3363×10^{-2}	1	4.1840	349.75
1 kJ mol^{-1} =	3.8088×10^{-4}	1.0364×10^{-2}	0.23901	1	83.593
1 cm^{-1} =	4.5563×10^{-6}	1.2399×10^{-4}	2.8592×10^{-3}	1.1967×10^{-2}	1

[a] From ref. 49.

For all structures, geometrical parameters will be quoted in angstroms and degrees; for optimized geometries bond lengths will be quoted to three decimal places, bond angles to one decimal place.

CHAPTER 2

STRUCTURES AND THERMOCHEMICAL STABILITIES OF THE C_2H_4O ISOMERS: ACETALDEHYDE, VINYL ALCOHOL AND ETHYLENE OXIDE

2.1 INTRODUCTION

Two C_2H_4O isomers, acetaldehyde and ethylene oxide, are well-known whereas a third isomer, vinyl alcohol, was for a long time thought to be too unstable for experimental identification. A study of these three isomers was undertaken with a number of objectives: (i) to calculate their structures and total energies, and, when possible, to compare the results with experimental data; (ii) to predict an experimental structure for vinyl alcohol, as such a structure is not available; (iii) to examine the kinetic stability of vinyl alcohol, i.e. the barrier for intramolecular rearrangement of vinyl alcohol to acetaldehyde.

Objectives (i) and (ii) will be dealt with in this chapter. The optimized geometries (gradient method) obtained with the STO-3G and the 4-31G basis set will be presented. The corresponding total energies are listed in Table 2.7. Objective (iii), relating to the kinetic stability of vinyl alcohol, will be dealt with in Chapter 4.

2.2 STRUCTURAL CONSIDERATIONS

There have been a number of previous *ab initio* calculations on acetaldehyde[45,46,50-53], vinyl alcohol[50,51,54] and ethylene oxide[55-60]. With the exception of ethylene oxide[59,60], these calculations did not include full optimizations of the molecular geometries. The aim of the present study was not only to fully optimize the structures, but also to obtain total energies at a consistent level of theory for these species, in order to get the relative energies, which are a measure of their thermodynamic stabilities.

2.2.1 *ACETALDEHYDE*

A standard geometry calculation with the 4-31G basis set had shown[51] that in its stable conformation acetaldehyde has a C-H single bond

Table 2.1 Optimized and Experimental Structural Parameters for Acetaldehyde (1).

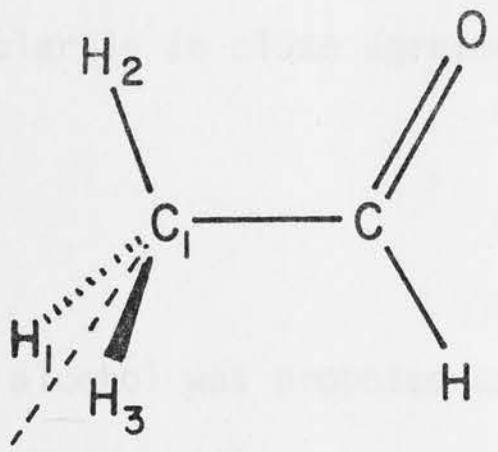

(1)

Parameter	STO-3G	4-31G	Experimental[a]
C_1-C	1.537	1.494	1.501
C=O	1.217	1.209	1.216
C-H	1.104	1.085	1.114
C_1-H_1	1.087	1.084	1.086[b]
C_1-H_2	1.085	1.079	..
$<C_1CO$	124.3	124.2	123.9
$<HCC_1$	114.3	116.0	117.5
$<H_2C_1C$	110.5	110.3	..
$<(H_{13})C_1C$	125.4	125.6	..
$<H_1CH_3$	108.1	107.3	108.3[c]

[a] From ref. 61.

[b] Assumed C_1-H_1 = C_1-H_2 = C_1-H_3

[c] Assumed $<H_1CH_3$ = $<H_1CH_2$ = $<H_2CH_3$.

eclipsing the adjacent C=O double bond, and therefore only this conformation of acetaldehyde (C_s symmetry) was considered. The optimized structural parameters are listed in Table 2.1, together with the experimentally determined[61]

parameters. The corresponding total energies are listed in Table 2.7. A comparison of the STO-3G, 4-31G and experimental structures shows that the 4-31G geometry in particular is in close agreement with the experimentally determined structure.

2.2.2 VINYL ALCOHOL

Although vinyl alcohol was proposed as a reaction intermediate nearly 100 years ago[62] it had, until very recently, not been identified experimentally. In 1973 Blank and Fisher[63] observed the CIDNP enhanced NMR spectrum of vinyl alcohol in solution, but only in late 1976 (after the present calculations had been completed) was the first gas-phase identification of vinyl alcohol reported by Saito[64], who generated the compound by thermal dehydration of ethylene glycol and was able to observe its microwave spectrum.

Although 4-31G//Std calculations had shown[46] that *syn* vinyl alcohol is lower in energy than *anti* vinyl alcohol, by 0.7 kJ mol^{-1}, it was decided to optimize both isomers (C_s symmetry) at the STO-3G and 4-31G levels, since such a small energy difference might well reverse upon optimization of the structures. Table 2.2 lists the optimized structural parameters; the corresponding total energies are listed in Table 2.7. It should be noted that optimization leads to an increase in the *syn/anti* energy difference, a result which was also shown by a previous partial optimization study[54]. There is no evidence for a non-planar *gauche* isomer as had been suggested by some experimental workers for the related methyl vinyl ether molecule.[65] Optimization starting from a structure with the CCOH dihedral angle set at 120° leads without activation energy to the *anti* structure.

Table 2.2 Optimized Structural Parameters for *Anti*-and *Syn*-Vinyl Alcohol [(2) and (3), respectively].

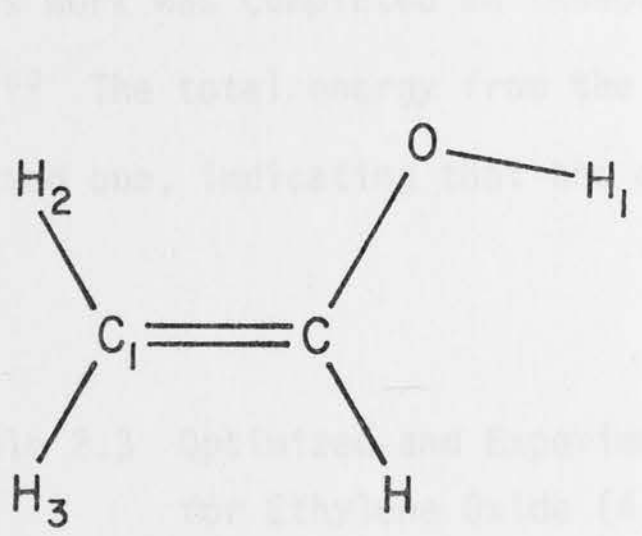

(2)

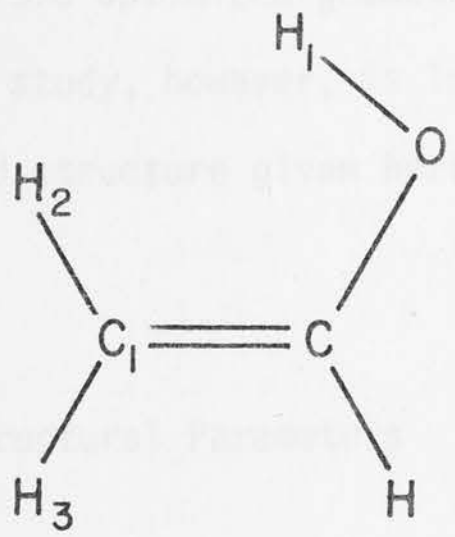

(3)

	(2)		(3)	
Parameter	STO-3G	4-31G	STO-3G	4-31G
C_1=C	1.312	1.311	1.312	1.315
C-O	1.398	1.378	1.390	1.371
C-H	1.090	1.073	1.089	1.068
O-H_1	0.988	0.948	0.990	0.952
C_1-H_2	1.079	1.070	1.080	1.073
C_1-H_3	1.078	1.070	1.077	1.069
<C_1CO	121.9	121.6	126.7	126.5
<HCC_1	121.5	122.7	122.2	123.5
<H_2C_1C	121.6	121.1	122.0	122.6
<H_3C_1C	121.1	120.7	121.2	120.5
<H_1OC	105.3	114.8	105.2	115.0

2.2.3 *ETHYLENE OXIDE*

An STO-3G geometry optimization (C_{2v} symmetry) of ethylene oxide was reported[59] in 1972, together with the STO-3G//STO-3G and the 4-31G//STO-3G

energies. To this has been added the 4-31G optimized structure (Table 2.3), which agrees quite well with a recently reported experimental geometry.[66] After this work was completed an independent 4-31G optimized geometry was reported.[60] The total energy from the present study, however, is lower than the reported one, indicating that the optimized structure given here is more accurate.

Table 2.3 Optimized and Experimental Structural Parameters for Ethylene Oxide (4).

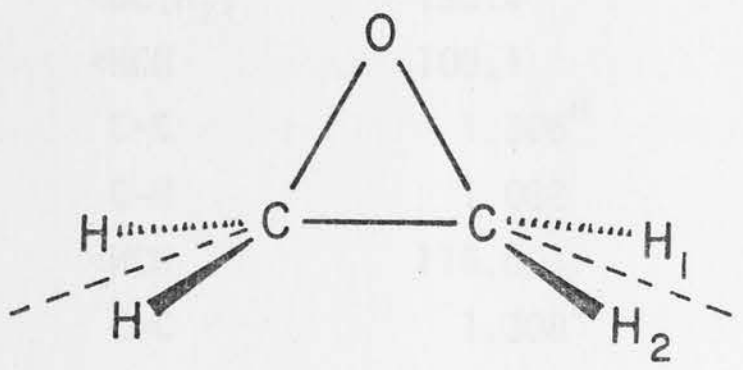

(4)

Parameter	STO-3G[a,b]	4-31G[b]	Experimental[c]
C-C	1.483	1.460	1.462
C-O	1.433	1.459	1.428
C-H	1.088	1.069	1.086
<COC	62.3	60.0	61.6
$<CC(H_{12})$	155.3	158.9	159.4
$<H_1CH_2$	114.5	115.6	116.9

[a] From ref. 59.

[b] 5 independent parameters.

[c] From ref. 66.

Table 2.4 Structural Data for Reference Molecules

Molecule	Parameter	STO-3G	4-31G	Exptl.
H_2O	O-H	0.990[a]	0.951[a]	0.957[b]
	<HOH	100.0	111.2	105.1
CH_3OH[c,d]	C-O	1.433[e]	1.429[f]	1.427[g]
	O-H	0.991	0.951	0.956
	C-H_u	1.092	1.076	1.096
	C-H	1.095	1.083	1.096
	<COH	103.8	113.2	108.9
	<OCH_u	107.7	106.2	106.6
	<OC(H_2)	130.4	129.6	126.0
	<HCH	108.1	109.2	109.0
CH_2CH_2	C=C	1.306[e]	1.316[e]	1.339[h]
	C-H	1.082	1.073	1.085
	<HCH	115.6	116.0	117.8
CH_3CHCH_2[i,j]	C=C	1.308[k]	1.318[l]	1.336[g]
	C-H_u	1.085	1.076	1.090
	C-H_c	1.081	1.074	1.091
	C-H_t	1.081	1.072	1.081
	<CCH_u	119.8	119.1	119.0
	<CCH_c	122.2	122.0	120.5
	<CCH_t	120.0	121.9	121.5
	<CCC	125.1	125.2	124.3
$FCHCH_2$[j]	C=C	1.312[f]	1.305[f]	1.332[g]
	C-H_u	1.092	1.066	1.071
	C-H_c	1.080	1.070	1.086
	C-H_t	1.079	1.069	1.079
	C-F	1.354	1.373	1.348
	<CCH_u	122.8	127.1	120.9[m]
	<CCH_c	121.8	121.5	120.7
	<CCH_t	120.8	120.2	118.8
	<CCF	123.4	121.5	121.2
CH_3OCHCH_2[i,j]	C=C	1.313[n]		1.341[o]
	C-O	1.392		1.360
	<CCH_u	120.9		117.5
	<CCO	129.5		127.7

Footnotes for Table 2.4

a From ref. 67.

b From ref. 68.

c H_u denotes the unique H of the CH_3 group in staggered CH_3OH.

d $<OC(H_2)$ denotes the angle between the C-O bond and the HCH plane.

e From ref. 70.

f This work.

g From ref. 69.

h From ref. 71.

i Full structures may be found in the listed references.

j H_u, H_c and H_t are the unique vinylic hydrogen and the hydrogens *cis* and *trans* to CH_3 (or F or OCH_3), respectively.

k From ref. 72.

l From ref. 73.

m The microwave rotational constants appear to be insensitive to the value of this angle. Electron diffraction studies[74] yield an improved estimate of 127.7°.

n From ref. 75.

o From ref. 54.

2.2.4 PREDICTION OF AN EXPERIMENTAL STRUCTURE FOR VINYL ALCOHOL

Since the present study confirmed that the preferred conformation of vinyl alcohol is *syn*, it was considered desirable to obtain reliable estimates of the experimental values of all the structural parameters in *syn* vinyl alcohol. The correction method employed here is based on the idea that it is possible to improve on the STO-3G and 4-31G predictions of bond lengths and bond angles in vinyl alcohol by recognizing the systematic deficiencies of these basis sets, utilizing data on related molecules whose experimental structures are known. Use has been made of STO-3G, 4-31G and experimental structural data (Table 2.4) for water[67,68], methanol[69,70], ethylene[70,71], propene[69,72,73], fluoroethylene[69,74] and methyl vinyl ether[54,75]. For the theoretical structures, methanol has been optimized with the 4-31G basis set, and fluoroethylene with both the STO-3G and the 4-31G basis set, since these optimized structures were not available; they are listed in Table 2.4. For

the experimental structures r_0 values have been selected, where possible, since the aim is to predict an r_0 structure for vinyl alcohol for comparison with experimental results.

The correction method is illustrated in Table 2.5 for the O-H length. The data in Table 2.4 suggest that STO-3G estimates for O-H bond lengths in this type of system are approximately 0.034 Å too long while 4-31G estimates are approximately 0.006 Å too short. The optimized STO-3G and 4-31G values of the O-H length in *syn* vinyl alcohol (Table 2.2) thus lead to corrected values of 0.956 Å and 0.958 Å, respectively, and hence a "best" value of 0.957 Å.

Table 2.5 Comparison of Theoretical and Experimental O-H Bond Lengths (r).

Molecule	Exptl.	STO-3G		4-31G	
		r	Δr[a]	r	Δr[a]
HO-H	0.957	0.990	+0.033	0.951	-0.006
CH_3O-H	0.956	0.991	+0.035	0.951	-0.005
Mean			+0.034		-0.006

[a] $\Delta r = r$(theoretical) - r(experimental).

The structural parameters with the greatest uncertainties resulting from the application of this procedure are the C-O length and the CCO and CCH_u bond angles (Fig. 2.1). It is thought that the remaining eight geometric parameters are predicted to an accuracy well within 0.01 Å in lengths and 1° in angles. It was possible to use the experimental rotational constants[64] to decide the best values for the C-O length and the CCO angle within the theoretically acceptable range. However, the calculated rotational constants

are quite insensitive to the value of the CCH_u angle, and it was not possible to refine the value for this parameter, which consequently has a somewhat greater uncertainty of approximately $\pm 2^{\circ}$.

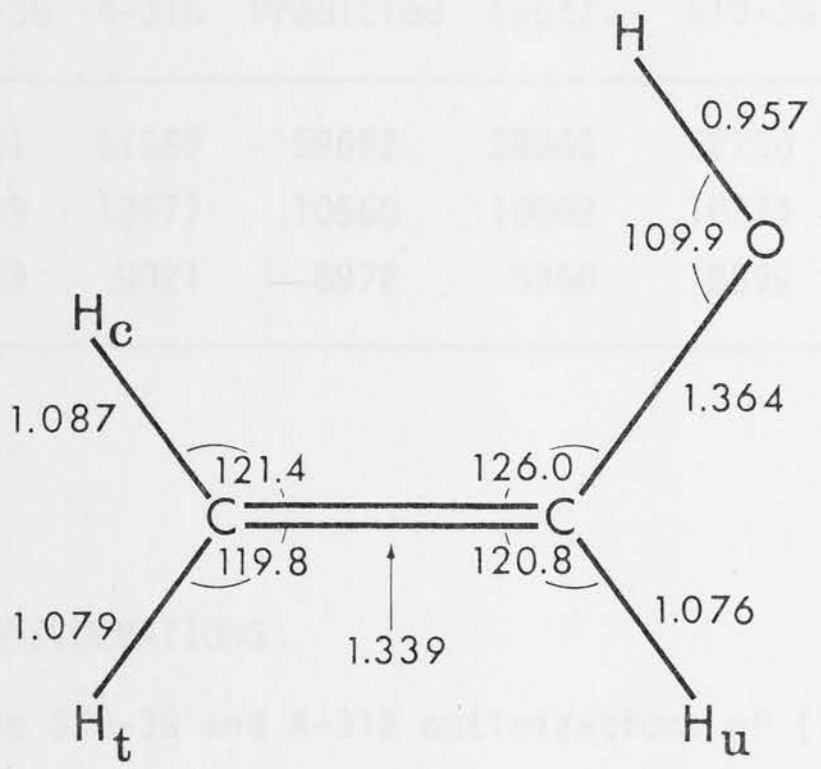

Fig. 2.1 Predicted Structure for Vinyl Alcohol

The resultant best structure for *syn* vinyl alcohol, i.e. the predicted r_0 structure, is shown in Fig. 2.1. In the microwave study[64] two parameters were determined, though it must be noted that all other geometrical parameters were assigned assumed values on the basis of experimental structures for vinyl chloride and methanol. The CCO angle (126.0°) obtained here is the same, but the C-O length (1.364) is somewhat shorter than the values (126.0° and 1.373 Å, respectively) derived in the microwave study. In particular it is noted that the assumed C=C length (1.332 Å) in the microwave study is significantly smaller than the predicted value (1.339 Å). The rotational constants calculated for the predicted structure (CH_2=CHOH and CH_2=CHOD) are compared with experimental values[64] in Table 2.6. Included, for comparison, are also the calculated rotational constants for the STO-3G optimized and the 4-31G optimized structures of *syn* vinyl alcohol. It is clear that the values for the predicted structure and the experimental values are in close agreement.

Table 2.6 Calculated and Experimental Rotational Constants (MHz) for *Syn* Vinyl Alcohol.

Constant	CH_2=CHOH				CH_2=CHOD			
	STO-3G	4-31G	Predicted	Exptl.	STO-3G	4-31G	Predicted	Exptl.
A	60131	61289	59662	59660	52750	54025	52637	52585
B	10499	10577	10560	10562	10274	10280	10308	10320
C	8939	9021	8972	8966	8599	8636	8620	8621

2.3 ENERGY CONSIDERATIONS

The STO-3G and 4-31G optimizations of (1)-(4) resulted in the STO-3G//STO-3G and 4-31G//4-31G energies. In addition the 4-31G//STO-3G energies were also calculated, for comparison. Although the STO-3G basis set is quite good for geometry predictions[45,46,50], it is not adequate for the calculation of relative energies. For this purpose the 4-31G basis set is thought to be better[46,50,51]. In order to provide better relative energies still, the total energies of the stable isomers (1), (3) and (4) have also been calculated at the 6-31G*//STO-3G and the 6-31G*//Exp levels. To obtain the latter the experimental structures for acetaldehyde (1) and ethylene oxide (4) from the literature[61,66], and the predicted experimental structure for vinyl alcohol (Fig. 2.1) have been used. All total and relative energies are listed in Table 2.7. The relative energies, of which the 6-31G*//Exp values should be the most accurate, can be compared with the relative energies obtained from the experimentally determined $\Delta H_f^o(0^o)$ values[76] of -155.4 kJ mol^{-1} for acetaldehyde and -40.1 kJ mol^{-1} for ethylene oxide. These have been corrected for zero-point vibrational energies (calculated as $\frac{1}{2}h\Sigma_i \nu_i$, where ν_i are experimental vibrational frequencies, using the reported vibrational frequencies for acetaldehyde[77] and ethylene oxide[78],

Table 2.7 Calculated Total Energies, and Theoretical and Experimental Relative Energies for the C_2H_4O Isomers.

	STO-3G//STO-3G Energy		4-31G//STO-3G Energy		4-31G//4-31G Energy		6-31G*//STO-3G Energy		6-31G*//Exp Energy		Expt.[a] Relative Energy
	Total	Rel.	Total	Rel.	Total	Rel.	Total	Rel.	Total	Rel.	
Acetaldehyde (1)	-150.94599	0	-152.68499	0	-152.68652	0	-152.91347	0	-152.91369	0	0
Vinyl Alcohol (*syn*) (3)	-150.91668	77.0	-152.66632	49.0	-152.67074	41.4	-152.88506	74.6	-152.88755	68.6	b
Vinyl Alcohol (*anti*) (2)	-150.91311	86.3	-152.66297	57.8	-152.66732	50.4	..	..	..	..	..
Ethylene Oxide (4)	-150.92850	45.9	-152.62444	159.0	-152.62676	156.9	-152.86455	128.4	-152.86605	125.1	111.7

[a] Calculated from $\Delta H_f(0^\circ)$ for (1) and (4), ref. 76, with zero-point vibration energy correction, see text.

[b] No experimental value available, see text.

leading to 141.4 and 145.0 kJ mol^{-1}, respectively) which results in the energy of ethylene oxide being 111.7 kJ mol^{-1} relative to acetaldehyde. For vinyl alcohol there is only an estimated $\Delta H_f^\circ(298^\circ)$ value[79] of -111 kJ mol^{-1} available, which should be compared with $\Delta H_f^\circ(298^\circ)$ of -166.2 kJ mol^{-1} for acetaldehyde[76], giving a relative energy of 55 kJ mol^{-1}. This estimated $H_f^\circ(298^\circ)$ value for vinyl alcohol, however, was obtained assuming additivity of bond energies, and is not very reliable. An experimental (ICR) value exists[80] for the keto-enol energy difference in the homologue of acetaldehyde, acetone, of 58.2 ± 8 kJ mol^{-1}. This experimental value is fairly close to the best value of 68.6 kJ mol^{-1}, with the 6-31G*//Exp approach. Other studies still in progress[81,82] show that the use of even larger basis sets and configuration interaction reduces the energy difference between (1) and (3) to ∿ 50 kJ mol^{-1}. For the acetaldehyde/ethylene oxide energy difference experimental and theoretical (6-31G*//Exp) results agree quite well (111.7 and 125.1 kJ mol^{-1}, respectively). Finally the calculated energy difference between *syn* and *anti* vinyl alcohol is worth noting. All three approaches used (Table 2.4) lead to values close to 9 kJ mol^{-1}, indicating that this is likely to be a reasonable estimate of the energy difference.

2.4 CONCLUSIONS

In this chapter, the calculated structures and energies for the three C_2H_4O isomers have been presented. The calculated relative energies at the 6-31G*//Exp level are in reasonable agreement with the available experimental data, while the calculated optimum geometries for acetaldehyde and ethylene oxide can be compared with experimentally determined structures, and agree quite well. For vinyl alcohol an experimental structure has been predicted, the rotational constants for which correlate well with experimental

data. A correction procedure as applied to vinyl alcohol may be generally useful in making structural predictions from small or medium-sized basis set calculations for molecules for which geometry optimizations with more sophisticated (e.g. double zeta + polarization + correlation) basis sets are currently not possible.

CHAPTER 3

EFFECT OF SUBSTITUENTS ON KETO-ENOL TAUTOMERISM IN THE ACETALDEHYDE/VINYL ALCOHOL SYSTEM

3.1 INTRODUCTION

It is well known[83] that the keto forms of simple aldehydes and ketones are considerably more stable than the corresponding enols, and theoretical calculations confirm this (cf. Chapter 2). However, it might be possible, by substituting the aldehyde or ketone in the α-position, to influence the relative stability of this isomer with respect to the substituted enol. In this chapter, a study will be presented of the effect of α-substituents on the acetaldehyde/vinyl alcohol energy difference. Since this study can be considered a prototype for keto-enol tautomerism in general, the substituted acetaldehydes will often be referred to as the keto isomer. The aim of the study is to identify those substituents which decrease the enol-keto energy difference [ΔE = E(enol) - E(keto)], and ideally to design a small system in which the enol isomer is lower in energy than the keto isomer. Using *ab initio* molecular orbital theory, Hehre and Lathan[84] were able to show that the difference in energy between the substituted keto (5) and enol (6) isomers of acetaldehyde is reduced when the substituent X is a π-electron-donating group (X = CH_3, NH_2, OH, F).

XCH_2CHO (5) $XCH{=}CHOH$ (6)

They found that when they calculated the stabilization energies (cf. Section 1.5) for these substituents, the enol isomer was stabilized more by substitution than the keto isomer. By finding substituents that have a similar, but more pronounced, effect, it is hoped to design a simple enol which would be more stable than its keto isomer.

3.2 METHOD

A general approach of 4-31G//Std calculations has been used on a number of conformations for each substituted isomer in order to identify the most stable one. For the enols this included all *cis*/*trans* and *syn*/*anti* isomers, while for the keto isomers the rotational potential energy surface corresponding to internal rotation about the C-C bond in XCH_2-CHO for XCCO dihedral angles [ϕ, cf. (7)] of 0, 60, 120 and 180° has been examined.

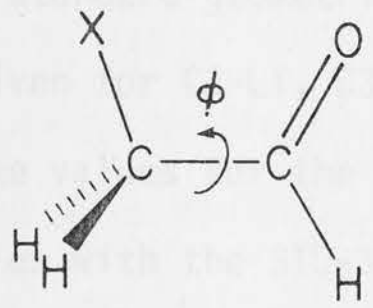

(7)

The energies calculated at these points were fitted to a truncated Fourier expansion (equation 1.21, cf. Section 1.6) which enabled the stationary points in the rotational potential surface to be determined. At these stationary points, additional calculations were performed. The potential constants, V_i, are indicative of the interaction of the substituent X with the formyl part of the acetaldehyde molecule.

Stabilization energies (E_S) for the keto and enol isomers were calculated according to equations 3.1 and 3.2 (see Section 1.5).

$$XCH_2CHO + CH_4 \rightarrow CH_3CHO + XCH_3 \qquad 3.1$$

$$XCHCHOH + CH_4 \rightarrow CH_2CHOH + XCH_3 \qquad 3.2$$

The energy change in these reactions measures the effect of a substituent in acetaldehyde or vinyl alcohol compared with its effect in methane. Finally, energy differences (ΔE) between enol and keto isomers were calculated.

3.3 SUBSTITUENTS THAT ARE π-ELECTRON DONORS (CH_3, NH_2, OH, F) AND SUBSTITUENTS THAT ARE π-ELECTRON ACCEPTORS (Li, BeH, BH_2)

In order to get a better understanding of the effect of substituents X on the keto-enol energy difference in (5) and (6) it was decided to examine a number of π-electron-accepting substituents (Li, BeH, BH_2) and to compare them with the π-electron-donating substituents (CH_3, NH_2, OH, F) which were studied by Hehre and Lathan.[84]

When assigning standard geometries[33-37], it was found that no standard bond lengths are given for C3-Li, C3-Be2, and C3-B3. It was therefore decided to take the values for the C-X bond lengths (X = Li, BeH, BH_2) from optimization studies with the STO-3G basis set of C-X bonds in selected conformations of (5) (<XCCO = 120°) and (6) (<XCCO = 180°, <CCOH = 0). These values are listed in Table 3.1.

Table 3.1 Lengths for C*m*-X*n* Bonds[a]

Bond	C4-Li	C4-Be2	C4-B3	C3-Li	C3-BeH	C3-B3
Length	2.03	1.71	1.59	1.91	1.64	1.52

[a] X*n* denotes an atom X joined to *n* other atoms.

In this study, the full set of conformers of (5) for X = Li, BeH, BH_2 has been examined; for the BH_2 substituent both planar and perpendicular orientations of the BH_2 group with respect to the BCC plane have been considered. For X = CH_3 and F, previously reported data[51,84] have been supplemented. Detailed studies for the NH_2 and OH substituents have been reported[85,86], and therefore it has not been necessary to examine further the conformational preferences for these substituents. The calculated energies

are displayed in Table 3.2, and the potential constants V_i are listed in Table 3.3. For the enol isomers (6) only the conformers for X = Li, BeH, BH_2 have been examined and the previously reported data[84] for the other substituents have been used. The calculated energies are listed in Table 3.5. Using the energies of the best conformers, the stabilization energies E_s and the energy differences ΔE, as shown in Table 3.4, can be calculated.

3.3.1 CONFORMATIONS OF KETO ISOMERS

Three types of rotational potential functions can be distinguished for the substituted acetaldehydes examined here. Examples of the first class are provided by those substituents for which the potential function has only a threefold component (X = H), or those for which the threefold term, although not the only one, is sufficiently large, relative to the other terms, to dominate the total potential function (X = CH_3). In this class, the well established tendency of single bonds of an XCH_2 group to eclipse an adjacent double bond, as for example in propene and 1-butene, is maintained[47,52,72,87,88]. For acetaldehyde itself (X = H), all the potential minima are equivalent and correspond to a methyl C-H eclipsing the C=O. The calculated threefold barrier (3.1 kJ mol^{-1})[51] is somewhat lower than the experimental estimate (4.85 kJ mol^{-1})[61] from microwave spectroscopy. The theoretical potential function and its Fourier components for propionaldehyde (X = CH_3)[51] are shown in Fig. 3.1. The most stable conformational isomer is the *cis* form (8) in which C-CH_3 eclipses C=O. There is an additional *skew* isomer (9) with ϕ = 117.4° lying 2.9 kJ mol^{-1} above (8).

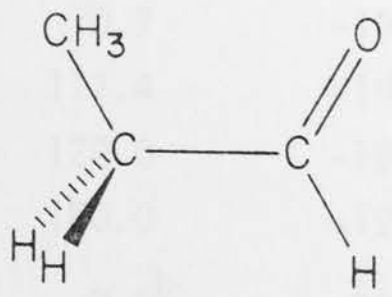

(8)

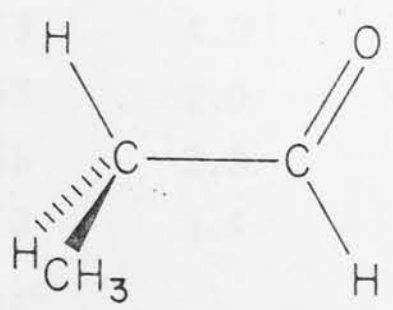

(9)

Table 3.2 Calculated Total Energies, Relative Energies and Dipole Moments of Conformations of Keto Isomers $XCH_2CH=O$.

Substituent X	Dihedral Angle XCCO	Total Energy	Relative Energy	Dipole Moment
H	0.0	-152.68475[a]	0	3.35
	60.0	-152.68358	3.1	3.29
Li	0.0	-159.52304	20.7	5.09
	60.0	-159.52952	3.7	6.95
	82.4	-159.53092	0	7.91
	120.0	-159.52445	17.0	8.94
	180.0	-159.50678	63.4	9.11
BeH	0.0	-167.28369	2.9	3.50
	60.0	-167.28459	0.6	3.50
	77.1	-167.28480	0	3.53
	120.0	-167.28131	9.2	3.45
	180.0	-167.27227	32.9	3.13
BH_2 (planar)	0.0	-177.87480	16.3	3.37
	60.0	-177.88009	2.4	3.45
	90.1	-177.88102	0	3.46
	120.0	-177.88034	1.8	3.39
	180.0	-177.87667	11.4	3.20
BH_2 (perp.)	0.0	-177.87967	3.3	3.50
	60.0	-177.87807	7.7	3.32
	120.0	-177.87610	12.9	3.20
	180.0	-177.87134	25.4	3.00
CH_3	0.0	-191.66266[a]	0	3.18
	60.0	-191.66116	3.9	3.21
	70.7	-191.66113	4.0	3.25
	117.4	-191.66156	2.9	3.42
	120.0	-191.66155	2.9	3.42
	180.0	-191.66060	5.4	3.37
NH_2	0.0[b]	-207.61945[c]		2.60

Table 3.2 (Cont'd)

Substituent X	Dihedral Angle XCCO	Total Energy	Relative Energy	Dipole Moment
OH	0.0[d]	-227.42270		3.49
F	0.0	-251.39849	17.0	4.80
	60.0	-251.39500	26.2	4.11
	67.6	-251.39488	26.5	3.94
	120.0	-251.39979	13.6	2.58
	180.0	-251.40497	0	1.18

[a] From ref. 51.
[b] < CCN: = 180°.
[c] From ref. 84.
[d] < CCOH = 0°.

The calculated *skew* → *cis* barrier is 1.1 kJ mol^{-1} and the *skew* → *skew* barrier is 2.5 kJ mol^{-1}. Other *ab initio* calculations[89] on propionaldehyde yield similar results. Microwave spectral studies[90] also indicate the *cis* form to be stable, with a *skew* structure (ϕ = 131°) lying 3.8 kJ mol^{-1} higher in energy. NMR measurements in the liquid phase[91] yield a *skew-cis* energy difference of 4.1 kJ mol^{-1}.

Examination of the potential constants in Table 3.3 shows that, for the remaining substituents (giving rise to the second and third classes of conformational behaviour), the potential function is dominated by V_1 and V_2 components rather than V_3. In these cases the tendency of a single bond in the XCH_2 group to eclipse the C=O bond is swamped by other factors.

The second class of potential functions is typified by the functions for X = Li (Fig. 3.2). The large positive V_1 indicates a preference for *cis* [(10), X = Li, ϕ = 0°] compared with *trans*

Table 3.3 Potential Constants for Internal Rotation in Keto Isomers $XCH_2CH{=}O$.

X	V_1	V_2	V_3
H	0	0	3.07
Li	37.33	-42.27	5.36
BeH	25.73	-17.40	4.25
BH_2 (planar)	- 3.71	-15.68	-1.20
BH_2 (perp.)	18.03	- 5.53	3.84
CH_3	2.93	0.97	2.48
F	-19.73	15.18	2.71

[(11), X = Li, $\phi = 180^\circ$] conformations and reflects the more favourable dipolar interactions in (10) (see also Table 3.2).

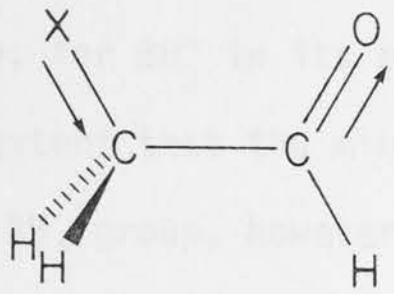

(10)

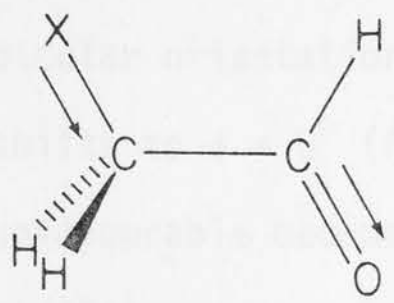

(11)

The large negative V_2 indicates a preference for XCCO perpendicular [(12), X = Li, $\phi = 90^\circ$] compared with XCCO planar ($\phi = 0, 180^\circ$) structures and can be rationalized in terms of the theory of geminal interactions[36,46,48,92,93]. This theory is based on the concept that in a disubstituted methane the interactions of the substituents through the methyl group can be analyzed by examining their electron-donating or electron-withdrawing properties (cf. Section 1.4). The π-electron-accepting nature of the CHO group and the σ-electron-donating nature of the Li substituent lead to a favourable interaction in the perpendicular structure as shown in (12), X = Li.

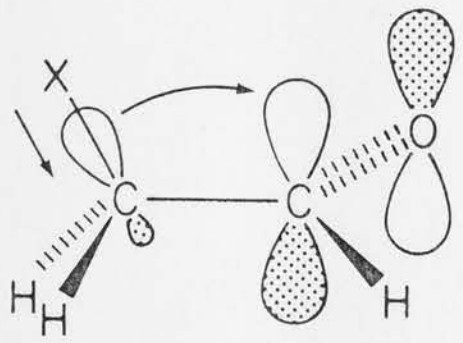

(12)

The net result of the large positive V_1 and the large negative V_2 is a minimum in the overall potential function for ϕ slightly less than 90°, i.e. ϕ = 82.4 , with maxima at the *cis* (20.7 kJ mol^{-1}) and *trans* (63.4 kJ mol^{-1}) structures.

Replacement of the Li substituent by the weaker σ-electron donors BeH and BH_2 leads to a reduction in magnitudes of both V_1 and V_2. For BeH, the potential function (Fig. 3.3, curve A) shows a minimum at $\phi = 77.1^{\circ}$, while, for BH_2 in its perpendicular orientation, the V_2 term is reduced to the extent that the minimum shifts to $\phi = 0^{\circ}$ (Fig. 3.3, curve B). A perpendicular BH_2 group, however, is unfavourable because of the σ-electron-withdrawing nature of the CHO substituent (13) and the planar orientation of BH_2 is consequently preferred. With a planar BH_2 arrangement, the conformations with ϕ = 0 and 180° are sterically unfavourable and the minimum in the potential function (Fig. 3.3, curve C) returns to a near-orthogonal position ($\phi = 90.1^{\circ}$).

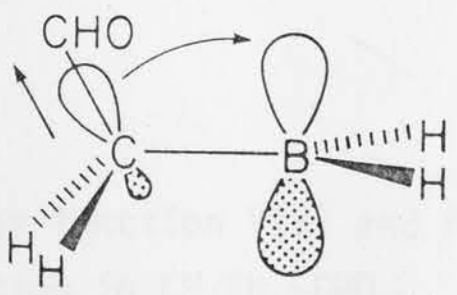

(13)

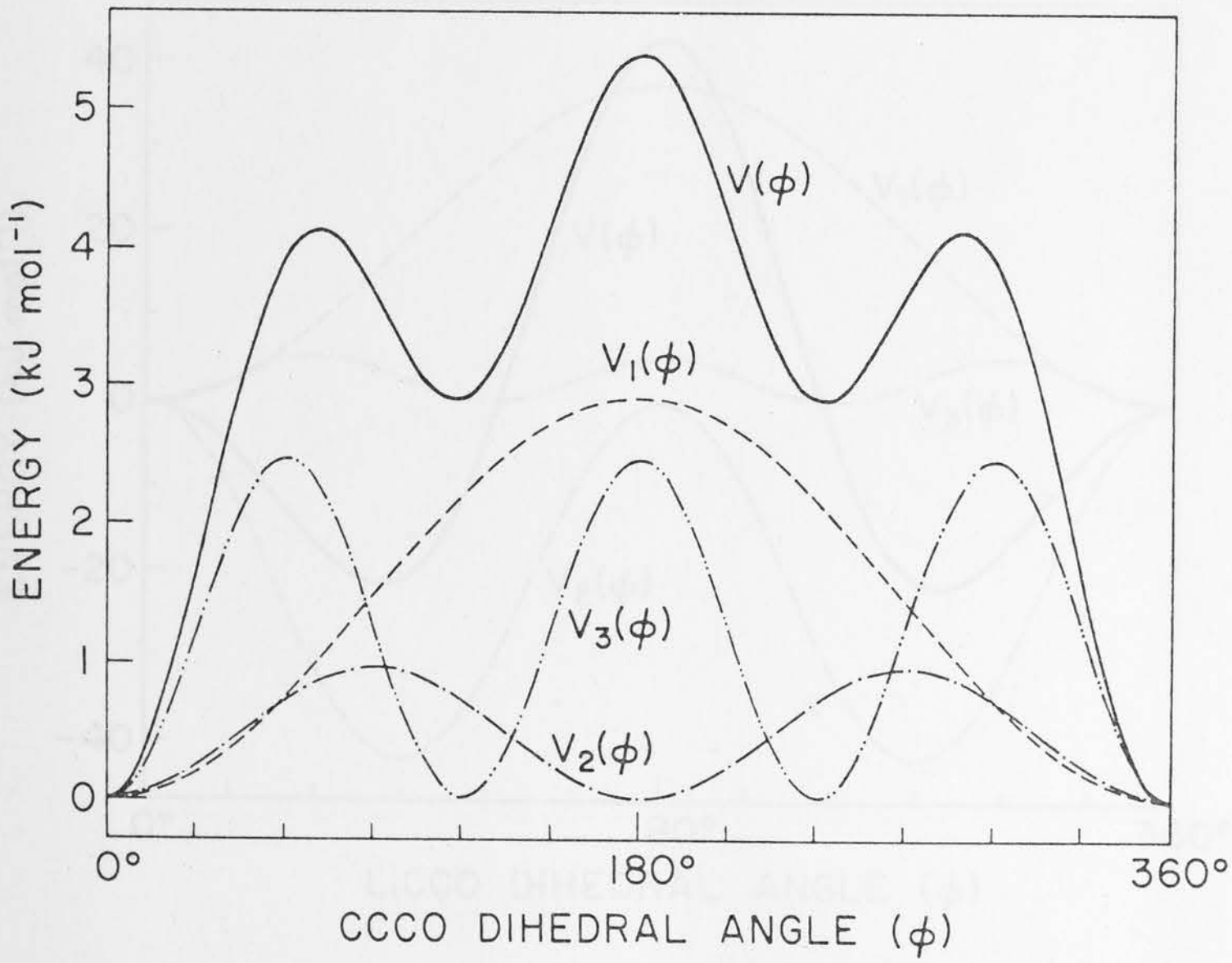

Fig. 3.1 Potential energy function $V(\phi)$ and Fourier components $V_n(\phi)$ describing internal rotation in CH_3CH_2-CHO.

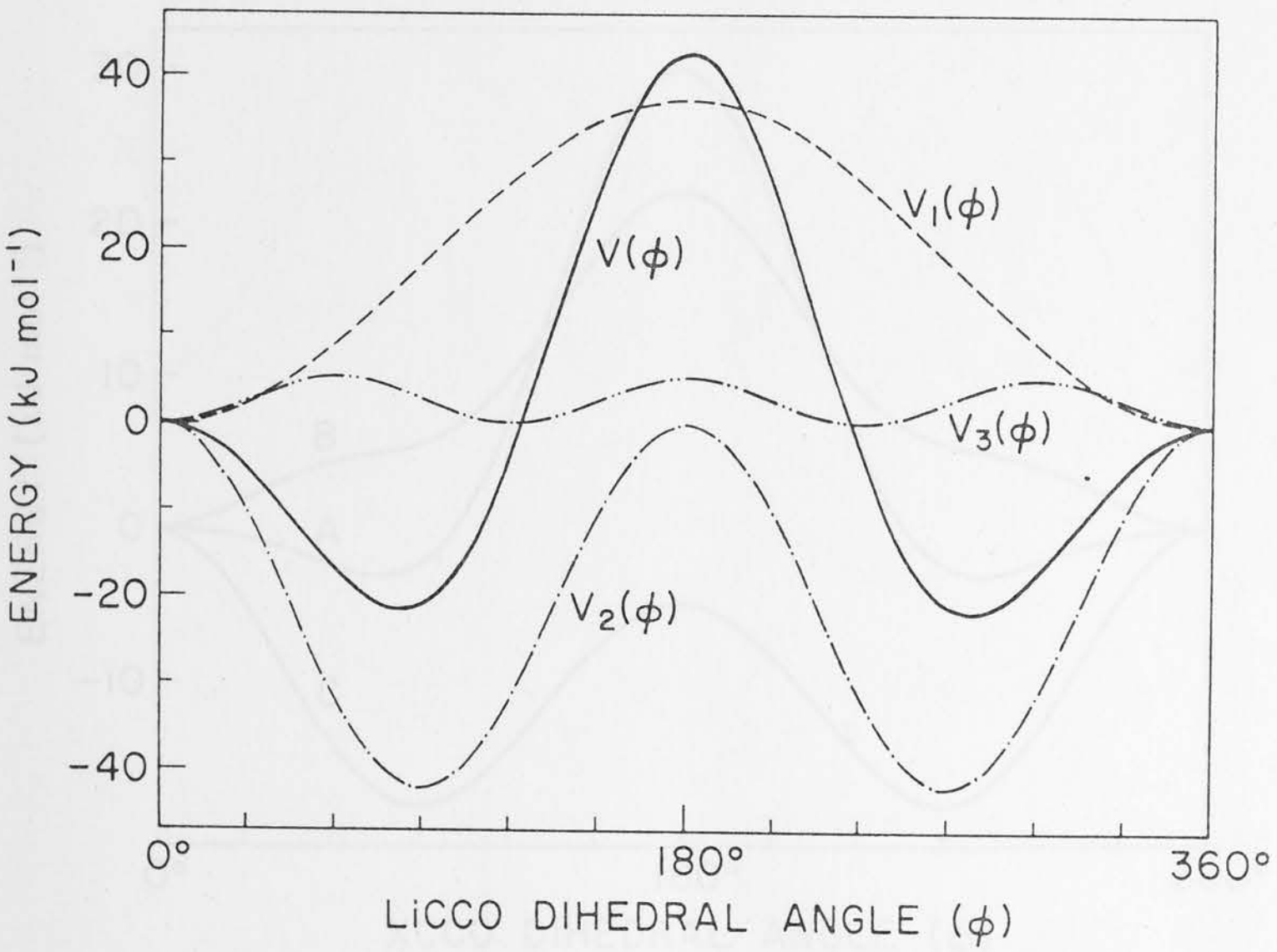

Fig. 3.2 Potential energy function $V(\phi)$ and Fourier components $V_n(\phi)$ describing internal rotation in $LiCH_2$-CHO.

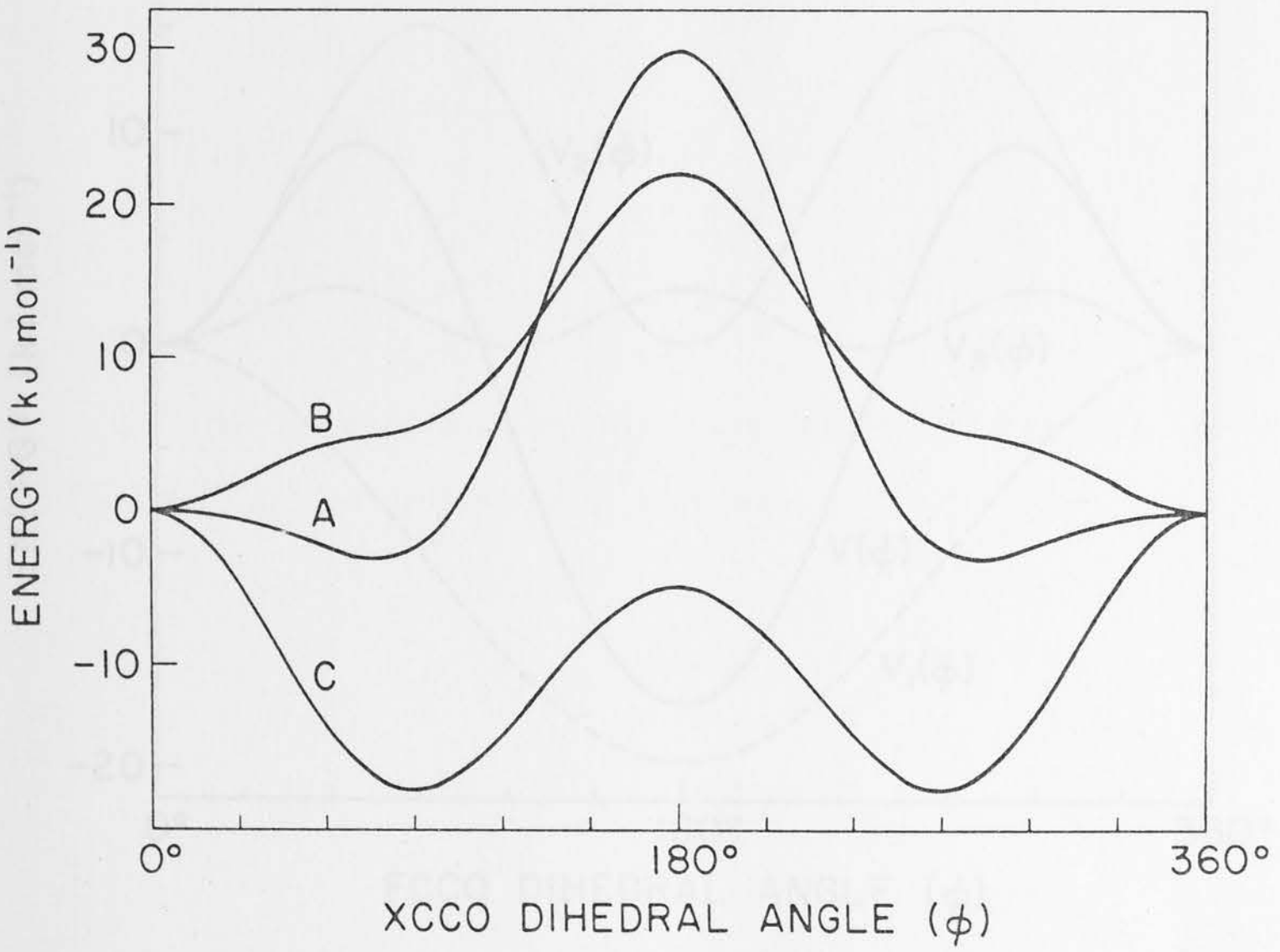

Fig. 3.3 Potential energy functions V(ϕ) describing internal rotation in (A) $BeHCH_2$-CHO, (B) BH_2CH_2-CHO (< HBCC = 90°), and (C) BH_2CH_2-CHO (< HBCC = 0°). Note that the zero levels for the three curves correspond to different *total* energies.

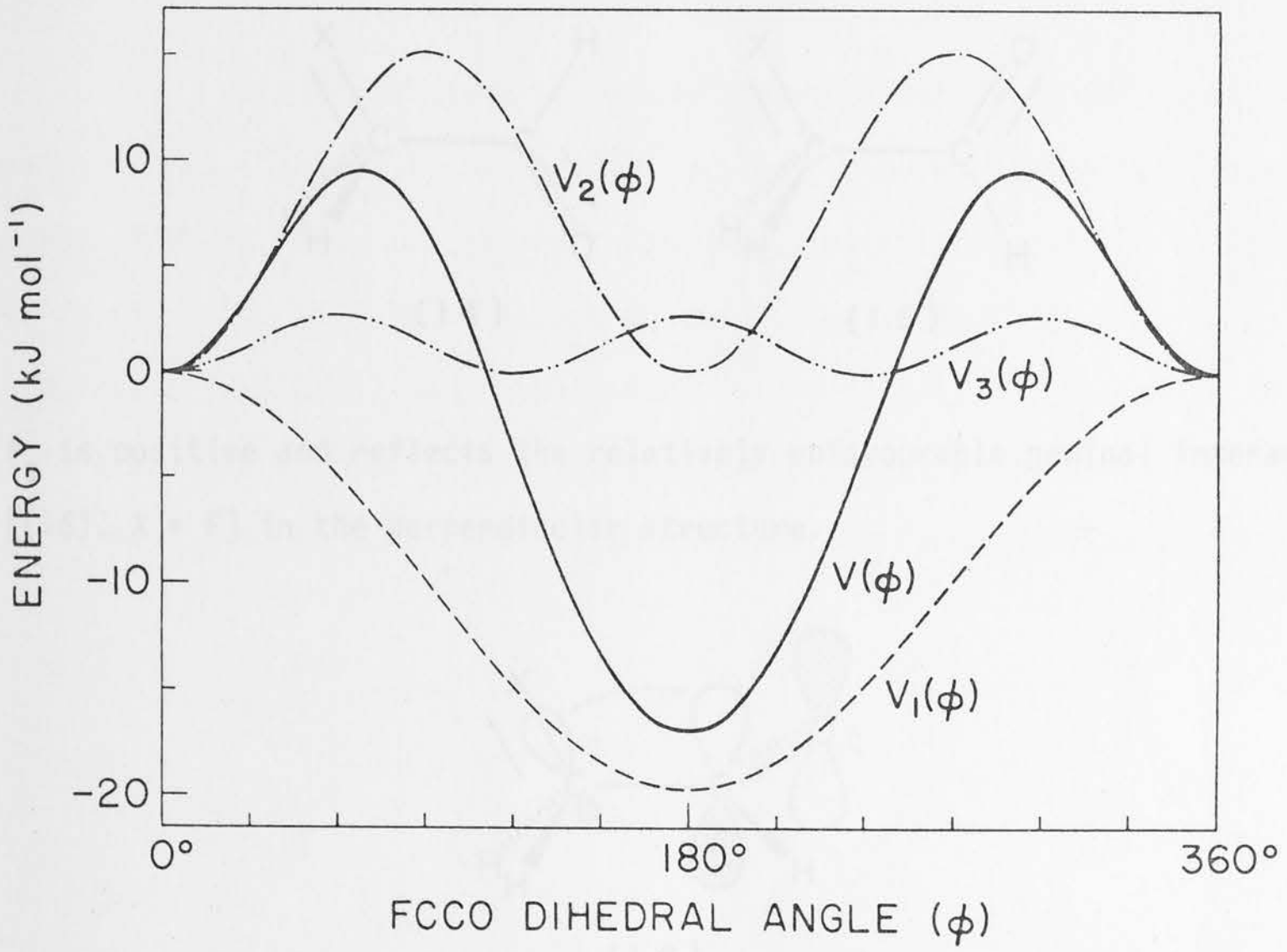

Fig. 3.4 Potential energy function $V(\phi)$ and Fourier components $V_n(\phi)$ describing internal rotation in FCH_2-CHO.

A typical member of the third class of potential functions, and in fact the only member of this class treated in this section, is the potential function for the σ-electron-accepting fluoro substituent (Fig. 3.4). In this case, V_1 is large and negative indicating a preference for *trans* [(14), X = F, $\phi = 180^{\circ}$] compared with *cis* [(15), X = F, $\phi = 0^{\circ}$] structures, consistent again with the dipolar interactions (cf. also Table 3.2).

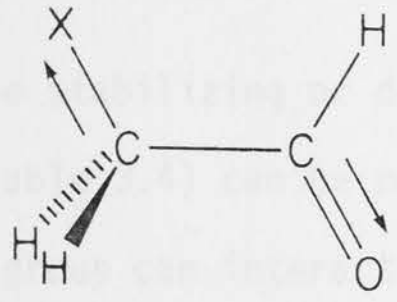

(14)

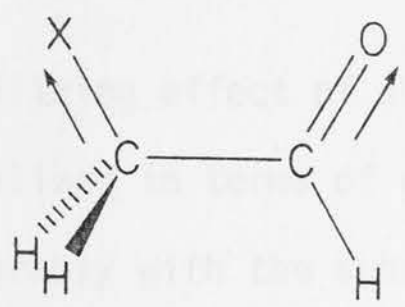

(15)

V_2 is positive and reflects the relatively unfavourable geminal interaction [(16), X = F] in the perpendicular structure.

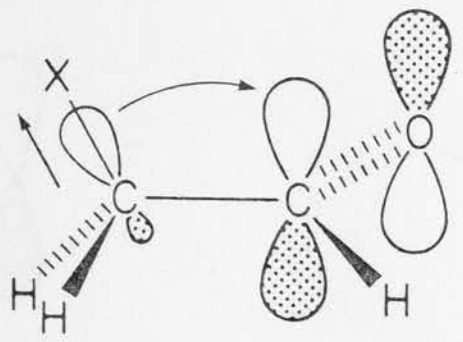

(16)

The overall result in this case is a potential function with minima at the *cis* and *trans* positions, the latter being favoured by 17.0 kJ mol^{-1}. Although there appears to be no relevant experimental information in the literature regarding the conformation of α-fluoroacetaldehyde itself, there are some data available for related molecules. Thus, the preferred conformation of fluoroacetone has FCCO *trans*[94], analogous to the favoured

conformation [(14), X = F] of α-fluoroacetaldehyde. Again, α-chloroacetaldehyde has been shown by microwave spectroscopy to exist in two conformations, the lower energy form having ClCCO *trans* and the higher energy form with ClCCO *cis*.[95] Finally, rotational isomers with FCCO *cis* and FCCO *trans* have also been found by microwave spectroscopy for fluoroacetyl fluoride.[96]

3.3.2 STABILIZATION ENERGIES FOR KETO ISOMERS

The stabilizing or destabilizing effect of substituents in the keto isomers (Table 3.4) can be rationalized in terms of geminal interactions. The CHO group can interact favourably with the substituent X in two ways. Firstly, if X is a π-electron donor, the σ-electron-withdrawing property of CHO leads to a stabilizing interaction (17). Secondly, if X is a σ-electron donor, the π-electron-withdrawing property of the CHO group will lead to a stabilizing interaction, as shown previously in (12).

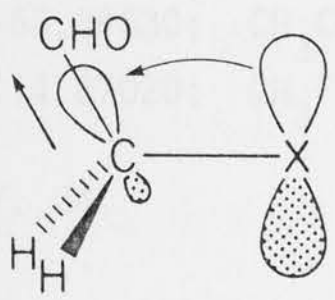

(17)

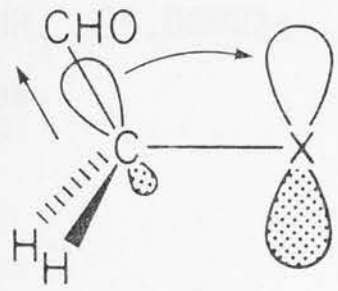

(18)

Thus the keto isomers are stabilized by π-electron donor substituents and by σ-electron donor substituents; conversely, they are destabilized by π-electron acceptors and σ-electron acceptors. The ordering of keto stabilization energies

$$Li > BeH > BH_2$$

can be understood on this basis. BH_2 is a stronger π-electron acceptor

Table 3.4 Calculated Stabilization Energies[a] (E_s) for Preferred Conformations of Keto and Enol Isomers, and Enol-Keto Energy Differences [ΔE = E(enol) - E(keto)].

Substituent X	E_s (keto)	E_s (enol)	ΔE
H	0	0	53.9
Li	+68.7	+40.7	81.9
BeH	+17.6	+27.1	44.3
BH_2	-27.5	+22.5	3.9
CH_3[b]	+ 6.9	+13.4	47.3
NH_2[b]	+16.3	+48.0	22.2
OH	+19.2	+34.8[b]	38.3
F	+ 8.6	+15.3[b]	47.2

[a] Calculated using 4-31G//Std energies from refs. 36 and 46 as follows: CH_4 -40.13955; CH_3Li -46.95957; CH_3BeH -54.73290; CH_3BH_2 -65.34630; CH_3CH_3 -79.11484; CH_3NH_2 -95.06803; CH_3OH -114.87020; CH_3F -138.85648 hartrees.

[b] From ref. 84.

than Li and so the destabilizing interaction (18) is greater for BH_2 than for Li. On the other hand, Li is a better σ-electron donor than BH_2 and so the stabilizing interaction in (12) is greater for Li.

Similar arguments based on (16) and (17) would predict an ordering

$$NH_2 > OH > F$$

of keto stabilization energies since NH_2 is the strongest π-electron donor and F the strongest σ-electron acceptor of these three substituents.

Examination of Table 3.4 shows, however, that the OH substituent does not fit into this pattern, having a keto stabilization energy somewhat higher than expected. The anomalous behaviour of OH can be understood by noting the likelihood of intramolecular hydrogen bonding in the favoured conformation[89,97] (19) of $HOCH_2CHO$, resulting in an additional stabilizing effect.

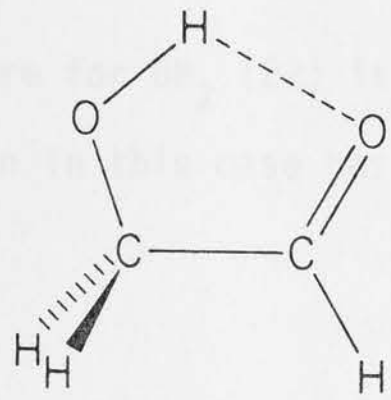

(19)

Although such an interaction could occur in principle for NH_2CH_2CHO as well, there is an extra cost in terms of bond eclipsing. The eclipsed-staggered energy differences (4-31G//Std) for methylamine and methanol are 8.9 and 4.7 kJ mol^{-1} respectively[48]. As a result, the preferred conformation[84,85] of NH_2CH_2CHO has a staggered NH_2 group and hence a less efficient intramolecular hydrogen bond.

3.3.3 CONFORMATIONS OF ENOL ISOMERS

There are several effects which appear to influence the conformations of the enol isomers. The preferred conformation (XCCO *cis*, CCOH *trans*) for Li and BeH substituents is favoured by both dipolar (20) and 1,4-donor-acceptor (21) interactions.

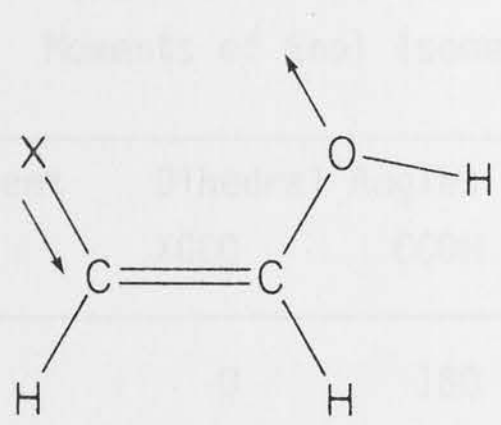

(20)

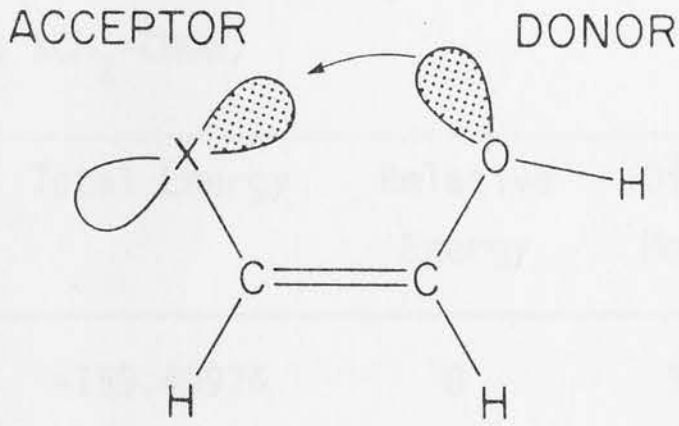

(21)

The corresponding structure for BH_2 (22) is sterically unfavourable and the preferred conformation in this case has BCCO *trans* and CCOH *cis* (23).

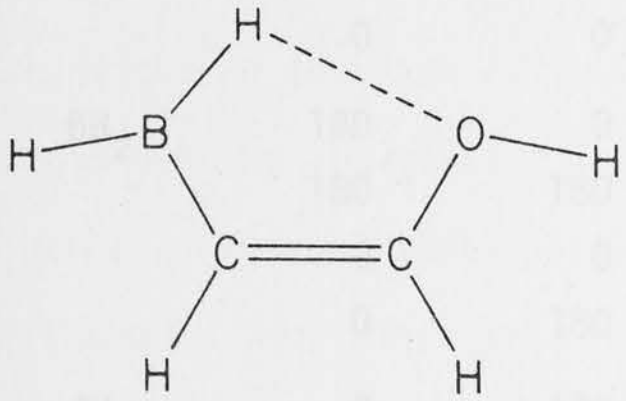

(22)

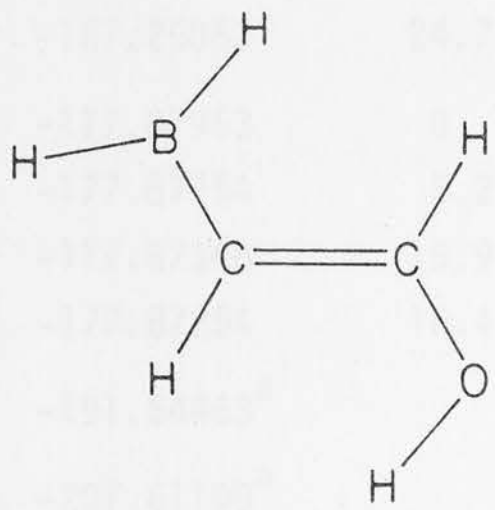

(23)

For NH_2, OH and F substituents, intramolecular hydrogen bonding can occur in the favoured conformations [e.g. (24)] reported previously.[84]

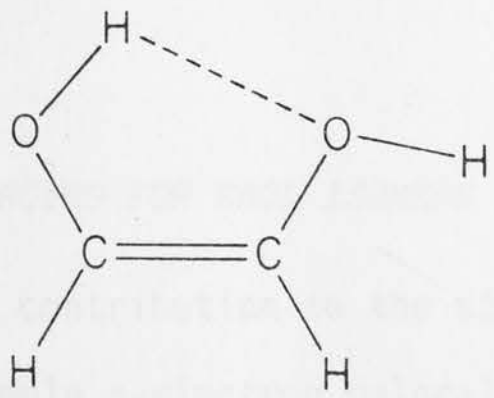

(24)

Table 3.5 Calculated Total Energies, Relative Energies and Dipole Moments of Enol Isomers XCH_2=CHOH.

Substituent X	Dihedral Angles XCCO	CCOH	Total Energy	Relative Energy	Dipole Moment
Li	0	180	-159.49974	0	3.30
	180	0	-159.49621	9.3	6.57
	180	180	-159.49330	16.9	6.45
	0	0	-159.49076	23.6	6.31
BeH	0	180	-167.26791	0	3.22
	180	0	-167.26620	4.5	1.11
	180	180	-167.26510	7.4	2.41
	0	0	-167.25852	24.7	1.29
BH_2	180	0	-177.87953	0	0.82
	180	180	-177.87754	5.2	2.82
	0	0	-177.87348	15.9	0.86
	0	180	-177.87254	18.4	3.44
CH_3	0	180	-191.64463[a]		
NH_2	0	180	-207.61100[a]		
OH	0	0[b]	-227.40813[a]		
F	0	0	-251.38699[a]		

[a] From ref. 84.

[b] < HOCC = 180°.

3.3.4 STABILIZATION ENERGIES FOR ENOL ISOMERS

An important contribution to the stabilization of the enol isomers is provided by simple π-electron delocalization (25) which should be particularly favourable for π-electron-accepting substituents X.

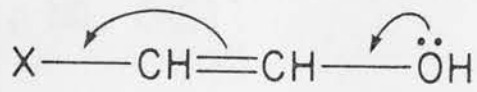

(25)

However, the calculated stabilization energies shown in Table 3.4 do not simply follow the order of π-electron-accepting power of the substituent, indicating that other forces must also be operative. It seems that any substituent that extends the π-system has a stabilizing effect. It can be seen, however, that the preferred conformations for Li, BeH and BH_2 substituents are consistent with a dominating role being played by interactions of the type (20)-(22), while, for NH_2, OH and F, the internal hydrogen-bonding interaction [e.g. (24)] seems to provide the overriding influence. The enol stabilization energies shown in Table 3.4 are determined by the interplay of these various forces.

3.3.5 ENOL-KETO ENERGY DIFFERENCES

The energy differences (ΔE) between the enol and keto isomers (Table 3.4) represent the combined effect of the keto and enol stabilizing or destabilizing interactions. It is interesting to note that the keto rather than the enol isomers show the greatest variation in substituent stabilization energies. For the Li substituent, the large value of the keto stabilization energy leads to a slightly increased ΔE (compared with X=H) while for BH_2, with a large destabilization of the keto isomer, ΔE is reduced to a value close to zero. Thus, it is found that the keto and enol isomers of the hypothetical BH_2CH_2CHO molecule have comparable energy.

3.4 SUBSTITUENTS THAT ARE π-ELECTRON ACCEPTORS AND σ-ELECTRON ACCEPTORS (CN, NO_2, NO, CHO)

In order to create a simple stable enol, ideally a substituent is required which both *stabilizes* the enol isomer, and *destabilizes* the keto isomer. Considerations based on the theory of geminal interactions showed in the previous section that such a substituent X should be both a σ-electron acceptor [e.g. (16)] and a π-electron acceptor [e.g. (18)], in order to have a *destabilizing* effect on the keto isomer. For this reason it was decided to examine the effect of four substituents that have these qualities, *viz.* CN, NO_2, NO and CHO, on the keto-enol equilibrium. These substituents are also expected to *stabilize* the enol form by allowing extensive delocalization (25).

3.4.1 CONFORMATIONS OF KETO ISOMERS

As before, the energies for various conformations of the substituted keto isomers $XCH_2CH{=}O$ were calculated by varying the XCCO dihedral angle [ϕ, cf. (7)]. For X = NO_2, NO and CHO there are a number of orientations of X possible; examined were, for X = NO_2: $<ONCC = 0^\circ$ (denoted NO_2-0) and $<ONCC = 90^\circ$ (NO_2-90); for X = NO: $<ONCC = 0^\circ$ (NO-0) and $<ONCC = 180^\circ$ (NO-180); and for X = CHO: $<OCCC = 0^\circ$ (CHO-0) and $<OCCC = 180^\circ$ (CHO-180). When fitting the calculated energies (Table 3.6) to the three-term Fourier expansion (equation 1.21), it was found that this expansion is not always accurate in describing the potential energy function. Problems arise because the three-term expansion cannot give rise to more than two stationary points within the range $0 < \phi < 180^\circ$ whereas such situations can exist in practice, most commonly when there are potential minima close to (but not coinciding with) $\phi = 0$ or 180°. In order to examine this problem, the energies of $XCH_2CH{=}O$ at

Table 3.6 Calculated Total Energies, Relative Energies and Dipole Moments for Keto Isomers $XCH_2CH=O$.

Substituent X	Dihedral Angle OYCC	XCCO	Total Energy	Relative Energy	Dipole Moment
CN		0	-244.26356	8.5	6.20
		60	-244.26173	13.3	5.38
		120	-244.26532	3.9	3.29
		180	-244.26680	0	1.25
NO	0[a]	0	-281.04170	162.3	
	0	60	-281.08724	42.8	
	0	120	-281.09885	12.3	
	0	180	-281.09418	24.5	
	180	0	-281.09713	16.8	
	180	60	-281.09751	15.8	
	180	120	-281.10078	7.2	
	180	180	-281.10353	0	
	120	180	-281.10280	1.9	
	60	180	-281.10168	4.9	
	0	180	-281.09418	24.5	
NO_2	0[a]	0	-355.77576	87.5	6.52
	0	60	-355.79805	29.0	5.85
	0	120	-355.80765	3.8	3.83
	0	180	-355.80910	0	1.81
	90	0	-355.80489	11.0	6.93
	90	60	-355.80146	20.0	5.95
	90	120	-355.80595	8.3	3.81
	90	180	-355.80886	0.6	1.93
CHO	-1.9[b]	138.5	-265.22867	0	
	0	0	-265.19832	79.7	
	0	60	-265.22049	21.5	
	0	120	-265.22347	13.7	
	0	180	-265.22510	9.4	
	60	60	-265.22413	11.9	
	60	120	-265.22712	4.1	

Table 3.6 (Cont'd)

Substituent X	Dihedral Angle OYCC	XCCO	Total Energy	Relative Energy	Dipole Moment
CHO	60	180	-265.22571	7.8	
	60	240	-265.22342	13.8	
	60	300	-265.21826	27.3	
	120	120	-265.22570	7.8	
	120	180	-265.22116	19.7	
	120	240	-265.22380	12.8	
	180	180	-265.22409	12.0	

a <ONCC

b <OCCC

ϕ = 0, 30, 60, 90, 120, 150 and 180° were calculated and fitted to a six-term Fourier expansion (equation 1.21). The potential constants V_i from both expansions are shown in Table 3.7. For the sake of brevity, only the energies for 60° intervals are shown in Table 3.6.

Examination of the potential constants in Table 3.7 suggests a division into three classes of conformational behaviour. The first class consists of CN, NO_2-90, and NO-180. For these substituents, the potential constants resemble those for the electron-withdrawing fluoro substituent (Section 3.3), which have been included for comparison in Table 3.7. V_1 is large and negative, indicating a preference for the *trans* conformation (14) over the *cis* conformation (15), consistent with the dipolar interactions. The magnitudes of the total dipole moments for X = CN and NO_2 are included in Table 3.6 and illustrate this effect. V_2 is positive and reflects a destabilizing interaction (16) in the perpendicular

Table 3.7 Potential Constants for Internal Rotation in Keto Isomers $XCH_2CH=O$.

X	V_1	V_2	V_3	V_4	V_5	V_6
F[a]	-19.73	15.18	2.71			
CN	-11.93	5.80	3.43			
	-11.88	5.74	3.43	0.06	-0.05	0.03
NO_2-90	-14.82	11.09	4.40			
	-15.08	10.94	4.40	0.15	0.26	0.05
NO-180	-16.93	4.14	0.12			
	-16.38	5.24	0.12	-1.10	-0.55	-0.11
NO-0	-112.18	-87.88	-25.60			
	-101.96	-69.51	-25.60	-18.37	-10.22	-4.08
NO_2-0	-75.16	-36.47	-12.37			
	-70.96	-28.16	-12.37	-8.31	-4.20	-1.44
CHO-0	-52.09	-35.95	-18.22			
	-55.09	-29.60	-18.22	-6.35	3.00	-6.95
CHO-180	9.73	4.06	-7.08			
	10.72	5.86	-7.08	-1.80	-0.99	-4.17

[a] From Table 3.3, included for comparison.

conformations associated with the σ-electron-withdrawing nature of X and and the π-electron-accepting nature of the CHO group. Finally, the positive values of V_3 (though of negligible magnitude for NO-180) reflect a tendency of C-X or C-H to eclipse the C=O double bond. The resulting potential energy curves (Fig. 3.5, 3.6 and 3.7) all show minima at $\phi = 180^\circ$; for CN and NO_2-90, secondary minima are found at $\phi = 0^\circ$ while for NO-180 there is a shallow secondary minimum at $\phi = 40^\circ$. In all three cases, the three-term and six-term expansions of the potential function yield almost identical results. The potential constants V_4, V_5 and V_6 in the six-term expansions are all very small.

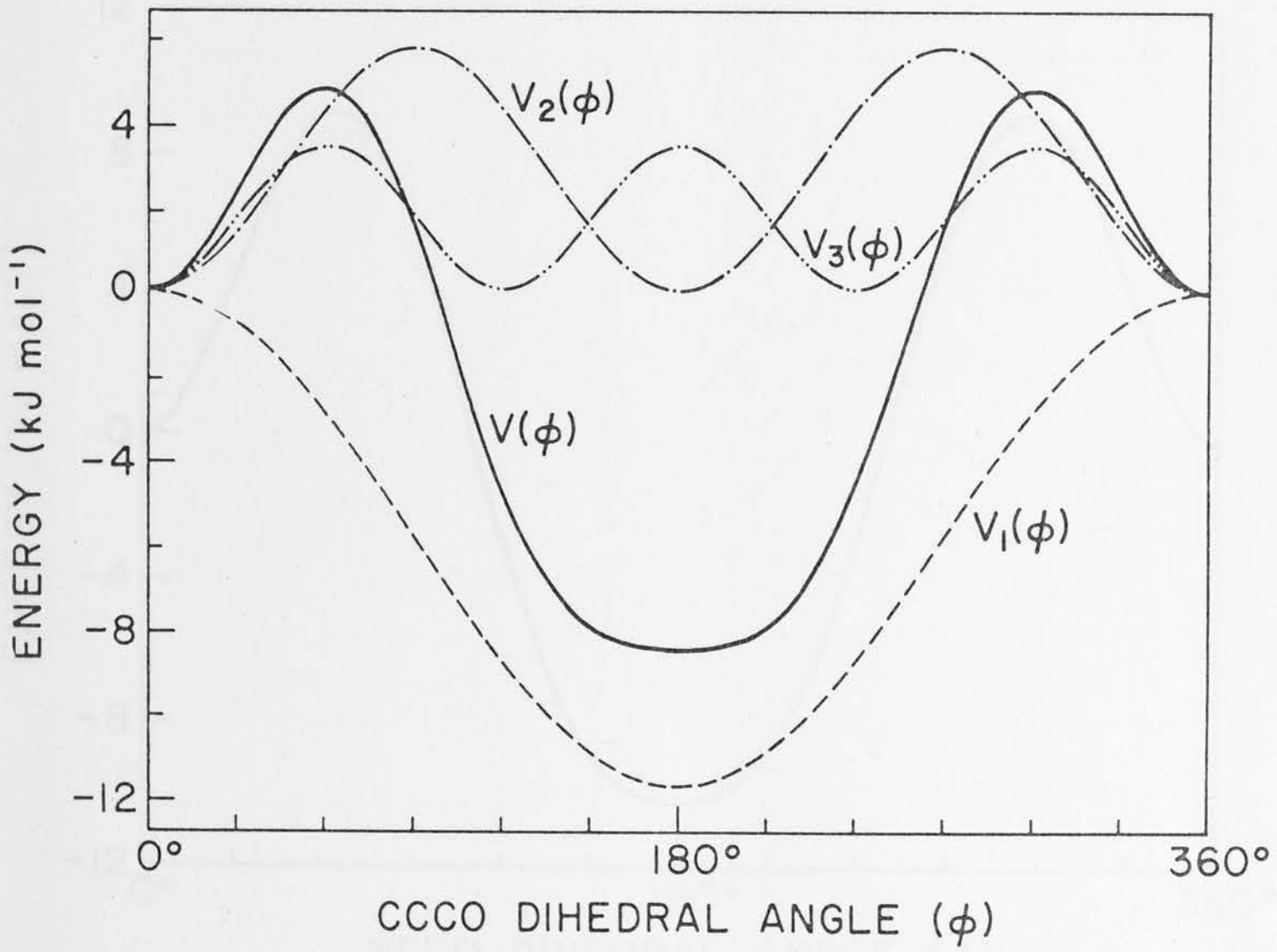

Fig. 3.5 Potential energy function $V(\phi)$ (from 6-term expansion; 3-term expansion coincides with 6-term expansion) and Fourier components $V_n(\phi)$ (from 6-term expansion) describing internal rotation in $NCCH_2$-CHO.

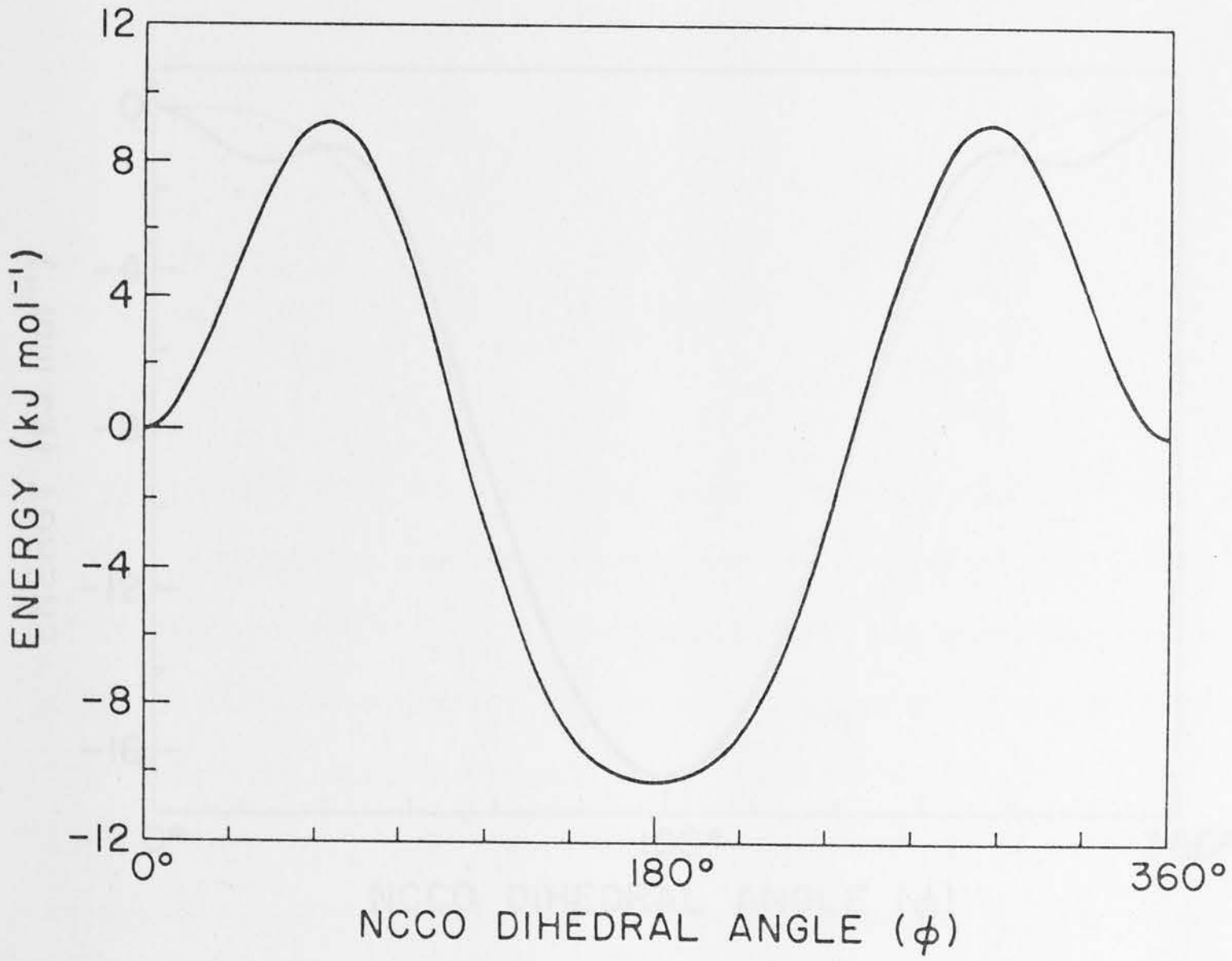

Fig. 3.6 Potential energy function $V(\phi)$ (from 6-term expansion; 3-term expansion coincides with 6-term expansion) describing internal rotation in O_2NCH_2-CHO, (< ONCC = 90°).

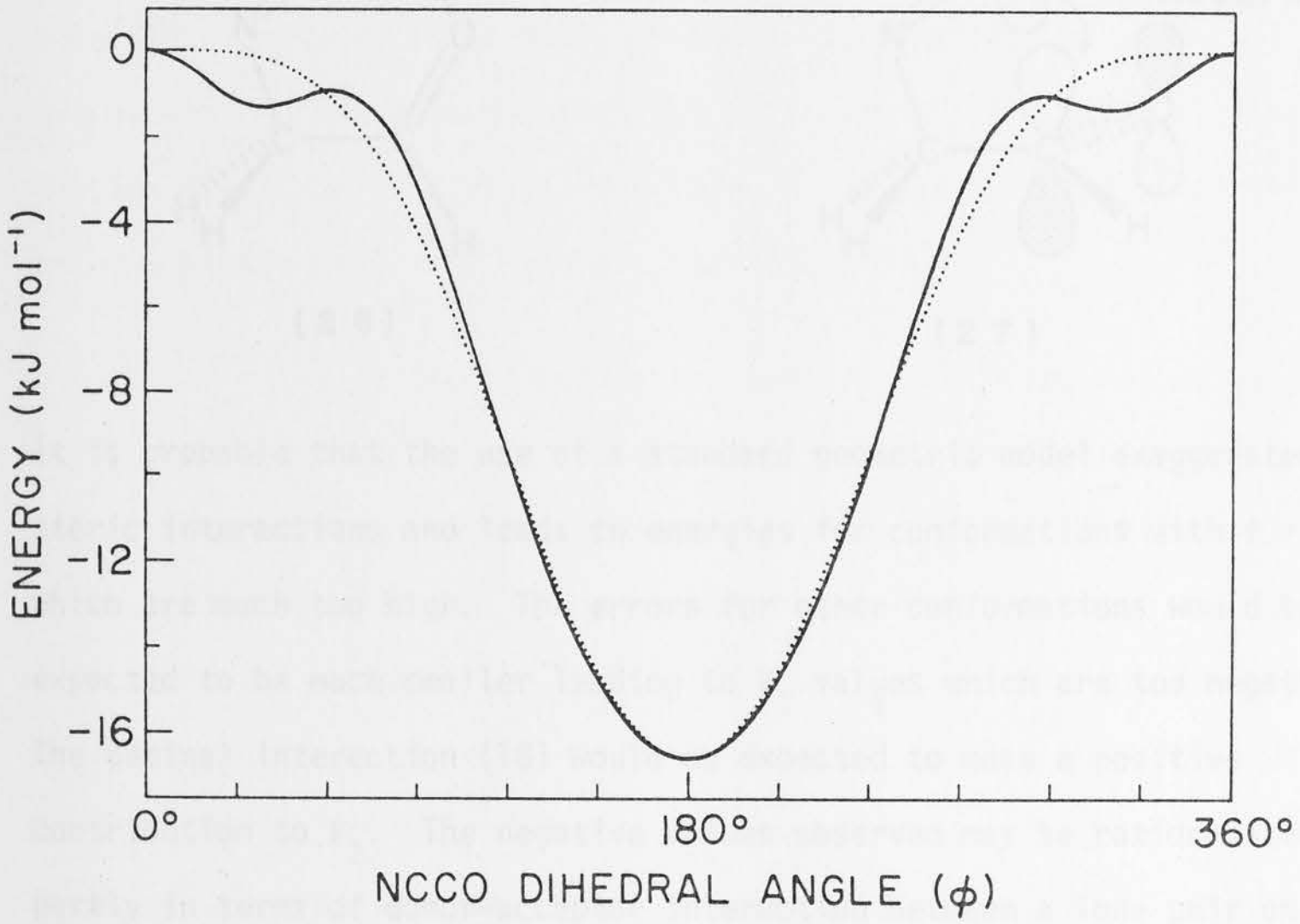

Fig. 3.7 Potential energy functions $V(\phi)$ (6-term expansion ——— ; 3-term expansion .....) describing internal rotation in $ONCH_2$-CHO (< ONCC = 180°).

The second class of substituents consists of NO-O, NO_2-O and CHO-O. Again, the dipolar interactions [(14) and (15)] contribute to a negative V_1 term, greatly enhanced by steric repulsion at $\phi = 0^\circ$ [e.g. (26)].

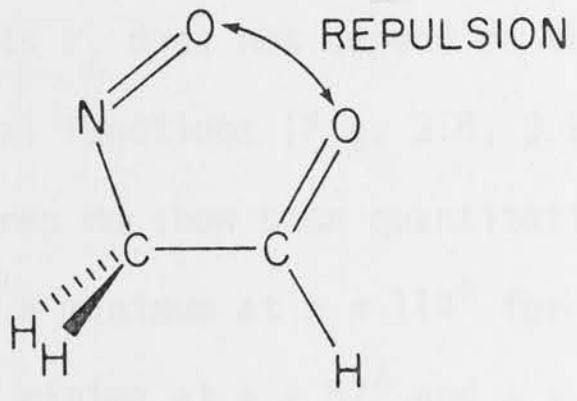

(26)

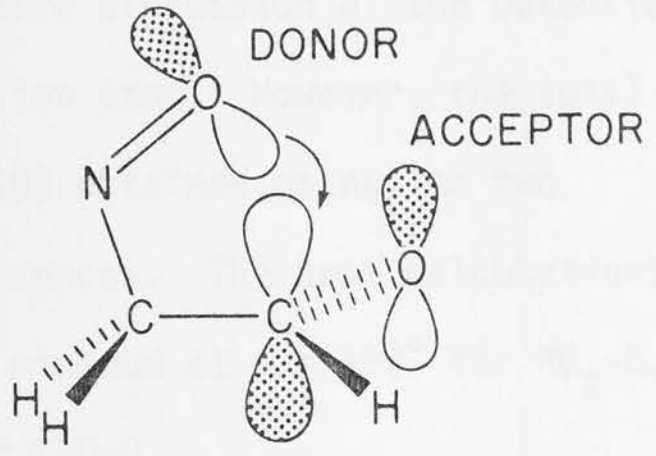

(27)

It is probable that the use of a standard geometric model exaggerates such steric interactions and leads to energies for conformations with $\phi = 0^\circ$ which are much too high. The errors for other conformations would be expected to be much smaller leading to V_1 values which are too negative. The geminal interaction (16) would be expected to make a positive contribution to V_2. The negative values observed may be rationalized partly in terms of donor-acceptor interaction between a lone pair on the oxygen atom of the substituent X and the antibonding π^* orbital of the C=O bond [e.g. (27)]. In addition, contributions to the negative V_2 and V_3 terms will arise through the extreme instability of the conformations with $\phi = 0^\circ$. This is apparent when the potential constants in the three-term Fourier expansion (equation 1.21) are expressed[98] as equations 3.3 and 3.4 where the terms staggered and eclipsed refer to the orientation of the CH_2X group with respect to the C=O bond.

$$V_2 = \tfrac{1}{2}\{\sum_{i=1}^{2} V[\phi_i(\text{orthogonal})] - \sum_{j=1}^{2} V[\phi_j(\text{coplanar})]\} \qquad 3.3$$

$$V_3 = \tfrac{1}{3}\{\sum_{i=1}^{3} V[\phi_i(\text{staggered})] - \sum_{j=1}^{3} V[\phi_j(\text{eclipsed})]\} \qquad 3.4$$

Both three-term and six-term Fourier expansions were obtained for these systems. The qualitative discussion of the potential constants V_i does not depend on the expansion used. However, the total potential functions (Fig. 3.8, 3.9 and 3.10) obtained using the two procedures do show some quantitative differences. The best calculations predict a minimum at $\phi = 114^\circ$ for NO-O, a minimum at $\phi = 180^\circ$ for NO_2-O, and two minima at $\phi = 87^\circ$ and $\phi = 150^\circ$ for CHO-O.

The potential constants for CHO-180 do not belong to either of the two previous classes and so the potential function for this substituent is treated separately. The V_1 term in the Fourier expansion is dominated by hydrogen bonding interaction which can occur when $\phi = 0^\circ$ [cf. (28)] but not when $\phi = 180^\circ$. This seems to be stronger than the dipole interaction, leading to a positive V_1. For $\phi = 90^\circ$ (29), there is a destabilizing hyperconjugative interaction [cf. (16)] while donor-acceptor interaction found in class two substituents [cf. (27)] cannot occur. V_2 is therefore positive. As with the previous class of substituents, V_3 is negative.

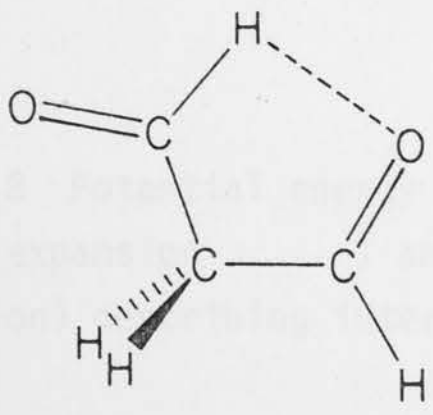

(28)

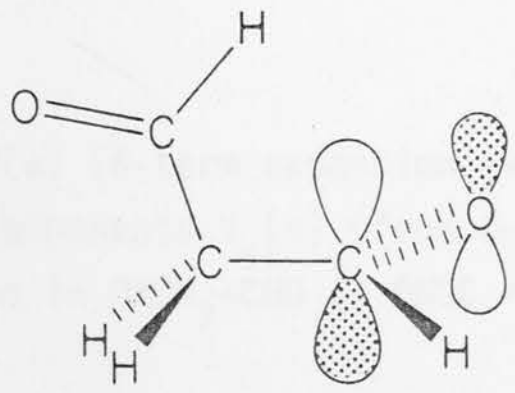

(29)

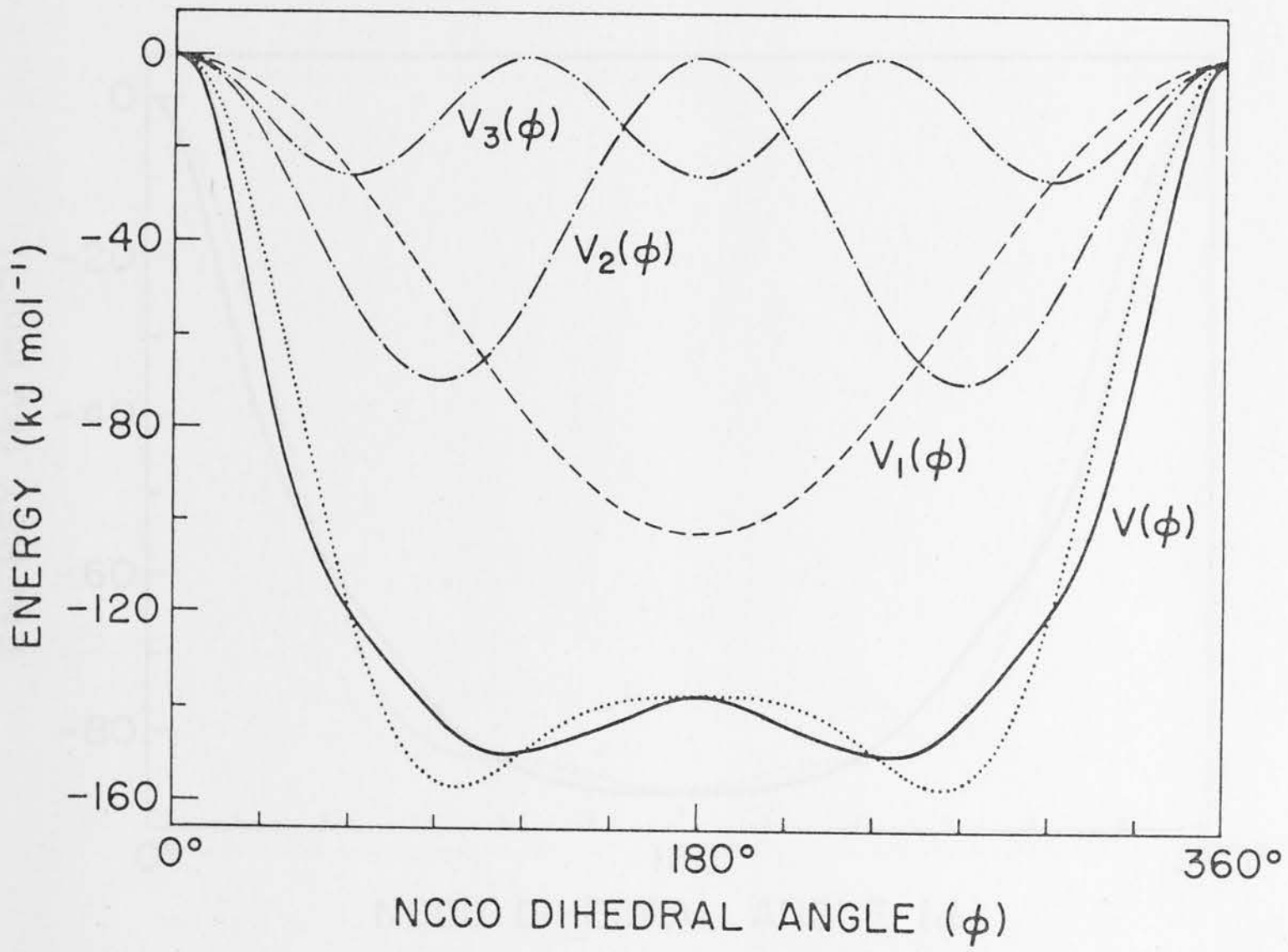

Fig. 3.8 Potential energy functions $V(\phi)$ (6-term expansion ——— ; 3-term expansion .....) and Fourier components $V_n(\phi)$ (from 6-term expansion) describing internal rotation in $ONCH_2$-CHO (< ONCC = 0°).

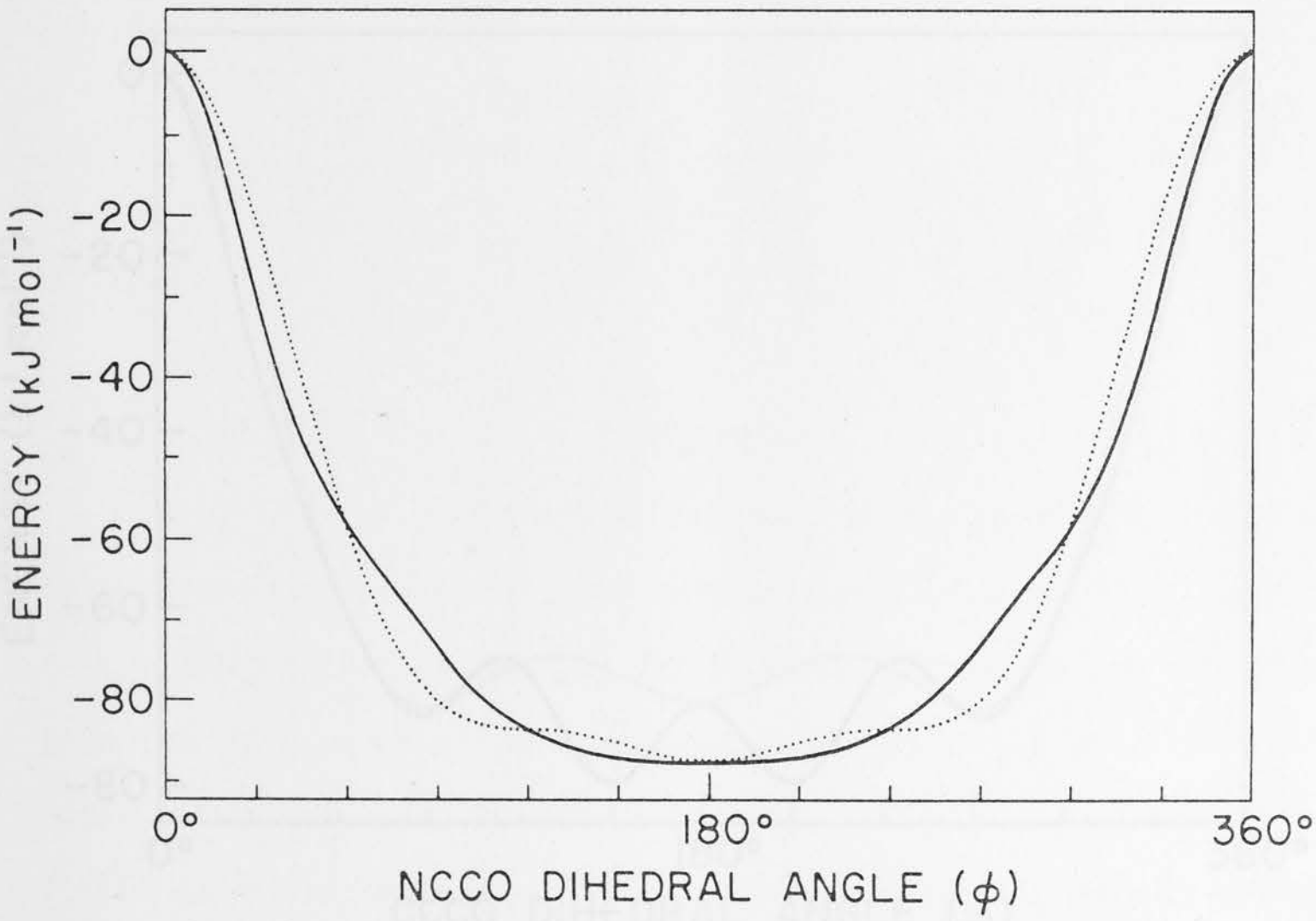

Fig. 3.9 Potential energy functions $V(\phi)$ (6-term expansion ——— ; 3-term expansion .....) describing internal rotation in $O_2NCH\text{-}CHO$ ($< ONCC = 0^0$).

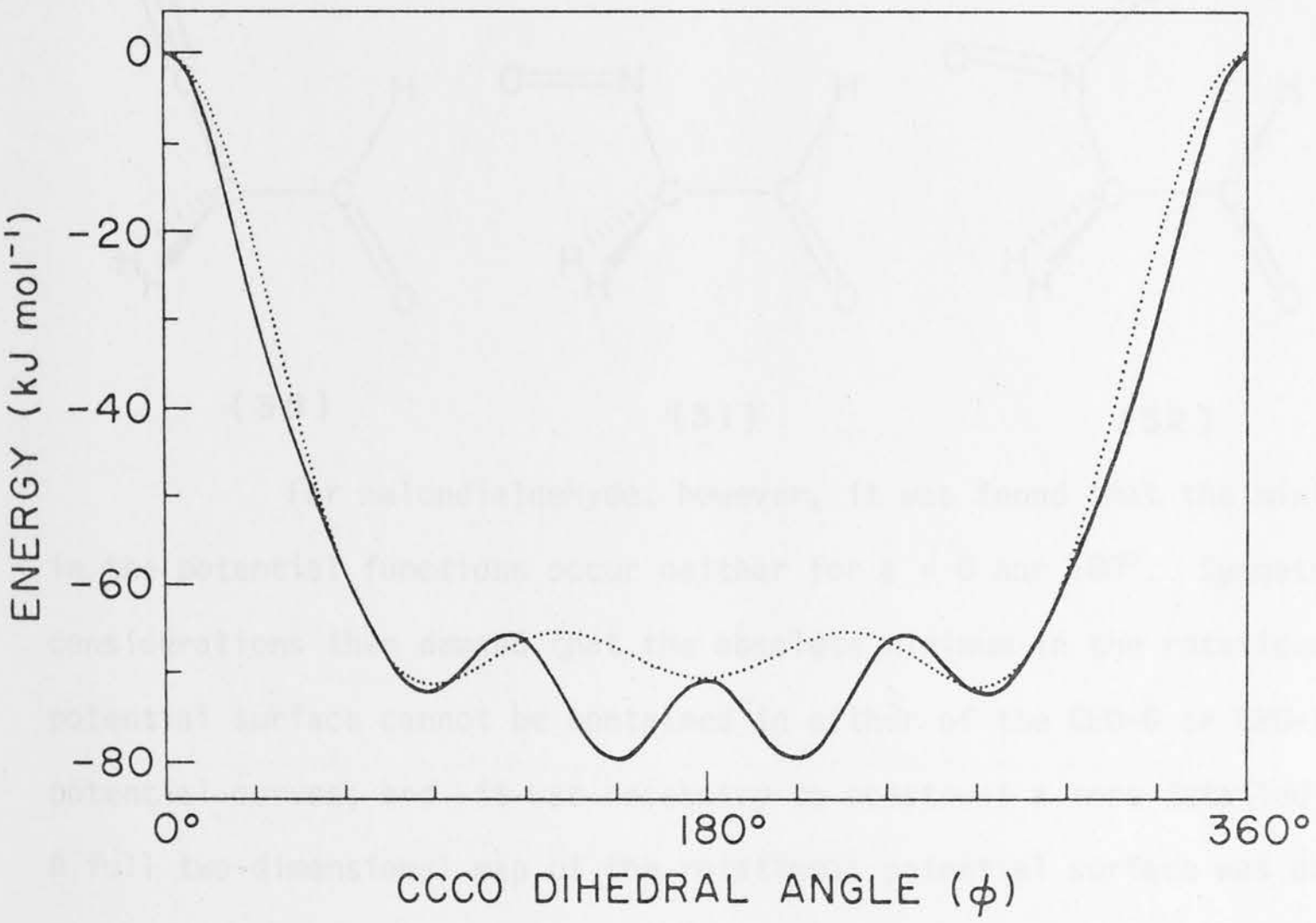

Fig. 3.10 Potential energy functions $V(\phi)$ (6-term expansion ——— ; 3-term expansion .....) describing internal rotation in $OHCCH_2$-CHO (< OCCC = 0°).

The resultant potential curves are shown in Figures 3.11 and 3.12. The six-term expansion exhibits a minimum at $\phi = 33^{\circ}$, with a secondary minimum at $\phi = 159^{\circ}$.

It is convenient at this stage to summarize the preferred conformations of the keto isomers. For cyanoacetaldehyde, nitrosoacetaldehyde and nitroacetaldehyde, these are shown respectively as (30)-(32).

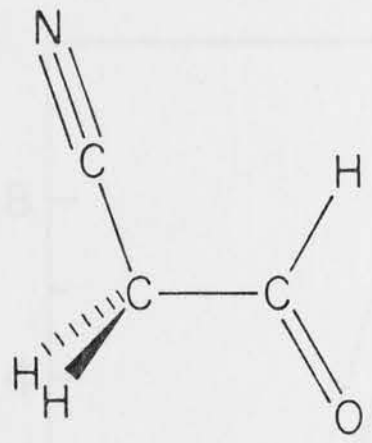

(30)

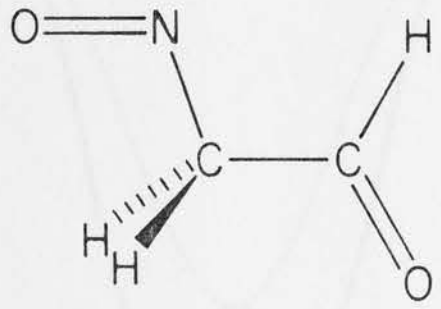

(31)

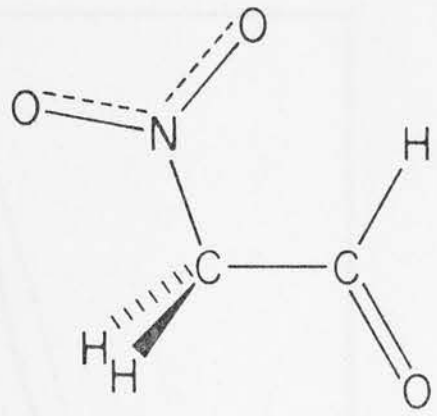

(32)

For malondialdehyde, however, it was found that the minima in the potential functions occur neither for $\phi = 0$ nor 180°. Symmetry considerations then demand that the absolute minimum in the rotational potential surface cannot be contained in either of the CHO-O or CHO-180 potential curves, and it was necessary to construct a more detailed surface. A full two-dimensional map of the rotational potential surface was obtained by performing calculations at a 30° (or, in some regions, finer) grid in the OCCC (ϕ_1) and CCCO (ϕ_2) dihedral angles as in (33). This resulted in the contour surface shown in Fig. 3.13.

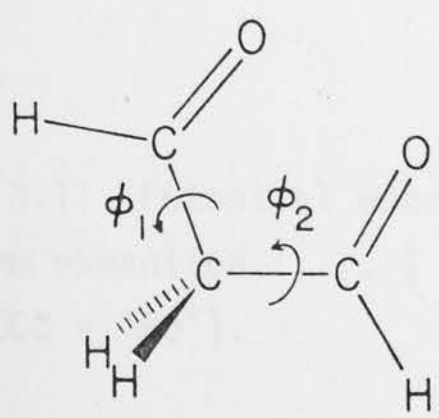

(33)

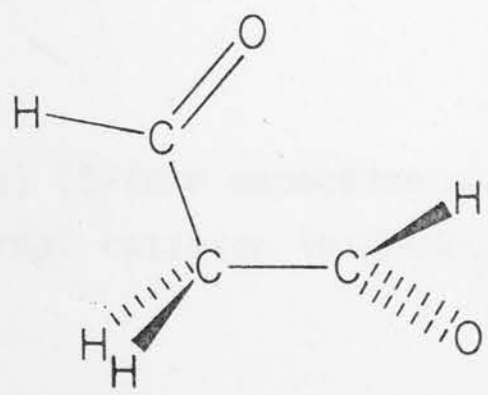

(34)

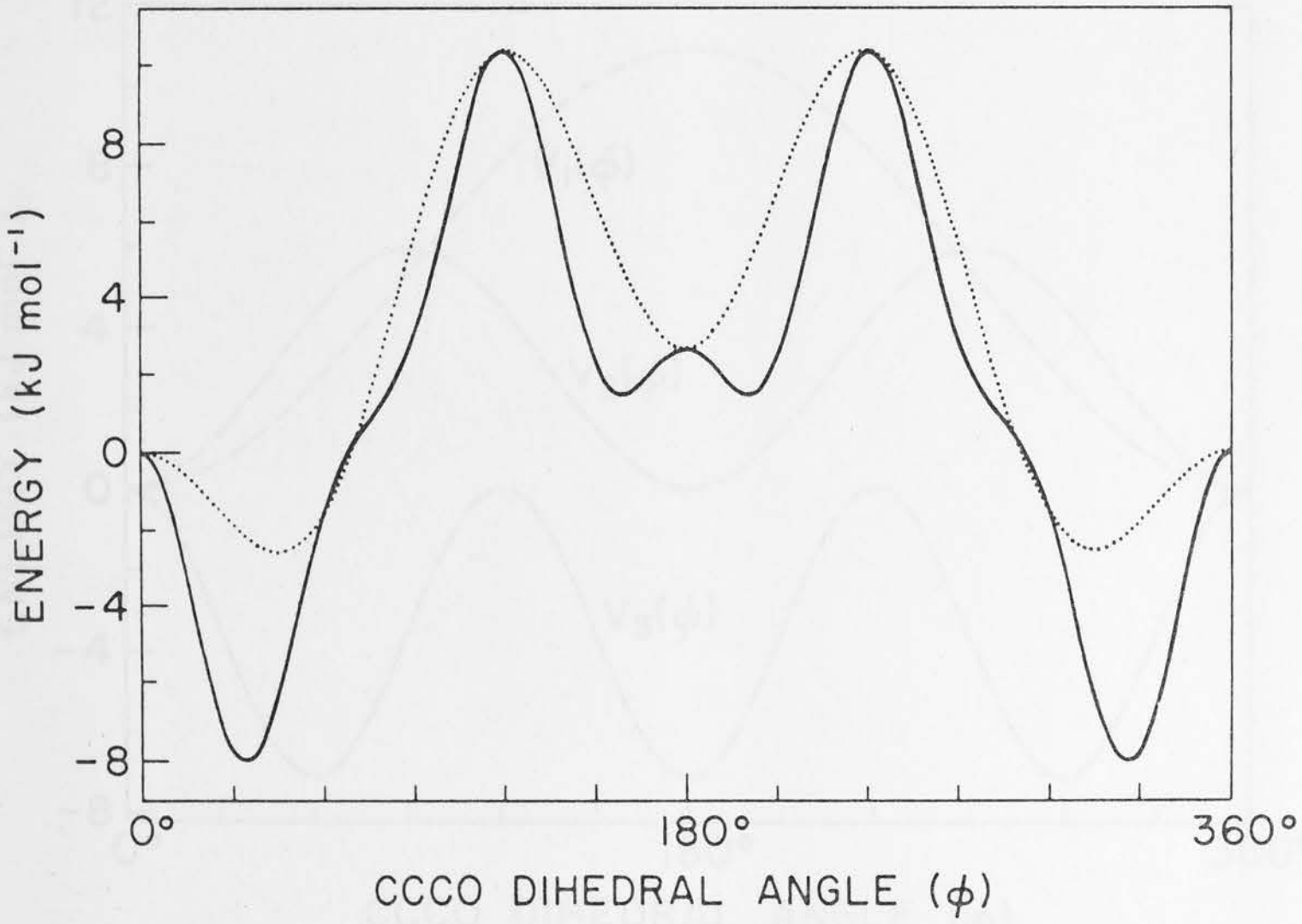

Fig. 3.11 Potential energy functions $V(\phi)$ (6-term expansion ——— ; 3-term expansion .....) describing internal rotation in $OHCCH_2$-CHO (< OCCC = 180°).

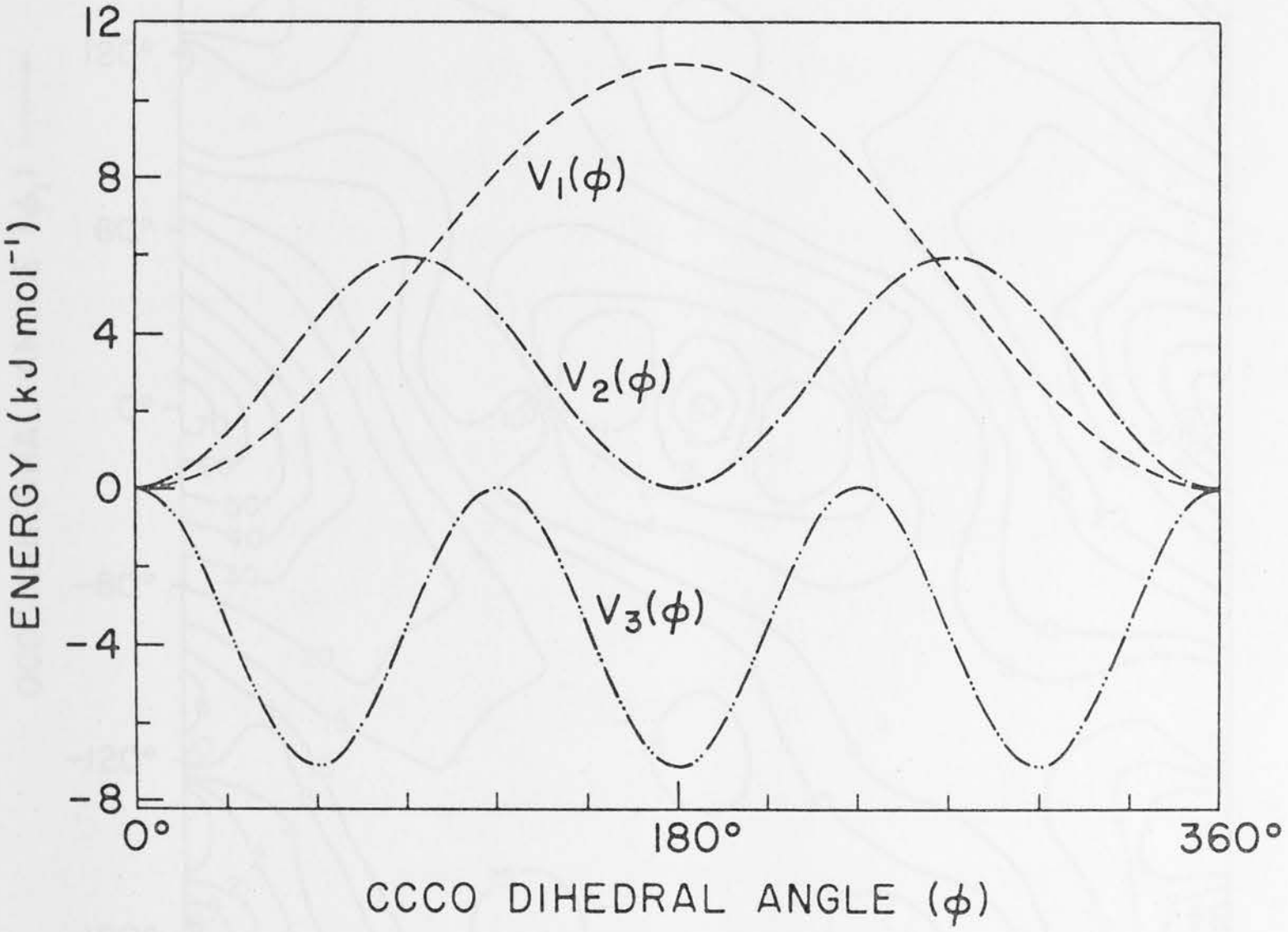

Fig. 3.12 Fourier components $V_n(\phi)$ (from 6-term expansion) of rotational potential function for $OHCCH_2$-CHO (< OCCC = 180°).

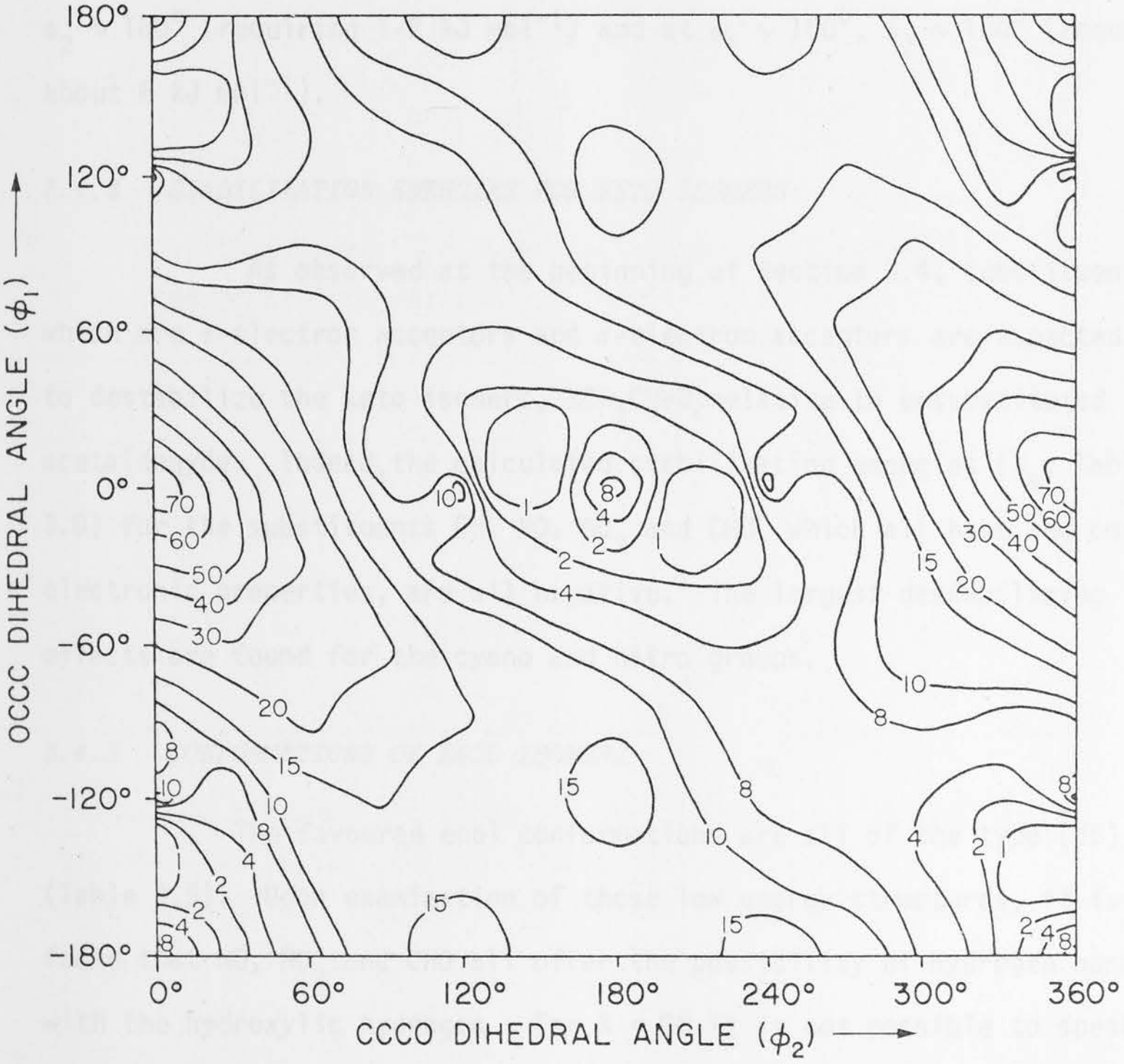

Fig. 3.13 Rotational potential surface $V(\phi_1,\phi_2)$ for OCH-CH_2-CHO. Contour energies in kJ mol^{-1}.

Optimization of ϕ_1 and ϕ_2 in the region around the absolute minimum in the surface yielded a lowest energy structure (34) with $\phi_1 = -1.9^{\circ}$ and $\phi_2 = 138.5^{\circ}$. Somewhat surprisingly, there appear to be no other significant minima in the potential surface. Equivalent structures of the type (34) can interconvert *via* saddle points at $\phi_1 \sim 30^{\circ}$, $\phi_2 \sim 180^{\circ}$ (requiring 1-2 kJ mol^{-1}) and at $\phi_1 \sim 100^{\circ}$, $\phi_2 \sim 100^{\circ}$ (requiring about 6 kJ mol^{-1}).

3.4.2 STABILIZATION ENERGIES FOR KETO ISOMERS

As observed at the beginning of Section 3.4, substituents which are π-electron acceptors and σ-electron acceptors are expected to destabilize the keto isomers, $XCH_2CH{=}O$, relative to unsubstituted acetaldehyde. Indeed, the calculated stabilization energies (E_S, Table 3.8) for the substituents CN, NO, NO_2 and CHO, which all have the correct electronic properties, are all negative. The largest destabilizing effects are found for the cyano and nitro groups.

3.4.3 CONFORMATIONS OF ENOL ISOMERS

The favoured enol conformations are all of the type (35) (Table 3.9). Upon examination of these low energy structures, it is found that NO, NO_2 and CHO all offer the possibility of hydrogen bonding with the hydroxylic hydrogen. For X = CN it is not possible to speak of a hydrogen bond in the conventional sense. However, examination of the Mulliken overlap populations shows a positive overlap of the hydroxylic hydrogen with the cyano group.

It is noted that for all the substituents examined here, conformations of the type (36) are of high energy because of unfavourable dipolar (and, in some cases, steric) interactions.

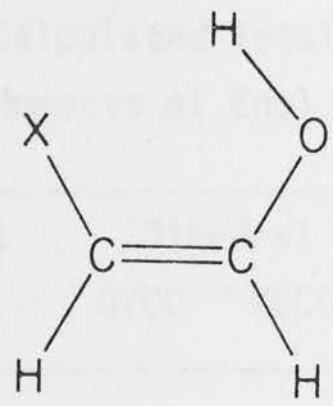

(35)

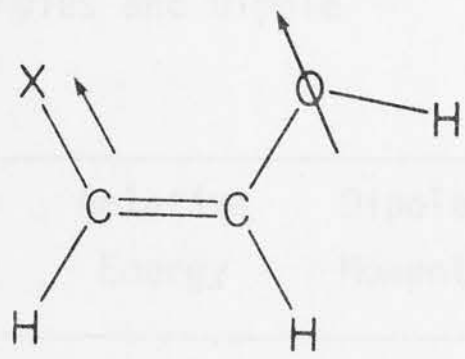

(36)

Table 3.8 Calculated Stabilization Energies[a] (E_s) for Preferred Conformations of Keto and Enol Isomers and Enol-Keto Energy Differences [ΔE = E (enol) - E (keto)].

Substituent X	E_s (keto)	E_s (enol)	ΔE
H	0	0	53.9
CN	-14.5	20.8	18.6
NO	-8.6	49.5	-4.2
NO_2	-17.1	32.5	4.4
CHO	-3.4	58.3	-7.7

[a] 4-31G//Std energies for reference structures: CH_3CHO -152.68475; CH_2CHOH -152.66422; CH_4 -40.13955; CH_3CN -131.72711; CH_3NO -168.56162; CH_3NO_2 -243.27040 from ref. 46 or this work (CH_3NO_2).

There have been a number of previous theoretical studies on the enol of malondialdehyde,[99-106] all of which were concerned with establishing whether in the hydrogen bonded structure the hydrogen occupies a symmetric position (C_{2v} symmetry) or an asymmetric position (C_s symmetry) with respect to the two oxygens. This problem is discussed in Chapter 4.

Table 3.9 Calculated Total Energies, Relative Energies and Dipole Moments of Enol Isomers XCH=CHOH.

Substituent X	Dihedral Angle OYCC	XCCO	CCOH	Total Energy	Relative Energy	Dipole Moment
CN		0	0	-244.25971	0	3.57
		180	180	-244.25934	1.0	4.87
		180	0	-244.25808	4.3	3.86
		0	180	-244.25728	6.4	6.81
NO	180[a]	0	0	-281.10513	0	
	180	180	180	-281.10205	8.1	
	180	180	0	-281.10153	9.5	
	180	0	180	-281.09626	23.3	
	0	180	180	-281.09319	31.3	
	0	180	0	-281.09227	33.8	
	0	0	0	-281.07768	72.1	
	0	0	180	-281.06815	97.1	
NO_2	0[a]	0	0	-355.80743	0	4.62
	0	180	180	-355.80648	2.5	6.13
	0	180	0	-355.80431	8.2	5.06
	0	0	180	-355.78803	50.9	8.05
CHO	0[b]	0	0	-265.23162	0	
	0	180	180	-265.22530	16.6	
	0	180	0	-265.22421	19.5	
	180	0	180	-265.22356	21.2	
	180	180	0	-265.22317	22.2	
	180	180	180	-265.22283	23.1	
	180	0	0	-265.21184	51.9	
	0	0	180	-265.20713	64.3	

[a] < ONCC

[b] < OCCC

The best calculations[101,103-105] all favour the asymmetric structure. Experimentally, malondialdehyde is known to occur as the enol, both in solution and in the gas-phase[107], while gas-phase studies show that the structure has C_s symmetry[108,109]. Therefore the C_{2v} structure has not been included in the present study.

3.3.3 STABILIZATION ENERGIES FOR ENOL ISOMERS

The four substituents examined in this section are all π-electron acceptors and, as such, are capable of extending the π-electron system of vinyl alcohol [cf. (25)]. It is therefore not surprising that the calculated stabilization energies (Table 3.8) are all positive. An additional contribution to the positive stabilization energy is provided, in the case of NO, NO_2 and CHO substituents, by hydrogen bonding interaction.

3.4.5 ENOL-KETO ENERGY DIFFERENCES

The net result of the destabilizing interaction of the substituent in the keto isomer and the stabilizing interaction in the enol isomer is shown by the enol-keto energy differences (ΔE, Table 3.8). It can be seen that all substituents lower the energy difference with respect to X = H (for which ΔE = 54 kJ mol^{-1}).

For X = CN, ΔE is reduced to 19 kJ mol^{-1} with the keto isomer still favoured. Cyanoacetaldehyde has been synthesised,[110,111] but its structure has never been investigated. Cyanoacetaldehyde and/or its enol is thought to have played a role in prebiotic chemistry.[112] Similarly, nitroacetaldehyde has been prepared,[113,114] and was assumed to have the keto structure, but the present calculations show that ΔE is very small. For the remaining two substituents, NO and CHO, the energy of the enol structure actually drops below that of the keto isomer, with ΔE values of

-4 and -8 kJ mol^{-1} respectively. Experimentally, the most stable structural isomer of the nitrosoacetaldehyde system is believed[115] to be the oxime, HON=CHCH=O. Observation of the enol will depend on the ease of rearrangement to the oxime. The rearrangement has been investigated and the results are reported in Chapter 5. Malondialdehyde, as stated before, has been characterized, both in solution and in the gas phase, to have the enol structure.[107-109]

3.5 A SIMPLE STABLE ENOL: THE DIAZONIUM SUBSTITUENT

In Sections 3.3 and 3.4, a number of substituents X were examined, and their effect on substituted acetaldehyde (5) and vinyl alcohol (6) was examined. Substituents X which are π-electron acceptors and σ-electron acceptors were found to be most suited to the purpose of creating a simple stable enol. A study of the properties of a number of diazonium ions[26,116] had shown that the diazonium substituent (N_2^+) is an extremely powerful σ-electron acceptor and π-electron acceptor. This being the case, it should be ideally suited for creating a simple enol which might be considerably more stable than its keto isomer. Previous calculations by Niemeyer[117] on $N_2^+CH{=}CHOH$ (37) and $N_2^+CH_2CH{=}O$ (38), carried out for a somewhat different purpose, are in agreement with this argument. However, Niemeyer's energy comparisons were carried out at the STO-3G level and, since the minimal STO-3G basis set is not always reliable for non-isodesmic comparisons,[45,50,72] it was felt desirable to carry out additional calculations at a higher level of theory with the split-valence 4-31G basis set. Preferred conformations of (37) and (38) were determined, as in Sections 3.3 and 3.4, by 4-31G//Std calculations on a number of conformations. However, in order to get a more accurate estimate of the energy difference (ΔE), the preferred conformers have been optimized and the 4-31G//STO-3G energies obtained.

3.5.1 *PREFERRED CONFORMATIONAL ISOMERS OF $N_2^+CH{=}CHOH$ AND $N_2^+CH_2CH{=}O$*

In order to identify the preferred conformers for the enol and keto isomers, preliminary 4-31G//Std calculations were carried out on a number of conformations. Since no appropriate standard values for the C3-$\overset{+}{N}$2 and C4-$\overset{+}{N}$2 bond lengths are available, these were assigned on the basis of optimization with the 4-31G basis set of the C-N lengths in (otherwise standard) ethylenediazonium and methanediazonium ions, yielding C3-$\overset{+}{N}$2 = 1.39Å and C4-$\overset{+}{N}$2 = 1.47Å. Previous work[116] had shown that the $\overset{+}{N}\equiv N$ bond in diazonium ions is close to the bond length in N_2 and therefore the standard length for N1-N1 was used for this bond. The energies thus obtained for conformations of (37) and (38) are listed in Table 3.10.

Table 3.10 Calculated Total Energies and Relative Energies of Standard Conformations of Enol Isomer $N_2^+CH{=}CHOH$ and Keto Isomer $N_2^+CH_2CH{=}O$.

$N_2^+CH{=}CHOH$				$N_2^+CH_2CH{=}O$		
Dihedral Angle NCCO	CCOH	Total Energy	Relative Energy	Dihedral Angle NCCO	Total Energy	Relative Energy
0	180	-260.51860	0	0	-260.50296	0
180	180	-260.51072	20.7	60	-260.49483	21.3
180	0	-260.50386	38.7	90.4	-260.49282	26.6
0	0	-260.49466	62.9	120	-260.49375	24.2
				180	-260.49483	21.3

For the enol isomer, the NCCO *cis*, CCOH *trans* structure is found to be the lowest in energy, in agreement with Niemeyer's results.[117] The

preference for this structure may in part be due to dipolar interactions. The theoretical charge distribution given by the Mulliken population analysis suggests that the local dipole moment of the $-\overset{+}{N}\equiv N$ group is directed towards the substituted nitrogen (39).

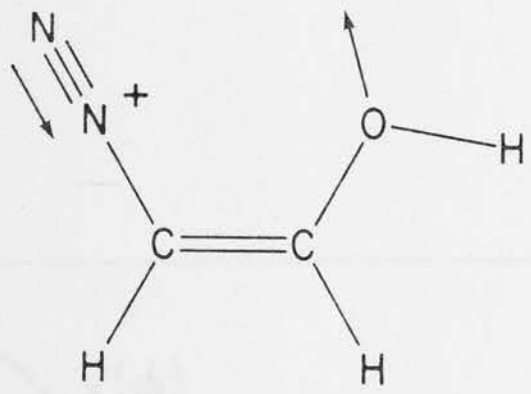

(39)

The calculated energies for the conformers of the keto isomer $N_2^+CH_2$-CHO with ϕ = 0, 60, 120 and 180° (ϕ = <NCCO) were fitted to the three-term Fourier expansion (equation 1.21) giving the total rotational potential (Fig. 3.14). The values of the rotational potential constants are: V_1 = 16.12, V_2 = 16.12, and V_3 = 5.22 kJ mol^{-1}, resulting in a total rotational potential with a minimum at ϕ = 0°, a maximum at ϕ = 90.4°, and a secondary minimum at ϕ = 180°. Clearly, the rotational barrier at 90.4° is the result of the V_2 term, which represents the hyperconjugative interaction between the N_2^+ substituent and the formyl part of the molecule [e.g. (16), X = N_2^+]. This is unfavourable relative to the interaction for X = H, and is largest when ϕ = 90°. The V_1 term is positive, and fairly large; it reflects the dipolar interactions. As for the enol isomer [e.g. (39)], the Mulliken charges show that the local dipole on the $-\overset{+}{N}\equiv N$ group is directed towards the substituted nitrogen (40). The positive V_3 term shows the tendency of the C=O bond to be eclipsed by the single bonds on the α-carbon, as found in other simply substituted acetaldehydes.

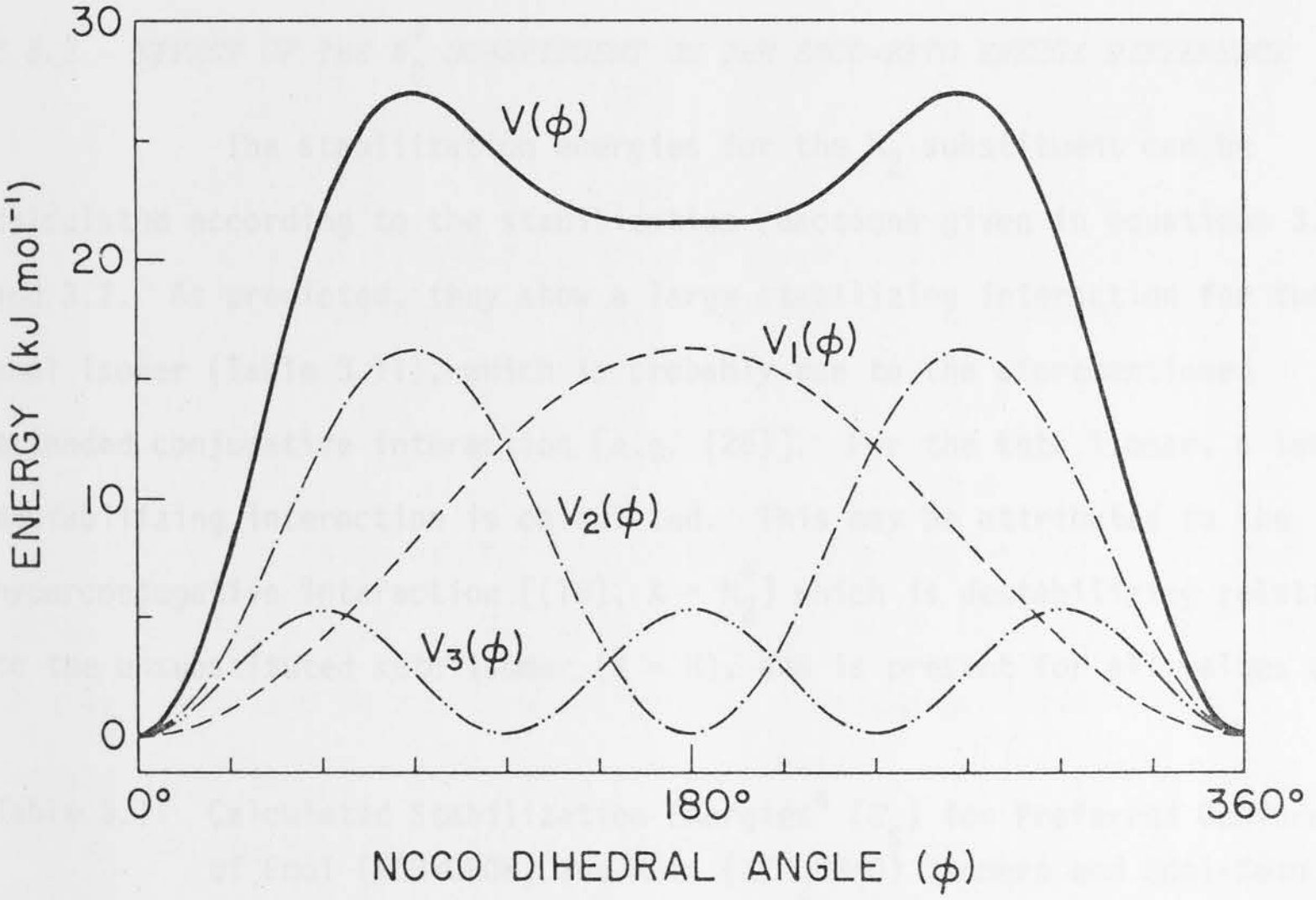

Fig. 3.14 Potential energy function $V(\phi)$ and Fourier components $V_n(\phi)$ describing internal rotation in $N_2^+CH_2$-CHO.

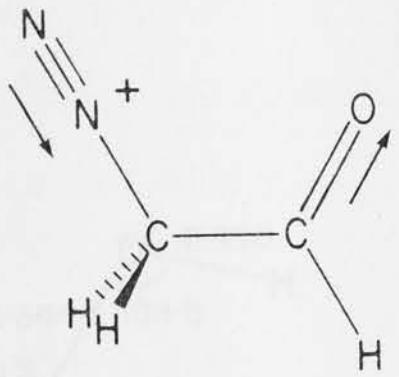

(40)

3.5.2 *EFFECT OF THE N_2^+ SUBSTITUENT ON THE ENOL-KETO ENERGY DIFFERENCE*

The stabilization energies for the N_2^+ substituent can be calculated according to the stabilization reactions given in equations 3.1 and 3.2. As predicted, they show a large stabilizing interaction for the enol isomer (Table 3.11), which is probably due to the aforementioned extended conjugative interaction [e.g. (25)]. For the keto isomer, a large destabilizing interaction is calculated. This may be attributed to the hyperconjugative interaction [(18), X = N_2^+] which is destabilizing relative to the unsubstituted keto isomer (X = H), and is present for all values of ϕ.

Table 3.11 Calculated Stabilization Energies[a] (E_s) for Preferred Conformations of Enol (XCH=CHOH) and Keto ($XCH_2CH=O$) Isomers and Enol-Keto Energy Differences [ΔE = E (enol) - E (keto)].

Substituent X	E_s (enol)	E_s (keto)	ΔE
H	0	0	53.9
NO[b]	49.5	-8.6	-4.2
CHO[b]	58.3	-3.4	-7.7
N_2^+	59.5	-35.4	-41.1

[a] The 4-31G//Std energies for reference structures: CH_3CHO -152.68475; CH_2CHOH -152.66422; CH_4 -40.13955; $CH_3N_2^+$ -147.97125 hartrees; from ref. 46 or this work ($CH_3N_2^+$).

[b] From Table 3.8, included for comparison.

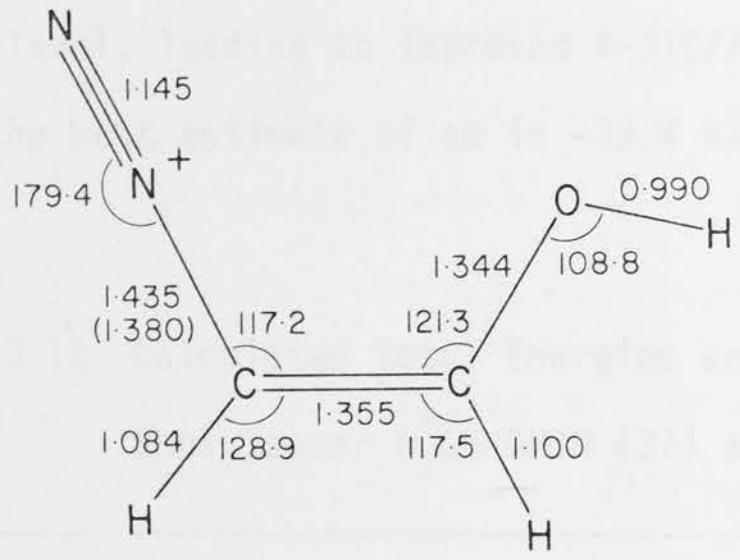

(37)

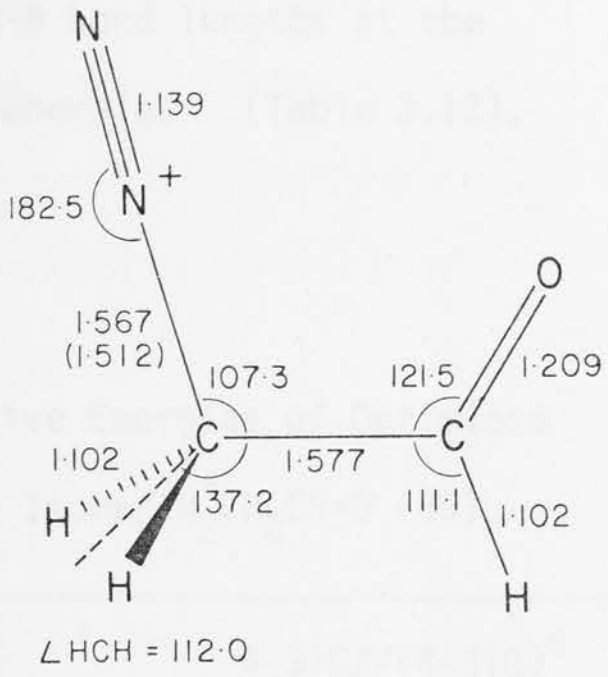

(38)

Fig. 3.15 STO-3G optimized geometries of $N_2^+CH{=}CHOH$ (37) and $N_2^+CH_2CH{=}O$ (38). The 4-31G - reoptimized C-N bond lengths are given in brackets.

The calculations with standard bond lengths and angles yield an energy difference (ΔE) of -41.1 kJ mol^{-1}, i.e. in favour of the enol isomer. In order to obtain an improved estimate of this energy difference the geometries of the best conformers of the enol- and keto-isomers were optimized with the STO-3G basis set(subject only to C_s symmetry constraints). Optimized geometries are displayed in Fig. 3.15. This approach gives ΔE at the STO-3G//STO-3G level as -8.2 kJ mol^{-1} (Table 3.12). This value differs considerably from a previous STO-3G estimate[117], based on CNDO/2 optimized structures, of $\sim$ -70 kJ mol^{-1}. For the optimized structures, the more reliable 4-31G//STO-3G energies were calculated, resulting in an energy difference of -36.4 kJ mol^{-1}. Finally, since it had been previously found[26,116] that STO-3G and 4-31G values of the C-$\overset{+}{N}$ lengths in diazonium ions differ substantially, the STO-3G optimized structures (37) and (38)

(Fig. 3.15) were refined by reoptimizing the C-N bond lengths at the 4-31G level, leading to improved 4-31G//STO-3G energies (Table 3.12). Thus the best estimate of ΔE is -39.4 kJ mol^{-1}.

Table 3.12 Calculated Total Energies and Relative Energies of Optimized Enol Isomer $N_2^+CH{=}CHOH$ (37) and Keto Isomer $N_2^+CH_2CH{=}O$ (38).

	STO-3G//STO-3G		4-31G//STO-3G		4-31G//(4-31G)[a]	
	Energy		Energy		Energy	
	Total	Rel.	Total	Rel.	Total	Rel.
(37)	-257.58532	-8.2	-260.50757	-36.4	-260.50916	-39.4
(38)	-257.58221	0	-260.49369	0	-260.49416	0

a Structures derived from 4-31G optimizations of the C-N lengths in the STO-3G optimized geometries.

3.6 CONCLUSIONS

In this chapter the effect of simple substituents on the enol-keto energy difference has been investigated. In the course of this study the conformational behaviour of α-substituted acetaldehydes (XCH_2CHO) has been analyzed. Three classes of rotational potential function have been distinguished for small substituents:

(i) When the substituent X is neither a strong σ-electron donor nor a strong σ-electron acceptor (X = H, CH_3), the rotational potential function is dominated by the threefold component, leading to minima for conformations where the C=O bond is eclipsed by one of the single bonds of the CH_2X group.

(ii) When the substituent X is a strong σ-electron donor (X = Li, BeH), geminal interactions favour a near perpendicular structure; domination of the rotational potential curve by the V_2 term results in a minimum for $\phi \sim 90^{\circ}$, and maxima at 0 and 180°.

(iii) When the substituent X is a strong σ-electron acceptor (X = F, CN), the reverse behaviour from class (ii) is found: the perpendicular structure is destabilized, and the stable conformations correspond to the *cis* and *trans* structures, with the latter being favoured.

From considerations based on the theory of geminal interactions, it was concluded that substituents X which are both σ-electron acceptors and π-electron acceptors are most effective in destabilizing the keto isomers. This was confirmed by explicit calculations in that examination of four such substituents (CN, NO_2, NO and CHO) showed a substantial reduction of the enol-keto energy difference (ΔE). The calculated stabilization energies (E_s) for substituents X in enol and keto isomers (6) and (5) showed clearly that these substituents, while stabilizing the enol isomer, destabilized the keto isomer. For the nitroso (NO) and formyl (CHO) substituents, the enol isomer is predicted to be slightly lower in energy than the keto form.

Finally, the diazonium substituent (N_2^+) has been examined. This substituent was known previously to be a powerful σ-electron acceptor and π-electron acceptor. Indeed, it is found that this substituent substantially stabilizes the enol isomer ($N_2^+CH{=}CHOH$) and destabilizes the keto isomer ($N_2^+CH_2CH{=}O$). As a consequence, the enol actually lies lower (by $\sim$ 39 kJ mol^{-1}) than the keto isomer, reversing the tautomeric preference in the parent system.

PART II

THEORETICAL STUDIES OF INTRAMOLECULAR REARRANGEMENTS

CHAPTER 4

1,3-AND 1,5-SIGMATROPIC HYDROGEN SHIFTS

4.1 INTRODUCTION

Since the advent of orbital symmetry rules, sigmatropic rearrangements have attracted considerable theoretical interest. Sigmatropic rearrangements are those reactions in which a σ-bond (in other words a substituent) moves across a conjugated system to a new site. Many different approaches to the problem have been presented, using a variety of methods based on orbital symmetry considerations[118-123]. In this chapter, a study of sigmatropic hydrogen rearrangements will be presented. There have been a number of quantitative studies of such rearrangements at both the semi-empirical[99,100,124-128] and *ab initio*[101-105,128-131] levels of theory. Most of these, however, have been restricted to studies where the transition states have been assumed to be symmetric. In this study, the *symmetric* 1,3-sigmatropic hydrogen shifts in propene and formic acid, the *symmetric* 1,5-sigmatropic hydrogen shifts in 1,3-pentadiene and β-hydroxyacrolein, as well as the corresponding *asymmetric* 1,3-shifts for the vinyl alcohol/acetaldehyde and the nitrosomethane/formaldoxime rearrangements have been examined. For the latter system an alternative rearrangement pathway has been examined as well, in which the nitrosomethane/formaldoxime isomerization involves two successive 1,2-hydrogen shifts, and is found to proceed *via* formaldonitrone as an intermediate.

4.2 METHOD

For all stable structures studied here, optimized geometries at the STO-3G basis set level have been obtained, while for the smaller systems (C_3H_6, CH_2O_2, C_2H_4O and CH_3NO) optimized geometries were also obtained at the 4-31G level. The optimized structures for vinyl alcohol and acetaldehyde have been reported in Chapter 2. Two different methods were used for locating

transition states, depending on whether or not they were expected to be symmetric with respect to the reaction coordinate. In the symmetric cases (e.g. the suprafacial and antarafacial 1,3-shifts in propene), transition states were determined by optimization of all geometric parameters subject to an appropriate symmetry constraint (C_s and C_2 respectively, in the propene example). In asymmetric cases (e.g. vinyl alcohol → acetaldehyde), the transition state was obtained by minimization of the gradient norm, using the transition state program (Section 1.3.2). In both situations it was verified that the matrix of second derivatives of the energy had one negative eigenvalue, i.e. that the derived structures were saddle points in the multidimensional energy surface. Single energy calculations with the 4-31G basis set (4-31G//STO-3G) were performed on all optimized structures. As had been done for the stable molecules, the transition states of the smaller systems (C_3H_6, CH_2O_2, C_2H_4O and CH_3NO) were optimized at the 4-31G level, affording 4-31G//4-31G energies.

It should be noted that single-determinant calculations are likely to be less satisfactory in describing "symmetry forbidden" than "symmetry allowed" reactions. As an initial step in remedying this situation, 3x3 configuration interaction (CI) calculations have been carried out, using the 4-31G basis set, on the structures optimized at the STO-3G level. Such an approach has been previously recommended[41,42] for problems of this type (Section 1.3.5).

When the optimized geometries are being discussed, the STO-3G data followed by the 4-31G data in brackets will be quoted; when relative energies are being discussed, the 3x3 CI/4-31G//STO-3G energies (in Sections 4.3 and 4.4) or the 4-31G//4-31G energies (in Section 4.5) will be quoted.

4.3 1,3-SIGMATROPIC HYDROGEN SHIFTS

For the 1,3-sigmatropic shifts studied here, the "model compound" is propene, where the 1,3-hydrogen shift is degenerate. When applying orbital symmetry considerations[118-123], it is found that a 1,3-sigmatropic shift is symmetry allowed if antarafacial (the moving hydrogen crosses the plane of heavy atoms, cf. (41)) and symmetry forbidden if suprafacial (the moving hydrogen stays on one side of the plane of heavy atoms). Although these labels should only be applied to symmetric (degenerate) rearrangements, these terms will also be used for similar transition states in non-symmetric cases (e.g. the vinyl alcohol/acetaldehyde rearrangement).

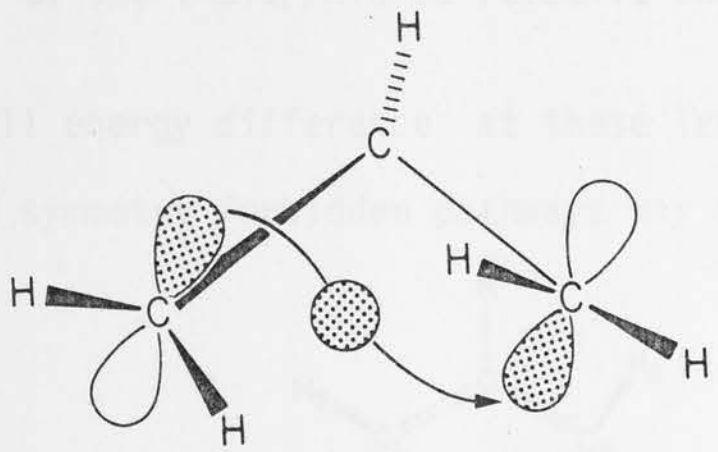

(41)

4.3.1 PROPENE → PROPENE

Two transition states are found for a 1,3-sigmatropic hydrogen shift [(42) → (42')] in propene, namely a structure with C_2 symmetry (43a) corresponding to a symmetry allowed (41) antarafacial process, and a structure with C_s symmetry (43b) corresponding to a symmetry forbidden suprafacial process. The moving hydrogen (H_1) in (43a) is bonded simultaneously to the terminal carbon atoms (C_1 and C_2), leading to a narrow CCC angle of 101.2 (108.9)°. On the other hand, in (43b) H_1 is bonded to the central carbon (C) with a bond length of 1.139 (1.245) Å and the CCC angle is considerably

wider at 127.4 (127.2)°. The C-C lengths in both (42a) [1.414 (1.401)Å] and (42b) [1.443 (1.406)Å] lie between the values for normal single and double bonds (Table 4.1). Whereas the optimized structures of the allowed transition state (43a) are much the same at the STO-3G and 4-31G levels, some differences are noted for the forbidden transition state (43b). At the STO-3G level, the moving hydrogen (H_1) is in a position above the central carbon atom (C), while the 4-31G basis set brings H_1 more forward (i.e. < H_1CX = 121.1°). The hydrogen atoms H_2 and H_4 are calculated to be on the same side of the CCC plane as H_1 at the STO-3G level, and are found to be on the opposite side to H_1 at the 4-31G level. However, the 4-31G//4-31G relative energies for the barriers are similar to the 4-31G//STO-3G relative energies.

The small energy difference at these levels between the symmetry allowed and symmetry forbidden pathways may seem surprising at first

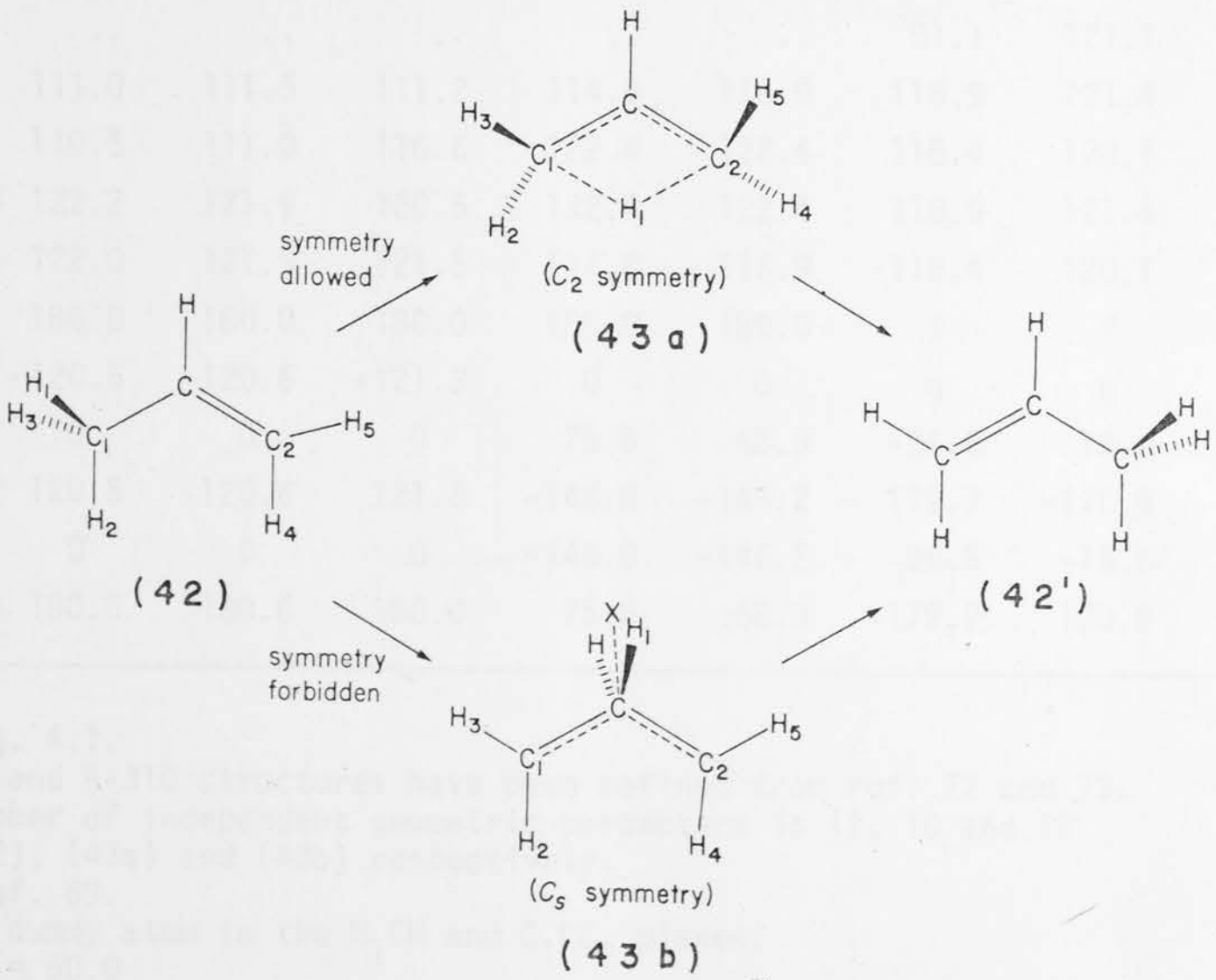

Fig. 4.1 Schematic diagram showing the 1,3-hydrogen shift in propene (42); for the optimized parameters see Table 4.1.

Table 4.1 Optimized Geometric Parameters[a] for Propene[b] (42) and Transition State Geometries (43a), (43b), for the 1,3-Hydrogen Shift[c]. Also Listed are the Experimental Parameters for Propene.

Parameter	(42), C_s			(43a), C_2		(43b), C_s	
	STO-3G	4-31G	Expt.[d]	STO-3G	4-31G	STO-3G	4-31G
$C\text{-}C_1$	1.521	1.501	1.501	1.414	1.401	1.443	1.406
$C\text{-}C_2$	1.308	1.318	1.336	1.414	1.401	1.443	1.406
C-H	1.085	1.076	1.090	1.086	1.076	1.087	1.074
$C_1\text{-}H_1$	1.088	1.085	1.098	1.394	1.532	1.831	1.643
$C\text{-}H_1$	..	..	..	1.763	1.839	1.139	1.245
$C_1\text{-}H_2$	1.086	1.082	1.085	1.085	1.076	1.078	1.071
$C_1\text{-}H_3$	1.088	1.085	1.098	1.090	1.079	1.078	1.067
$C_2\text{-}H_4$	1.081	1.074	1.091	1.090	1.079	1.078	1.071
$C_2\text{-}H_5$	1.081	1.072	1.081	1.085	1.076	1.078	1.067
$\angle C_1CC_2$	124.9	125.2	124.3	101.2	108.9	127.4	127.4
$\angle HCC_2$	119.9	119.2	119.0	129.4	125.55	..	..
$\angle H_1C_1C$	110.5	111.0	110.6	77.8	77.5	..	..
$\angle HCX$[e]	..	..	..	..	..	18.0	-9.4
$\angle H_1CX$	..	..	..	..	..	91.1	121.1
$\angle H_2C_1C$	111.0	111.5	111.2	114.8	116.9	118.9	121.4
$\angle H_3C_1C$	110.5	111.0	110.6	122.4	122.4	118.4	120.1
$\angle H_4C_2C$	122.2	121.9	120.5	122.4	122.4	118.9	121.4
$\angle H_5C_2C$	122.0	121.9	121.5	114.8	116.9	118.4	120.1
$\angle HCC_2C_1$	180.0	180.0	180.0	180.0	180.0	f	f
$\angle H_1C_1CC_2$	-120.5	-120.6	-121.3	0	0	g	g
$\angle H_2C_1CC_2$	0	0	0	75.6	68.3	-26.8	15.6
$\angle H_3C_1CC_2$	120.5	120.6	121.3	-146.0	-146.2	179.7	-170.9
$\angle H_4C_2CC_1$	0	0	0	-146.0	-146.2	26.8	-15.6
$\angle H_5C_2CC_1$	180.0	180.0	180.0	75.6	68.3	-179.7	170.9

[a] See Fig. 4.1.
[b] STO-3G and 4-31G structures have been refined from ref. 72 and 73.
[c] The number of independent geometric parameters is 12, 10 and 12 for (42), (43a) and (43b) respectively.
[d] From ref. 69.
[e] X is a dummy atom in the H_1CH and C_1CC_2 planes.
[f] $\angle HCXC_2 = 90.0$
[g] $\angle H_1CXC_2 = -90.0$

glance, particularly when it is realized that the latter is likely to benefit to a greater extent from a more sophisticated treatment. When 3x3 CI is included, the forbidden transition state (43b) is slightly lower in energy than the allowed structure (43a), the barrier being 390 kJ mol^{-1} (Table 4.4). This qualitative result was foreshadowed several years ago by Berson and Salem[122,132], who postulated that symmetry forbidden transition states for sigmatropic rearrangements are stabilized through subjacent and superjacent orbital interactions. If the transition states in the propene rearrangement are considered as interacting allyl and hydrogen fragments as shown in Fig. 4.2, the primary interaction is A, which can occur in C_2 distorted structures [e.g. (43a)] but not in C_s structures [e.g. (43b)]. On the other hand, interactions B and C with subjacent and superjacent levels can stabilize (43b). Although these interactions are likely to be somewhat weaker than A, the unfavourable steric interactions in (43a) make (43b) energetically competitive.

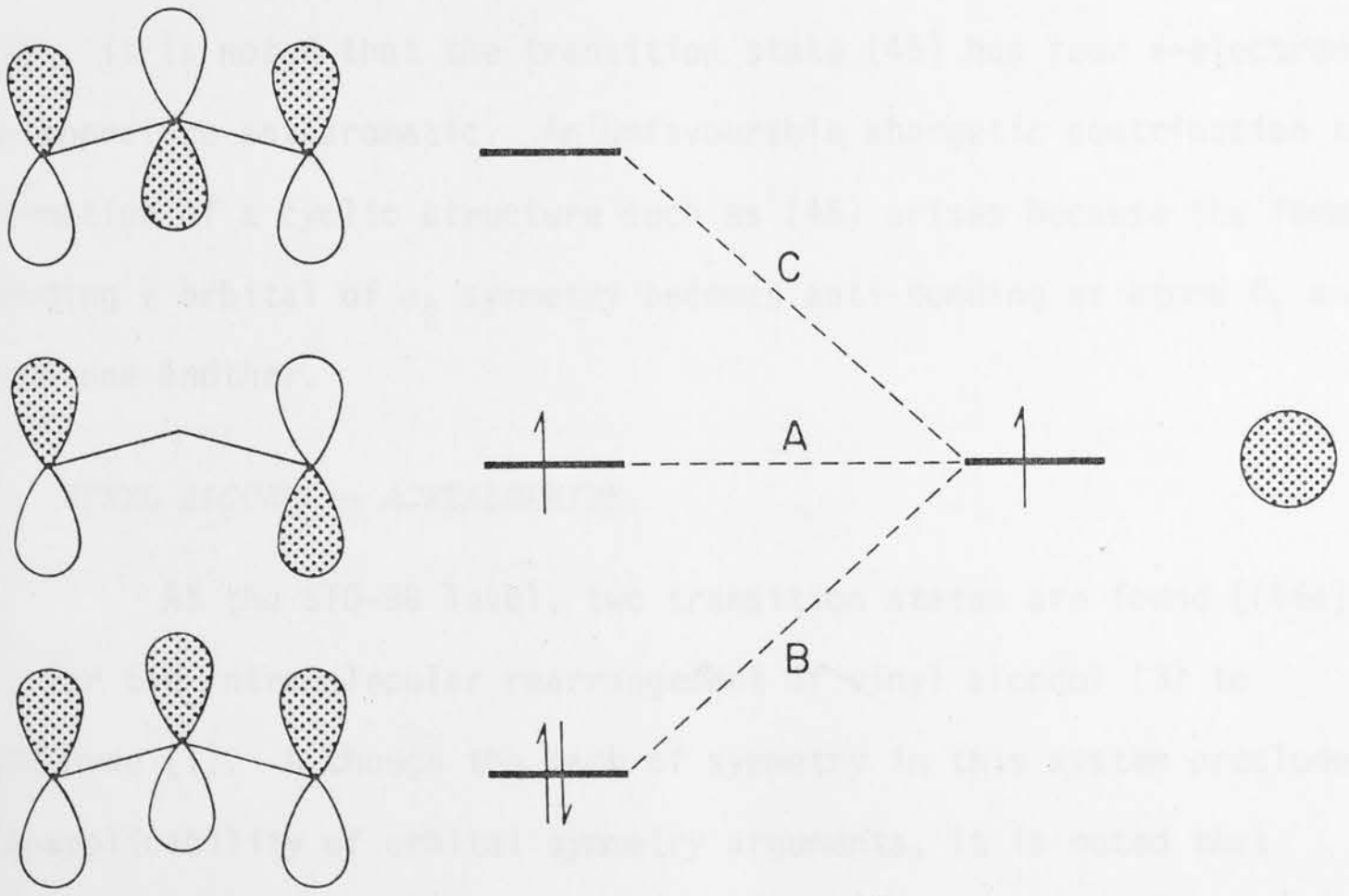

Fig. 4.2 Interaction diagram for orbitals of allyl radical and hydrogen, showing primary (A), subjacent (B) and superjacent (C) interactions.

4.3.2 FORMIC ACID → FORMIC ACID

Only a single transition state (45) is found for the rearrangement (44) → (44') in formic acid. Again, the moving hydrogen is simultaneously bonded to the terminal atoms O_1 and O_2, leading to a small OCO angle [102.6 (108.5)°]. The barrier for the rearrangement is quite high at 263 kJ mol^{-1}. Previous *ab initio* calculations[129,130] with partial geometry optimization yielded barriers of 550 and 310 kJ mol^{-1}. The high barrier for the 1,3-shift can be rationalized in terms of interaction diagrams similar to Fig. 4.1 between the formate fragment and a hydrogen atom. Both the highest occupied π-orbital and the highest occupied σ-orbital (corresponding to a combination of the in-plane lone pairs) of formate are antisymmetric with respect to the symmetry plane perpendicular to the molecule (i.e. have a_2 and b_2 symmetries, respectively) and cannot interact with a hydrogen 1s orbital in a planar C_{2v} structure. Stabilization of the transition state can therefore only occur through subjacent and superjacent interactions. In addition, it is noted that the transition state (45) has four π-electrons and is therefore antiaromatic. An unfavourable energetic contribution to the formation of a cyclic structure such as (45) arises because the formally non-bonding π orbital of a_2 symmetry becomes anti-bonding as atoms O_1 and O_2 approach one another.

4.3.3 VINYL ALCOHOL → ACETALDEHYDE

At the STO-3G level, two transition states are found [(46a) and (46b)] for the intramolecular rearrangement of vinyl alcohol (3) to acetaldehyde (1). Although the lack of symmetry in this system precludes the strict applicability of orbital symmetry arguments, it is noted that transition state (46a) resembles the symmetry allowed transition state (43a) in propene while (46b) resembles the symmetry forbidden transition state (43b).

Table 4.2 Optimized Geometric Parameters for Formic Acid (44) and the Transition State (45) for the 1,3-Hydrogen Shift.[a] Also Listed are the Experimental Parameters for Formic Acid.

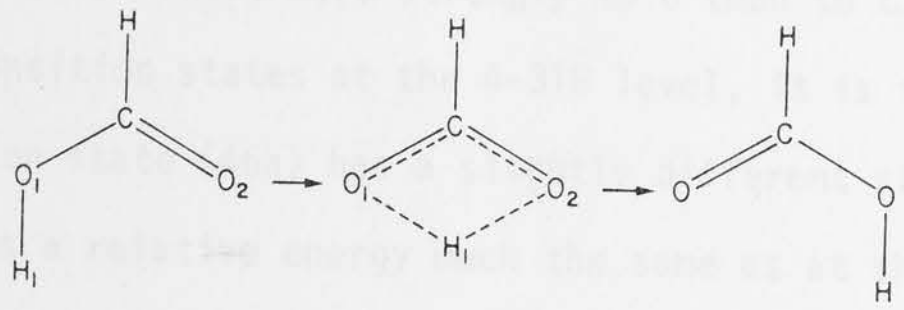

(44) (45) (44')

Parameter	(44), C_s			(45), C_{2v}	
	STO-3G[b]	4-31G	Expt.[c]	STO-3G	4-31G
$C-O_1$	1.385	1.342	1.343	1.297	1.269
$C-O_2$	1.214	1.200	1.202	1.297	1.269
$C-H$	1.104	1.072	1.097	1.095	1.065
O_1-H_1	0.991	0.956	0.972	1.239	1.335
$C-H_1$	..	..	..	1.526	1.590
$<O_1CO_2$	123.9	124.6	124.9	102.6	108.5
$<HCO_2$	125.9	125.0	124.1	128.7	125.75
$<H_1O_1C$	104.8	114.9	106.3	74.0	75.2

[a] The number of independent geometric parameters is 7 and 4 for (44) and (45) respectively.

[b] From ref. 67.

[c] From ref. 133.

The structure of (46a) resembles that of the higher energy isomer, vinyl alcohol, more than that of the lower energy isomer, acetaldehyde, consistent with the expectations of the Hammond postulate.[134] For example, the moving hydrogen H_1 in (46a) is bonded more strongly to O than to C_1. When optimizing the transition states at the 4-31G level, it is found that the "allowed" transition state (46a) has a slightly different structure (see Table 4.3), but has a relative energy much the same as at the 4-31G//STO-3G level. For the "forbidden" transition state (46b), it was difficult to calculate the exact structure, since the gradient norm did not reach the minimum value required. However, the gradient norm for the reported structure was close to zero (0.51×10^{-4} compared with the normal convergence limit of 0.5×10^{-4}), and the matrix of the second derivatives of the energy had one negative eigenvalue. A continuation of the search for this transition state led to the "allowed" transition state. This seems to indicate that at the 4-31G level there is only a very small barrier, or a nearly flat potential energy surface, separating the forbidden transition state from the allowed one. There are some differences in the structure of (46b) calculated at the two levels. The most striking feature is the position of the moving hydrogen (H_1), which has shifted forward with 4-31G (i.e. $< H_1C_1O = 62.2^{\circ}$). As was the case for propene, the calculated barriers (3x3CI/4-31G//STO-3G) for the two rearrangement pathways *via* (46a) and (46b) are very similar (within 4 kJ mol^{-1}). Thus the activation energy for the vinyl alcohol/acetaldehyde isomerization is about 394 kJ mol^{-1}. This activation energy is sufficiently large for vinyl alcohol to be stable with respect to intramolecular rearrangement. Indeed, after this study was completed, the microwave spectrum of vinyl alcohol was reported[64], which established vinyl alcohol as an observable isomer of acetaldehyde in the gas phase.

Table 4.3 Optimized Geometric Parameters[a] for the Transition States (46a, 46b) for the 1,3-Hydrogen Shift in the Vinyl Alcohol/Acetaldehyde System.[b,c]

Parameter	(46a), C_1		(46b), C_1	
	STO-3G	4-31G	STO-3G	4-31G[d]
$C\text{-}C_1$	1.448	1.411	1.413	1.367
C-O	1.293	1.281	1.378	1.362
C-H	1.097	1.071	1.098	1.080
$O\text{-}H_1$	1.163	1.277	1.662	1.511
$C\text{-}H_1$	1.616	1.665	1.164	1.208
$C_1\text{-}H_1$	1.475	1.546	1.743	1.709
$C_1\text{-}H_2$	1.087	1.083	1.080	1.071
$C_1\text{-}H_3$	1.082	1.072	1.080	1.072
$<OCC_1$	102.6	108.5	124.6	124.3
$<HCC_1$	136.5	131.6	115.3	116.5
$<H_1C_1C$	67.1	68.4	41.7	44.6
$<H_2C_1C$	108.1	112.6	119.8	119.3
$<H_3C_1C$	118.8	121.7	121.5	120.9
$<HCC_1O$	183.1	182.9	188.5	181.7
$<H_1C_1CO$	3.3	7.5	75.3	62.2
$<H_2C_1CO$	-81.8	-70.3	10.4	-1.2
$<H_3C_1CO$	151.7	150.4	183.8	-184.1

[a] See Fig. 4.3.

[b] The number of independent geometric parameters is 15 for both (46a) and (46b).

[c] See Tables 2.1 and 2.2 for the structures of (1) and (3).

[d] Optimization not fully completed; gradient norm 0.5×10^{-4}.

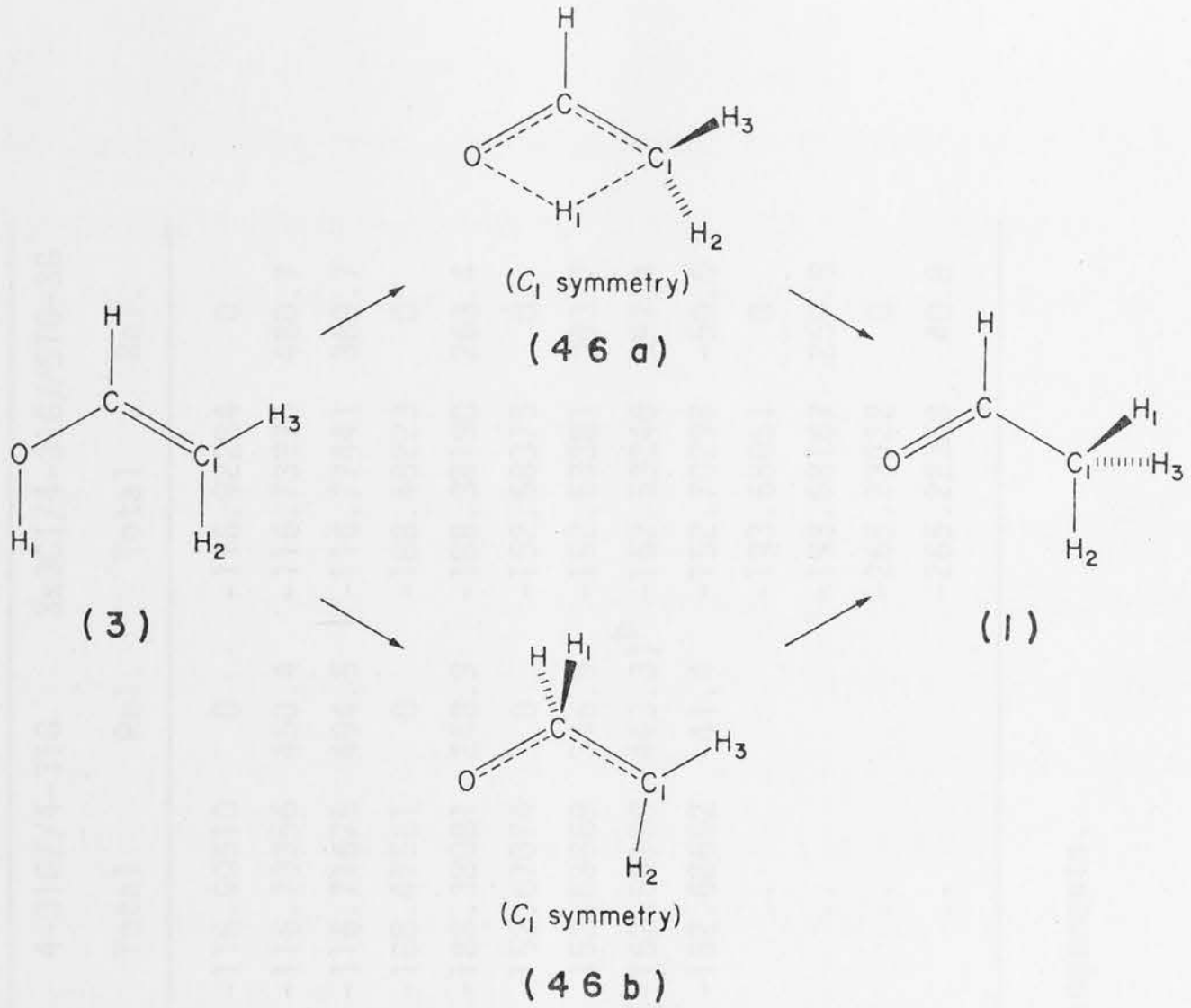

Fig. 4.3 Schematic diagram showing the 1,3-hydrogen shift in vinyl alcohol (3); for the optimized parameters see Table 4.3.

4.4 1,5-SIGMATROPIC HYDROGEN SHIFTS

In contrast to a 1,3-sigmatropic hydrogen shift, which is symmetry allowed when antarafacial [e.g. (41)], a 1,5-sigmatropic hydrogen shift is allowed when suprafacial [e.g. (47)].

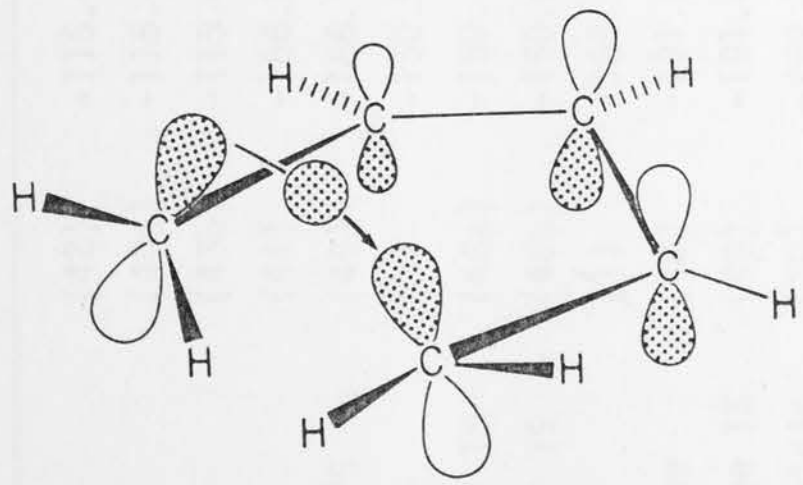

(47)

Table 4.4 Calculated Total and Relative Energies for STO-3G and 4-31G Optimized Structures, Showing the Barriers for Sigmatropic Rearrangements.

Structure[a]		STO-3G//STO-3G		4-31G//STO-3G		4-31G//4-31G		3x3CI/4-31G//STO-3G	
		Total	Rel.	Total	Rel.	Total	Rel.	Total	Rel.
Propene	(42)	-115.66030	0	-116.90458	0	-116.90510	0	-116.92284	0
Propene TS	(43a)	-115.44749	558.7	-116.72660	467.3	-116.73356	450.4	-116.73975	480.7
Propene TS	(43b)	-115.40792	662.6	-116.70719	518.2	-116.71675	494.5	-116.77441	389.7
Formic Acid	(44)	-186.21788	0	-188.46994	0	-188.47561	0	-188.48223	0
Formic Acid TS	(45)	-186.12743	237.5	-188.37254	255.7	-188.38081	248.9	-188.38190	263.4
Vinyl Alcohol	(3)	-150.91668	0	-152.66632	0	-152.67074	0	-152.68375	0
Vinyl Alcohol TS	(46a)	-150.77052	383.7	-152.53144	354.1	-152.53869	346.9	-152.53381	393.7
Vinyl Alcohol TS	(46b)	-150.68740	602.0	-152.49927	438.6	(-152.50189	443.3)[b]	-152.53240	397.4
Acetaldehyde	(1)	-150.94599	-77.0	-152.68499	-49.0	-152.68652	-41.4	-152.70298	-50.5
1,3-Pentadiene	(48)	-191.59799	0	-193.67121	0	..		-193.68051	0
1,3-Pentadiene TS	(49)	-191.47884	312.8	-193.56807	270.8	..		-193.58167	259.5
β-Hydroxyacrolein	(50)	-262.15587	0	-265.23331	0	..		-265.23922	0
β-Hydroxyacrolein TS	(51)	-262.14532	27.7	-265.21689	43.1	..		-265.22368	40.8

[a] Structures labelled TS are transition states for the various rearrangements.

[b] Not fully optimized, the gradient norm is 0.5×10^{-4}, see text.

Investigations have been carried out on two symmetric 1,5-sigmatropic hydrogen shifts, in 1,3-pentadiene and β-hydroxyacrolein, and the asymmetric 1,5-hydrogen shift in nitrosovinyl alcohol, which will be described in Chapter 5.

4.4.1 1,3-PENTADIENE → 1,3-PENTADIENE

As stated previously, the 1,5-hydrogen shift in 1,3-pentadiene is symmetry allowed when suprafacial (47) and a preliminary investigation of such a pathway has been carried out. A planar heavy-atom skeleton was assumed for both 1,3-pentadiene (48) and for the transition state (49). An interesting structural feature (Table 4.5) is the distance (1.374Å) of the migrating hydrogen (H_1) to the terminal carbons (C_3 and C_4), which is comparable to the value (1.394Å) in the symmetry allowed transition state for the propene rearrangement. Although the calculated barrier is substantially smaller than the corresponding value for the 1,3-shift in propene, as might have been expected from qualitative considerations, it is still quite large at 260 kJ mol^{-1}. It will be of interest to examine the effect of an improved geometric model and of higher levels of theory on the theoretical barrier.

4.4.2 β-HYDROXYACROLEIN → β-HYDROXYACROLEIN

The 1,5-hydrogen shift in β-hydroxyacrolein, the enol of malondialdehyde, has attracted studies with a somewhat different emphasis: the question being asked is whether or not the hydrogen bond in this system is symmetric, i.e. is (51) lower or higher in energy than (50)? The best *ab initio* calculations to date include optimizations at the double zeta level and have also examined the effect of electron correlation on the energy difference between (50) and (51). At the SCF level, (51) is found[101] to lie 48 kJ mol^{-1} higher in energy than (50), while an extensive configuration interaction treatment[104] lowers this value only slightly to 42 kJ mol^{-1}.

Table 4.5 Optimized Geometric Parameters for 1,3-Pentadiene (48) and the Transition State (49) for the 1,5-Hydrogen Shift.[a,b]

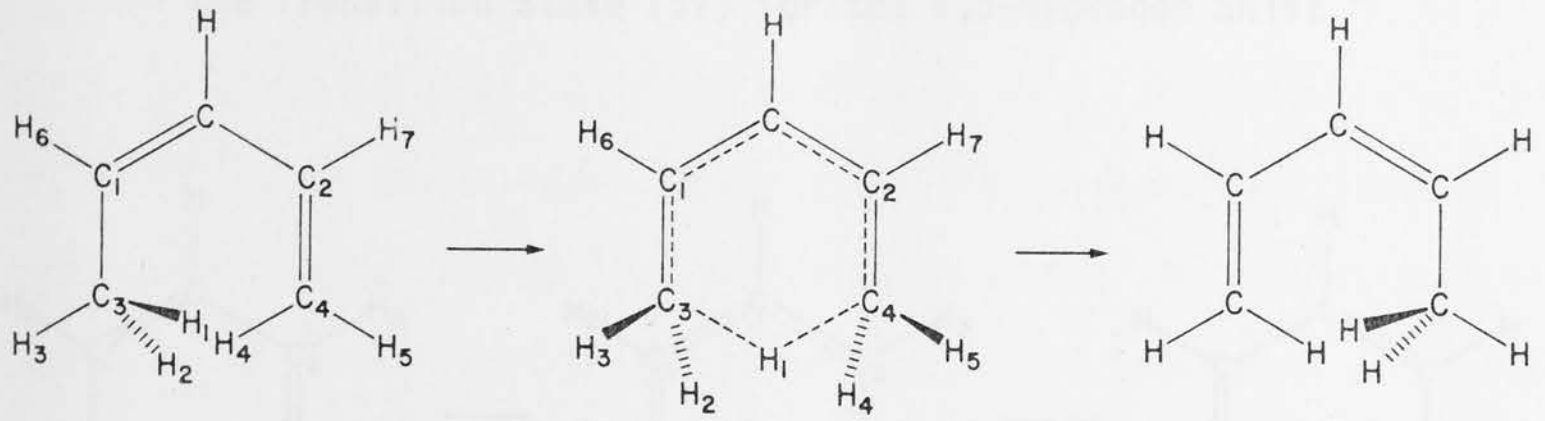

(48) (49) (48')

Parameter	(48), C_s	(49), C_s	Parameter	(48), C_s	(49), C_s
$C\text{-}C_1$	1.319	1.382	$<C_1CC_2$	130.5	121.0
$C\text{-}C_2$	1.490	1.382	$<CC_1C_3$	128.0	121.3
$C_1\text{-}C_3$	1.524	1.425	$<CC_2C_4$	128.0	121.3
$C_2\text{-}C_4$	1.316	1.425	$<HCC_2$	113.0	119.5
C-H	1.084	1.082	$<H_1C_3C_1$	111.6	..
$C_3\text{-}H_1$	1.087	1.374	$<H_1CH$	..	167.8
$C\text{-}H_1$	..	2.418	$<H_2C_3C_1$	111.6	118.0
$C_3\text{-}H_2$	1.087	1.083	$<H_3C_3C_1$	109.9	114.4
$C_3\text{-}H_3$	1.086	1.088	$<H_4C_4C_2$	123.4	118.0
$C_4\text{-}H_4$	1.077	1.083	$<H_5C_4C_2$	121.0	114.4
$C_4\text{-}H_5$	1.081	1.088	$<H_6C_1C$	117.3	118.9
$C_1\text{-}H_6$	1.084	1.086	$<H_7C_1C$	113.6	118.9
$C_2\text{-}H_7$	1.085	1.086	$<H_1C_3C_1C$	-62.7	c
			$<H_2C_3C_1C$	62.7	73.0
			$<H_3C_3C_1C$	0.0	-147.1
			$<H_4C_4C_2C$	0.0	-73.0
			$<H_5C_4C_2C$	0.0	147.1

a The number of independent geometric parameters is 22 and 15 for (48) and (49), respectively.

b For (49), H, H_6 and H_7 were assumed to be in the C_1CC_2 plane.

c $<H_1CHC_2 = -90^\circ$.

Table 4.6 Optimized Geometric Parameters for β-Hydroxyacrolein (50) and the Transition State (51) for the 1,5-Hydrogen Shift.[a]

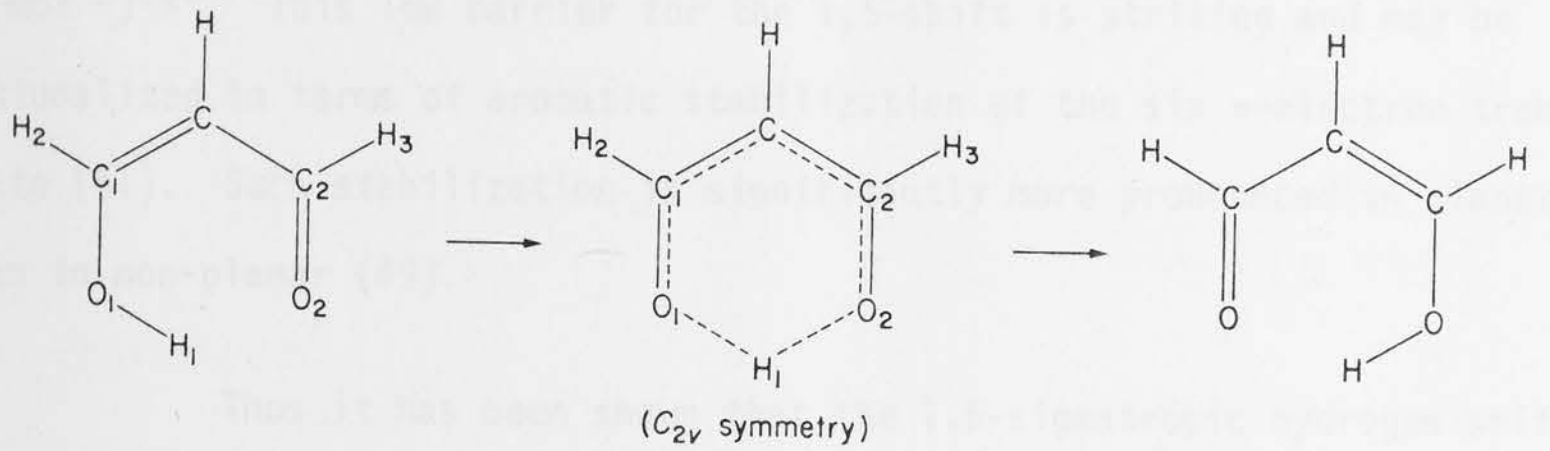

(50) (51) (50')

Parameter	(50), C_s	(51), C_{2v}	Parameter	(50), C_s	(51), C_{2v}
$C-C_1$	1.334	1.401	$<C_1CC_2$	119.3	114.6
$C-C_2$	1.484	1.401	$<CC_1O_1$	124.5	121.3
C_1-O_1	1.366	1.288	$<CC_2O_2$	122.1	121.3
C_2-O_2	1.234	1.288	$<HCC_2$	119.1	122.7
C-H	1.076	1.072	$<H_1O_1C_1$	103.9	..
$O-H_1$	0.998	1.167	$<H_1CH$	..	180.0
$C-H_1$	..	2.262	$<H_2C_1C$	122.1	120.7
C_1-H_2	1.092	1.099	$<H_3C_2C$	116.8	120.7
C_2-H_3	1.103	1.099			

[a] The number of independent geometric parameters is 15 and 8 for (50) and (51), respectively.

This lends confidence to the predictions of calculations within the Hartree-Fock framework for problems of this type.

The results obtained in this study are in agreement with the previous *ab initio* calculations[101,103,104] and with experiment[108,109] in finding (51) higher in energy than (50), i.e. the hydrogen bond is asymmetric.

The calculated barrier for the 1,5-hydrogen shift in β-hydroxyacrolein is 43.1 kJ mol^{-1} at the SCF level and is lowered slightly after 3x3 CI to 40.8 kJ mol^{-1}, in close agreement with the best previously calculated value (42 kJ mol^{-1})[104]. This low barrier for the 1,5-shift is striking and may be rationalized in terms of aromatic stabilization of the six π-electron transition state (51). Such stabilization is significantly more pronounced in planar (51) than in non-planar (49).

Thus it has been shown that the 1,5-sigmatropic hydrogen shifts require considerably less energy than the 1,3-shifts. The activation energy for the 1,5-shift in 1,3-pentadiene is still substantial, and this must be ascribed to the steric requirements for this suprafacial shift (47) which lead to a quite strained transition state.

4.5 THE NITROSOMETHANE → FORMALDOXIME REARRANGEMENT

Nitrosomethane is known to be less stable than its isomer formaldoxime and original attempts to isolate this molecule failed due to its speedy isomerization to formaldoxime[135]. More recently, however, the dimer of nitrosomethane has been prepared[135-138], and has been shown in the gas phase to be in equilibrium with the monomer[139]. The microwave spectrum and the structure of nitrosomethane have been reported[140], establishing nitrosomethane as a stable isomer of formaldoxime.

The nitrosomethane/formaldoxime system is isoelectronic with the acetaldehyde/vinyl alcohol system, and provides another system for which a study of a 1,3-sigmatropic hydrogen shift is of interest. The nitroso-methane/formaldoxime rearrangement, however, is particularly interesting since there is also the possibility of nitrosomethane rearranging to formaldoxime by

successive 1,2-hydrogen shifts, *via* formaldonitrone as as intermediate. Thus there are two possible pathways (A and B, Scheme 4.1) for the rearrangement. Note that in pathway A the isomerization of *syn* formaldoxime to its *anti* isomer has been included since microwave spectral studies[141,142] have shown that the *anti* form is the more stable isomer.

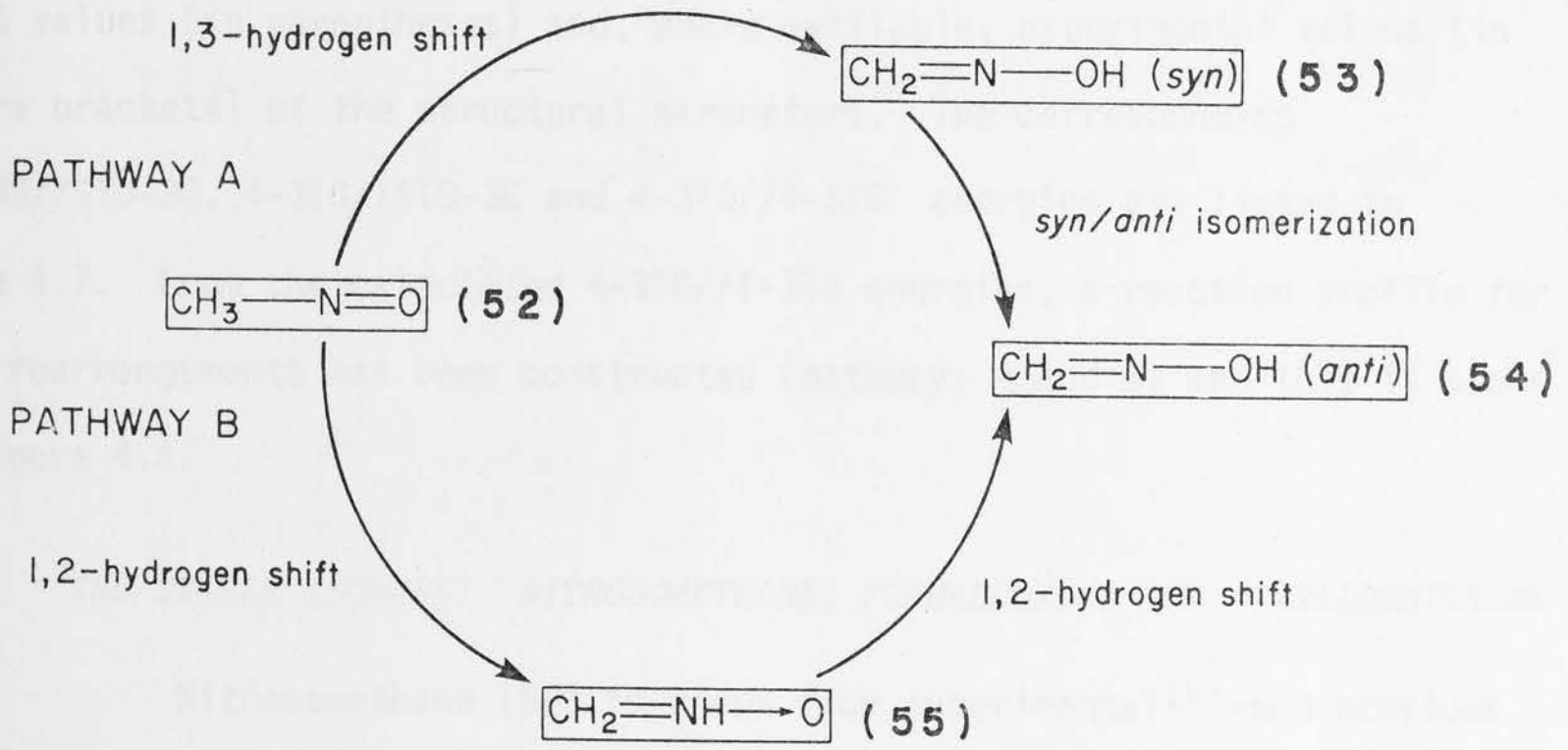

SCHEME 4.1

The aim of the study presented in this section is to examine the structures and energies of nitrosomethane (52), *syn* and *anti* formaldoxime [(53) and (54), respectively] and the intermediate, formaldonitrone (55), as well as the four transition states [(56) - (59)] involved in pathways A and B. In this way, it is hoped to establish the potential energy surface connecting nitrosomethane with *anti* formaldoxime. There have been several previous *ab initio* molecular orbital calculations on nitrosomethane[46,50,52,143-147], formaldoxime[46,50,143,148-151] and formaldonitrone[143]. Most of these calculations were carried out with experimental, assumed or standard geometries and were concerned largely with the individual stable isomers and

associated conformational problems. None of the previous studies examined the hydrogen-shift rearrangements described here.

The stable isomers [(52) - (55)] and the transition states [(56) -(59)] have been studied at both the STO-3G and the 4-31G levels. The optimized geometries are displayed within the text, and include STO-3G values, 4-31G values (in parentheses) and, where available, experimental values (in square brackets) of the structural parameters. The corresponding STO-3G//STO-3G, 4-31G//STO-3G and 4-31G//4-31G energies are listed in Table 4.7. From the calculated 4-31G//4-31G energies, a reaction profile for both rearrangements has been constructed (pathways A and B) and this is shown in Figure 4.4.

4.5.1 THE STABLE ISOMERS: NITROSOMETHANE, FORMALDOXIME AND FORMALDONITRONE

Nitrosomethane (52) is known from experimental[140] and previous theoretical[52,144,145,147] studies to have a preferred conformation in which the N=O bond is eclipsed by a neighbouring C-H bond of the methyl group. An optimized geometry (double zeta basis set) for (52) has been previously reported[147]. In this study the STO-3G and 4-31G geometries and energies have been calculated. Examination of the structural parameters displayed in (52) shows that agreement with the experimental structure[140] is good.

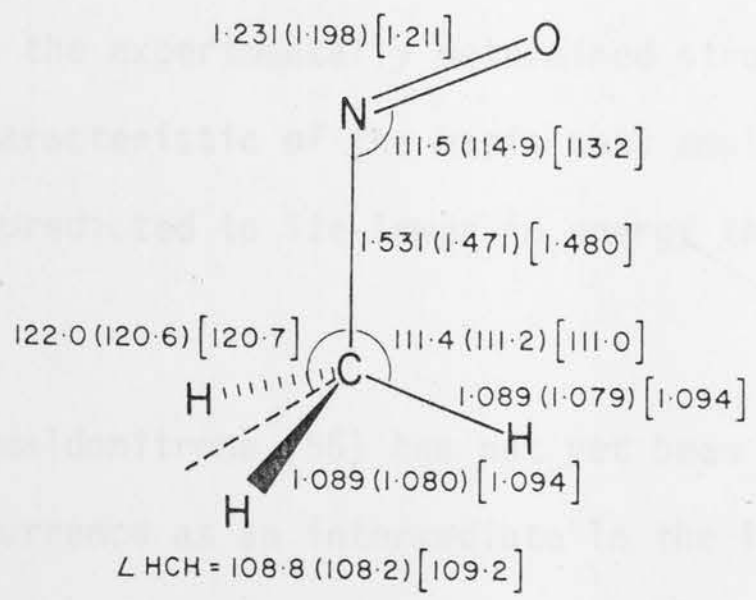

(52)

For formaldoxime, both the *syn* (53) and the *anti* (54) isomers have been optimized. The *syn/anti* energy difference had been previously calculated[46,50] using standard geometries and the STO-3G and 4-31G basis sets, yielding values of 24 and 45 kJ mol^{-1}, respectively, in favour of the *anti* isomer. Calculations[151] using floating spherical gaussian orbitals (FSGO) produced a difference of 29 kJ mol^{-1}. STO-3G and 4-31G optimized structures of (54) have been reported[150], but no total energies were given. These parameters have been refined for (54), and (53) has been fully optimized.

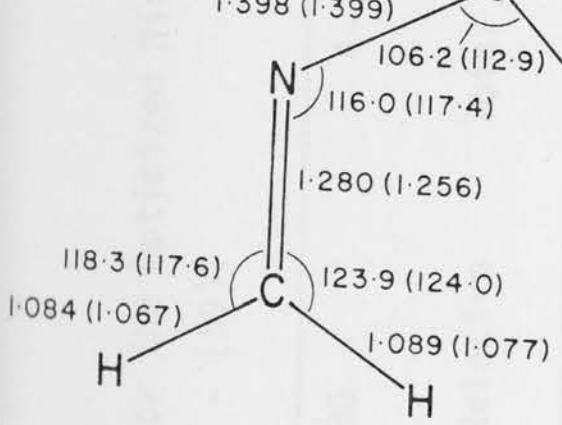

(53)

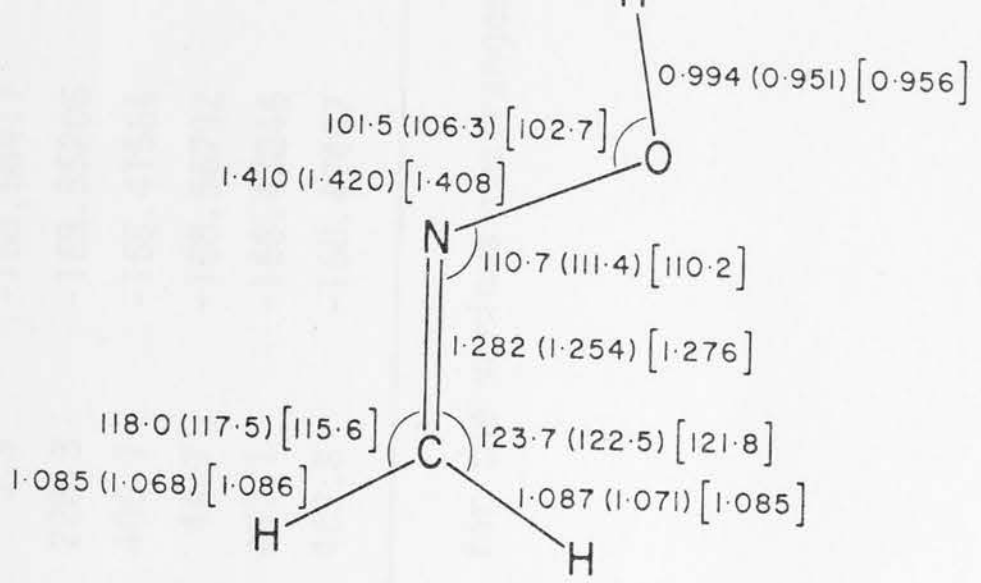

(54)

Total and relative energies shown in Table 4.7 demonstrate the fact that (54) is lower in energy than (53), with the best estimate of the energy difference being 37 kJ mol^{-1}. The optimized geometries for (54) can be compared with the experimentally determined structure[142]. The differences are small and characteristic of the basis sets employed (cf. ref. 150). Formaldoxime is predicted to lie lower in energy than nitrosomethane by about 62 kJ mol^{-1}.

Formaldonitrone (55) has not yet been observed experimentally although its occurrence as an intermediate in the 1,3-cycloaddition of

Table 4.7 Total Energies and Relative Energies for the Optimized Nitroso, Oxime and Nitrone Isomers (52) - (55), and the Related Transition States (56) - (59).

Structure[a]		STO-3G//STO-3G Energy		4-31G//STO-3G Energy		4-31G//4-31G Energy	
		Total	Relative	Total	Relative	Total	Relative
Nitrosomethane	(52)	-166.65373	0	-168.56066	0	-168.56479	0
Formaldoxime (*syn*)	(53)	-166.64349	26.9	-168.57004	-24.6	-168.57448	-25.4
Formaldoxime (*anti*)	(54)	-166.65225	3.9	-168.58417	-61.7	-168.58855	-62.4
Formaldonitrone	(55)	-166.56679	228.3	-168.55206	22.6	-168.55812	17.5
TS: 1,3-H shift	(56)	-166.49881	406.7	-168.41564	380.8	-168.42447	368.4
TS: *syn* → *anti*	(57)	-166.63672	44.7	-168.56792	-19.1	-168.57221	-19.5
TS: 1,2-H shift	(58)	-166.46592	493.1	-168.43846	320.8	-168.44351	318.4
TS: 1,2-H shift	(59)	-166.47706	463.8	-168.47407	227.3	-168.47388	238.7

[a] Structures labelled TS are transition states for the various rearrangements.

formaldoxime with monosubstituted alkenes[152] has been suggested. Isomer (55) is the parent compound of known substituted nitrones[153-155]. In agreement with the only previous *ab initio* study[143] on (55), our results show this isomer slightly higher in energy (by 18 kJ mol^{-1}) than its nitroso isomer (52). It is noted that the relative energies obtained at the STO-3G level do not describe the energy differences at all well (Table 4.7). The optimized geometries of (55) are reasonably consistent with the results of an X-ray study[156] of *N*-methyl-*p*-chlorophenyl nitrone: C=N = 1.309Å, N-O = 1.280Å and <CNO = 125.5°.

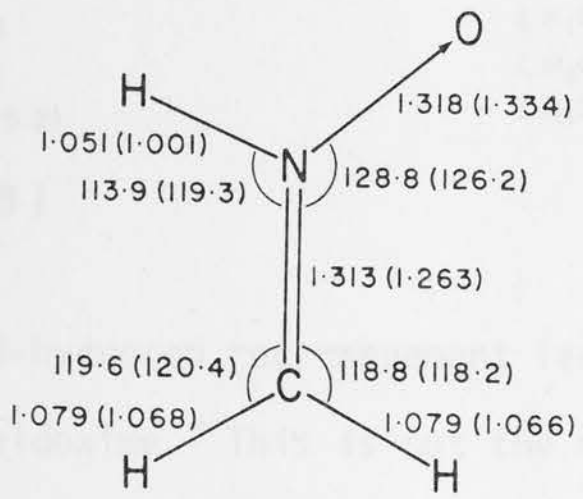

(55)

4.5.2 THE REARRANGEMENT VIA A 1,3-HYDROGEN SHIFT

In Section 4.3, where 1,3-hydrogen shifts were studied, substantial barriers for such rearrangements were found. Even though an antarafacial hydrogen shift is classified as "allowed" from orbital symmetry considerations[118], it seems that the steric problems involved in such a strained transition state contribute to a high energy of activation. The transition state (56) for the 1,3-hydrogen shift in the nitrosomethane (52)/ formaldoxime (53) system is found to be quite high in energy, being

368 kJ mol^{-1} above (52). The moving hydrogen (H_1) is clearly bonded simultaneously to the carbon and the oxygen in (56) as demonstrated by the small CNO angle [cf. the CNO angles in (52) and (53)].

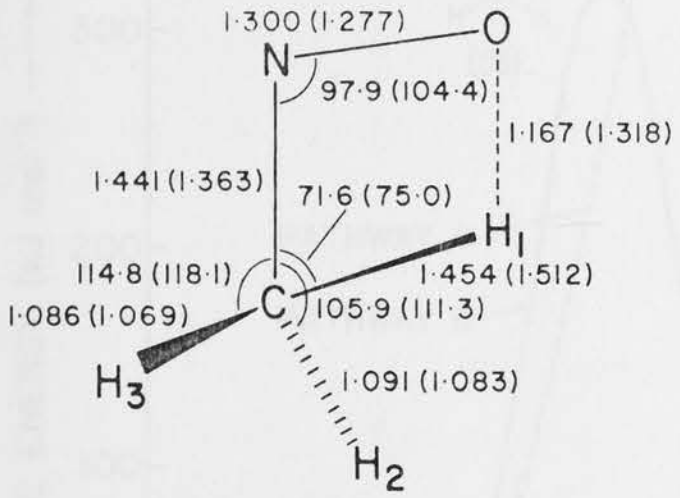

$\angle H_1CNO = -3{\cdot}7\ (-6{\cdot}8)$
$\angle H_2CNO = 82{\cdot}2\ (69{\cdot}8)$
$\angle H_3CNO = -155{\cdot}6\ (-155{\cdot}2)$

(56)

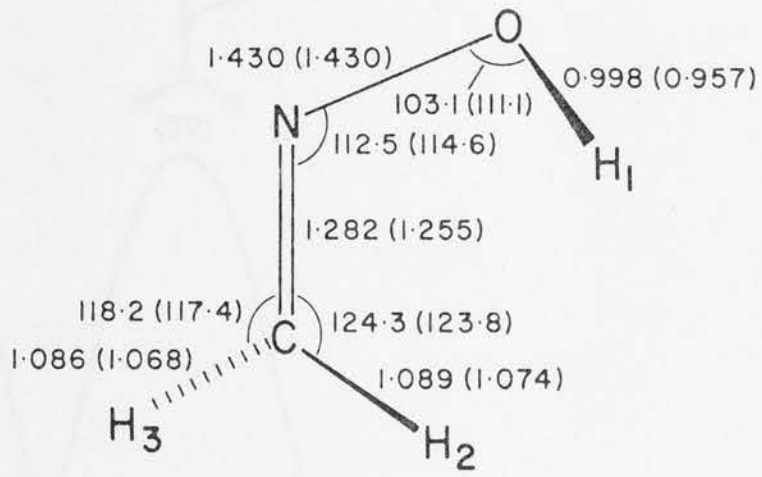

$\angle H_1ONC = 69{\cdot}6\ (54{\cdot}3)$
$\angle H_2CNO = -3{\cdot}2\ (-1{\cdot}1)$
$\angle H_3CNO = 177{\cdot}9\ (178{\cdot}3)$

(57)

The 1,3-hydrogen rearrangement leads to the formation of the *syn* isomer (53) of formaldoxime. This is not the most stable isomer of formaldoxime and therefore the transition state (57) for the subsequent isomerization to the preferred *anti* isomer (54), involving a rotation about the N-O bond, has also been investigated. The transition state for rotation from *syn* formaldoxime occurs for $\angle H_1ONC = 54^{\circ}$, and the barrier is calculated to be only 5.9 kJ mol^{-1} (Table 4.7). A somewhat larger barrier (19.2 kJ mol^{-1}) was obtained in a recent FSGO study[151] but is considered less reliable than that of the present work because of the smaller basis set and use of a rigid rotor approximation in the FSGO calculations. Experimentally, there is little known about the *syn/anti* isomerization since the only observed species is *anti* formaldoxime[141,142,157]. The overall reaction profile for this isomerization of (52) to (54) is shown as pathway A in Figure 4.4.

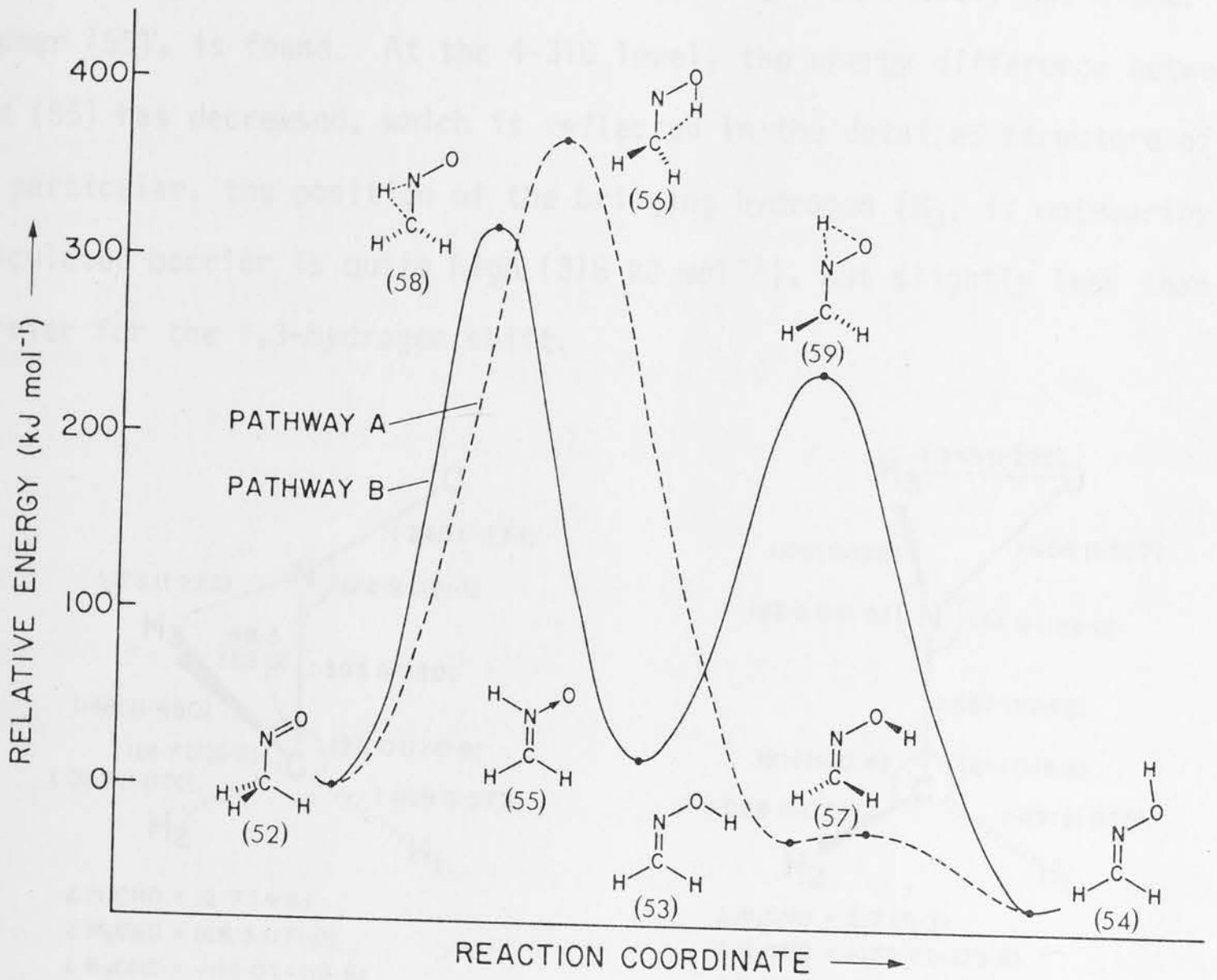

Fig. 4.4 Reaction profile (from 4-31G//4-31G energies) for the intramolecular rearrangement of nitrosomethane (52) to formaldoxime (54) by two possible pathways, A and B, as indicated.

4.5.3 *THE REARRANGEMENT VIA SUCCESSIVE 1,2-HYDROGEN SHIFTS*

In the examination of this reaction pathway, the transition state (58) for the initial 1,2-hydrogen shift, corresponding to the isomerization of nitrosomethane (52) to its nitrone isomer (55), was located first. The position of the moving hydrogen (H_3) in the calculated transition state (58) is quite sensitive to the basis set employed. This can be explained by the fact that, at the STO-3G level, the nitrone (55) is much higher in energy than nitrosomethane (52) (see Table 4.7). In agreement with the Hammond

postulate[134], a structure for (58), resembling more closely the higher energy isomer (55), is found. At the 4-31G level, the energy difference between (52) and (55) has decreased, which is reflected in the detailed structure of (58). In particular, the position of the bridging hydrogen (H_3) is noteworthy. The calculated barrier is quite high (318 kJ mol^{-1}), but slightly less than the barrier for the 1,3-hydrogen shift.

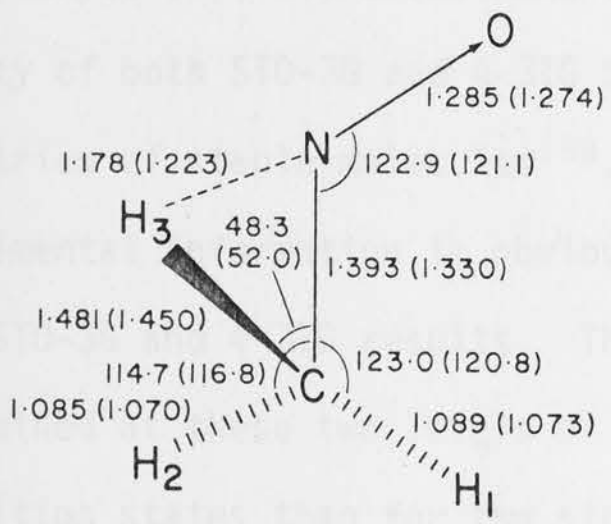

(58)

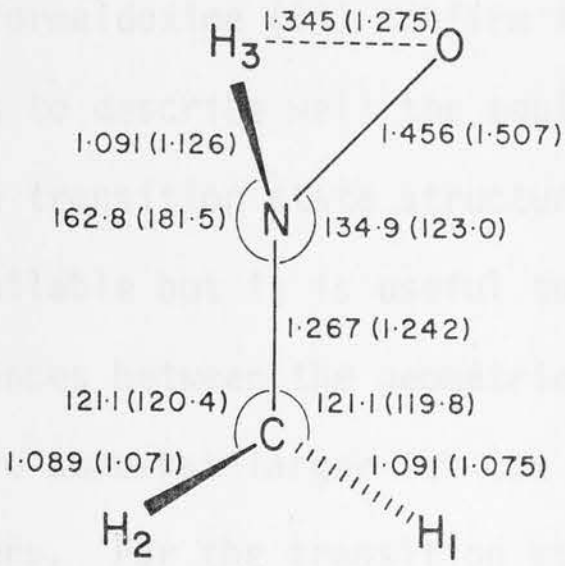

(59)

The transition state (59) for the second 1,2-hydrogen shift is associated with the isomerization of formaldonitrone (55) to the more stable formaldoxime isomer (54). Again differences in the STO-3G and 4-31G structures of (59) are found which can be ascribed to the high relative energy of (55) at the STO-3G level. The position of the moving hydrogen (H_3) in (59) is in agreement with expectations based on the Hammond postulate. The calculated barrier for the isomerization of (55) to (54) is somewhat lower than the barriers associated with transition states (56) and (58), but is still substantial (221 kJ mol^{-1}). The reaction profile for pathway B is also included in Fig. 4.4.

4.6 COMPARISON OF THEORETICAL PROCEDURES

With this study of small systems (C_3H_6,CH_2O_2,C_2H_4O and CH_3NO) and their associated intramolecular rearrangements having been completed at both the STO-3G and the 4-31G level, it is possible to make a comparison of the results at the various levels employed. The results for the experimentally known structures of propene (44), formic acid (45), acetaldehyde (1), nitrosomethane (52) and formaldoxime (54) confirm the ability of both STO-3G and 4-31G basis sets to describe well the equilibrium geometries of stable molecules[158]. For the transition state structures, experimental information is obviously unavailable but it is useful to compare here STO-3G and 4-31G results. The differences between the geometries determined at these two levels of theory are somewhat larger for the transition states than for the stable isomers. For the transition states, the position of the moving hydrogen is the most sensitive when going from STO-3G to 4-31G. The relative energies at the STO-3G level are generally in poor agreement with the 4-31G values. This is not unexpected since it is well established[45,50] that STO-3G is not very suited for studying non-isodesmic[45] energy comparisons. Noteworthy, however, is the close correspondence between the 4-31G//STO-3G and the 4-31G//4-31G relative energies. The agreement is good, even for the transition states for which some differences between the geometries calculated at the two levels were noted. This does not imply that it will always be sufficient to determine transition states at the STO-3G level since the overall potential energy surface might not be well described at this level. This is exemplified by the difficulties experienced in locating the vinyl alcohol "forbidden" transition state at the 4-31G level. When it is possible to do energy comparisons with STO-3G optimized structures, however, the 4-31G//STO-3G

(or higher level//STO-3G) approach represents a substantial saving in computational expense.

4.7 CONCLUSIONS

In this chapter a number of intramolecular rearrangements have been examined. The results lend quantitative support to the qualitative predictions concerning sigmatropic hydrogen shifts. For example, 1,5-shifts are found to require considerably less energy than 1,3-shifts. In addition, forbidden pathways for 1,3-shifts are found in some instances to be favoured over allowed pathways. The effect of inclusion of 3x3 CI is to preferentially favour these forbidden pathways. For the (allowed) 1,5-shift in β-hydroxyacrolein, results reported here are in close agreement with those of a previous[104] extensive CI study. The following points should be noted with regard to the asymmetric rearrangements in vinyl alcohol and nitrosomethane:

(i) The barrier for rearrangement *via* a 1,3-hydrogen shift in vinyl alcohol is sufficiently high to make such a rearrangement unlikely. This stability of vinyl alcohol with respect to intramolecular rearrangement is consistent with the experimental observation[64] of vinyl alcohol.

(ii) For nitrosomethane, rearrangement either *via* a 1,3-hydrogen shift (pathway A), or *via* successive 1,2-hydrogen shifts (pathway B), requires high activation energies. Thus nitrosomethane is predicted to be quite stable with respect to intramolecular rearrangement. This agrees with

experimental results: nitrosomethane is an observable isomer[140] of formaldoxime.

(iii) The rotational isomerization of *syn* to *anti* formaldoxime is associated with a small energy barrier of 6 kJ mol^{-1} and is exothermic by about 37 kJ mol^{-1}.

(iv) Formaldonitrone, which is an intermediate in the isomerization of nitrosomethane (pathway B), is only slightly higher in energy (by 18 kJ mol^{-1}) than nitrosomethane. It is separated from both nitrosomethane and formaldoxime by substantial potential energy barriers (301 and 221 kJ mol^{-1}, respectively), and therefore offers a reasonable prospect of experimental observation under appropriate conditions.

Finally, a close agreement is noted between relative energies calculated at the 4-31G//STO-3G and 4-31G//4-31G levels, even for transition states.

CHAPTER 5

NITROSOACETALDEHYDE

AND ITS ENOL AND OXIME ISOMERS

5.1 INTRODUCTION

In Chapter 3 the effect of substituents on the acetaldehyde/vinyl alcohol system was examined, the aim being to identify substituents that would reverse the relative stabilities of vinyl alcohol and acetaldehyde. It was found that the nitroso substituent had the desired effect, and it was calculated that nitrosoacetaldehyde [O=NCH$_2$CH=O, (60)] is actually slightly higher in energy than its enol isomer, nitrosovinyl alcohol [O=NCH=CHOH, (61)]. Thus nitrosovinyl alcohol appeared to be a good candidate for a simple, stable enol. Intramolecular enol-keto tautomerism [(61) → (60)] is not likely (cf. Section 4.3), nor is the possibility of nitroso-oxime tautomerism, by which nitrosoacetaldehyde (60) could isomerize to its oxime isomer, glyoxal monoxime [HON=CHCH=O, (62)]. A prototype for this isomerization was studied in Section 4.5. Apart from these isomerizations *via* 1,3-hydrogen shifts there is a further possibility of nitrosovinyl alcohol (61) rearranging *via* a 1,5-sigmatropic hydrogen shift, directly to the oxime isomer (62).

In this chapter, the relationship to one another of the keto (60), enol (61) and oxime (62) isomers of the $C_2H_3NO_2$ system will be examined. The main points of interest are the thermochemical and kinetic stabilities of the enol (61) with respect to the other isomers.

5.2 METHOD

The preferred conformations of (60) and (61) have been established in the study of the substituted keto and enol isomers (Tables 3.6 and 3.9) using the 4-31G//Std approach. The same approach has been used here to examine the conformations of the oxime isomer (62). The preferred conformers (60), (61a) and (62a), as well as three additional conformations (61b), (62b)

and (62c), which are relevant to the 1,5-shift, have been optimized at the STO-3G level. For the optimizations, the gradient procedure was used, and symmetry constraints were applied as specified. The transition state for the asymmetric 1,5-hydrogen shift (63) was obtained by the transition state optimization procedure. Energy comparisons have been made at the 4-31G//STO-3G level, and allow the construction of a reaction profile for the 1,5-hydrogen shift in nitrosovinyl alcohol.

5.3 PREFERRED CONFORMATIONS OF THE KETO, ENOL AND OXIME ISOMERS

For the keto isomer ($O{=}NCH_2CH{=}O$), the lowest energy conformer obtained in the 4-31G//Std study reported in Chapter 3 was optimized. This structure has <ONCC *trans* and <NCCO *trans*. The optimized structure (60) is shown in Fig. 5.1. For nitrosovinyl alcohol (O=NCH=CHOH), two structures were optimized, one with <ONCC *trans*, <NCCO *cis* and <CCOH *cis* (61a) and the other with <ONCC *cis*, <NCCO *cis* and <CCOH *cis* (61b). The former had emerged with lowest energy in the 4-31G//Std study of (61).

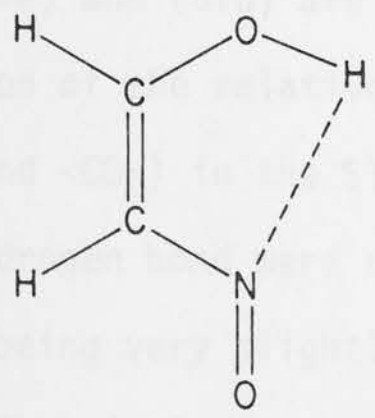

(61a)

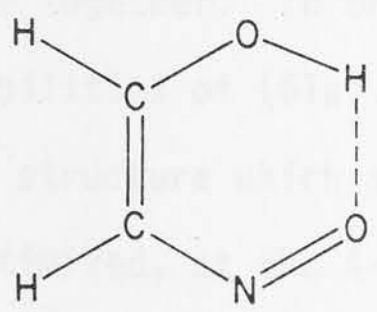

(61b)

It was desirable to optimize the structure of (61b) for two reasons. In the first place, the presence of an intramolecular hydrogen bond in (61b) should make the energy particularly sensitive to geometry optimization and secondly, (61b) is the conformation of nitrosovinyl alcohol most naturally

Table 5.1 Calculated Total Energies and Relative Energies for Conformations of HON=CHCH=O (62).

Conformation[a]			4-31G//Std	
<HONC	<ONCC	<NCCO	Total Energy	Relative Energy
0	0	0	-281.08326	137.5
0	0	180	-281.08393	135.7
0	180	0	-281.10829	71.7
180	0	0	-281.10977	67.8
0	180	180	-281.11867	44.5
180	0	180	-281.13053	13.3
180	180	0	-281.12650	23.9
180	180	180	-281.13561	0

[a] Dihedral angles in degrees.

involved in the 1,5-hydrogen shift. The optimized structures of (61a) and (61b) are shown in Fig. 5.1 and the corresponding energies in Table 5.2. Optimization does indeed have a large effect on (61b) and, after optimization, the energies of (61a) and (61b) are close together. In order to probe further the question of the relative stabilities of (61a) and (61b), the two angles (<ONC and <COH) in the STO-3G structure which are most directly involved in the hydrogen bond were re-optimized, at the 4-31G level. This resulted in (61b) being very slightly favoured (by 0.3 kJ mol^{-1}) over (61a) (see Table 5.2). Thus it is found that (61a) and (61b) have very similar energies.

Glyoxal monoxime (HON=CHCH=O) has not been studied previously and therefore initial calculations with the 4-31G basis set and standard

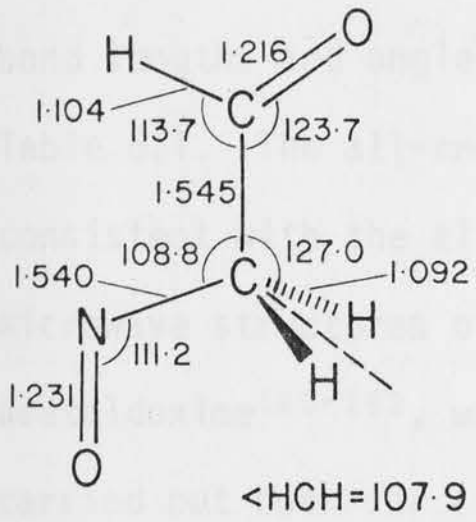

<HCH=107·9

(60)

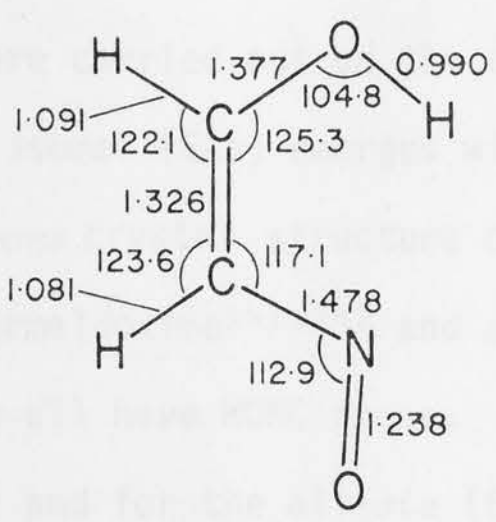

(61a)

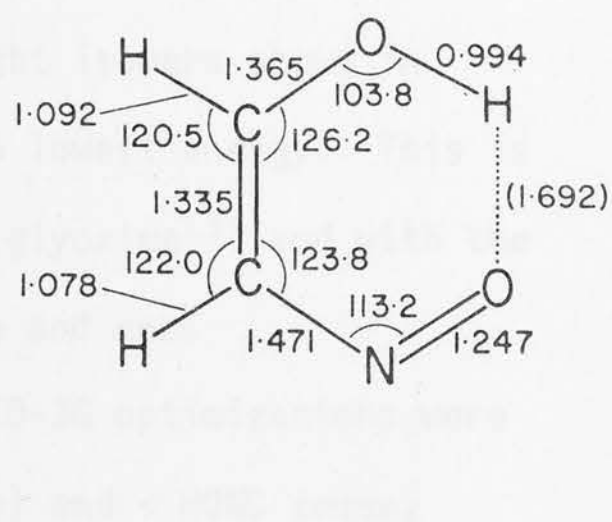

(61b)

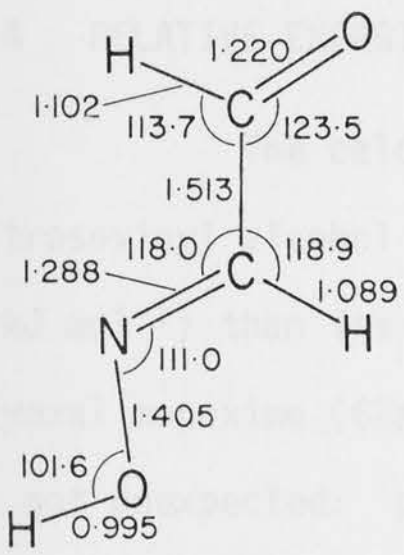

(62a)

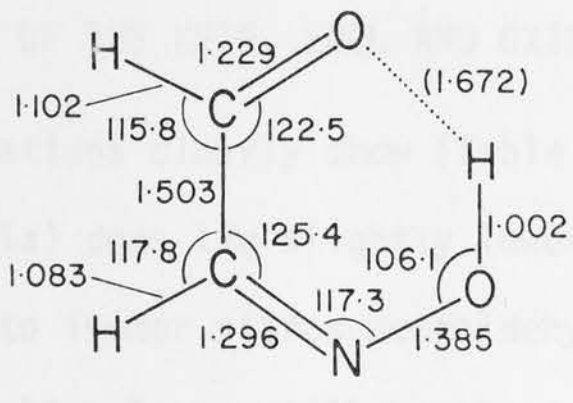

(62b)

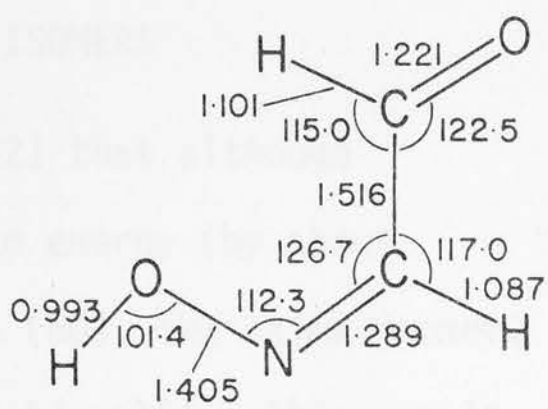

(62c)

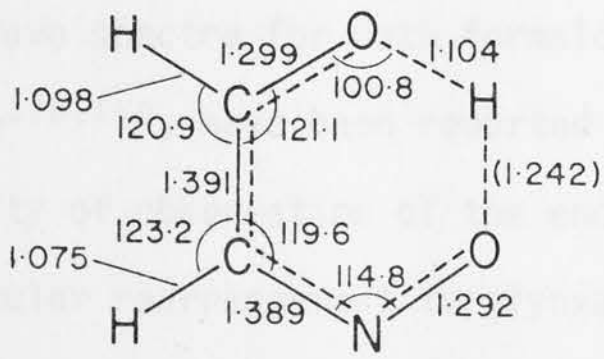

(63)

Fig. 5.1 STO-3G optimized geometries for conformations of nitrosoacetaldehyde (60), nitrosovinyl alcohol (61a), (61b), glyoxal monoxime (62a), (62b), (62c) and the transition state (63) for the rearrangement (61b) → (62b); C_s symmetry constraint in each case.

bond lengths and angles were carried out on the eight isomers shown in Table 5.1. The all-*trans* isomer (62a) emerges with lowest energy. This is consistent with the all-*trans* crystal structure of glyoxime[159] and with the microwave structures of formaldoxime[141,142] and *syn* and *anti* acetaldoxime[160-162], which all have HONC *trans*. STO-3G optimizations were carried out both for (62a) and for the all-*cis* (62b) and < HONC *trans*, < ONCC *cis*, < NCCO *trans* (62c) structures. These confirm (Table 5.2) that the preferred conformation of glyoxal monoxime is (62a).

5.4 RELATIVE ENERGIES OF THE KETO, ENOL AND OXIME ISOMERS

The calculations clearly show (Table 5.2) that although nitrosovinyl alcohol (61a) does lie slightly lower in energy (by about 6 kJ mol^{-1}) than its keto isomer nitrosoacetaldehyde (60), the oxime isomer, glyoxal monoxime (62a), lies lower still by about 86 kJ mol^{-1}. This result is not unexpected: primary and secondary nitroso compounds are generally thought to exist in solution (where thermodynamic equilibrium is rapid) as their oxime tautomers[163]. There are, however, several instances where both the nitroso and oxime isomers have been characterized. For example, the preparation and microwave spectra for both formaldoxime[142] and its nitroso isomer, nitrosomethane[138,140], have been reported (cf. Section 4.5). Clearly, the possibility of observation of the enol is dependent on the barrier for intramolecular rearrangement to glyoxal monoxime.

5.5 THE 1,5-SIGMATROPIC HYDROGEN SHIFT FROM NITROSOVINYL ALCOHOL TO GLYOXAL MONOXIME.

There are two possible pathways by which nitrosovinyl alcohol might rearrange intramolecularly to its lower energy isomer, glyoxal monoxime, as shown in Scheme 5.1 (page 120).

Table 5.2 Calculated Total Energies and Relative Energies for the $C_2H_3NO_2$ Isomers.

Structure[a]	STO-3G//STO-3G		4-31G//Std		4-31G//STO-3G	
	Total	Rel.	Total	Rel.	Total	Rel.
(60)	-277.87050	29.7	-281.10353	84.2	-281.10102	91.8
(61a)	-277.85942	58.8	-281.10513	80.0	-281.10328	85.9[b]
(61b)	-277.85958	58.4	-281.07768	152.1	-281.10249	88.0[b]
(62a)	-277.88182	0	-281.13561	0	-281.13600	0
(62b)	-277.87560	16.3	-281.08326	137.5	-281.12186	37.1
(62c)	-277.87947	6.2	-281.13053	13.3	-281.13302	7.8
(63)	-277.85205	78.2	-	-	-281.09072	118.9

[a] See Fig. 5.1.

[b] Partial optimization at the 4-31G level leads to
(61a), <HOC = 113.3°, <CNO = 115.0°, total energy = -281.10617
(61b), <HOC = 112.7°, <CNO = 117.5°, total energy = -281.10629

Pathway A involves successive 1,3-hydrogen shifts. The first shift is an enol → keto interconversion. Previously, it was shown (Section 4.3) for the parent rearrangement, vinyl alcohol → acetaldehyde, that the barrier to such a shift is substantial i.e., that vinyl alcohol should be stable with respect to a 1,3-intramolecular hydrogen shift. Approximate calculations, involving the attachment of a standard nitroso group to the STO-3G optimized structures (Table 4.3) of vinyl alcohol, acetaldehyde, and the two transition states for the 1,3-sigmatropic shift, indicate that this conclusion is unlikely to be modified by the presence of a nitroso substituent. The second shift in pathway A involves interconversion of nitroso and oxime isomers. A detailed

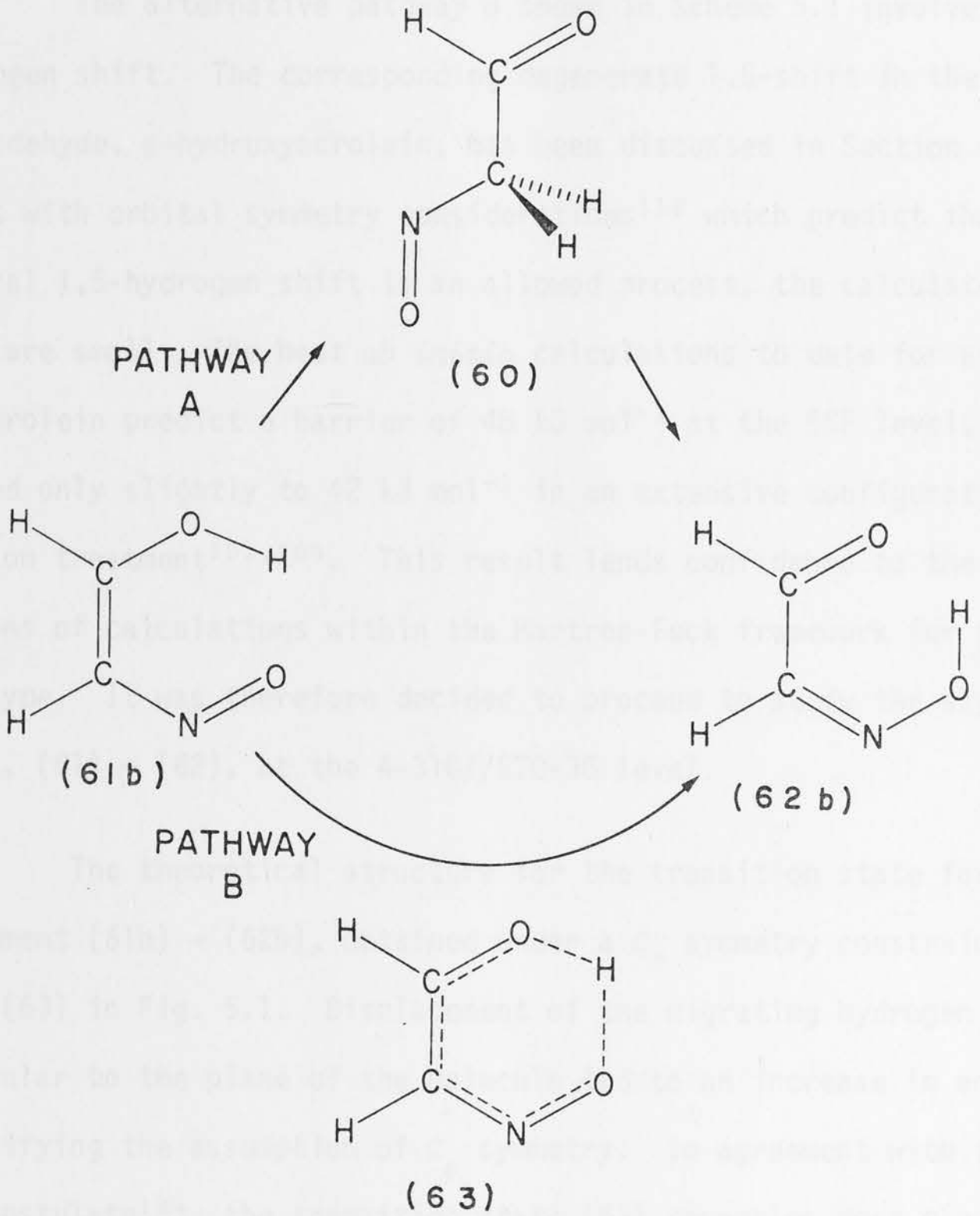

SCHEME 5.1

study of such a rearrangement for the parent system, nitrosomethane → formaldoxime, has been presented in Section 4.5, and shows a substantial barrier. However, regardless of the barrier for this second step, the high barrier calculated for the first step ensures that pathway A does not present a viable means for conversion of (61) → (62).

The alternative pathway B shown in Scheme 5.1 involves a 1,5-hydrogen shift. The corresponding degenerate 1,5-shift in the enol of malondialdehyde, β-hydroxyacrolein, has been discussed in Section 4.4. In agreement with orbital symmetry considerations[118] which predict that the suprafacial 1,5-hydrogen shift is an allowed process, the calculated barriers are small. The best *ab initio* calculations to date for β-hydroxyacrolein predict a barrier of 48 kJ mol^{-1} at the SCF level, which is reduced only slightly to 42 kJ mol^{-1} in an extensive configuration interaction treatment[101,104]. This result lends confidence to the predictions of calculations within the Hartree-Fock framework for problems of this type. It was therefore decided to proceed to study the asymmetric 1,5-shift, (61) → (62), at the 4-31G//STO-3G level.

The theoretical structure for the transition state for the rearrangement (61b) → (62b), obtained under a C_s symmetry constraint, is shown as (63) in Fig. 5.1. Displacement of the migrating hydrogen perpendicular to the plane of the molecule led to an increase in energy, thus justifying the assumption of C_s symmetry. In agreement with the Hammond postulate[134], the transition state (63) resembles more closely the higher-energy isomer (61b) than the lower-energy isomer (62b). The barrier to rearrangement is quite low at 30.9 kJ mol^{-1} (4-31G//STO-3G). It is somewhat lower than the corresponding calculated barrier [43.1 kJ mol^{-1}, Table 4.4] for the enol of malondialdehyde, which is not surprising in the light of the exothermicity of the process (61) → (62). The cyclic transition state contains six π-electrons and is therefore formally aromatic. The reaction profile for the 1,5-hydrogen shift in nitrosovinyl alcohol is shown in Fig. 5.2.

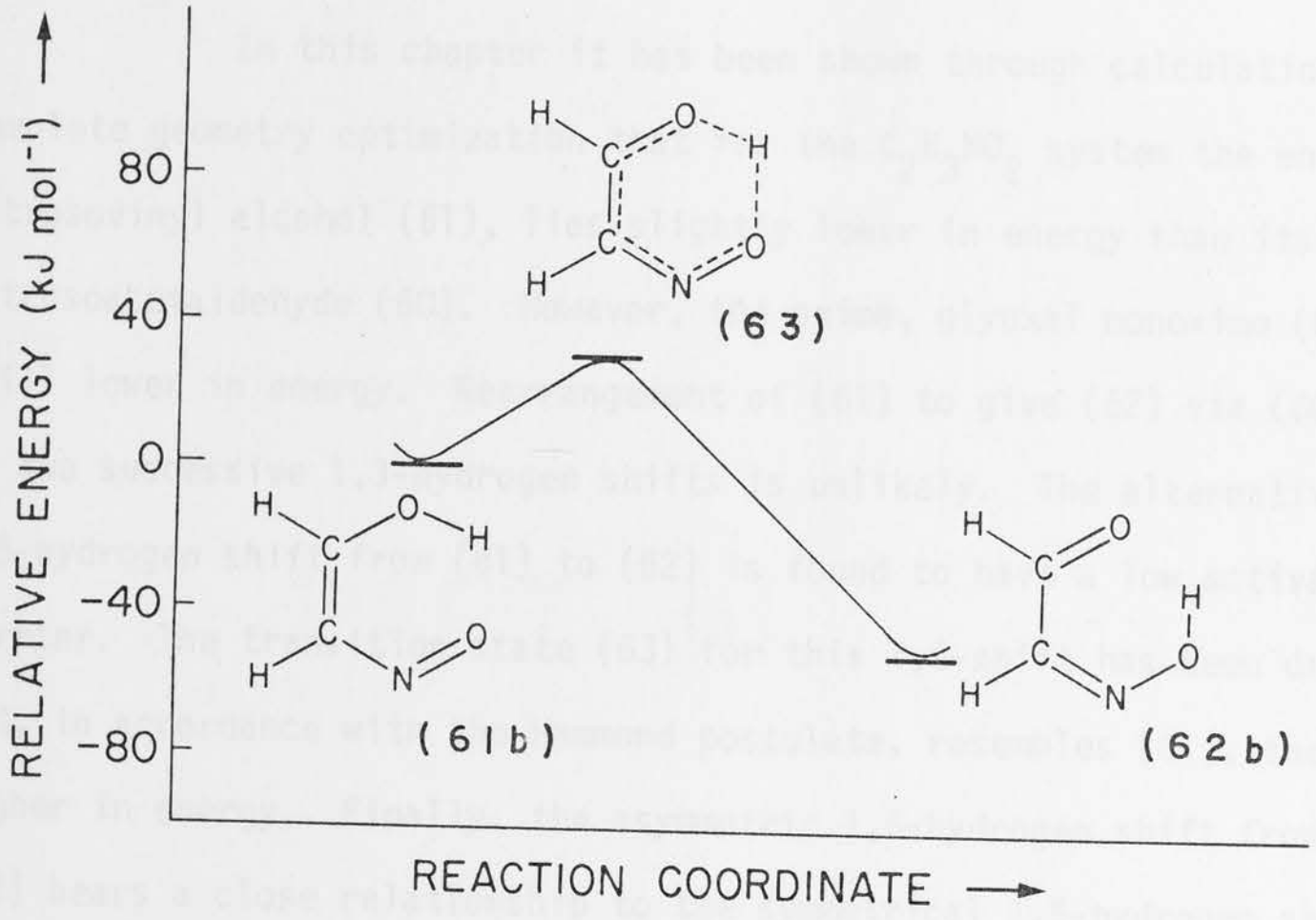

Fig. 5.2 Reaction profile for the 1,5-sigmatropic hydrogen shift of nitrosovinyl alcohol (61b) to glyoxal monoxime (62b).

Whereas it was found that (61b) is likely to be the most stable isomer of (61), (62b) is not the lowest energy form of (62). It is of interest to examine the energy required to convert (62b) to the more stable isomers (62a) and (62c). Transformation of the *cis-cis-cis* structure (62b) to the *trans-cis-trans* structure (62c) requires rotation about the O-N and C-C *single* bonds. Such rotations normally have small barriers and hence (62c) should be readily formed from (62b). On the other hand, formation of the *trans-trans-trans* isomer (62a) requires, in addition, rotation about the N=C *double* bond or inversion at nitrogen and, by analogy with related systems, such processes should have considerably larger barriers[148,149]. It may well be that the product ultimately formed from a 1,5-hydrogen shift in nitrosovinyl alcohol will be (62c) rather than the lower energy [but less accessible from (62b)] isomer (62a).

5.6 CONCLUSIONS

In this chapter it has been shown through calculations with complete geometry optimization that for the $C_2H_3NO_2$ system the enol, nitrosovinyl alcohol (61), lies slightly lower in energy than its keto isomer nitrosoacetaldehyde (60). However, the oxime, glyoxal monoxime (62), lies still lower in energy. Rearrangement of (61) to give (62) via (60) by means of two successive 1,3-hydrogen shifts is unlikely. The alternative 1,5-hydrogen shift from (61) to (62) is found to have a low activation barrier. The transition state (63) for this 1,5-shift has been determined and, in accordance with the Hammond postulate, resembles (61), the reactant higher in energy. Finally, the asymmetric 1,5-hydrogen shift from (61) to (62) bears a close relationship to the symmetrical 1,5-hydrogen shift in the enol of malondialdehyde, which was discussed in Chapter 4.

PART III

THEORETICAL AND EXPERIMENTAL STUDIES OF GAS-PHASE ION STRUCTURES

CHAPTER 6

A THEORETICAL STUDY OF $CH_2O^{+\cdot}$ ISOMERS

6.1 INTRODUCTION

The study and understanding of structures and structural isomerism of positively-charged ions is an important aspect of mass spectrometry[164], and has received considerable attention. To obtain more information about systems of small isomeric ions, a theoretical and experimental study of a number of $C_nH_{2n}O^{+\cdot}$ isomers has been undertaken. In this chapter, a theoretical study of the structures and relative energies of three possible $CH_2O^{+\cdot}$ isomers, the formaldehyde and hydroxymethylene radical cations [(64) and (65), respectively] and the oxonium ion (66), is discussed.

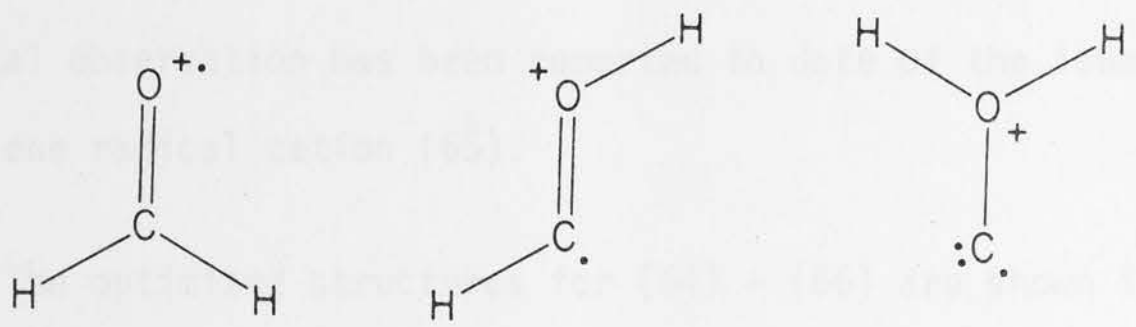

(64) (65) (66)

To determine the kinetic stability of the hydroxymethylene radical cation (65), the 1,2-hydrogen shift leading to the formaldehyde radical cation (64) has been investigated. In this study, both the RHF and the UHF procedures have been used. Although the UHF procedure produces lower energies than the RHF procedure, it is known to cause problems occasionally, due to contamination from states of higher spin multiplicity[23]. This study provides a comparison of the two procedures at the 4-31G//4-31G level. In order to obtain better estimates of the relative energies, the 6-31G* basis set has been used for obtaining relative energies at the RHF/6-31G*//RHF/4-31G level.

6.2 STRUCTURES AND THERMODYNAMIC STABILITIES OF THE $CH_2O^{+\cdot}$ ISOMERS

There have been numerous theoretical studies on the neutral CH_2O isomers[70,165-172], including some extensive studies[170-172] on the rearrangement of hydroxymethylene to formaldehyde. The CH_2O radical cations, however, have received far less attention[70,173]. *Ab initio* FSGO calculations[173] on the formaldehyde radical cation (64) have shown it to be planar, and in a more extensive *ab initio* study[70], minimal basis set (UHF/STO-3G) calculations were reported for (64) and (65). The formaldehyde radical cation is well known experimentally from photoionization[174], ESR[175] and mass spectrometric (ref. 1-9 of ref. 176) studies, and its ion/molecule reactions have been studied[176]. No experimental observation has been reported to date of the isomeric hydroxymethylene radical cation (65).

The optimized structures for (64) - (66) are shown in Fig. 6.1. For (64), a $^2B_2$ ground state, corresponding to ionization from a b_2 lone pair orbital of formaldehyde, is found. The hydroxymethylene radical cation (65) has a $^2A'$ ground state while the third isomer, the oxonium ion (66), has a $^2B_2$ ground state. The optimized structure for the ion (64) can be compared with the 4-31G optimized structure of formaldehyde[166,172], which shows a lengthening of the C=O bond and a widening of the HCH angle for the ion. For all three structures [(64) - (66)], very similar results are obtained with the RHF/4-31G and the UHF/4-31G methods (see Fig. 6.1 and Table 6.1).

The best estimate of the relative energies for the $CH_2O^{+\cdot}$ isomers is provided by the RHF/6-31G*//RHF/4-31G calculations, which show that the formaldehyde ion (64) is the more stable ion, with the hydroxymethylene ion (65) 41 kJ mol^{-1} and the oxonium ion (66) 258 kJ mol^{-1} higher in energy. The energy difference between (64) and (65) can be compared with the results

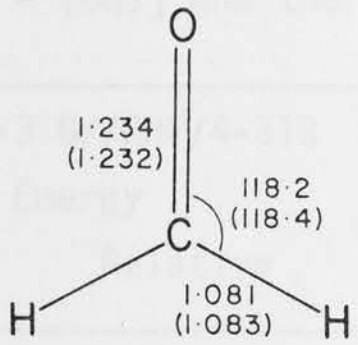

(64)

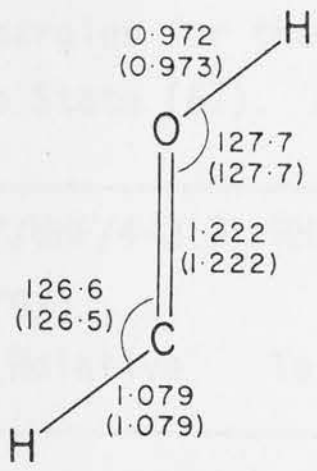

(65)

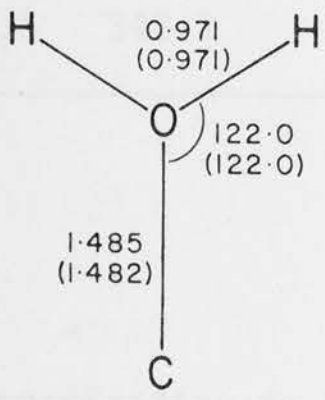

(66)

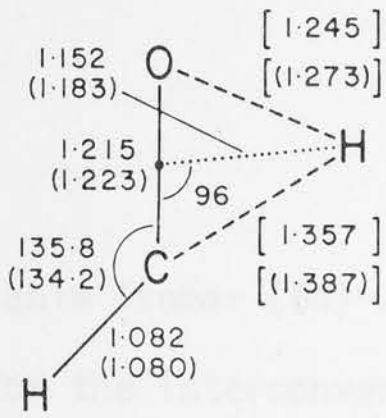

(67)

Fig. 6.1 Optimized geometries of the $CH_2O^{+\cdot}$ isomers [(64) - (66)], and the transition state (67), obtained at the RHF/4-31G (UHF/4-31G) levels. Non-independent parameters are shown in brackets.

obtained in a study of the corresponding neutral systems[172], where formaldehyde was found to be 217 kJ mol^{-1} lower in energy than hydroxymethylene, at a similar level of theory (6-31G*//6-31G*).

6.3 THE KINETIC STABILITIES OF THE $HCOH^{+\cdot}$ AND THE $COH_2^{+\cdot}$ RADICAL CATIONS

6.3.1 THE $HCOH^{+\cdot}$ ISOMER

Whether the hydroxymethylene ion (65) is stable with respect to

Table 6.1 Calculated Total and Relative Energies for the $CH_2O^{+\cdot}$ Isomers [(64) - (66)] and the Transition State (67).

Isomer	RHF/4-31G//RHF/4-31G Energy		UHF/4-31G//UHF/4-31G Energy		RHF/6-31G*//RHF/4-31G Energy	
	Total	Relative	Total	Relative	Total	Relative
(64)	-113.34212	0	-113.34733	0	-113.51403	0
(65)	-113.32769	37.9	-113.32947	46.9	-113.49862	40.5
(66)	-113.27534	175.3	-113.27679	185.2	-113.41592	257.6
(67)[a]	-113.21175	342.3	-113.22286	326.8	-113.40395	289.0

[a] $\alpha = 96^{\circ}$.

intramolecular isomerization to its more stable isomer (64) will depend on the barrier for the 1,2-hydrogen shift needed for the interconversion. This rearrangement has been studied by optimizing structures and energies corresponding to various values of the parameter α shown in (67a), X being the midpoint of the C-O bond. By varying α from its value in the hydroxymethylene ion to its value in the formaldehyde ion, and optimizing the

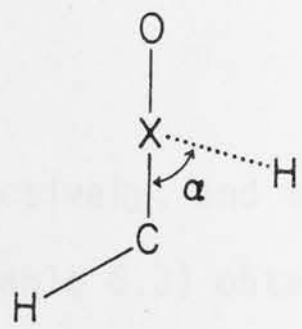

(67a)

intermediate structures for various values of α, reaction profiles (Fig. 6.2) have been constructed from the calculated energies (Table 6.2). Both the RHF/4-31G and the UHF/4-31G methods predict a barrier at $\alpha = 96^{\circ}$ of

Table 6.2 Calculated Total Energies and Relative Energies for Intermediate Structures for the 1,2-Hydrogen Shift from $HCOH^{+\cdot}$ (65) to $H_2CO^{+\cdot}$ (64).

α[a]	RHF/4-31G Energy		UHF/4-31G Energy	
	Total	Relative	Total	Relative
155.0	-113.32535	6.1	-113.32714	6.1
147.5[b]	-113.32769	0	-113.32947	0
120.0	-113.28309	117.1	-113.28515	116.4
105.0	-113.23151	252.5	-113.23670	243.6
99.0	-113.21535	294.9	-113.22477	274.9
97.0	-113.21243	302.6	-113.22315	279.1
96.0	-113.21175	304.4	-113.22286	279.9
93.0	-113.21371	299.3	-113.22410	276.6
90.0	-113.22037	281.8	-113.22844	265.3
75.0	-113.27071	149.6	-113.27595	140.5
60.0	-113.31695	28.2	-113.32221	19.1
40.2[c]	-113.34212	-37.9	-	-
40.1[c]	-	-	-113.34733	-46.9

[a] See (67a).

[b] Fully optimized structure of (65).

[c] Fully optimized structure of (64).

304 and 280 kJ mol^{-1} respectively, and the reaction profiles (Fig. 6.2) and intermediate structures (Table 6.3) obtained from the two methods are very similar. The considerable height of the barrier can be understood after examination of the singly occupied molecular orbital (SOMO) of a number of structures along the reaction path. This shows that the atomic orbital corresponding to the migrating hydrogen changes sign in the transition state, which indicates an avoided crossing of orbitals [e.g. (68) and (69)].

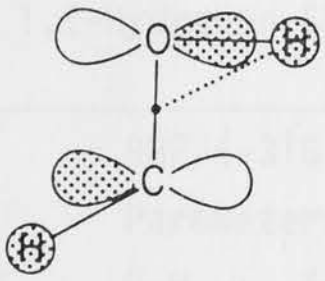

$\alpha > 96°$

(68)

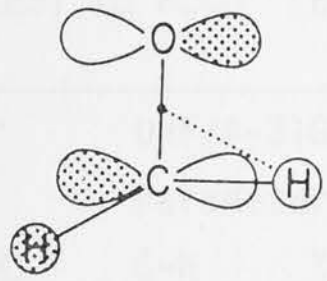

$\alpha < 96°$

(69)

At the 6-31G*//4-31G level (Table 6.1), a barrier of 248 kJ mol^{-1} is found, which is quite substantial, and only slightly reduced from the 4-31G results (see also Fig. 6.2).

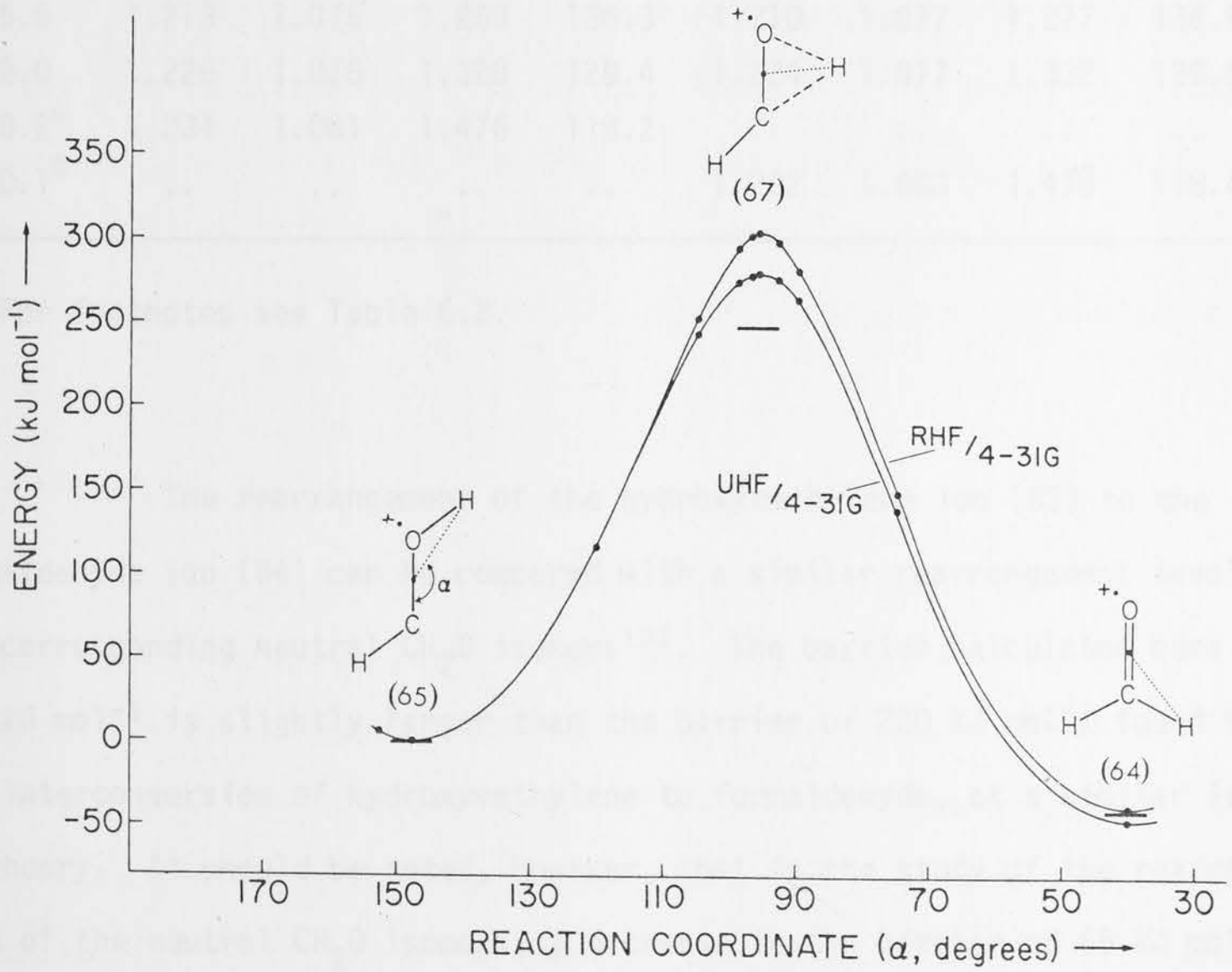

Fig. 6.2 Reaction profiles (RHF/4-31G and UHF/4-31G) for the conversion of the hydroxymethylene radical cation (65) to the formaldehyde radical cation (64). The RHF/6-31G*//RHF/4-31G energies for (64), (65) and the transition state (67) are indicated by solid lines (—).

Table 6.3 Optimized Structural Parameters for Intermediate Structures for the 1,2-Hydrogen Shift from $HCOH^{+\cdot}$ (65) to $H_2CO^{+\cdot}$ (64)†.

α[a]	RHF/4-31G Parameters				UHF/4-31G Parameters			
	O-C	C-H	X-H	<HCO	O-C	C-H	X-H	<HCO
155.0	1.216	1.080	1.481	126.2	1.217	1.080	1.482	126.1
147.5[b]	1.222	1.079	1.430	126.6	1.222	1.079	1.431	126.5
120.0	1.230	1.080	1.227	130.1	1.231	1.079	1.227	130.0
105.0	1.226	1.082	1.151	131.8	1.228	1.081	1.162	131.8
99.0	1.221	1.082	1.138	133.8	1.225	1.081	1.169	133.2
97.0	1.217	1.082	1.144	135.1	1.224	1.081	1.178	133.8
96.0	1.215	1.082	1.152	135.8	1.223	1.080	1.183	134.2
93.0	1.209	1.080	1.198	138.4	1.220	1.080	1.198	135.4
90.0	1.205	1.079	1.237	139.5	1.216	1.079	1.215	136.7
75.0	1.213	1.076	1.269	136.3	1.210	1.077	1.277	136.9
60.0	1.226	1.076	1.328	129.4	1.224	1.077	1.332	129.8
40.2[c]	1.234	1.081	1.476	118.2	..	..	..	..
40.1[c]	..	..	..	..	1.232	1.083	1.478	118.4

† For footnotes see Table 6.2.

The rearrangement of the hydroxymethylene ion (65) to the formaldehyde ion (64) can be compared with a similar rearrangement involving the corresponding neutral CH_2O isomers[172]. The barrier calculated here of 248 kJ mol^{-1} is slightly larger than the barrier of 220 kJ mol^{-1} found for the interconversion of hydroxymethylene to formaldehyde, at a similar level of theory. It should be noted, however, that in the study of the rearrangement of the neutral CH_2O isomers, a decrease in the barrier of 65 kJ mol^{-1} was found upon inclusion of configuration interaction. If this effect operates for the $CH_2O^{+\cdot}$ isomers as well, this could decrease the barrier to $\sim$ 180 kJ mol^{-1}. A striking difference between the results for the neutral CH_2O

isomers and the $CH_2O^{+\cdot}$ isomers is the lower relative energy of the hydroxymethylene radical cation (relative to the formaldehyde radical cation) compared with neutral hydroxymethylene (relative to formaldehyde), namely 41 vs 217 kJ mol^{-1}, respectively.

Finally, the possibility that the hydroxymethylene radical cation can undergo O-H bond fission, to give HCO^+ and $H^\cdot$, has been examined. An estimate of $\Delta H_f^\circ(0^\circ)$ for (65) can be arrived at by using the known experimental $\Delta H_f^\circ(0^\circ)$ value[76] of 936 kJ mol^{-1} for (64), and the calculated energy difference between (64) and (65) of 41 kJ mol^{-1}. From the experimental $\Delta H_f^\circ(0^\circ)$ values[76,174] of 822 kJ mol^{-1} for HCO^+ and 216 kJ mol^{-1} for $H^\cdot$ and the calculated $\Delta H_f^\circ(0^\circ)$ value of 977 kJ mol^{-1} for $HCOH^{+\cdot}$, it is estimated that dissociation of $HCOH^{+\cdot}$ will be endothermic by 61 kJ mol^{-1}. Although this is a relatively low value, it may still be possible to observe hydroxymethylene ions of low internal energies. It is noted (using an experimental[76] $\Delta H_f^\circ(0^\circ)$ for $CO^{+\cdot}$ of 1238 kJ mol^{-1}) that an alternative dissociation of $HCOH^{+\cdot}$ to $CO^{+\cdot} + H_2$ is highly endothermic and therefore unlikely.

6.3.2 THE $COH_2^{+\cdot}$ ISOMER

Even though this isomer (66) was found to be very high in energy, it was interesting to examine (in somewhat less detail than for $HCOH^{+\cdot}$) the potential energy surface for the 1,2-hydrogen shift needed for the isomerization of the oxonium isomer (66) to the hydroxymethylene radical cation (65). This has been investigated by optimizing a few intermediate structures [cf. (70)] along the reaction path while constraining the angle β to fixed values.

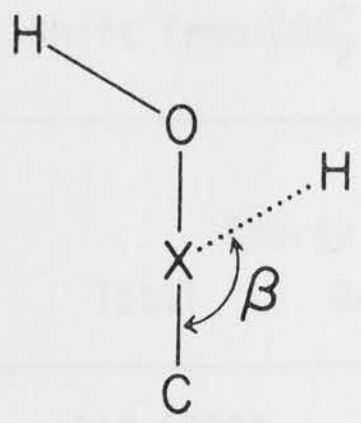

(70)

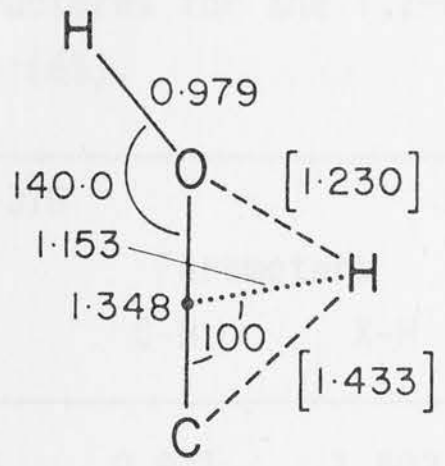

(70a)

This study has been carried out at the RHF/4-31G level and the resulting energies and structural parameters are listed in Table 6.4. The structure with $\beta = 100^{\circ}$ (70a) is the highest energy structure and is an approximation for the transition state for the 1,2-hydrogen shift under study. The calculated barrier (Table 6.4) of 269 kJ mol^{-1} reduces to 225 kJ mol^{-1} at the RHF/6-31G*//RHF/4-31G level, which is still substantial. However, the high energy of the oxonium ion (66) is likely to facilitate dissociation of the ion into COH^+ and $H^{\cdot}$. For (66) an estimate of $\Delta H_f^{\circ}(0^{\circ})$ of 1225 kJ mol^{-1} is obtained from the relative energy of (66) vs (64) and $\Delta H_f^{\circ}(0^{\circ})$ for (64). Since COH^+ is calculated† to be 91 kJ mol^{-1} higher than HCO^+, the total heat of formation of COH^+ and $H^{\cdot}$ is 91 kJ mol^{-1} higher than that for $HCO^+ + H^{\cdot}$ (which is 1038 kJ mol^{-1}, see Section 6.3.1). Thus the dissociation of COH_2^+ to COH^+ and $H^{\cdot}$ is found to be exothermic by 96 kJ mol^{-1}.

---

† The 4-31G optimized geometries are: HCO^+, H-C 1.078Å, C-O 1.098Å; HOC^+, H-O 0.976Å, O-C 1.160Å.

The 4-31G//4-31G energies are: HCO^+ -112.77931 hartrees; HOC^+ -112.74464 hartrees.

Table 6.4 Calculated Total Energies, Relative Energies and Structural Parameters for Intermediate Structures for the 1,2-Hydrogen Shift from $COH_2^{+\cdot}$ (66) to $HCOH^{+\cdot}$ (65).

	RHF/4-31G					
	Energy		Parameters			
β[a]	Total	Relative	O-C	O-H	X-H	<HOC
146.8[b]	-113.27534	0	1.485	0.971	1.503	122.0
120.0	-113.22723	126.3	1.445	0.973	1.214	144.0
110.0	-113.19415	213.2	1.415	0.975	1.146	146.2
100.0[c]	-113.17288	269.0	1.348	0.979	1.153	140.0
90.0	-113.18252	243.7	1.280	0.982	1.268	133.8
34.7[d]	-113.32769	-137.4	1.222	0.972	1.524	127.7

[a] See (70).

[b] Fully optimized structure of (66).

[c] RHF/6-31G*//RHF/4-31G energy: -113.33015.

[d] Fully optimized structure of (65).

6.4 CONCLUSIONS

The theoretical study of the $CH_2O^{+\cdot}$ isomers described in this chapter has confirmed that the most stable isomer is the formaldehyde radical cation (64) and that of the two other possible isomers, the hydroxymethylene radical cation (65) is only slightly higher (41 kJ mol^{-1}) in energy than (64). The third isomer, the oxonium ion [$COH_2^{+\cdot}$, (66)], is very high in energy, and even though there is a large barrier to its rearrangement to the hydroxymethylene radical cation, it is unlikely to be observed due to its possible dissociation into COH^+ and $H^\cdot$. The barrier to intramolecular rearrangement (*via* a 1,2-hydrogen shift) of the hydroxymethylene radical cation (65) to the more stable formaldehyde radical cation (64) is substantial, the best estimate

being 248 kJ mol^{-1}. The dissociation of $HCOH^{+\cdot}$ into HCO^{+} and $H^{\cdot}$ is predicted to be endothermic by about 60 kJ mol^{-1}. The conclusion of this study is, therefore, that under appropriate conditions the hydroxymethylene radical cation might be an observable species.

CHAPTER 7

STRUCTURES AND STABILITIES OF $C_2H_4O^{+\cdot}$ ISOMERS: A REVIEW

7.1 INTRODUCTION

Ions have long been known or suspected to play a major role in various physical and biological phenomena. The majority of these phenomena occur in condensed phases, but ions also play an important role in gas-phase phenomena. One area of importance is the interstellar atmosphere, where the tremendous temperatures and radiation densities give rise to relatively high concentrations of ions which have resulted from single and multiple ionization of a wide variety of materials; such ions can lead to other ions through ion/molecule reactions[177]. Ions and free electrons also determine many of the physical and chemical properties of the earth's upper atmosphere[177]. Important areas of research include the study of the emission spectra of atomic ions for elucidation of the structure of atoms, and the study of emission spectra of molecular ions for elucidation of the electronic structure of molecules[178]. Another important area of research is the study of gas-phase ions in the course of chemical analysis, where materials are identified by detection of the molecular ions and/or the fragment ions that can be derived from the given material. The most obvious example of this is the mass spectrometric study of molecular ions and fragment ions of chemical compounds. In these studies the knowledge of the exact structure of the ions under investigation is of great importance[164]. It is for this reason that a study has been undertaken of one such system, namely $C_2H_4O^{+\cdot}$, for which a number of isomeric structures are possible. The $C_2H_4O^{+\cdot}$ isomers have been studied by means of ion cyclotron resonance spectrometry, which will be described in Chapters 9 and 10. A detailed theoretical study of the $C_2H_4O^{+\cdot}$ isomers has also been carried out, and is described in Chapter 8.

In this chapter, a review will be given of the available experimental information on the $C_2H_4O^{+\cdot}$ isomers. Four main areas of research

on the $C_2H_4O^{+\cdot}$ isomers can be distinguished:

(i) Thermochemical measurements.

(ii) Metastable ion studies.

(iii) Collisional activation studies.

(iv) Studies of ion/molecule reactions.

The instrumental techniques will be discussed briefly; for an excellent review of these techniques see ref. 179.

7.2 EXPERIMENTAL DATA FOR THE $C_2H_4O^{+\cdot}$ ISOMERS

Of the $C_2H_4O^{+\cdot}$ isomers, the acetaldehyde (ethanal) and ethylene oxide (oxirane) radical cations ($CH_3CHO^{+\cdot}$ and $C_2H_4O^{+\cdot}$) have long been known, since they can be obtained by ionization of the stable parent molecules. Mass spectra for ethylene oxide[180] and acetaldehyde[181] have been reported, in which the structures of the molecular ions have been assumed to be the same as the parent neutral molecules. The third $C_2H_4O^{+\cdot}$ isomer which is considered to be well-established is the vinyl alcohol (ethenol) radical cation, which can be obtained as a secondary ion in the mass spectra of γ-hydrogen containing aliphatic aldehydes (unsubstituted on the α-carbon) *via* the McLafferty rearrangement[181,182]. Other methods of obtaining the vinyl alcohol radical cation are by way of rearrangements in the mass spectra of alkyl vinyl ethers[182-184], and in the mass spectrum of cyclobutanol[185]. The confirmation of the structures of these isomers will be discussed in the following sections and in Chapter 10. Other $C_2H_4O^{+\cdot}$ isomers have been postulated as possible or transient species, namely the hydroxyethylidene radical cation[186] ($CH_3COH^{+\cdot}$), the C---C ring-opened ethylene oxide ion[187,188] (CH_2-O-$CH_2^{+\cdot}$), and the C---O ring-opened ethylene oxide ion[189,190] (CH_2-CH_2-$O^{+\cdot}$).

7.2.1 THERMOCHEMICAL MEASUREMENTS

An early source of information on molecular ions has been the use of emission and absorption spectroscopy[191] of the corresponding stable (neutral) molecules, which yielded the ionization potential (IP) for ethylene oxide as 10.565 eV (1020 kJ mol^{-1}) and the IP for acetaldehyde as 10.229 eV (987 kJ mol^{-1})[192]. Another method of obtaining ionization potentials is through photoionization studies[193], which confirmed the above IP value for ethylene oxide, and resulted in an IP of 10.21 eV (985 kJ mol^{-1}) for acetaldehyde[194]. Photoelectron spectroscopy[195] studies of these ionization potentials gave similar results, and showed that acetaldehyde and ethylene oxide are ionized by removal of an electron from the lone pair on the oxygen atom[196,197] . The above methods give thermochemical information derived from stable molecules. Other techniques used for studying the thermochemistry of ions in the gas phase are electron impact[198] and photon impact[199] mass spectrometry. From the ionization potential of a molecular ion, the appearance potential obtained for the fragment ion under study, and the known heat of formation for the neutral molecule and/or radical involved in the formation of the fragment ion, the heat of formation of that ion can be calculated. In a recent study by Holmes, Terlouw and Lossing[79] of the $C_2H_4O^{+\cdot}$ isomers, the $\Delta H_f^\circ(298^\circ)$ values for three isomers were reported. This study also described the $\Delta H_f^\circ(298^\circ)$ values of $^m/_z$ 44 ions obtained from 1,3-dioxolane and 2,3-epoxypropanol, which are different from the values found for the three "established" isomers, the ethylene oxide, acetaldehyde, and vinyl alcohol radical cations (Table 7.1). A study[200] of tetrahydrofuran showed that a fragment ion of $^m/_z$ 44, produced by ionization of the parent compound, had an appearance potential of 12.27 eV, which resulted in a ΔH_f value for the fragment ion of 950 kJ mol^{-1}, slightly lower than the value observed for the ethylene oxide molecular ion. Finally it should be noted that in a photoionization and ion cyclotron resonance study[187] an "activated" ethylene oxide ion was observed, for which the

Table 7.1 Heats of Formation of $C_2H_4O^{+\cdot}$ ions[a].

Precursor Molecule	Structure	$\Delta H_f^\circ(298^\circ)$
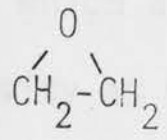	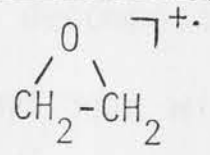	966[b]
CH_3CHO	$CH_3CH{=}O^{+\cdot}$	820[b]
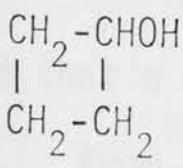	$CH_2{=}CHOH^{+\cdot}$	761
$CH_3(CH_2)_2CHO$	$CH_2{=}CHOH^{+\cdot}$	757
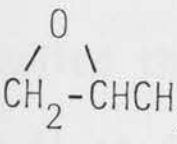	?	856
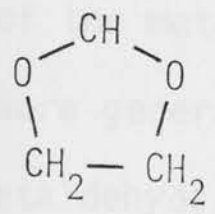	?	860

[a] From ref. 79.
[b] See also ref. 201.

$CH_2\text{-}O\text{-}CH_2^{+\cdot}$ structure was proposed (see Section 7.2.4) and for which a heat of formation of 845 kJ mol^{-1} was estimated.

7.2.2 *METASTABLE ION STUDIES*

The technique of metastable ion analysis is based on the fact that ions decomposing within a narrow time frame (e.g. in the field-free region of a mass spectrometer), which are identical in structure and energy, should exhibit identical decomposition patterns[202,203]. Identification of such processes in a complex mass spectrum is facilitated by the use of special

instrumental techniques, e.g. MIKES (mass-analysed ion kinetic mass spectrometry) or DADI (direct analysis of daughter ions)[204,205], Barber-Elliott "defocussing"[206] and "linked" metastable ion scans[207]. A "metastable peak" which arises from a particular decomposition will be characteristic in intensity as well as in peak shape and peak width at half height. The latter is dependent on the amount of energy that is released during the decomposition[208,209].

A metastable ion study[210] of ethylene oxide and acetaldehyde showed that a prominent metastable peak at $^{m}/_{z}$ 19.1 (corresponding to the loss of $CH_3^{\cdot}$ from the molecular ion) in the spectrum of ethylene oxide is not present in the spectrum of acetaldehyde. In a more extensive metastable ion study, Holmes and Terlouw[188] examined the fragmentation $C_2H_4O^{+\cdot} \rightarrow C_2H_3O^{+} + H^{\cdot}$, and studied the metastable ion characteristics for this fragmentation occurring in the first field-free region of a double focussing mass spectrometer. The shape of the metastable ion peak was examined for a number of $C_2H_4O^{+\cdot}$ ions which were generated by electron impact from a series of suitable compounds. The acetaldehyde, ethylene oxide and vinyl alcohol radical cations could be distinguished by the peak shapes and the kinetic energy released in the fragmentation. The vinyl alcohol radical cation was observed to be produced from ethyl vinyl ether, unbranched aldehydes, cyclic alcohols (e.g. cyclobutanol) and 2-haloethanols. Some compounds were found to produce composite metastable ion peaks, indicating a mixture of $C_2H_4O^{+\cdot}$ isomers. For the $C_2H_4O^{+\cdot}$ isomer produced in the mass spectrum of 1,3-dioxolane a mixture of ethylene oxide and vinyl alcohol ions was proposed, whereas for the $C_2H_4O^{+\cdot}$ isomer produced in the spectrum of isopropanol a mixture of acetaldehyde and vinyl alcohol ions was reported. In a previous study[186] of the mass spectrum of pyruvic acid, the $CH_3COH^{+\cdot}$ structure had been proposed as a transient species for the fragment ion at $^{m}/_{z}$ 44, which supposedly rearranged to the acetaldehyde

ion. Holmes and Terlouw[188] also studied the metastable fragmentation of this $^{m}/_{z}$ 44 ion from pyruvic acid and proposed that it had the vinyl alcohol structure. Although the mass spectrum of ethylene glycol dimethyl ether produced only a very small $^{m}/_{z}$ 44 peak, a study of its fragmentation indicated that it was a mixture of acetaldehyde and ethylene oxide ions; nevertheless the possibility that some of the ions might have the $CH_2\text{-}O\text{-}CH_2^{+\cdot}$ structure was not excluded[188].

7.2.3 COLLISIONAL ACTIVATION STUDIES

When organic ions with high translational energy collide inelastically with neutral atoms or molecules, they become electronically excited at the expense of their translational energy. The excitation energy enables a wide range of dissociation processes to occur, and the intensity relationships of the fragment ions yield information about the structure of the parent ions. This technique is known as collisional activation (CA) mass spectrometry[211-213].

In a "collision induced dissociation" study[214] of acetaldehyde and ethylene oxide in a time of flight mass spectrometer, the molecular ions were accelerated and then allowed to collide with helium, and the fragmentation spectra were recorded for various kinetic energies of the $C_2H_4O^{+\cdot}$ ions. It was found that during the time of flight through the mass spectrometer (4×10^{-6} sec) the ethylene oxide and acetaldehyde ions remained distinct. From the threshold values for the energy of the molecular ions for which certain dissociations took place, the heats of formation could be determined as 10.2 ± 0.2 eV (985 kJ mol^{-1}) and 8.2 ± 0.2 eV (791 kJ mol^{-1}) for the ethylene oxide and acetaldehyde ions, respectively. In an extensive collisional activation study by Van de Sande and McLafferty[215], three $C_2H_4O^{+\cdot}$ isomers, the ethylene oxide, acetaldehyde, and vinyl alcohol radical cations, were readily distinguished. As reference

structures to establish basic fragmentation patterns the molecular ions of ethylene oxide and acetaldehyde were taken, together with the $^{m}/_{z}$ 44 ions produced from aliphatic aldehydes[180]. The collisional activation spectra of these three ions were used to identify $C_2H_4O^{+\cdot}$ ions from other sources. Cyclic alcohols, alkyl vinyl ethers, aliphatic epoxides and 2-haloethanols were all shown to produce ions with the vinyl alcohol structure. For 1,4- and 1,3-butanediol a mixture of acetaldehyde and ethylene oxide ions was found, and for 1,3-dioxolane a mixture of ethylene oxide and vinyl alcohol ions was proposed.

7.2.4 ION/MOLECULE REACTIONS

There are a number of techniques available for the study of ion/molecule reactions[164,216,217]. They include ion cyclotron resonance (ICR) spectrometry[218], high pressure ion source mass spectrometry[219,220], flowing afterglow mass spectrometry[221] and high pressure time of flight mass spectrometry[222]. High pressure mass spectrometry studies for the acetaldehyde and ethylene oxide ions have been carried out[223,224]. Both studies showed the presence of protonated monomers which were reported to arise in part from reactions of the molecular ions. Pulsed ion source mass spectrometry studies by Pritchard and Harrison[225] and Blair and Harrison[226] showed detailed reactions for the ethylene oxide and acetaldehyde radical cations. For the ethylene oxide ion, a reaction with neutral ethylene oxide to give protonated ethylene oxide was found (reaction 7.1) and at longer lifetimes a second product, $C_3H_5O^{+}$, was observed, and presumed to be from a reaction of an "activated" ethylene oxide ion ($C_2H_4O^{+\cdot *}$, reactions 7.2 and 7.3)

$$C_2H_4O^{+\cdot} + C_2H_4O \rightarrow C_2H_5O^{+} + C_2H_3O^{\cdot} \qquad 7.1$$

$$C_2H_4O^{+\cdot} + C_2H_4O \rightarrow C_2H_4O^{+\cdot *} + C_2H_4O \qquad 7.2$$

$$C_2H_4O^{+\cdot *} + C_2H_4O \rightarrow C_3H_5O^{+} + CH_3O^{\cdot} \qquad 7.3$$

The ethylene oxide ion was also found to react with dimethyl ether-d_6 *via* charge transfer, proton transfer, and deuteride abstraction, e.g. reactions 7.4 - 7.6.

$$C_2H_4O^{+\cdot} + (CD_3)_2O \longrightarrow \begin{cases} (CD_3)_2O^{+\cdot} + C_2H_4O & 7.4 \\ (CD_3)_2OH^{+} + C_2H_3O^{\cdot} & 7.5 \\ C_2H_4OD^{+} + CD_3OCD_2^{\cdot} & 7.6 \end{cases}$$

With neutral acetone and acetaldehyde, a transfer of $CH_2^{+\cdot}$ from the ethylene oxide molecular ion was observed[226] to give ions at m/z 72 and m/z 58 (reactions 7.7 and 7.8).

$$C_2H_4O^{+\cdot} + (CH_3)_2CO \rightarrow C_4H_8O^{+\cdot} + CH_2O \qquad 7.7$$

$$C_2H_4O^{+\cdot} + CH_3CHO \rightarrow C_3H_6O^{+\cdot} + CH_2O \qquad 7.8$$

For the acetaldehyde radical cation, a proton transfer or hydride abstraction was observed with neutral acetaldehyde (reaction 7.9).

$$CH_3CHO^{+\cdot} + CH_3CHO \rightarrow CH_3CHOH^{+} + C_2H_3O^{\cdot} \qquad 7.9$$

In a mixture of acetaldehyde and dimethyl ether-d_6 the acetaldehyde ion was found to react with the dimethyl ether-d_6 molecule, but the reaction channels were not identified. With ethylene oxide-d_4 both proton transfer and deuteride abstraction were observed (e.g. reactions 7.10 and 7.11).

$$CH_3CHO^{+\cdot} + C_2D_4O \longrightarrow \begin{cases} C_2D_4OH^{+} + C_2H_3O^{\cdot} & 7.10 \\ CH_3CHOD^{+} + C_2D_3O^{\cdot} & 7.11 \end{cases}$$

In an earlier ICR study by Beauchamp and Dunbar[227] the occurrence of reaction 7.3 had also been observed, although no mention of an "activated" ethylene oxide ion was made. In subsequent ICR studies[228] another $CH_2^{+\cdot}$ transfer reaction for the ethylene oxide ion was reported (equation 7.12), and a mechanism for reaction 7.3 was proposed[187] on the basis of deuterium labelling studies.

$$C_2H_4O^{+\cdot} + PH_3 \rightarrow CH_2PH_3^{+\cdot} + CH_2O \qquad 7.12$$

These studies[187] showed that reaction 7.3 could be explained if the structure of the activated ion ($C_2H_4O^{+\cdot *}$) was assumed to be a C---C ring-opened ethylene oxide ion e.g. reaction 7.13.

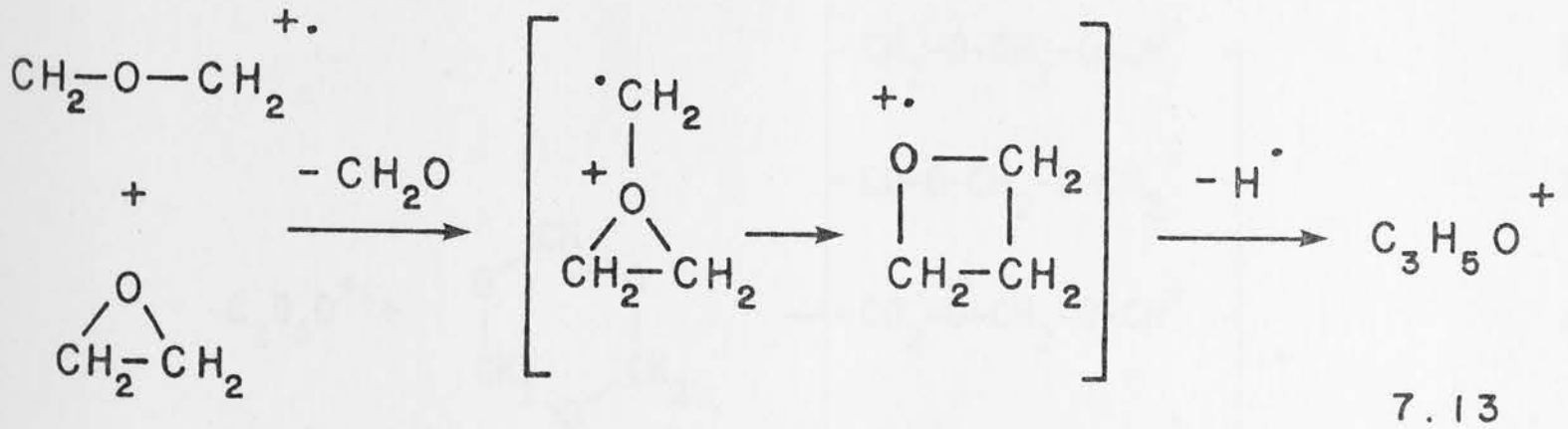

7.13

Finally, high pressure mass spectrometry studies by Kumakura and coworkers of reactions of the ethylene oxide[189,190,229,230] and acetaldehyde[189,231-234] molecular ions have been reported. For the ethylene oxide molecular ion, reactions 7.1, 7.14-7.29 were reported with ethylene oxide, acetaldehyde and trioxane.

$$C_2H_4O^{+\cdot} + C_2H_4O \begin{cases} \rightarrow CH_2CH_2O{=}CH^+ + CH_3O^\cdot & 7.14 \\ \rightarrow CH_2CH_2O{=}CH_2^{+\cdot} + CH_2O & 7.15 \end{cases}$$

$C_2H_4O^{+\cdot}$ + CD_3CDO and/or $CD_3CDO^{+\cdot}$ + C_2H_4O

→ $CH_2CH_2O\text{-}CD_2^{+\cdot}$ + CD_2O	7.16
→ $CH_2CHO\text{-}CD_3^{+\cdot}$ + CDHO	7.17
→ $CD_3CO\text{-}CH_3^{+\cdot}$ + CDHO	7.18
→ $CD_3CDO\text{-}CH_2^{+\cdot}$ + CH_2O	7.19
→ $CH_2CH_2O\text{-}CD_3^{+}$ + $CDO^{\bullet}$	7.20
→ $CD_3CDO\text{-}CH_3^{+}$ + $CHO^{\bullet}$	7.21

$C_2D_4O^{+\cdot}$ + 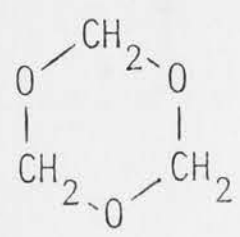

→ $C_2D_4OH^{+}$ + $C_3H_5O_3^{\cdot}$		7.22
→ $CH_2\text{-}O\text{-}CH_2\text{-}O\text{-}CH^{+}$		7.23
→ $CD\text{-}O\text{-}CH_2\text{-}O\text{-}CH_2^{+}$		7.24
→ $CD_2\text{-}O\text{-}CH_2\text{-}O\text{-}CH^{+}$	+	7.25
→ $CD\text{-}CD_2\text{-}O\text{-}CH_2\text{-}O^{+}$	fragments	7.26
→ $CD_2\text{-}CD_2\text{-}O\text{-}CH\text{-}O^{+}$		7.27
→ $CD_2\text{-}CD_2\text{-}O\text{-}CH_2\text{-}O^{+\cdot}$		7.28
→ $CD_2\text{-}CD_2O\text{-}CH_2\text{-}OH^{+}$		7.29

It should be noted that reactions 7.16 - 7.21 can arise from either or both sets of reactants, as indicated, and that these cannot be distinguished by the experimental method employed. For reactions 7.16 - 7.21 and 7.23 - 7.29 the intermediacy of a C---O ring-opened ethylene oxide species ($CH_2\text{-}CH_2\text{-}O^{+\cdot}$) was postulated[189,190]. The acetaldehyde radical cation was reported to react with

acetaldehyde, ethylene oxide, trioxane and *n*-propylacetate (reactions 7.9, 7.16 - 7.21 and 7.30 - 7.39).

$$CD_3CHO^{+\cdot} + CD_3CHO \rightarrow \begin{cases} CD_3CHO\text{-}CD^+ + CD_2HO^\cdot & 7.30 \\ CD_3CHO\text{-}CD_2^{+\cdot} + CDHO & 7.31 \\ CD_3CO\text{-}CD_3^{+\cdot} + CH_2O & 7.32 \\ CD_3CHO\text{-}CD_3^+ + CHO^\cdot & 7.33 \end{cases}$$

$$CD_3CDO^{+\cdot} + \begin{array}{c} O \diagup CH_2 \diagdown O \\ | \qquad\qquad | \\ CH_2 \diagdown O \diagup CH_2 \end{array} \rightarrow \begin{cases} CD_3CDOH^+ + C_3H_5O_3^\cdot & 7.34 \\ CD_3CO\text{-}CH_2O^+ \\ CD_3CDO\text{-}CHO^+ \\ CD_3CDO\text{-}CH_2O^+ \\ CD_3CDO\text{-}CH_2OH^+ \end{cases} \begin{array}{l} 7.35 \\ + \\ \text{fragments} \\ \\ \end{array} \begin{array}{l} \\ 7.36 \\ \\ 7.37 \\ 7.38 \end{array}$$

$$CD_3CDO^{+\cdot} + CH_3COOC_3H_7 \rightarrow CH_3COOC_3H_7D^+ + CD_3CO^\cdot \qquad 7.39$$

7.3 EVALUATION

In the preceding section, experimental information which was available or was reported during the present study (Chapters 8 and 10) of the $C_2H_4O^{+\cdot}$ isomers has been reviewed. There are substantial differences in the experimental methods utilized and the limitations of these, as they affect the interpretation of the results, are discussed below.

The thermochemical data show that the ethylene oxide and acetaldehyde ions are well-established, distinguishable $C_2H_4O^{+\cdot}$ isomers. The heat

of formation reported for the vinyl alcohol ion shows it to be different from the other two isomers. However, since this ΔH_f value was obtained from appearance potential measurements, it must be taken as an upper limit to the true value[164,179]. This also applies to the ΔH_f value obtained for the m/z 44 ion from 1,3-dioxolane. One limitation of this method is that, by definition, only ions formed at or just above threhold can be studied.

The metastable ion studies have verified the thermochemical measurements regarding the distinguishability of the ethylene oxide, acetaldehyde and vinyl alcohol ions. It must be stressed, however, that with the two methods ions of different lifetimes and stabilities are examined. Whereas the thermochemical measurements look at stable ions of low energy, metastable ion studies are concerned with ions which are unstable, and decompose within narrow time frames. This fragmentation occurs before the ions have traversed the mass spectrometer, and thus their lifetimes are short (10^{-7} to 10^{-5} sec). It should be noted that in the metastable ion study the possibility that a fourth $C_2H_4O^{+\cdot}$ isomer (CH_2-O-$CH_2^{+\cdot}$) might exist was discussed.

The collisional activation studies involve stable ions (i.e. with lifetimes $\gtrsim 10^{-5}$ sec), which through collisions are transformed into higher energy, fragmenting ions. In such a study, the ethylene oxide, acetaldehyde and vinyl alcohol ions were distinguished, but the possibility of other $C_2H_4O^{+\cdot}$ isomers existing in addition to the three known isomers was not examined.

The identification of isomers by way of ion/molecule reactions is a very sound method, since it is concerned with stable ions of long lifetimes and thus of low energies, and is analogous to similar methodology used in

solution chemistry. In ion cyclotron resonance experiments, ions with lifetimes of 10^{-3} sec or greater can be studied. The pulsed ion source and high pressure mass spectrometry techniques have one great disadvantage, in that the reacting ion which is proposed to be involved in an ion/molecule reaction can only *indirectly* be identified. This problem does not occur in ICR spectrometry, where the double resonance technique makes it possible to identify the reacting ion (see Chapter 9). Ion/molecule reaction studies have proposed the existence of two $C_2H_4O^{+\cdot}$ ions apart from the three well-established ones. One proposal[187] involves a C---C ring-opened ethylene oxide isomer, the other[189,190] a C---O ring-opened ethylene oxide ion. For neither definitive proof of its existence was given.

CHAPTER 8

STRUCTURES AND STABILITIES OF $C_2H_4O^{+\cdot}$ ISOMERS: THEORETICAL STUDY

8.1 INTRODUCTION

As stated in Chapter 7, the identification of the structures of the different isomers of gas-phase cations is important since knowledge of the structures and relative energies of these ions can assist in understanding mass spectrometric rearrangement and fragmentation processes. For this reason, and in combination with an ICR study (Chapter 10) of the $C_2H_4O^{+\cdot}$ isomers, an *ab initio* molecular orbital study has been undertaken of these isomers. Eleven potentially stable species have been examined [(71) - (81)].

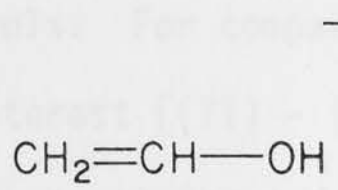

(71)

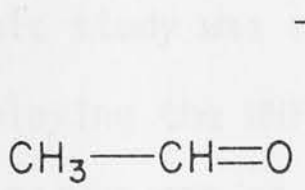

(72)

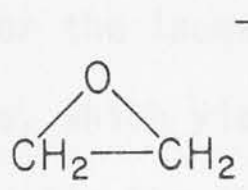

(73)

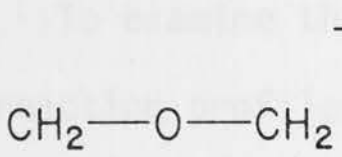

(74)

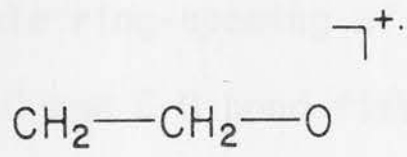

(75)

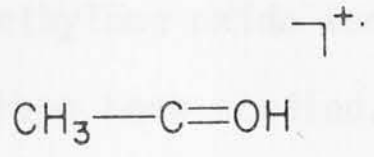

(76)

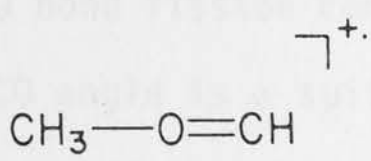

(77)

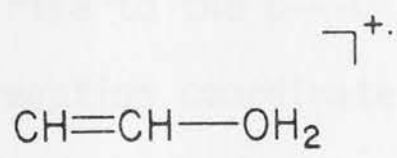

(78)

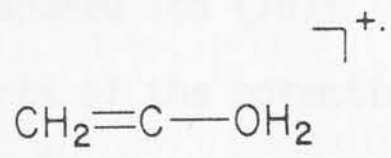

(79)

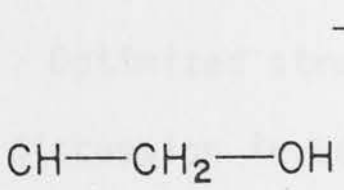

(80)

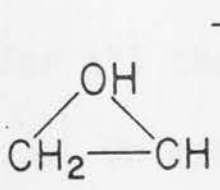

(81)

The study described in this chapter was undertaken with three principal objectives, namely to determine: (i) those isomers which are at minima in the $C_2H_4O^{+\cdot}$ potential energy surface, and thus might occur as stable ionic

species, (ii) the structures of these isomers and, (iii) the relative energies of these isomers.

8.2 METHOD

The study of the $C_2H_4O^{+\cdot}$ isomers was performed at various levels of theory. It involved, for all isomers, a complete optimization of the geometry, subject only to specified symmetry constraints (C_{2v} for (73), C_1 for (81), C_s for the remaining isomers), using the RHF procedure at the STO-3G level, followed by single energy calculations at the 4-31G and the 6-31G* levels. For comparison, this study was repeated for the isomers of special interest [(71) - (75)] employing the UHF procedure, which yielded UHF/STO-3G geometries and UHF/4-31G//UHF/STO-3G energies. Finally, the isomers (71) - (75) were reoptimized at the RHF/4-31G level.

To examine the possible ring-opening of the ethylene oxide ion (73), the reaction profiles for C-C and C-O bond fission have been studied, using the UHF/4-31G//UHF/STO-3G approach. C-C bond fission will lead to the C---C ring-opened form (74), and a suitable reaction coordinate is the COC angle. C-O bond fission can give rise to the C---O ring-opened ion (75); here the CCO angle is a suitable reaction coordinate. Parts of the potential energy surface interconnecting some of the additional $C_2H_4O^{+\cdot}$ isomers were also examined (at the RHF/4-31G//RHF/STO-3G level) and are discussed below.

Optimized structures for all the ions studied are displayed within the discussion in Section 8.3. Unless otherwise noted, these refer to RHF/STO-3G results. For ions (71) - (75), where optimizations were also carried out at the UHF/STO-3G and RHF/4-31G levels, all three sets of parameters are shown in the order RHF/STO-3G, UHF/STO-3G and RHF/4-31G. In the discussion, reference will be made to RHF/6-31G*//RHF/STO-3G energies, unless otherwise stated.

8.3 STRUCTURES, ENERGIES AND RELATIVE STABILITIES OF THE $C_2H_4O^{+\cdot}$ ISOMERS

Since experimental techniques had established the existence of (71), (72) and (73) as stable, non-interconverting isomers of $C_2H_4O^{+\cdot}$, and (74) and (75) had been postulated as possible fourth and fifth isomers (Chapter 7), an initial study of these species was carried out. All five isomers were optimized at the RHF/STO-3G, UHF/STO-3G and RHF/4-31G levels. Though producing lower energies than RHF, the UHF procedure is known to run occasionally into problems due to contamination from states of higher spin multiplicity[23]. The present study provides a further comparison between the two procedures.

CH_2=CH-$OH^{+\cdot}$ (71). In agreement with thermochemical measurements[79], the vinyl alcohol radical cation is found to be the lowest energy $C_2H_4O^{+\cdot}$ isomer. Noteworthy is the position of the hydroxyl hydrogen, which is found to be *anti* in the radical cation, whereas in neutral vinyl alcohol it is found to be *syn*, both experimentally[64] and theoretically (Chapter 2).

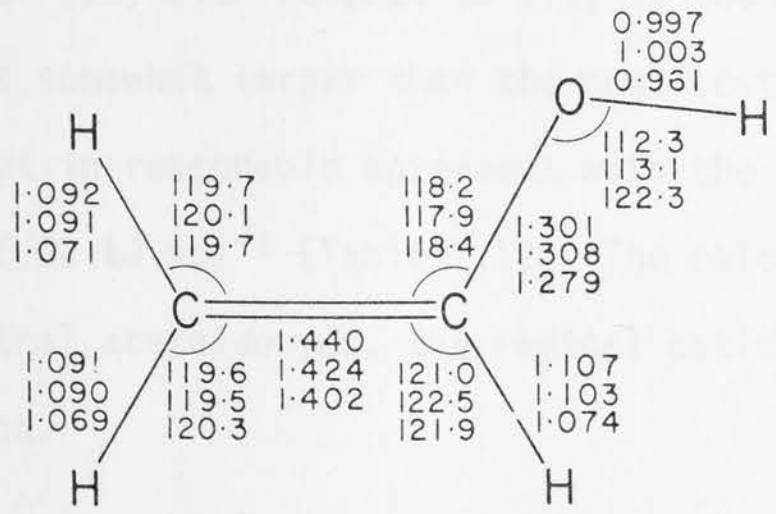

(71)

For the radical cation, the *syn* isomer is found to be 12.6 kJ mol^{-1} (with

RHF/4-31G//RHF/STO-3G as well as UHF/4-31G//UHF/STO-3G) higher than the *anti* isomer[†]. Examination of the highest occupied molecular orbital (HOMO) in the neutral, and the singly occupied molecular orbital (SOMO) in the radical cation, shows that the electron has been removed from a π-orbital (82). Removal of an electron from this orbital would be expected to, and indeed does, lead to a lengthening of the C=C bond (+0.13 Å with RHF/STO-3G, +0.11 Å with UHF/STO-3G, and +0.09 Å with RHF/4-31G, cf. Chapter 2), and a shortening of the C-O bond (e.g. -0.09 Å with RHF/4-31G).

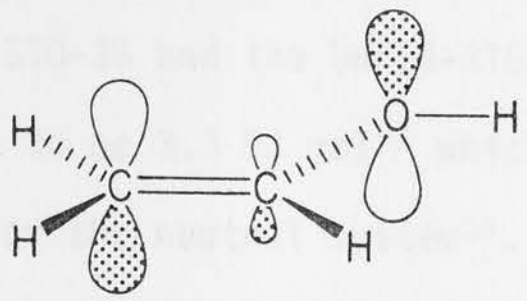

(82)

CH_3-CH=O (72). The best estimate (RHF/6-31G*//RHF/STO-3G) of the relative energy of (72) with respect to (71) is found to be 52.3 kJ mol^{-1} (Table 8.1), which is somewhat larger than the next best value of 46.4 kJ mol^{-1} (RHF/4-31G level), but in reasonable agreement with the experimentally determined[79] value of 62 kJ mol^{-1} (Table 7.1). The calculations show that, as found for the neutral acetaldehyde, the radical cation has one C-H bond eclipsing the C=O bond.

---

† Optimized structural parameters [RHF/STO-3G(UHF/STO-3G)] for the *syn* vinyl alcohol radical cation are: C=C 1.448 (1.430), C-O 1.296 (1.306), C-H_c 1.091 (1.091), C-H_t 1.090 (1.090), C-H_u 1.108 (1.104), O-H 0.998 (1.005), <CCO 125.3 (124.1), <H_cCC 120.9 (121.3), <H_tCC 119.1 (119.1) <H_uCC 120.8 (122.3), <HOC 113.0 (113.6), where H_c and H_t denote the hydrogens *cis* and *trans* with respect to the hydroxyl group, and H_u denotes the unique hydrogen. Total energies are: RHF/STO-3G -150.68669, RHF/4-31G//RHF/STO-3G -152.36654, UHF/STO-3G -150.69425 and UHF/4-31G//UHF/STO-3G -152.37039.

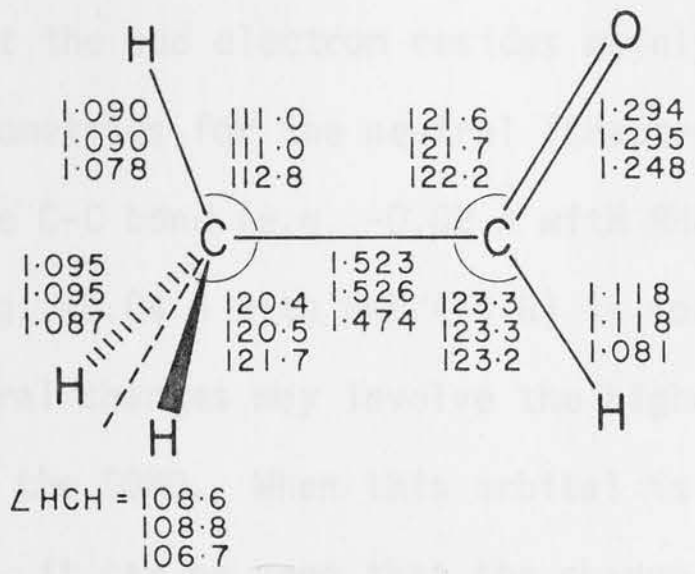

(72)

At both the RHF/4-31G//RHF/STO-3G and the UHF/4-31G//UHF/STO-3G levels† the rotational barrier is found to be 3.3 kJ mol^{-1} which is close to the barrier calculated (3.1 kJ mol^{-1}) for the neutral system[51]. Examining the HOMO for neutral acetaldehyde and the SOMO for the radical cation, it is found that the orbital in each case is a σ-orbital, with the largest coefficient on the oxygen (83).

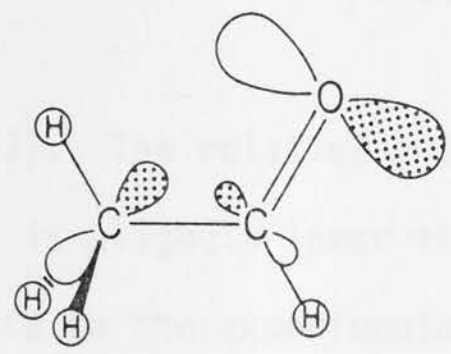

(83)

† Optimized structural parameters [RHF/STO-3G(UHF/STO-3G)] for the staggered acetaldehyde radical cation are; C-C 1.528 (1.520), C=O 1.295 (1.295), C-H_t 1.088 (1.089), C-H_s 1.095 (1.094), C-H 1.119 (1.118), <CCO 121.4 (121.4), <H_tCC 109.1, <CCH_{ss} 122.8 (123.2), <HCC 124.0 (124.1), < H_sCH_s 109.0 (109.2), where H_t denotes the methyl hydrogen *trans* with respect to O, H_s denotes the methyl hydrogens staggered with respect to O, and H_{ss} denotes the H_sCH_s plane. Total energies are: RHF/STO-3G -150.70797, RHF/4-31G//RHF/STO-3G -152.35418, UHF/STO-3G -150.71285 and UHF/4-31G//UHF/STO-3G -152.35824.

This implies that the odd electron resides mainly on the oxygen. Comparing the optimized geometries for the neutral (Chapter 2) and the ion, a slight shortening of the C-C bond (e.g. -0.02 Å with RHF/4-31G) and a lengthening of the C=O bond (e.g. +0.04 Å with RHF/4-31G) is found. This suggests that the observed structural changes may involve the highest occupied π-orbital even though it is not the SOMO. When this orbital is examined for the neutral (84) and the ion (85), it can be seen that the change in this orbital is consistent with the observed structural change upon ionization: the antibonding character in the C-C bond has decreased, and also the bonding character in the C=O bond has decreased.

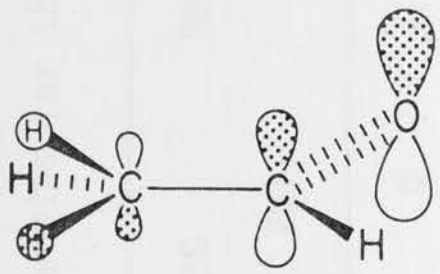

(84)

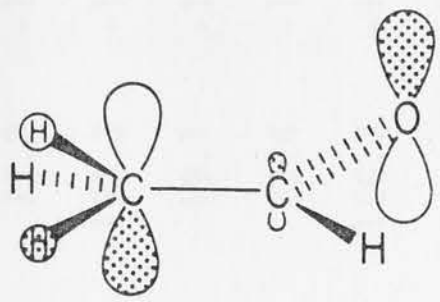

(85)

$\overline{CH_2\text{-}O\text{-}CH_2}^{+\cdot}$ (73). The relative energy of this ion is calculated to be 182.6 kJ mol^{-1}, which is slightly lower than the 4-31G basis set calculations, but quite close to the experimental value[79] of 209 kJ mol^{-1}. The HOMO and SOMO of ethylene oxide and its radical cation have π-symmetry and are almost exclusively located on the oxygen (86). This is in agreement with photoelectron studies[235], which show that (73) is formed by removal of an electron from the $2b_1$ π-type orbital which is largely localized on the oxygen atom.

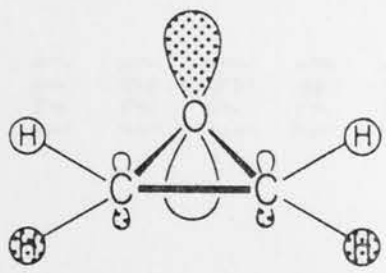

(86)

Table 8.1 Calculated Total Energies and Relative Energies for the $C_2H_4O^{+\cdot}$ Isomers.

Isomer[a]	Symmetry	State	RHF/STO-3G		RHF/4-31G//RHF/STO-3G		RHF/6-31G*//RHF/STO-3G	
			Total	Rel.	Total	Rel.	Total	Rel.
(71)	C_s	$^2A''$	-150.68963	0	-152.37139	0	-152.59996	0
(72)	C_s	$^2A'$	-150.70959	-52.4	-152.35545	41.9	-152.58005	52.3
(73)	C_{2v}	$^2B_1$	-150.68291	17.6	-152.29780	193.2	-152.53041	182.6
(74)	C_s	$^2A'$	-150.66022	77.2	-152.32124	131.7	-152.55238	124.9
(75)	C_s	$^2A''$	-150.63240	150.3	-152.29583	198.4	-152.50958	237.3
(76)	C_s	$^2A'$	-150.68232	19.1	-152.34367	72.8	-152.57244	72.3
(77)	C_s	$^2A'$	-150.66169	73.4	-152.31730	142.0	-152.54788	136.7
(78)	C_s	$^2A'$	-150.63008	156.3	-152.31161	157.0	-152.51891	212.8
(79)	C_s	$^2A'$	-150.62694	164.6	-152.30408	176.7	-152.51114	233.2
(80)	C_s	$^2A'$	-150.57823	292.5	-152.25879	295.6	-152.48131	311.5
(81)	C_1	^2A	-150.64318	122.0	-152.28058	238.4	-152.51634	219.5

[a] For geometries, see text.

Table 8.1 (Cont'd)

Isomer	UHF/STO-3G Total	UHF/STO-3G Rel.	UHF/4-31G//UHF/STO-3G Total	UHF/4-31G//UHF/STO-3G Rel.	RHF/4-31G Total	RHF/4-31G Rel.
(71)	-150.69695	0	-152.37521	0	-152.37806	0
(72)	-150.71438	-45.8	-152.35950	41.2	-152.36040	46.4
(73)	-150.68566	29.6	-152.30109	194.6	-152.30389	194.7
(74)	-150.66250	90.4	-152.32344	135.9	-152.32724	133.4
(75)	-150.63354	166.5	-152.29761	203.7	-152.30221	199.1

Comparison of the optimized geometries of neutral ethylene oxide (Chapter 2) and its radical cation, however, shows a lengthening of the C-O bonds (e.g. +0.14 Å with RHF/4-31G) upon ionization.

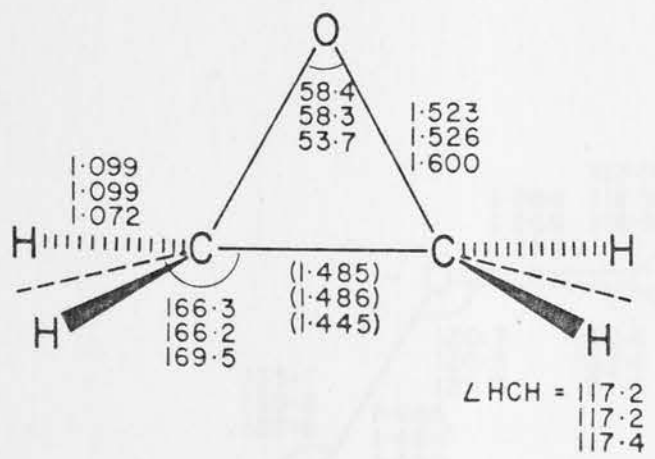

(73)

A rationalization of this increase can be found by looking at the highest doubly-occupied π-type orbital (not the HOMO) for the neutral (87) and the ionic (88) species. Whereas in (87) the molecular orbital is providing bonding between all three heavy atoms, the molecular orbital in (88) is centered mainly on the carbon atoms, which may account for the observed shortening of the C-C and lengthening of the C-O bonds.

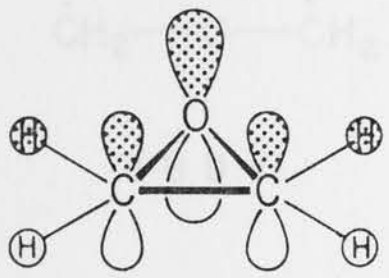

(87)

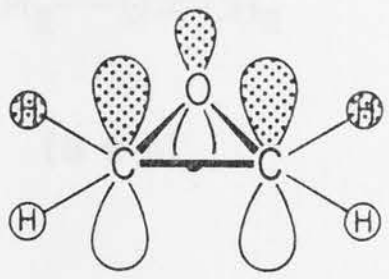

(88)

$\underline{CH_2\text{-}O\text{-}CH_2}^{+\cdot}$ (74). In Chapter 7, it was reported that a $C_2H_4O^{+\cdot}$ isomer of this structure had been proposed by Beauchamp[187] as the reacting species in the ion/molecule reaction of ionized ethylene oxide with neutral ethylene oxide (reaction 7.13). Ion (74) can be considered to arise from the ethylene oxide ion by C-C bond cleavage. The calculations show that this C---C ring-opened ethylene oxide ion is about 58 kJ mol^{-1} lower in energy than the ethylene oxide radical cation (73).

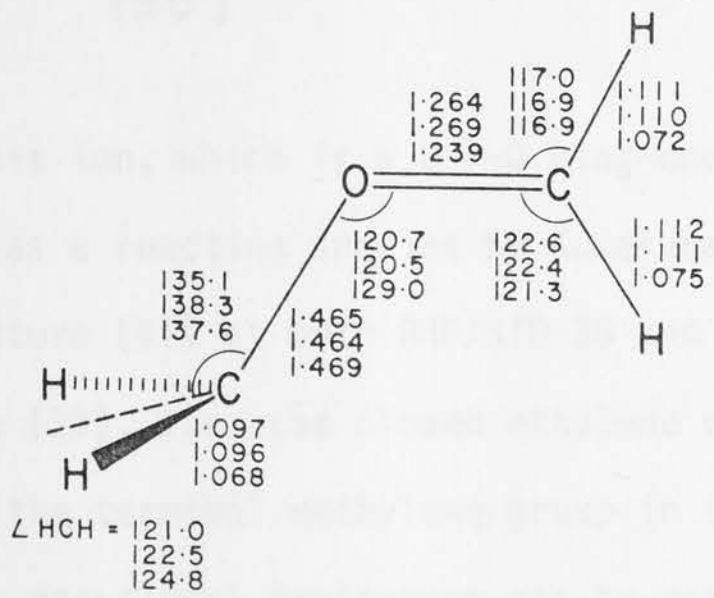

(74)

The calculated geometry of (74) has some interesting features. One C-O bond is much shorter than the other, and the CH_2 group on the side with the weaker C-O bond is perpendicular to the plane of the rest of the molecule. This suggests a significant contribution of the asymmetric valence structure (89b).

(89a) (89b)

This geometry provides an immediate rationalization for the observed ion/molecule reactions[187,226,228] of (74) (see Chapters 7 and 10), in which it transfers a $CH_2^{+\cdot}$ moiety to the neutral molecule with which it reacts. The SOMO (90) of (74) demonstrates the radical character at the carbon of the perpendicular CH_2 group.

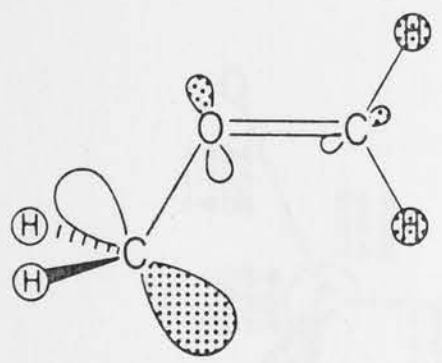

(90)

$\underline{CH_2\text{-}CH_2\text{-}O}^{+\cdot}$ (75). This ion, which is a C---O ring-opened ethylene oxide ion isomer, was proposed as a reacting species by Kumakura *et al.*[189,190]. Initial optimization of structure (91) at both RHF/STO-3G and UHF/STO-3G levels led directly to structure (73), i.e. the closed ethylene oxide radical cation. However, rotation of the terminal methylene group in (91) did lead to a stable structure (75). This rotational preference can be rationalized by hyperconjugative interaction. The oxygen is strongly σ-electron withdrawing, and has therefore a relative destabilizing interaction with the neighbouring cationic centre (91a). Thus (75) is found to have the preferred conformation shown below, a result similar to that obtained[93,236] for $F\text{-}CH_2\text{-}CH_2^{+}$.

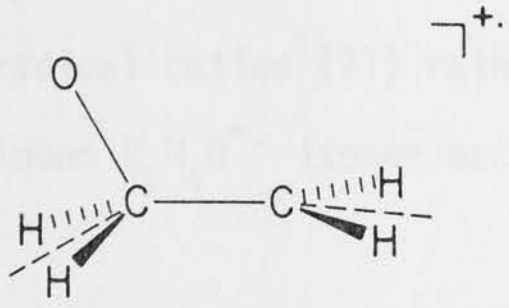

(91)

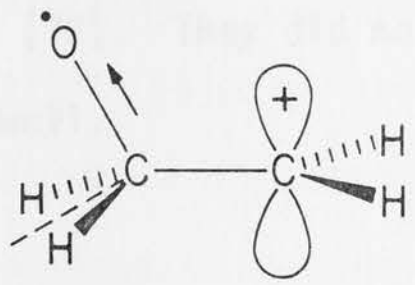

(91 a)

The energy of (75) relative to (73) is 54.7 kJ mol^{-1} (RHF/6-31G*//RHF/STO-3G). In this case, the relative energy is substantially larger with 6-31G* than 4-31G.

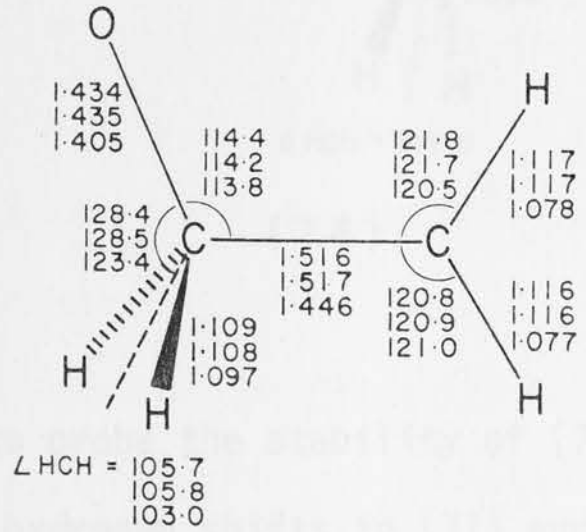

(75)

For the remaining $C_2H_4O^{+\cdot}$ isomers [(76) - (81)], optimizations were only carried out at the RHF/STO-3G level.

CH_3-C=O$H^{+\cdot}$ (76). This isomer has a surprisingly low energy of 72 kJ mol^{-1} relative to (71). The occurrence of (76) as an unstable intermediate formed by CO_2 loss from the pyruvic acid molecular ion had been previously postulated by Turro *et al.*[186], where they assumed subsequent isomerization of (76) to the acetaldehyde radical cation (72). In their metastable ion study, Holmes and Terlouw[188] also studied the m/z 44 ion

from the pyruvic acid molecular ion, and found it to correspond to the vinyl alcohol radical cation (71) rather than to (72). They did note the possibility of an unknown $C_2H_4O^{+\cdot}$ isomer occurring as well.

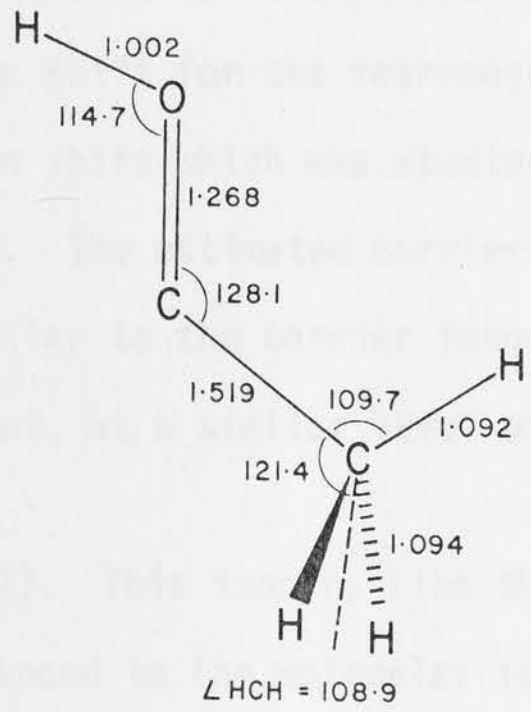

(76)

In order to probe the stability of (76), two possible isomerizations of (76), by way of 1,2-hydrogen shifts to (71) and (72), have been examined. An approximation to the barriers has been obtained by optimizing structures in which the moving hydrogen was constrained to be halfway along the C-C or C-O bond [(92), (93)].

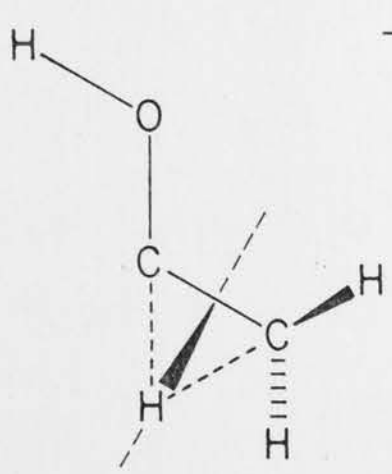

(92)

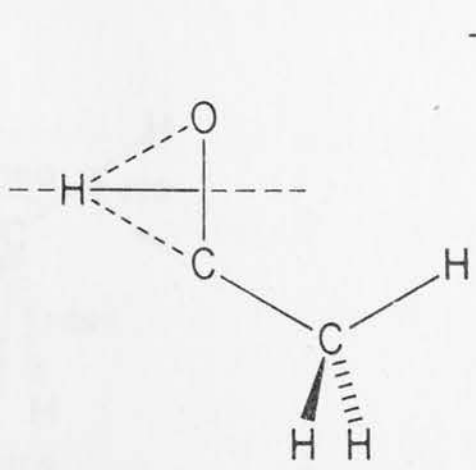

(93)

This leads to lower limits for the barriers of 167 and 264 kJ mol^{-1}, respectively (RHF/4-31G//RHF/STO-3G). These results support the experimental findings of Holmes and Terlouw [namely that (76) is more likely to rearrange to (71) than to (72)], but also suggest that under the appropriate conditions (76) might be sufficiently stable to be experimentally observed. It should be noted that the 1,2-hydrogen shift for the rearrangement of (76) to (72) is similar to the 1,2-hydrogen shift which was studied for the hydroxymethylene radical cation (Chapter 6). The estimated barrier height for the rearrangement discussed here is very similar to the barrier found for the hydroxymethylene radical cation rearrangement, at a similar level of theory.

$\underline{CH_3\text{-}O{=}CH^{+\cdot}}$ (77). This isomer, like the one previously discussed, can be considered to correspond to the molecular ion of a carbenoid species, in this case methoxymethylene. The energy calculated relative to (71) is 137 kJ mol^{-1}, which is lower than that of one of the observed isomers, (73). Although it has not yet been detected experimentally, there seems to be a reasonable prospect of (77) occurring as a stable $C_2H_4O^{+\cdot}$ isomer if a suitable precursor ion species can be found.

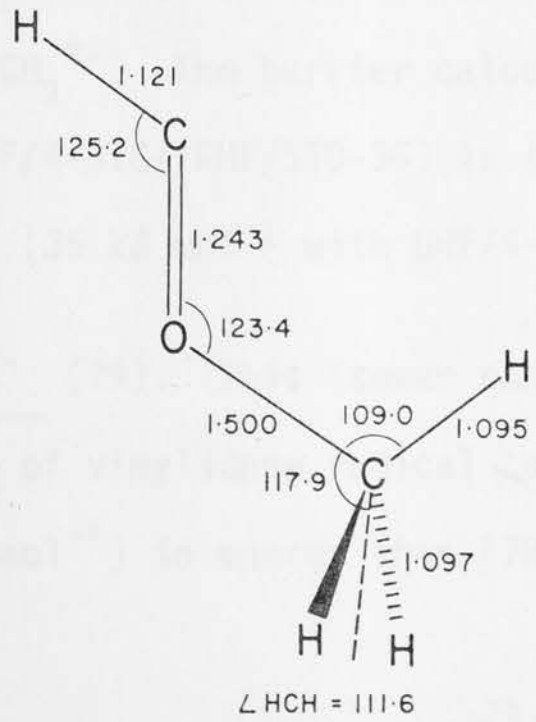

(77)

CH=CH-$OH_2^{+\cdot}$ (78). This isomer, which is somewhat higher in energy, was also found to lie at a potential minimum in the $C_2H_4O^{+\cdot}$ surface. The short C-C bond and the long C-O bond suggest that it might be considered a complex of H_2O and $HC{\equiv}CH^{+\cdot}$.

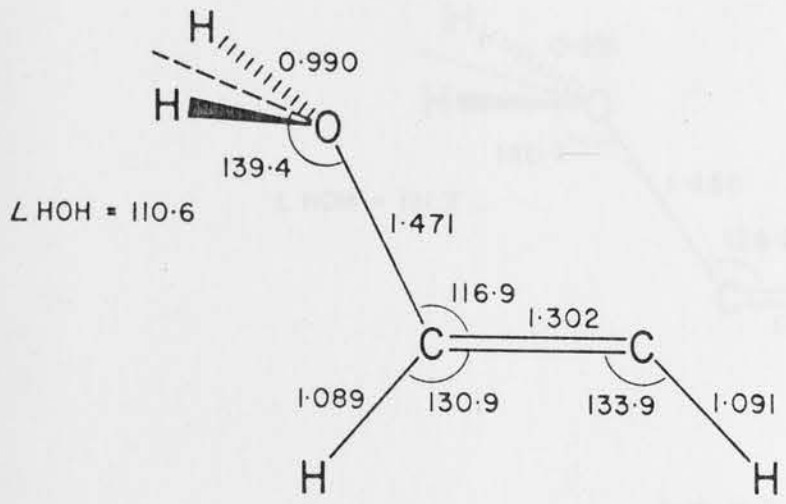

(78)

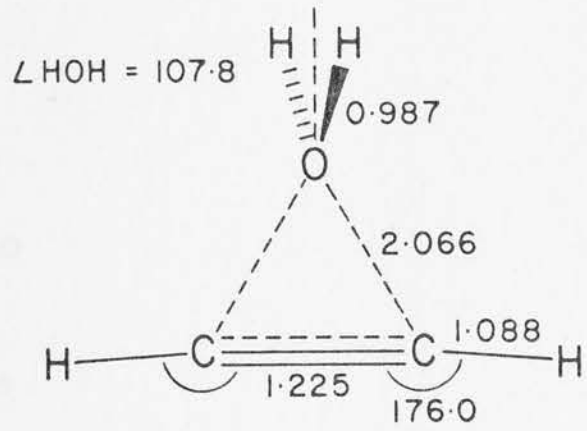

(94)

At the RHF/4-31G//RHF/STO-3G level, this complex is calculated to be 162 kJ mol^{-1} more stable than separated H_2O and $HC{\equiv}CH^{+\cdot}$[†]. When the C-O bond length is selected as reaction coordinate, it is found that dissociation of the complex passes through a structure with C_{2v} symmetry. The optimized C_{2v} structure (94) can be considered to be the transition state for the degenerate isomerization of (78). This isomerization is similar to that previously studied[237] for the complex of H_2O and $H_2C{=}CH_2^{+\cdot}$. The barrier calculated for the isomerization of (78) (73 kJ mol^{-1} at RHF/4-31G//RHF/STO-3G) is somewhat higher than the barrier found for CH_2-CH_2-$OH_2^{+\cdot}$ (35 kJ mol^{-1} with UHF/4-31G//UHF/STO-3G).

CH_2=C-$OH_2^{+\cdot}$ (79). This isomer can, by analogy with (78), be considered as a complex of vinylidene radical cation and water. It is only slightly higher (20 kJ mol^{-1}) in energy than (78). However, it should be

---

[†] 4-31G//STO-3G energy for H_2O: -75.90324[70]; RHF/4-31G//RHF/STO-3G energy for $HC{\equiv}CH^{+\cdot}$: -76.34686 with C≡C = 1.247 Å, C-H = 1.101 Å.

noted that an isomerization by means of a 1,2-hydrogen shift could lead to the most stable $C_2H_4O^{+\cdot}$ isomer, (71). Considering that (79) is 233 kJ mol^{-1} higher in energy than (71), the barrier for this isomerization might be small [cf. the barriers calculated for 1,2-hydrogen shifts in (76)].

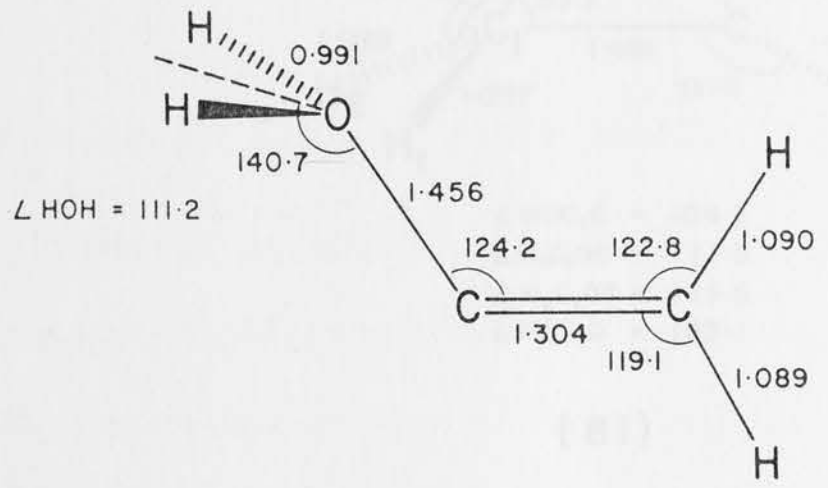

(79)

$\underline{CH\text{-}CH_2\text{-}OH^{+\cdot}}$ (80). Included in this study as another possible isomer is (80). The structure is found to prefer C_s symmetry with distortions leading to an increase in energy. (80) is found to be extremely high in energy, and is thus unlikely to be significant experimentally.

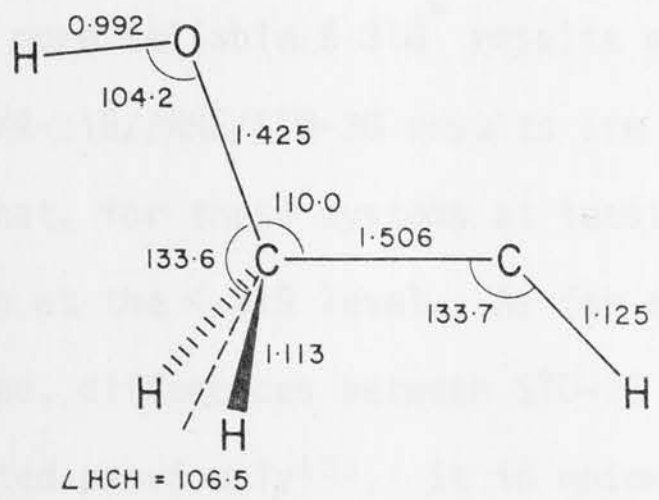

(80)

$\overline{\underline{CH\text{-}CH_2\text{-}OH^{+\cdot}}}$ (81). Structure (81) is a ring-closed isomer of (80) and is also of quite high energy. Although (81) is significantly lower in energy than (80), the ring closure is not found to occur without a barrier.

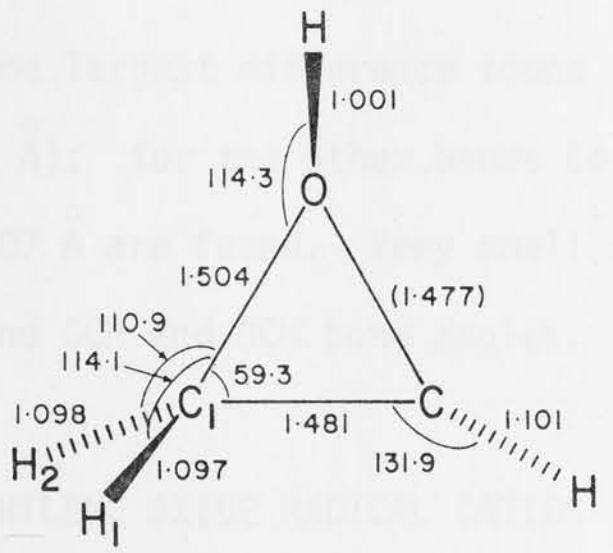

$\angle HOC_1C = 104{\cdot}2$
$\angle H_1C_1OC = -111{\cdot}9$
$\angle H_2C_1OC = 113{\cdot}5$
$\angle HCC_1O = 103{\cdot}1$

(81)

8.4 COMPARISON OF THEORETICAL PROCEDURES

Since the $C_2H_4O^{+\cdot}$ isomers (71) - (75) were studied in detail with various approaches, it is possible to compare the RHF/6-31G*//RHF/STO-3G results with the RHF/4-31G//RHF/STO-3G, UHF/4-31G//UHF/STO-3G and the RHF/4-31G results. The relative energies calculated with all four methods are generally very similar, with only isomer (75) showing a substantial difference between the more reliable 6-31G* results and those of the simpler calculations. The RHF/4-31G//RHF/STO-3G results are very similar to those with RFH/4-31G indicating that, for these systems at least, there is no significant advantage in optimizing at the 4-31G level. As far as the optimized geometries are concerned, differences between STO-3G and 4-31G results are similar to those reported previously[158]. It is noteworthy, however, that STO-3G and 4-31G predict similar *changes* in geometry when going from the neutral species to the corresponding ions. Finally, the generally good agreement between the RHF and UHF structures for the $C_2H_4O^{+\cdot}$ isomers (71) - (75) is noted. Even for multiple bonds, for which the differences between UHF and RHF have been previously found to be large because of contamination

of UHF by states of higher multiplicity[23], the results obtained by the two methods are very similar. The largest difference found in this study is for the C=C bonds of (71) (0.016 Å); for the other bonds between heavy atoms differences smaller than 0.007 Å are found. Very small differences are also found for C-H bond lengths and CCH and OCH bond angles.

8.5 RING OPENING IN THE ETHYLENE OXIDE RADICAL CATION

In order to assess the stability of the closed ethylene oxide ion (73) with respect to ring opening to give the open ethylene oxide ions (74) or (75), the potential energy surfaces linking (73) with (74) and (73) with (75) have been examined using the 4-31G//STO-3G approach. For the study of the ring opening, the UHF method has been employed, in the expectation that this method should provide a better description of intermediate regions on the $C_2H_4O^{+\cdot}$ potential energy surface.

8.5.1 FISSION OF THE CARBON-CARBON BOND

The COC angle was chosen as a convenient reaction coordinate. For fixed values of <COC, a number of structures were fully optimized, subject only to a C_s symmetry constraint. For the closed ethylene oxide ion (73), it was found that the best structure actually has C_{2v} symmetry, leading to a ground state of $^2A''(C_s) \rightarrow {}^2B_1(C_{2v})$. In this structure there are five electrons in π-type orbitals, as indicated in Figure 8.1. As the COC angle widens from its value in (73), the optimized structures continue to have C_{2v} symmetry, and the energy rises rapidly. When <COC is larger than 72°, the $^2A'(C_s)$ state (with six π-electrons) becomes energetically more favourable. For <COC between 72° and 90°, these structures prefer C_{2v} symmetry over C_s symmetry.

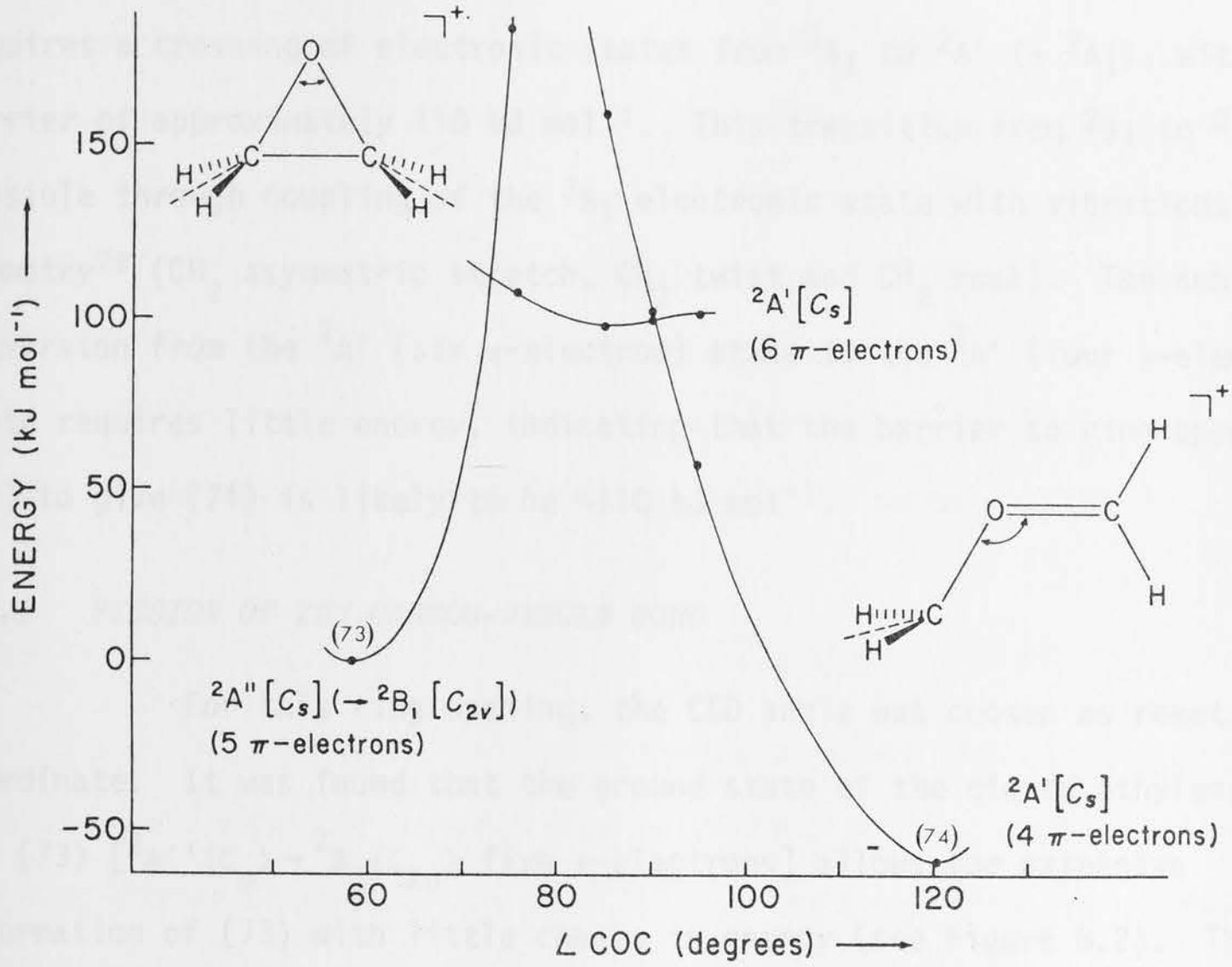

Fig. 8.1 Reaction profile for the ring opening of the closed ethylene oxide ion (73) by C-C bond fission. The number of π-electrons for the systems described by the individual potential curves is shown in brackets.

This state has a potential energy minimum at ‹COC = 75.6° (UHF/STO-3G), which at the 4-31G//STO-3G level has shifted somewhat towards a larger COC angle. At ‹COC = 90° this $^2A'$ state becomes isoenergetic with a second $^2A'$ (C_s) state with four π-electrons. The latter leads to the open ethylene oxide ion (74) which has a stable minimum for ‹COC = 120.5°. Going from the $^2A'$ (six π-electron) state to the $^2A'$ (four π-electron) state requires rotation of one of the CH_2 groups by 90° leading to coplanarity of this group with the heavy-atom system. This rotation is likely to take place when ‹COC ∼ 90°. Optimization of an ion with ‹COC = 90°, and one CH_2 group rotated through 45°, showed only a slight increase in energy (∼ 4 kJ mol^{-1}) over the unrotated form.

Thus it is found that interconversion of (73) to (74) initially requires a crossing of electronic states from $^2B_1$ to $^2A'$ ($\rightarrow {}^2A_1$), with a barrier of approximately 110 kJ mol^{-1}. This transition from $^2B_1$ to $^2A_1$ is possible through coupling of the $^2B_1$ electronic state with vibrations of b_1 symmetry[78] (CH_2 asymmetric stretch, CH_2 twist and CH_2 rock). The subsequent conversion from the $^2A'$ (six π-electron) state to the $^2A'$ (four π-electron) state requires little energy, indicating that the barrier to ring opening of (73) to give (74) is likely to be $\sim$110 kJ mol^{-1}.

8.5.2 FISSION OF THE CARBON-OXYGEN BOND

For this ring opening, the CCO angle was chosen as reaction coordinate. It was found that the ground state of the closed ethylene oxide ion (73) [$^2A''(C_s) \rightarrow {}^2B_1(C_{2v})$, five π-electrons] allows for extensive deformation of (73) with little change in energy (see Figure 8.2). The

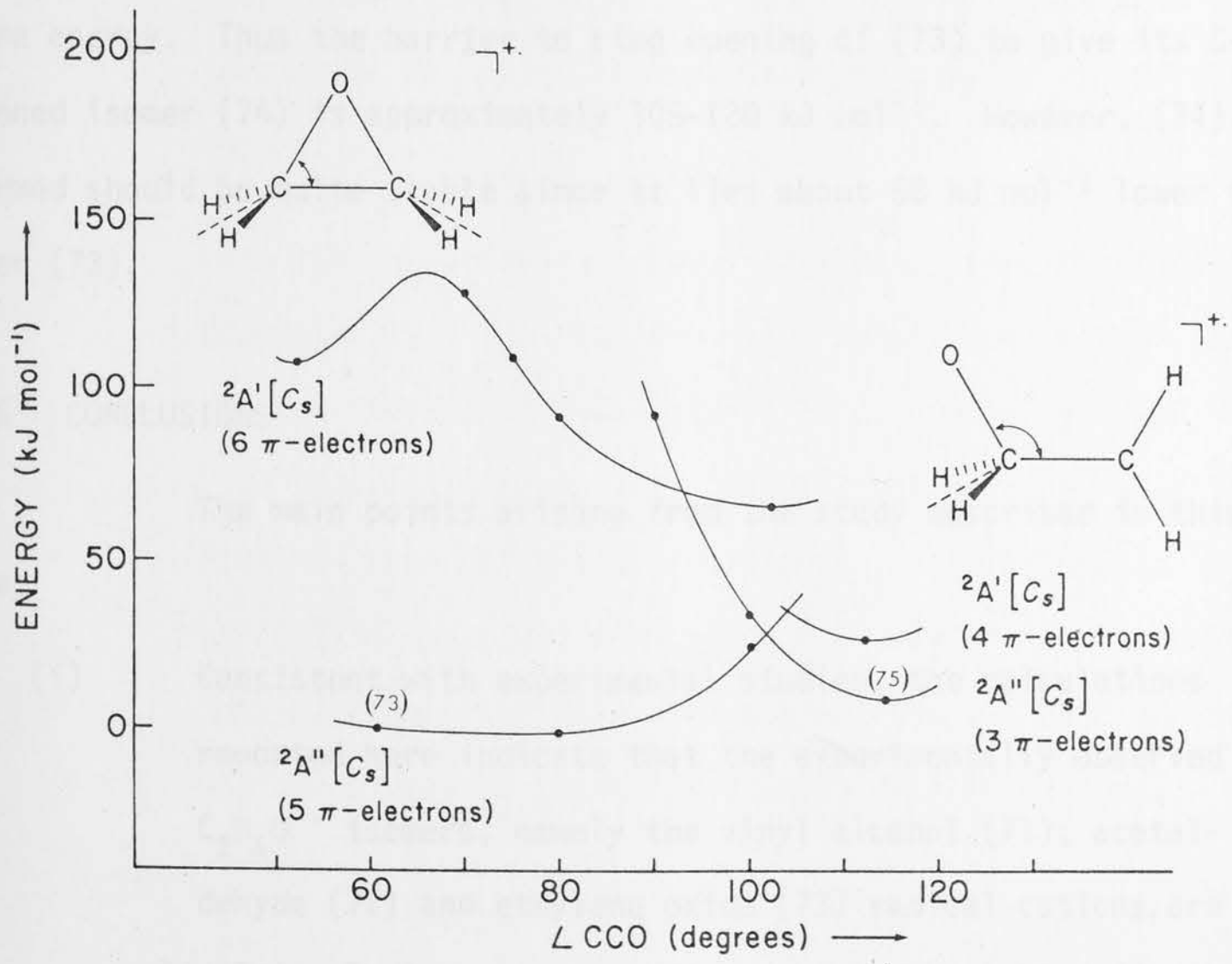

Fig. 8.2 Reaction profile for the ring opening of the closed ethylene oxide ion (73) by C-O bond fission. The number of π-electrons for the systems described by the individual potential curves is shown in brackets.

excited state of (71) [$^2A'(C_s)$, six π-electrons] lies higher in energy. The C---O ring-opened form of the ethylene oxide ion (75) has a $^2A''$ (three π-electron) ground state with a $^2A'$ (four π-electron) state lying several kJ mol^{-1} higher in energy. Rearrangement of (75) to (73) can take place by rotation of the terminal methylene group through 90°, coupled with ring closure. At the UHF/4-31G//UHF/STO-3G level, the barrier is 25-30 kJ mol^{-1} and occurs at $<CCO \sim 102°$. At the 6-31G* level, the relative energy of (75) is increased and the barrier to rearrangement to (73) is likely to be decreased.

8.5.3 THE STABILITY OF THE ETHYLENE OXIDE RADICAL CATION

This study of the two possible modes of ring opening indicates that the C-O bonds in (73) are relatively weak, and can easily be broken, i.e. the ring-closed ethylene oxide ion (73) and its C---O ring-opened isomer (75) are separated by only a small energy barrier. Fission of the C-C bond requires more energy. Thus the barrier to ring opening of (73) to give its C---C ring-opened isomer (74) is approximately 105-120 kJ mol^{-1}. However, (74) when formed should be quite stable since it lies about 58 kJ mol^{-1} lower in energy than (73).

8.6 CONCLUSIONS

The main points arising from the study described in this chapter are:

(i) Consistent with experimental studies, the calculations reported here indicate that the experimentally observed $C_2H_4O^{+\cdot}$ isomers, namely the vinyl alcohol (71), acetaldehyde (72) and ethylene oxide (73) radical cations, are relatively low energy species which are stable with respect

to intramolecular rearrangement. The calculated relative energies for these three isomers are in reasonable agreement with thermochemical data. In addition to these three $C_2H_4O^{+\cdot}$ isomers, a fourth isomer, the C---C ring-opened ethylene oxide ion (74), was found to be a low energy isomer, in agreement with experimental findings (see Chapter 10).

(ii) The C---O ring-opened ethylene oxide cation (75) has an energy higher than that of the ring-closed form (73).

(iii) Fission of the C-C bond in the closed ethylene oxide ion (73) to produce the more stable C---C ring-opened isomer (74) requires about 105-120 kJ mol^{-1}.

(iv) Four other isomers [(76) - (79)] of $C_2H_4O^{+\cdot}$ have been identified as having reasonable prospects for experimental observation.

(v) From the comparison of theoretical procedures for studying isomers (71) - (75) two important points are noted: (a) For the radical cations studied here, the RHF and UHF methods give comparable results. (b) The relative energies obtained from RHF/4-31G single point calculations at RHF/STO-3G optimized structures are very similar to those obtained from full RHF/4-31G optimizations. This demonstrates the usefulness of the RHF/4-31G//RHF/STO-3G approach.

CHAPTER 9

STRUCTURES AND STABILITIES OF $C_2H_4O^{+\cdot}$ ISOMERS: EXPERIMENTAL TECHNIQUE

9.1 INTRODUCTION: ION CYCLOTRON RESONANCE (ICR) SPECTROMETRY

Ion cyclotron resonance spectrometry is a well-established technique for studying ion/molecule reactions in the gas phase at low pressures. Ions in a magnetic field move in a circular motion with an angular velocity characteristic of the $^{m}/_{z}$ value of the ions for a given strength of the magnetic field. The detection of ions is possible by applying an electric rf field; when the frequency of the applied rf field is equal to the frequency of the ion motion, energy transfer to that ion is possible. This is called the resonance phenomenon.

The ICR principle was first applied by Hipple *et al.*[238], who developed the omegatron for ionic mass determination. The first ICR spectrometer for studying ion/molecule reactions was developed by Wobschall *et al.*[239], and in 1965 an ICR spectrometer became commercially available from Varian Associates, Palo Alto, California[240]. Since then the technique has gradually become more popular, and several reviews on ICR spectrometry have appeared in recent years[179,218,241-248]. In the ICR experiments described in this thesis, an ICR instrument manufactured by Dynaspec Inc. of California, which is a development of the original Varian instrument, has been employed. The Dynaspec spectrometer as purchased was equipped with a square, three section cell and can be used to study both positive and negative ions in the drift or trapped modes. In the following description of the ICR technique, emphasis will be placed on the Dynaspec instrument, for the study of positive ions only.

9.2 THE ICR TECHNIQUE

9.2.1 ION MOTION IN THE ICR CELL

Ions of mass m and charge z which are moving in a plane perpendicular to a uniform magnetic field B with a velocity v, undergo a

force F,

$$F = zvB \tag{9.1}$$

which will be perpendicular to both B and v. This will result in circular motion of the ions, for which the acceleration, a, is equal to v^2/r, where r is the radius of the ion path. Thus

$$ma = mv^2/r = zvB \tag{9.2}$$

If ω_c is the angular frequency of the ion in rad sec^{-1}, then

$$mv/r = m\omega_c = zB \tag{9.3}$$

or

$$\omega_c = zB/m \tag{9.4}$$

Equation 9.4 shows that the angular frequency of an ion is independent of its velocity, and only dependent on its mass (m) and charge (z), and the external magnetic field (B). In practice, it is more convenient to consider the cyclotron frequency (ν_c) for an ion which is expressed in kHz.

$$\nu_c = \omega_c/2\pi \tag{9.5}$$

If a static electric field E is applied normal to the magnetic field B, a drift motion is superimposed on the circular motion of the ions. In this crossed-field geometry, the ions move in cycloidal orbits with cyclotron frequency ν_c and drift with the velocity v_d:

$$v_d = E/B \tag{9.6}$$

in the direction perpendicular to B and E.

An ICR cell which has been designed on the basis of these principles is shown in Figure 9.1.

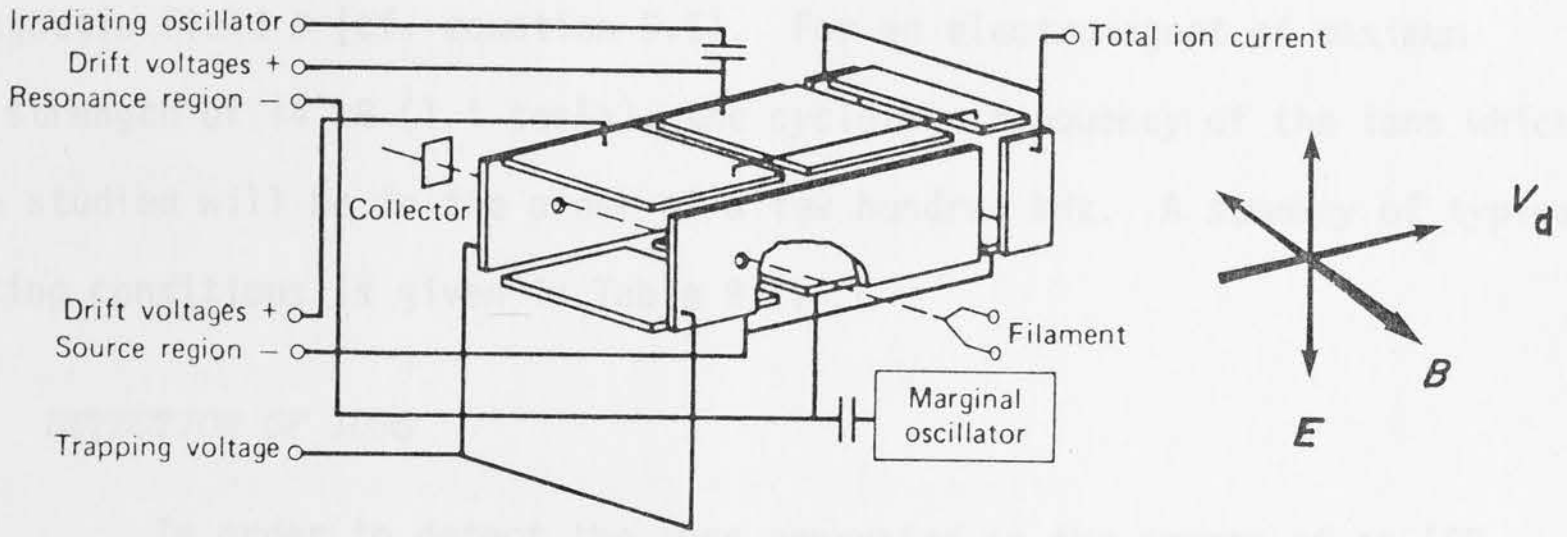

Fig. 9.1 Schematic diagram of a "flat" three section ICR cell. The sections are, from front to rear: the source region, the analyser region and the ion collector region.

The sample is ionized by electron impact, the ionizing electrons being emitted from a hot wire filament and collimated by a potential difference (electron voltage) between the filament and the cell. The electron current falling on the collector plate is measured as the emission current. The side plates of the cell carry a small positive potential called a trapping voltage (<2V) which keeps the ions that have been generated from drifting to the sides of the cell. The upper and lower plates of the cell have drift voltages imposed on them; the resulting electric field will cause the ions to drift through the cell from the source region to the resonance or analyser region, and finally to the ion collector region. The side plates in the ion collector region are at ground potential, and the ions move outward to the plates. The current is measured by an electrometer, and is usually only a few pA.

Typical dimensions of a "square" ICR cell are 2.54 x 2.54 x 12.7 cm

and of a "flat" ICR cell are 1.27 x 2.54 x 12.7 cm, and typical residence times for the ions are in the order of 10^{-3} seconds[248]. For a fixed drift potential the residence time of an ion depends directly on the strength of the magnetic field B (cf. equation 9.6). For an electromagnet of maximum field strength of 14 kG (1.4 tesla), the cyclotron frequency of the ions which can be studied will be in the order of a few hundred kHz. A summary of typical operating conditions is given in Table 9.1.

9.2.2 DETECTION OF IONS

In order to detect the ions generated in the source of an ICR cell, an electrical oscillator is used to generate an rf field that will excite ions which have a cyclotron frequency equal to the frequency of the oscillator at a given value of B. The oscillating voltage is applied to the upper and lower plates of the analyzer region of the cell. When ions are in resonance they absorb energy and gain velocity, which results in an increase in the radius of the cyclotron motion (see Fig. 9.2).

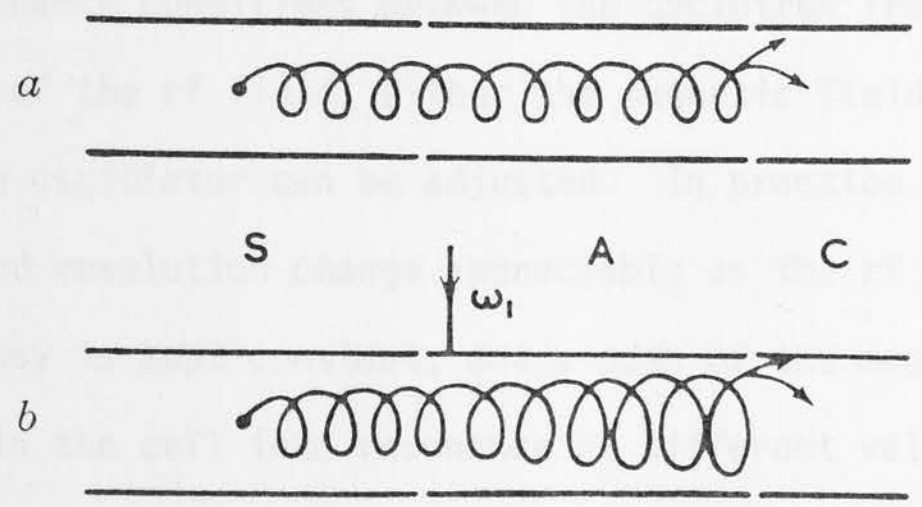

Fig. 9.2 Schematic diagram showing the ion motion in the ICR cell; a, ion motion in the absence of the rf field; b, ion motion when the rf frequency ($\omega_1/2\pi$) is equal to the cyclotron frequency (ν_c) of the ion.
S = source region, A = analyzer region and C = collector region.

Table 9.1 Example of Typical Operating Conditions and Dimensions of a "Square" Cell.

Dimension of the cell	2.54 x 2.54 x 12.7 cm
Separation of drift plates	2.54 cm
Operating Pressures	10^{-4} - 10^{-7} torr (10^{-2} - 10^{-5} N m^{-2})
Trapping Voltage	∿ 0.25 V
Drift Voltage	∿ 0.50 V
Ionizing Potential	20 eV
Emission Current	0.03 μA

For $CO_2^{+\cdot}$, m/z = 44, magnetic field B = 10000 gauss:

$\nu_c = \omega_c/2\pi$ = 350 kHz

With E = 0.20 V cm^{-1} $\quad v_d$ = 4 x 10^3cm s^{-1}

τ (time spent in the cell by the ion) = 2.5 x 10^{-3} s

D (diameter of the cyclotron orbit of the ion) = 0.4 mm

d (distance of drift during one revolution) = 0.011 mm

To obtain resonance conditions between the cyclotron frequency of the ion and the frequency of the rf field, either the magnetic field (B) or the frequency ($\omega_1/2\pi$) of the oscillator can be adjusted. In practice, because both sensitivity and resolution change appreciably as the rf frequency is altered, the rf frequency is kept constant, and a scan of the magnetic field brings the various ions in the cell into resonance at different values of B, depending on the m/z values of the ions. Due to the problem of decreased sensitivity and resolution at low rf values, the lowest fixed value of $\omega_1/2\pi$ used for the observing oscillator is about 75 kHz, which for a maximum field strength of 14 kG gives a range of up to m/z 280. The absorption of the applied rf energy by an ion in resonance is monitored by signal modulation and phase-sensitive detection.[249] Either some resonance condition or the supply of ions is

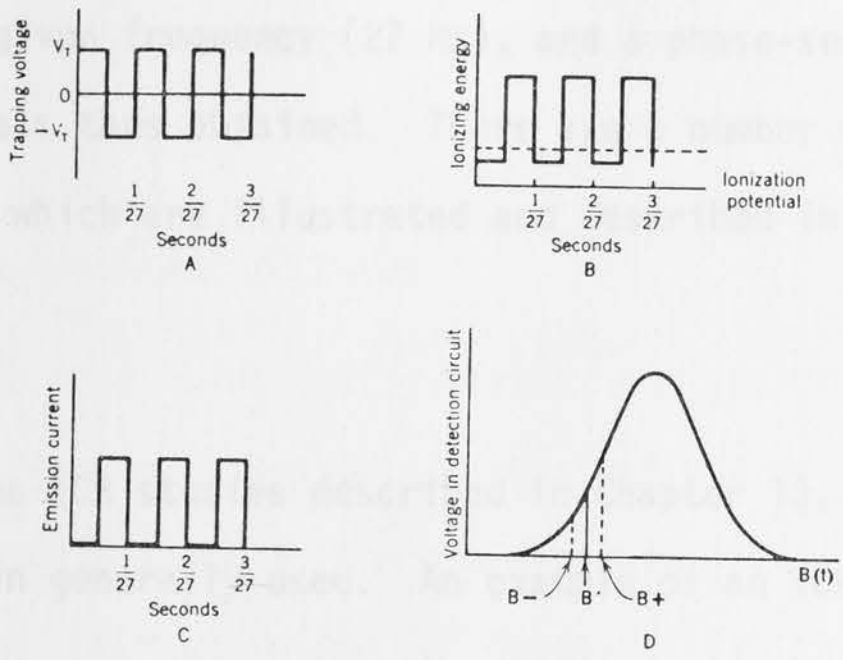

Fig. 9.3 Ion pulsing and signal modulation schemes.

A. Trapping modulation. The trapping voltage (V_T) is modulated by a square wave on one trapping plate. When it is at $-V_T$, no ions leave the cell[250].

B. Electron energy modulation. The energy of the ionizing electrons is modulated, usually from below to above the ionization potential[251]. At the low value, no ions are formed.

C. Emission current modulation. A grid is placed between the filament and the cell and a voltage is pulsed on it to keep electrons from reaching the cell[252].

D. Field modulation. The magnetic field is modulated over a range of a few gauss. B(t) sweeps across the absorption curve. Helmholtz coils, set just inside the magnetic pole caps, repeatedly impose a small incremental field B+, then an equal decremental field B-, on B(t). The detector compares the signal at B+ to that at B-. As *B* sweeps through the curve, a derivative trace is produced.

interrupted at a given frequency (27 Hz), and a phase-sensitive detector compares the signals thus obtained. There are a number of ways available for signal modulation which are illustrated and described in Fig. 9.3.

In the ICR studies described in Chapter 10, electron energy modulation has been generally used. An example of an ICR spectrum is given in Fig. 9.4.

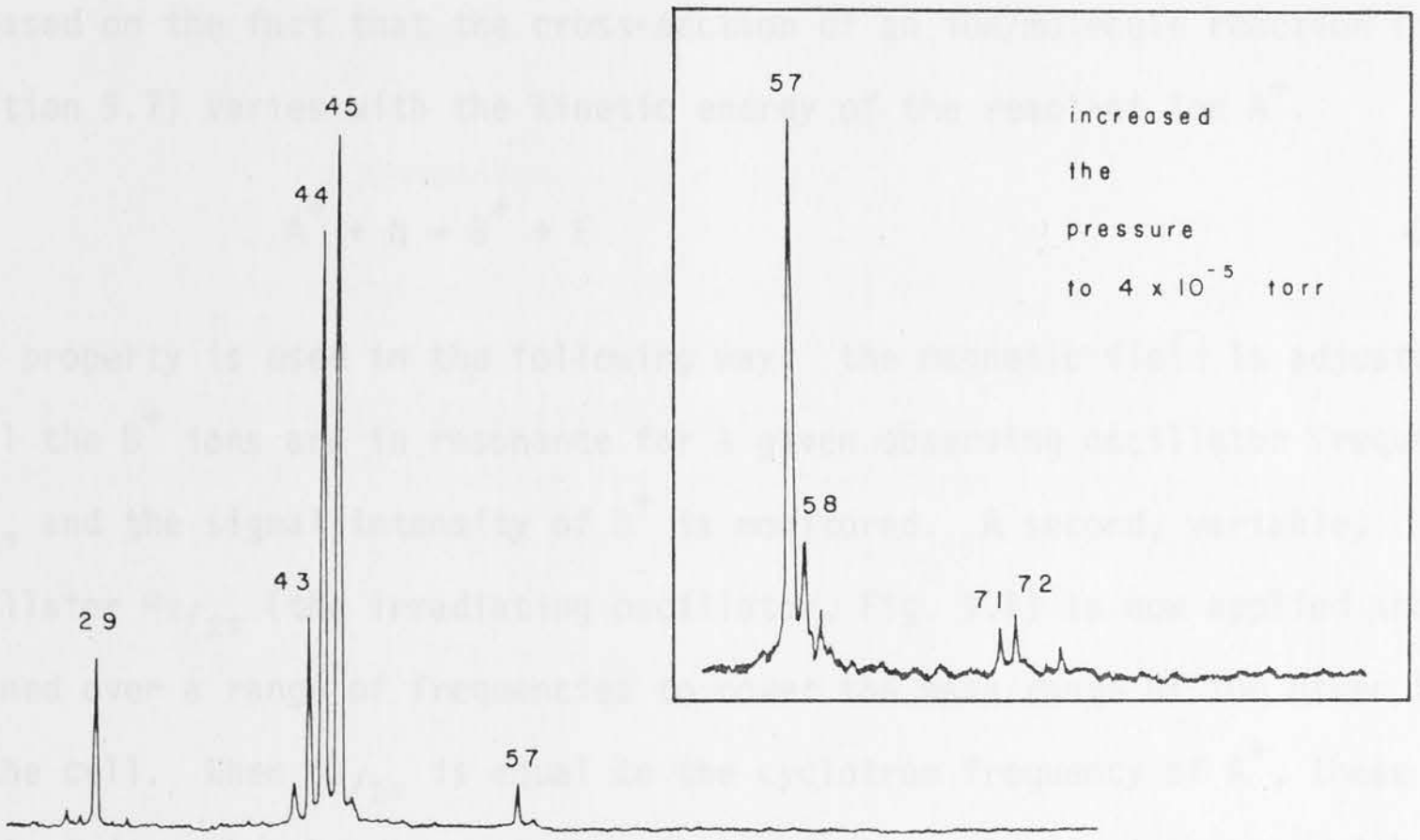

Fig. 9.4 ICR spectrum of ethylene oxide from $^{m}/_{z}$ 25 to $^{m}/_{z}$ 90. Electron energy 20 eV, emission current 0.024 μA. Rf field 153.26 kHz, electron energy modulation. Sample pressure 2 x 10^{-5} torr. Every signal at $^{m}/_{z}$ > 44 is the product of an ion/molecule reaction.

For the studies described in this thesis the pressure of the neutral gas(es) did not need to be known accurately; the pressures as measured by the current

produced in the vac ion pump which is pumping the cell have been used, and are satisfactory.

9.2.3 THE DOUBLE RESONANCE TECHNIQUE

Due to their slow drift velocity and cyclotron motion, ions travel for long distances ($\sim$ 1 or 2 metres) in the cell and as a result ion/molecule reactions occur readily, even at low pressures ($\sim 10^{-5}$ - 10^{-6} torr), and the product ions can be observed in the ICR spectrum (cf. Fig. 9.4). For the identification of the ion/molecule reactions that give rise to a particular product ion B^+, the double resonance technique[253,254] is used. This technique is based on the fact that the cross-section of an ion/molecule reaction (cf. reaction 9.7) varies with the kinetic energy of the reactant ion A^+.

$$A^+ + N \rightarrow B^+ + F \qquad 9.7$$

This property is used in the following way: the magnetic field is adjusted until the B^+ ions are in resonance for a given observing oscillator frequency $\omega_1/2\pi$ and the signal intensity of B^+ is monitored. A second, variable, oscillator $\omega_2/2\pi$ (the irradiating oscillator, Fig. 9.1) is now applied and is scanned over a range of frequencies to cover the mass range of the other ions in the cell. When $\omega_2/2\pi$ is equal to the cyclotron frequency of A^+, these reactant ions absorb energy so that their angular velocity increases, with the result that a change in the intensity of the product ion B^+ is observed due to a change in the rate of reaction 9.7. At a fixed magnetic field the following relation holds:

$$m_B \times \omega_1 = m_A \times \omega_2 \qquad 9.8$$

so that the m/z value of the reactant ion A^+ that gives rise to the product ion B^+ can readily be calculated. Moreover, since the composition and the molecular weight of the reacting neutral species (N) is known, the composition of the

fragment or fragments F can be deduced. A typical double resonance scan is shown in Fig. 9.5.

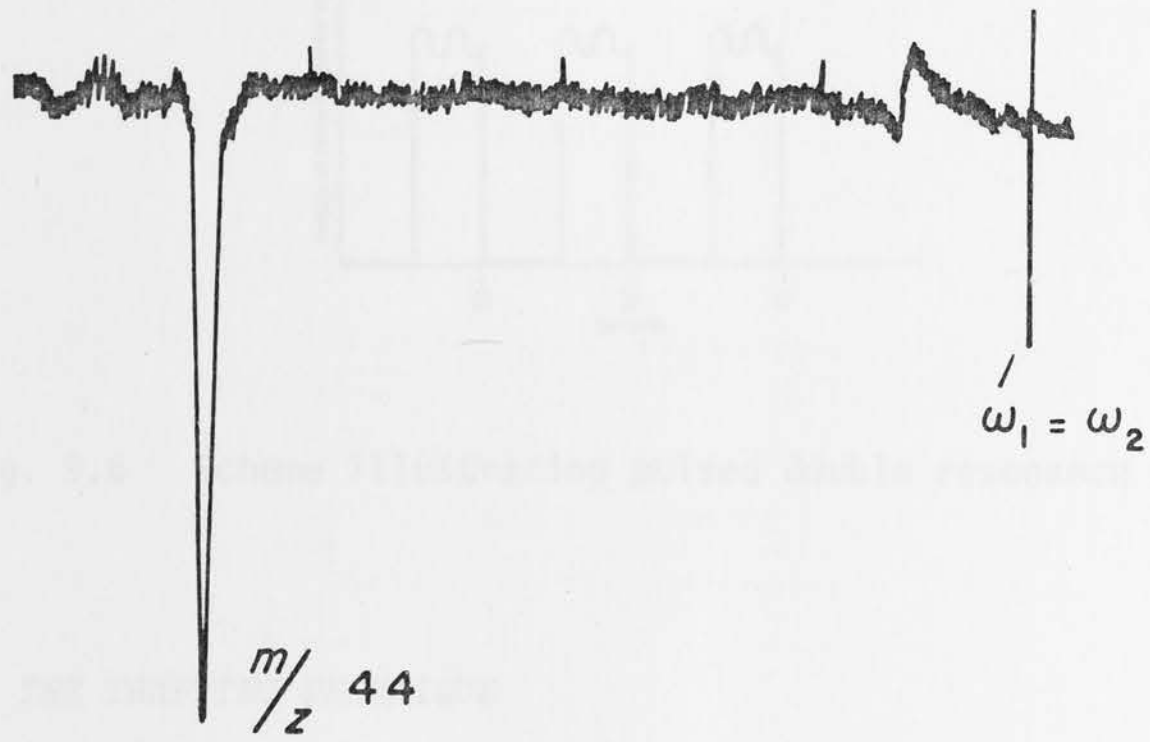

Fig. 9.5 Double resonance scan of the ion at m/z 93 in the ICR spectrum of a mixture of ethylene oxide and pyridine. Total pressure is 2.5×10^{-5} torr, electron energy 20 eV, emission current 0.03 μA, $\omega_1/2\pi$ = 113.31 kHz, electron energy modulation. The double resonance oscillator has an amplitude of 0.32 V and is swept from 110 to 270 kHz, which corresponds to a mass range of 95 to 39. Double resonance occurs at 239.5 kHz, which corresponds to the m/z 44 ion. Reaction: $C_2H_4O^{+\cdot} + C_5H_5N \rightarrow [C_5H_5N\text{---}CH_2]^{+\cdot} + CH_2O$ (see Chapter 10).

The double resonance signal can also arise because, at a sufficiently large amplitude of the second irradiating oscillator, the reactant ion A^+ will absorb enough energy to come in contact with the upper or lower plates of the cell (cf. Fig. 9.2). The ions are swept out of the cell[255], and the intensity of B^+ is reduced to almost zero if A^+ is the only procursor. This is called the ion ejection technique. The double resonance technique permits another method of signal modulation, that of pulsing the irradiating oscillator (Fig. 9.6).

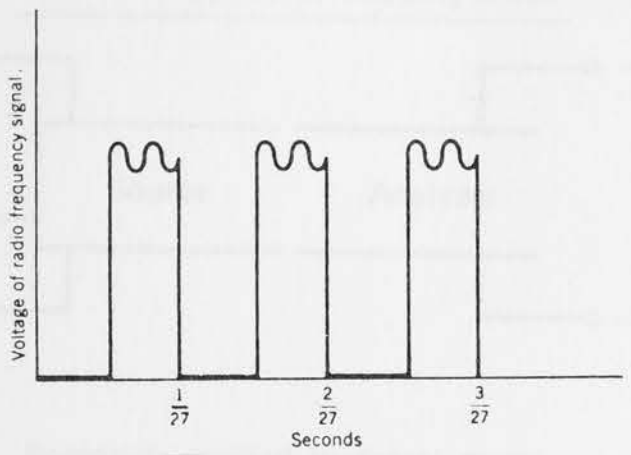

Fig. 9.6 Scheme illustrating pulsed double resonance modulation.

9.2.4 THE TRAPPING TECHNIQUE

A modification of the drift cell (Fig. 9.1) is the ion-trapping cell. A single section trapped ion cell was designed by McIver[256,257], whereas McMahon and Beauchamp modified a drift cell to trap ions[258]. Ion trapping cells derive their unique capabilities from their pulsed operation. Ions are formed by a short electron-beam pulse (τ_1), followed by a double resonance pulse (τ_2) and a reaction (trapping) time τ_3 (1 ms - 1000 ms) in which the product ions are allowed to interact with neutrals. After the desired reaction time τ_3, the ions are detected during the time τ_4 after which the ion signals are quenched and the pulse sequence repeated. In the modified drift cell[258], which was incorporated in the Dynaspec instrument, trapping of the ions in the source region is effected by keeping the source drift plates and a new rear plate at near ground potential, the analyser drift plates at a negative potential and the trapping plates at a positive potential. Ion detection after $(\tau_1 + \tau_2 + \tau_3)$ is effected by switching all voltages, under computer control, to appropriate values for the normal drift mode operation, and the ions are observed during τ_4 in the normal way (see Fig. 9.7). The trapping technique

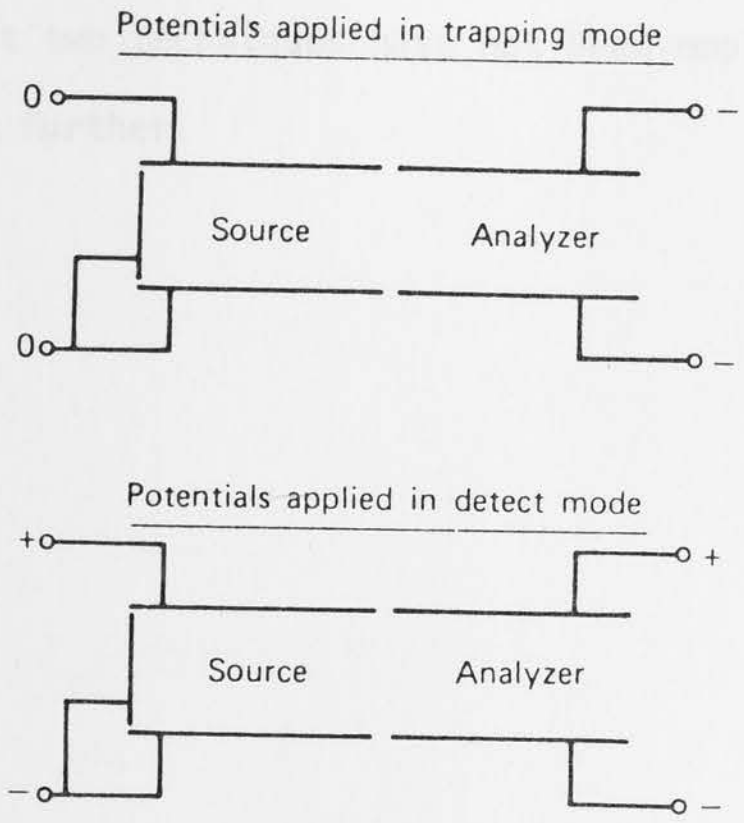

Fig. 9.7 Typical potentials applied to the trapped cell[258] in trapping and detect modes.

is used a great deal for studying ions of long lifetimes and for studying reaction kinetics and acid/base equilibria.

9.3 FINAL REMARKS

ICR spectrometry is now a well-established technique for studying ion/molecule reactions. The double resonance technique is a powerful tool for determining the identity of the reacting ions which are responsible for the formation of the observed product ions. The trapped ion technique enables the study of ions of long lifetimes, as well as the study of the time dependence of product formation.

More recently Fourier transform ICR spectrometry has been developed, which permits much faster scanning, higher sensitivity, higher mass range and a substantially better resolution[259-261]. Another new technique is rapid scan ICR spectrometry[262] which uses a capacitance bridge detector instead of a

marginal oscillator, and produces a very high resolution for ions up to $^{m}/_{z}$ 1000. These last two techniques have not been employed here, and will therefore not be discussed further.

CHAPTER 10

STRUCTURES AND STABILITIES OF $C_2H_4O^{+\cdot}$ ISOMERS: AN ICR EXPERIMENTAL INVESTIGATION

10.1 INTRODUCTION

In this chapter, the experimental investigation of the $C_2H_4O^{+\cdot}$ isomers, which has been carried out to complement the theoretical studies, will be described. ICR spectrometry has been employed to study the ion/molecule reactions of the three $C_2H_4O^{+\cdot}$ isomers which are considered well-established stable isomers, the vinyl alcohol, acetaldehyde and ethylene oxide radical cations [(71) - (73)]. The methodology is that originally used for the study of the gas-phase $C_3H_6O^{+\cdot}$ keto and enol ions[263], namely identification of ion structures by differences in their reactions with selected neutral molecules. The study has also been concerned with two $C_2H_4O^{+\cdot}$ isomers which have been postulated as observable $C_2H_4O^{+\cdot}$ species, the C---C ring-opened and C---O ring-opened ethylene oxides [(74) and (75)]. Finally the possibility of observing other stable $C_2H_4O^{+\cdot}$ isomers, which were shown to be of low energy in the theoretical study (Chapter 8), will be briefly discussed.

10.2 ICR INVESTIGATION

A Dynaspec ICR spectrometer was used in this study to record ion/molecule reactions under standard drift operating conditions (Table 9.1). The spectrometer is equipped with a dual sample inlet system, which allows for the pressure of two sample gases to be controlled independently (see also Fig. 10.1).

10.2.1 THE VINYL ALCOHOL RADICAL CATION

10.2.1.1 Reaction with Cyclobutanol

Since it was known that the vinyl alcohol radical cation (71) can be generated from a number of suitable precursors[181-185], three such precursors, cyclobutanol, ethyl vinyl ether and *n*-hexanal, have been used in this study.

Fig. 10.1 The Dynaspec ICR spectrometer. On the left the magnet unit, with the sample inlet system and a foreline pump for initial pumping (the ICR cell is pumped by an ion pump). To the right is the control console where operating conditions are monitored and set, and where the spectra are recorded. At the lower right is a small computer which controls the ion-trapping experiments.

Cyclobutanol is found to produce a strong signal at $^{m}/_{z}$ 44, which by CA studies[215] and thermochemical measurements[79] had been shown to be a $C_2H_4O^{+\cdot}$ ion distinguishable from the ethylene oxide and acetaldehyde radical cations. A feature of the ICR spectrum of cyclobutanol at pressures > 10^{-6} torr is a signal at $^{m}/_{z}$ 70 which by double resonance can be shown to be the product ion of an

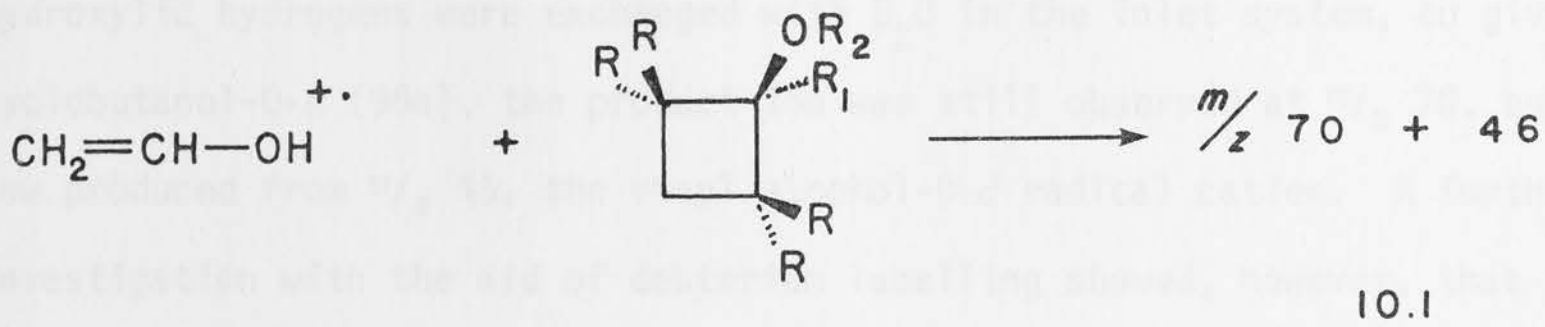

10.1

(71)

(95) $R = R_1 = R_2 = H$

(95a) $R = R_1 = H$, $R_2 = D$

(95b) $R = D$, $R_1 = R_2 = H$

(95c) $R = R_1 = D$, $R_2 = H$

exclusive reaction of the vinyl alcohol radical cation [(71), $^{m}/_{z}$ 44] with neutral cyclobutanol (95) (reaction 10.1). A similar reaction had been observed[263] for the homologue of the vinyl alcohol radical cation, the enol ion of acetone, when generated from 1-methylcyclobutanol. The mechanism which was proposed[263] for that reaction involved loss of water and an ethylene fragment (reaction 10.2). A similar mechanism would account for the observation of $^{m}/_{z}$ 70 in reaction 10.1.

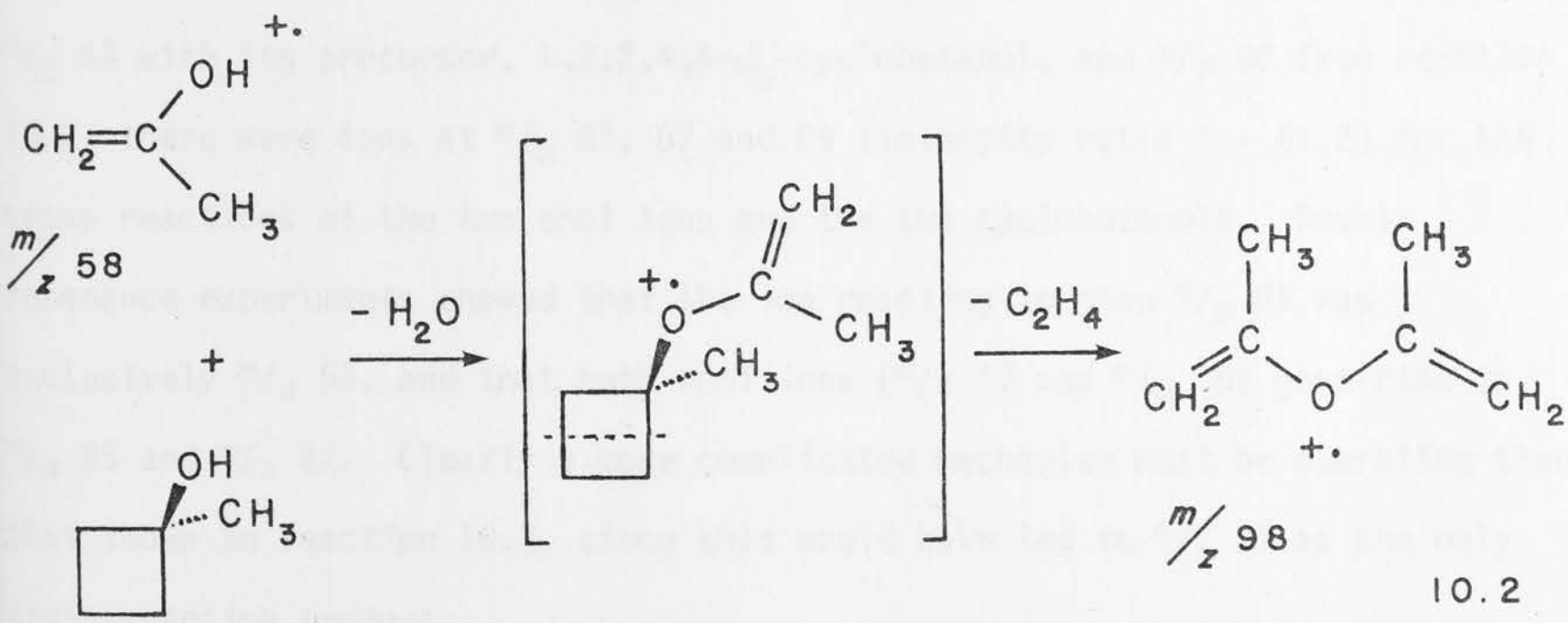

10.2

It was possible to show by labelling experiments that in reaction 10.1 both hydroxylic hydrogens are lost and that the carbinol hydrogens [R_1, (95)] are

retained, in keeping with the above mechanism (reaction 10.2). When the hydroxylic hydrogens were exchanged with D_2O in the inlet system, to give cyclobutanol-O-*d* (95a), the product ion was still observed at $^m/_z$ 70, but was now produced from $^m/_z$ 45, the vinyl alcohol-O-*d* radical cation. A further investigation with the aid of deuterium labelling showed, however, that the reaction proceeds in a more complicated way than reaction 10.2 suggests. When the ICR spectrum of 2,2,4,4-d_4-cyclobutanol (95b) is examined, product ions from the reaction of the 2,2-d_2-vinyl alcohol radical cation ($^m/_z$ 46) are found at $^m/_z$ 72 and $^m/_z$ 74, while with 1,2,2,4,4-d_5-cyclobutanol (95c), the same ion/molecule process gives rise to product ions at $^m/_z$ 74 and $^m/_z$ 76, in a ratio of $\sim$ 4:3, both showing $^m/_z$ 47 as the precursor ion. If the proposed mechanism (reaction 10.2) were correct, the d_4-cyclobutanol (95b) should show only $^m/_z$ 74 as the product ion, and the d_5-compound (95c) only $^m/_z$ 76. In order to probe this ion/molecule reaction further, a mixture of 1-methyl-cyclobutanol and 1,2,2,4,4-d_5-cyclobutanol (95c) was introduced into the ICR spectrometer *via* the dual inlet system to give a total pressure of 1.5×10^{-5} torr, such that the ratio of the two enol ions $^m/_z$ 58 to $^m/_z$ 47 was 1.0 : 0.7. As well as observing the product ions at $^m/_z$ 74 and 76 from the reaction of $^m/_z$ 47 with its precursor, 1,2,2,4,4-d_5-cyclobutanol, and $^m/_z$ 98 from reaction 10.2, there were ions at $^m/_z$ 85, 87 and 89 (intensity ratio 1 : 6: 2) for the cross reactions of the two enol ions and the two cyclobutanols. Double resonance experiments showed that the ion reacting to give $^m/_z$ 89 was exclusively $^m/_z$ 58, and that both enol ions ($^m/_z$ 47 and $^m/_z$ 58) gave rise to $^m/_z$ 85 and $^m/_z$ 87. Clearly a more complicated mechanism must be operating than that shown in reaction 10.2, since this would have led to $^m/_z$ 87 as the only cross-reaction product.

From the labelling experiments, it seems likely that the initial step is the loss of water and the formation of an exocyclic ether (96), since

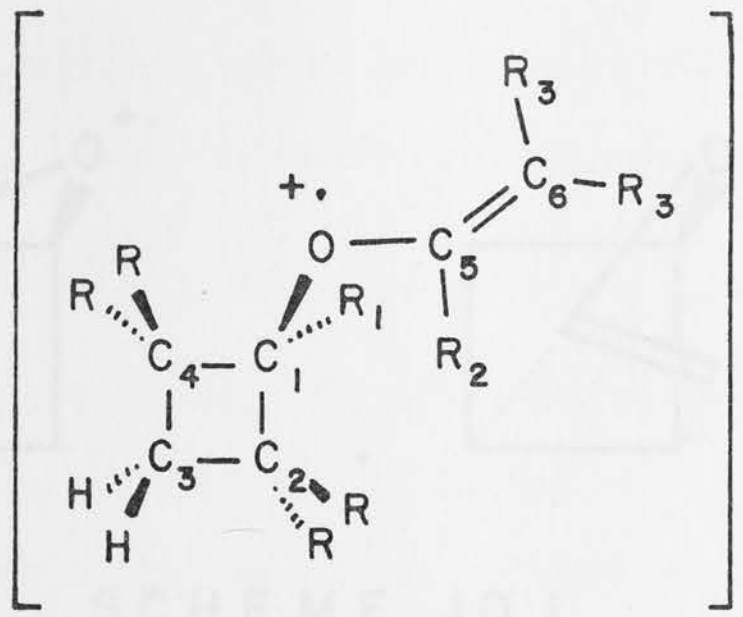

(96) $R = R_1 = R_2 = R_3 = H$

(96a) $R = R_3 = D$, $R_1 = R_2 = H$

(96b) $R = R_1 = R_2 = R_3 = D$

(97) $R = R_1 = D$, $R_2 = CH_3$, $R_3 = H$

it was shown that both hydroxylic hydrogens are lost. The postulated intermediate (96), which is not a detectable species, then eliminates ethylene in such a way that every combination of C_2, C_3, C_4 and C_6 [i.e. any two of the four methylene groups in (96) - (97)] is lost in near statistical fashion. This necessitates proposing a mechanism by which these four methylene groups become equivalent. No scrambling of the hydrogen and deuterium atoms is observed, i.e. there are no losses of C_2H_3D or C_2D_3H from (96a) - (97). The observed product ions can be explained if, for the complexes (96) - (97), a rapid exchange of an ethylene unit between the ring and the exocyclic double bond occurs, which is a degenerate process for (96). The ethylene exchange can take place in two distinct ways (Scheme 10.1). If C_2 and C_4 in (96) are not identical a single exchange in (96) will produce four different species (Scheme 10.2).

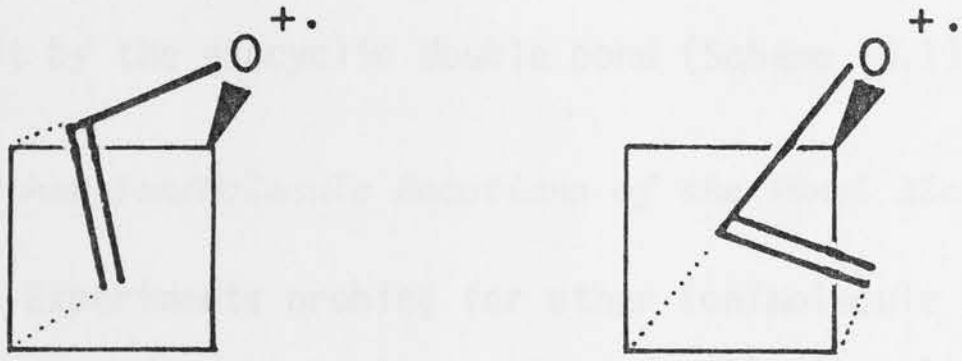

SCHEME 10.1

Subsequent exchanges (dashed arrows) will lead to a random distribution for C_2, C_3, C_4 and C_6 in the ring and the exocyclic position.

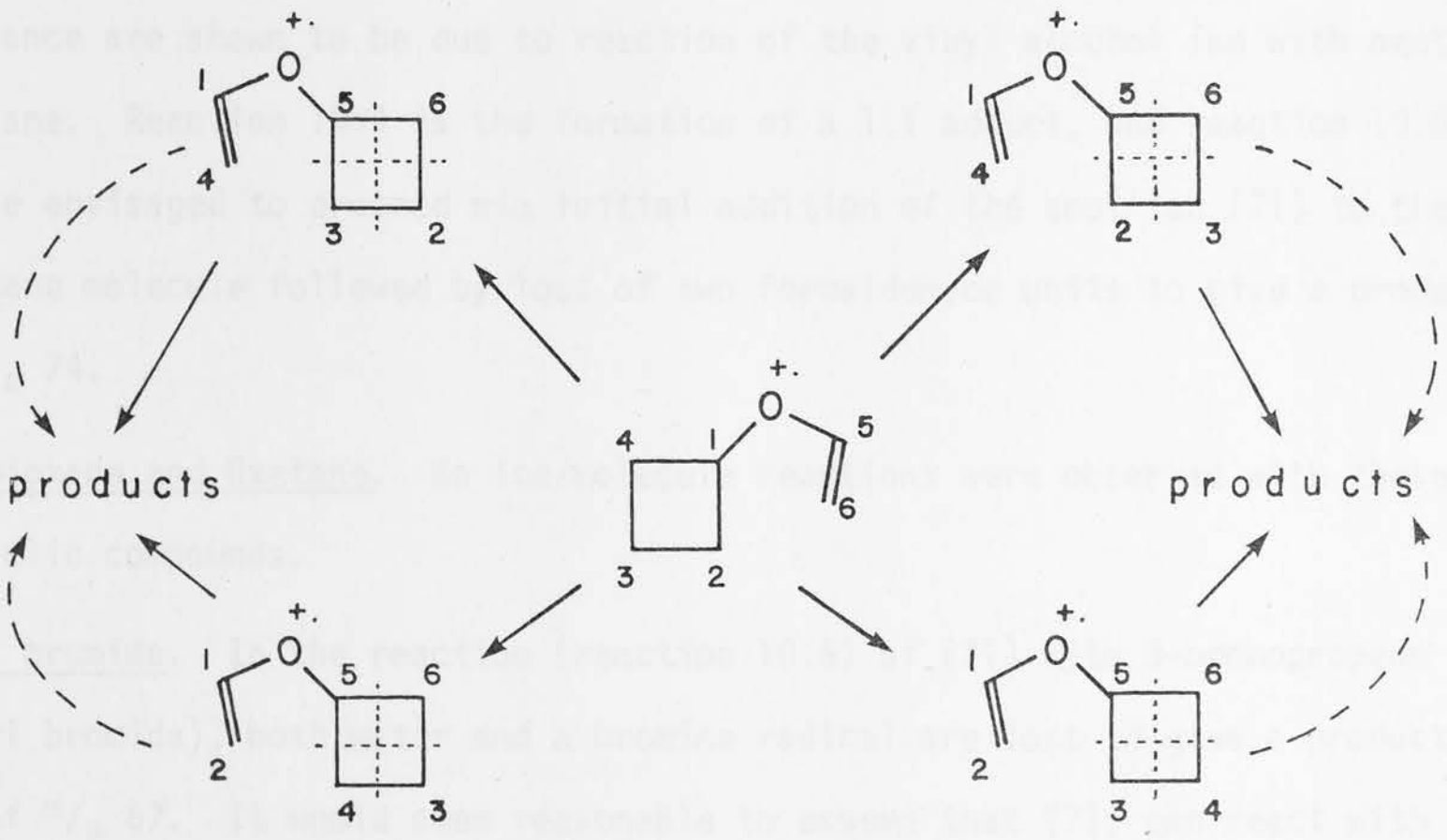

SCHEME 10.2

The observed product ions are formed by loss of ethylene from all the contributing species in a retro [2 + 2] process. The proposed mechanism (Schemes 10.1 and 10.2) implies that the exchange of an ethylene unit proceeds on a faster time

scale than the loss of such a unit. In other words, the intramolecular exchange of an ethylene unit can be envisaged as the trapping of a departing ethylene unit by the exocyclic double bond (Scheme 10.1).

10.2.1.2 Other Ion/Molecule Reactions of the Vinyl Alcohol Radical Cation

Experiments probing for other ion/molecule reactions which are specific for the vinyl alcohol radical cation, i.e. they are not observed for other $C_2H_4O^{+\cdot}$ isomers, were carried out and were successful in a number of cases. The results are presented in Table 10.1 and are discussed here. Unless otherwise stated, cyclobutanol was used for generating the vinyl alcohol radical cation (71).

Trioxane. Two product ions at $^m/_z$ 74 and $^m/_z$ 134 are observed which by double resonance are shown to be due to reaction of the vinyl alcohol ion with neutral trioxane. Reaction 10.4 is the formation of a 1:1 adduct, and reaction 10.5 can be envisaged to proceed *via* initial addition of the enol ion (71) to the trioxane molecule followed by loss of two formaldehyde units to give a product of $^m/_z$ 74.

1,4-Dioxane and Oxetane. No ion/molecule reactions were observed with these oxocyclic compounds.

Allyl bromide. In the reaction (reaction 10.6) of (71) with 3-bromopropene (allyl bromide), both water and a bromine radical are lost to give a product ion of $^m/_z$ 67. It would seem reasonable to assume that (71) can react with substrates which contain a double or triple bond in much the same way as the methyl vinyl ether radical cation. The latter is known to react[264-266] to give a four-centre complex which can eliminate a new olefin molecule (e.g. reaction 10.12).

Table 10.1 Ion/Molecule Reactions Observed for the Vinyl Alcohol Radical Cation (71).

Neutral Substrate	Fragments lost	Product Ion ($^{m}/_{z}$) (intensity[a])	Reaction
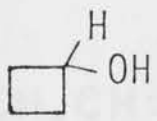	18,28	70 (l)	10.1
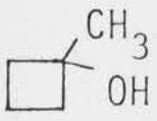	18,28	84 (m)	10.3
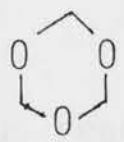	-	134 (s)	10.4
	30,30	74 (m)	10.5
	No reaction		
	No reaction		
CH_2=CH-CH_2Br	18,Br·	67 (m)	10.6
CH≡C-CH_2Br	Br·	83 (s)	10.7
CH_2=CH-CH_2OH	18,28	56 (s)	10.8
	18,28,H·	55 (s)	10.9
CH≡C-CH_2OH	18,H·	81 (s)	10.10
CH_2=CH-CH_3	28	58 (vs)	10.11
CH_3OH	No reaction		
C_6H_5-C≡N	No reaction		

[a] Intensity: vs = very small; s = small; m = medium; l = large.

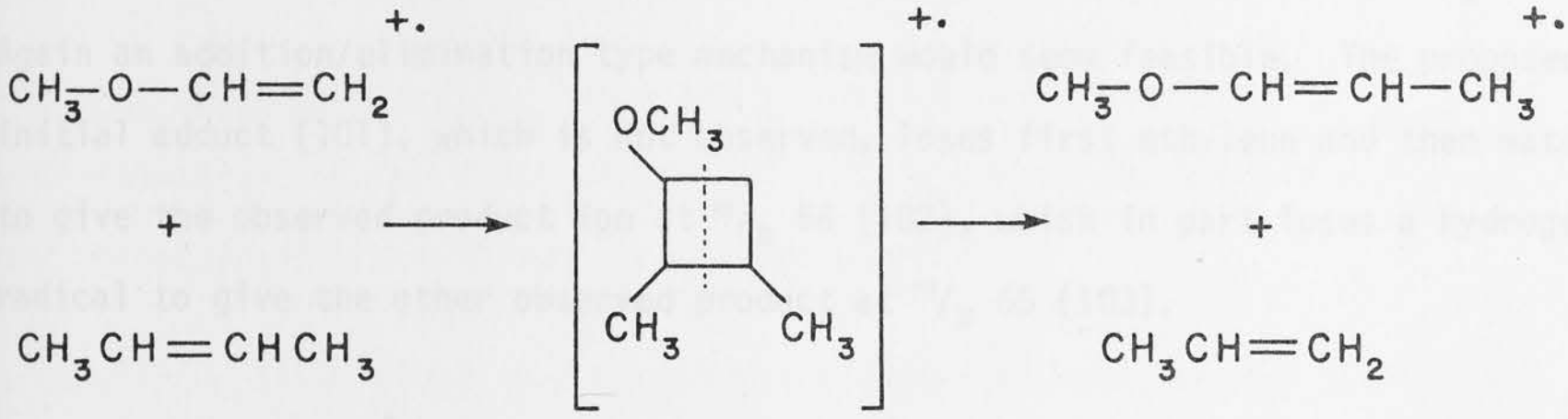

10.12

Thus reaction 10.6 might proceed *via* the intermediate complex (98), which through loss of bromine and water could lead to the allylic cation (99).

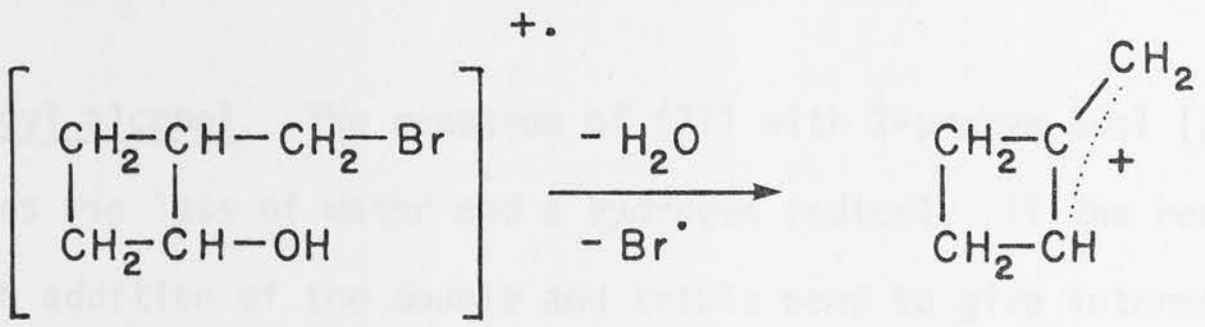

(98) (99)

Propargyl bromide. The addition of (71) to 3-bromopropyne (propargyl bromide) can lead to a cyclobutene intermediate which is stabilized by loss of a bromine radical to give a product ion (100) of $^{m}/_{z}$ 83, similar to (99) proposed above.

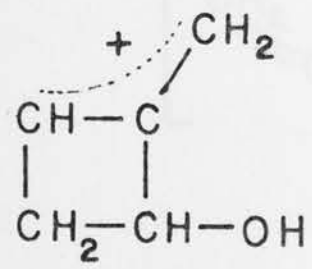

(100)

Allyl alcohol. This substrate reacts with the $^{m}/_{z}$ 44 enol ion (71) with loss of mass 46 (most likely water and ethylene) to give the product ion at $^{m}/_{z}$ 56. Again an addition/elimination type mechanism would seem feasible. The proposed initial adduct (101), which is not observed, loses first ethylene and then water to give the observed product ion at $^{m}/_{z}$ 56 (102), which in part loses a hydrogen radical to give the other observed product at $^{m}/_{z}$ 55 (103).

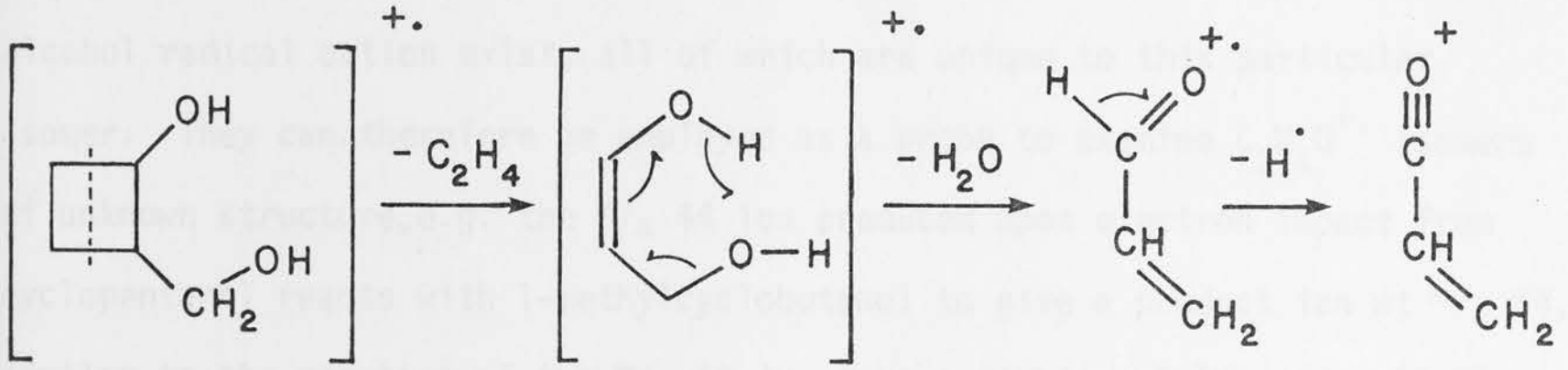

(101) (102) (103)

Propargyl alcohol. The reaction of (71) with 2-propyn-1-ol (propargyl alcohol) proceeds *via* loss of water and a hydrogen radical. If the reaction proceeds through addition of the double and triple bond to give intermediate (104), loss of ethylene as in (101) is not possible. Elimination of water and loss of H· will lead to a stable even-electron ion of $^{m}/_{z}$ 81 (105).

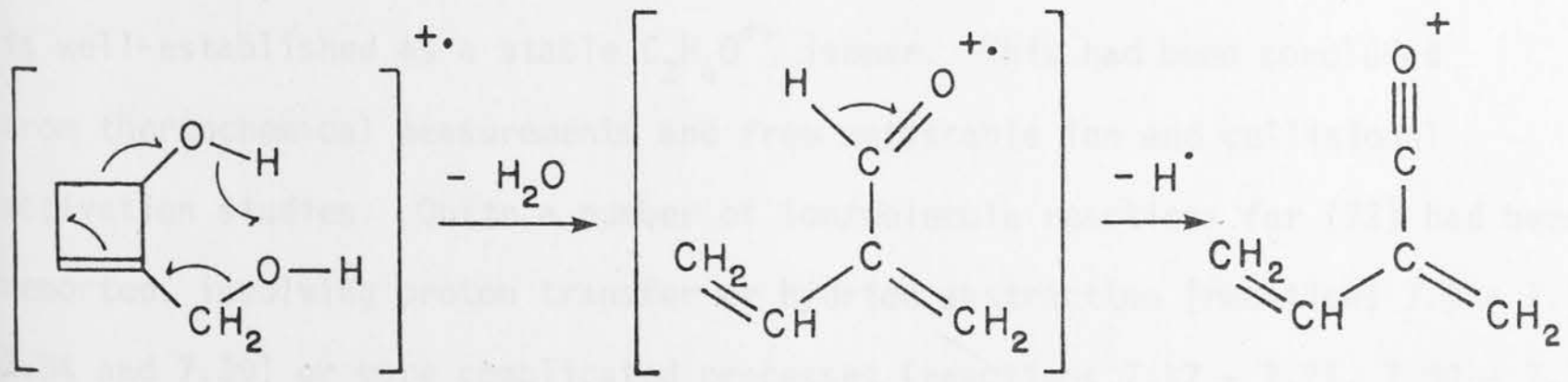

(104) (105)

Propene. The ion/molecule reaction with propene (reaction 10.11) is analogous to the reaction of the methyl vinyl ether cation with propene (cf. reaction 10.12).

The observed product ion (CH_3-CH=CH-$OH^{+\cdot}$) is only present in small quantity, but the double resonance spectrum definitely shows (71), $^m/_z$ 44, as precursor.

Methanol and benzonitrile. These two substrates were examined as representatives of two other classes of organic compounds, but did not show any characteristic ion/molecule reactions with (71).

It is clear that a reasonable number of reactions of the vinyl alcohol radical cation exist, all of which are unique to this particular isomer. They can therefore be employed as a probe to examine $C_2H_4O^{+\cdot}$ isomers of unknown structure, e.g. the $^m/_z$ 44 ion produced upon electron impact from cyclopentanol reacts with 1-methylcyclobutanol to give a product ion at $^m/_z$ 84, similar to the reaction of the $^m/_z$ 44 ion from cyclobutanol (reaction 10.3). The $^m/_z$ 44 ion produced by electron impact from *n*-hexanal reacts with trioxane to give a product at $^m/_z$ 74 as found in reaction 10.5. Thus the $C_2H_4O^{+\cdot}$ ions produced from cyclobutanol, cyclopentanol and *n*-hexanal react in identical fashion and can be said to have the same structure (71), a result also deduced by McLafferty in a collisional activation study[215].

10.2.2 THE ACETALDEHYDE RADICAL CATION

In Chapter 7 it was shown that the acetaldehyde radical cation (72) is well-established as a stable $C_2H_4O^{+\cdot}$ isomer. This had been concluded from thermochemical measurements and from metastable ion and collisional activation studies. Quite a number of ion/molecule reactions for (72) had been reported, involving proton transfer or hydride abstraction (reactions 7.9 - 7.11, 7.34 and 7.39) or more complicated processes (reactions 7.17 - 7.21, 7.30 - 7.33, 7.35 - 7.38). However, since no ICR studies using the double resonance technique for the identification of the reactant ions had been carried out, these reported reactions cannot be considered as well-established reactions of the acetaldehyde radical cation.

In the course of this study, acetaldehyde was examined in the ICR spectrometer together with a number of different compounds (Table 10.2), in order to identify any typical ion/molecule reaction of the acetaldehyde radical cation (72). In no case, however, was any such reaction found and, in fact, this ion proved to be notably unreactive. Where substrates were involved that could give rise to other $C_2H_4O^{+\cdot}$ ions, either acetaldehyde-d_4 was utilized as the source of the aldehyde ion (72), or deuterated substrates were used.

Table 10.2 Substrates Examined for Possible Ion/Molecule Reactions with the Acetaldehyde Radical Cation (72).

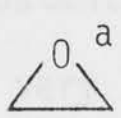 [a]		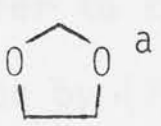 [a]	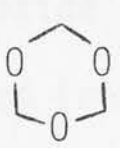
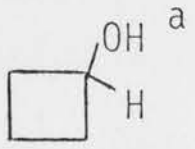 [a]	CH_3OH	$CH_2{=}CH{-}CH_3$	CH_3NO_2
$CH_3{-}C{\equiv}N$	$CH{\equiv}C{-}CH_2Br$	$N(C_2H_5)_3$	

[a] Checked by deuterium labelling.

Especially noteworthy is the result that the ion/molecule reactions reported by Kumakura (see Section 7.2.4) for (72) and ethylene oxide, and (72) with trioxane, could not be confirmed by ICR experiments and must therefore be considered to be tenuous.

Proton transfers and hydride abstractions have been reported for (72), and while they are not very suitable for identifying this ion, they have been examined here since they have been found to be the only ion/molecule reactions that can be observed for (72). In a mixture of acetaldehyde and acetaldehyde-d_4, two reactions are observed, both involving proton or deuteron transfer (reactions 10.13 and 10.14).

$$CH_3CHO^{+\cdot} + CD_3CDO \rightarrow CD_3CDOH^{+} + CH_3CO^{\cdot} \qquad 10.13$$

$$CD_3CDO^{+\cdot} + CH_3CHO \rightarrow CH_3CHOD^{+} + CD_3CO^{\cdot} \qquad 10.14$$

No hydride or deuteride abstraction was observed. When a mixture of acetaldehyde and ethylene oxide-d_4 is examined, the acetaldehyde radical cation shows a substantial amount of proton transfer to the ethylene oxide (reaction 7.10), but very little deuteride abstraction by (72) is observed (reaction 7.11). The ethylene oxide-d_4 radical cation, however, does not show any D^+ transfer to acetaldehyde.

$$CH_3CHO^{+\cdot} + C_2D_4O \begin{cases} \rightarrow C_2D_4OH^{+} + C_2H_3O^{\cdot} & (7.10) \\ \rightarrow CH_3CHOD^{+} + C_2D_3O^{\cdot} & (7.11) \end{cases}$$

10.2.3 THE ETHYLENE OXIDE RADICAL CATION

In Chapter 7 a number of reactions for the ethylene oxide radical cation (73) were discussed. It was originally suggested[226] that the reacting ion was an "activated" ethylene oxide ion, but in a later study[187] a C---C ring-opened structure was postulated for this reactive species. A detailed study of this C---C ring-opened ethylene oxide ion is reported in the next section.

This creates a dilemma. If the detected reactions are due to a

different isomer [e.g. (74)], the ethylene oxide ion proper remains to be identified. A study of a mixture of ethylene oxide and ethylene oxide-d_4 showed that the formation of protonated ethylene oxide (reaction 7.1) is due to proton transfer to neutral ethylene oxide from (73) and other fragment ions, and not to any detectable extent to hydride abstraction by the ethylene oxide molecular ions. It should be noted that this proton transfer from (73) is not as efficient as the proton transfer from the acetaldehyde molecular ion (72) to ethylene oxide (reaction 7.10). Examination of a mixture of acetaldehyde and ethylene oxide-d_4 shows that proton transfer from (73) to give protonated acetaldehyde does not occur.

10.2.4 IDENTIFICATION OF A FOURTH STABLE $C_2H_4O^{+\cdot}$ ISOMER: THE C---C RING-OPENED ETHYLENE OXIDE ION.

10.2.4.1 $CH_2^{+\cdot}$ Transfer

Beauchamp proposed[187] that the $C_2H_4O^{+\cdot}$ ion generated by electron impact from ethylene oxide which reacts with neutral ethylene oxide (reaction 7.3, see Fig. 9.4) is the C---C ring-opened ethylene

$$C_2H_4O^{+\cdot *} + C_2H_4O \rightarrow C_3H_5O^{+} + CH_3O^{\cdot} \qquad (7.3)$$

oxide ion (74). If experimental proof for the existence of this isomer could be given, it would establish (74) as a fourth stable $C_2H_4O^{+\cdot}$ isomer. In contrast to the proposal by Beauchamp, Kumakura and coworkers postulated[189,190] a C---O ring-opened ethylene oxide ion (75) as the reacting species in ion/molecule reactions of ionized ethylene oxide (see Section 7.2.4). The *ab initio* molecular orbital calculations reported earlier (Chapter 8) show that ion (74) should be a stable species whereas ion (75) was found to be higher in energy than its precursor, the ring-closed ethylene oxide ion (73).

Initial studies of the reactions of the $^{m}/_{z}$ 44 ion generated by electron impact of ethylene oxide revealed that it undergoes ion/molecule reactions with a large number of substrates (see Table 10.3). A common feature is the transfer of a $CH_2^{+\cdot}$ moiety, as proposed by Beauchamp (reaction 7.13), which initially leads to an odd-electron product ion. In a number of cases, further stabilization is obtained by loss of a hydrogen or halide radical, to give an even-electron ion as the final product. The observed reactions are summarized in Table 10.3. Noteworthy are the reactions with nitriles (reactions 10.27, 10.28 and 10.29) and with pyridine (reaction 10.52), which show large cross-sections for the product ions resulting from the $CH_2^{+\cdot}$ transfer from $^{m}/_{z}$ 44.

10.2.4.2 The Structure of the Ring-Opened Ion

In order to substantiate that the $CH_2^{+\cdot}$ transfer from ionized ethylene oxide was occurring *via* the C---C ring-opened isomer (74) and not the C---O ring-opened isomer (75), an alternative source of this ion was investigated. 1,3-Dioxolane (106) fragments under electron impact to give a predominant ion at $^{m}/_{z}$ 44 which could correspond to either (74) or (75). Collisional activation studies[215] led to the proposal that the $C_2H_4O^{+\cdot}$ ion from (106) was a mixture of the closed ethylene oxide ion (73) and the vinyl alcohol ion (71). However, measurements[79] of the heat of formation of this ion show it to be significantly lower in energy than (73) but higher than (71) (see Table 7.1), in agreement with the theoretical calculations reported in Chapter 8. These calculations also predict (74) to be substantially lower in energy than (75).

The $^{m}/_{z}$ 44 ion from 1,3-dioxolane (106) shows the same $CH_2^{+\cdot}$ transfer reactions as the ionized ethylene oxide ion (Table 10.3), but does not show the typical reactions of the enol ion (71) (Table 10.1). In order to

Table 10.3 Ion/Molecule Reactions Observed for the C---C Ring-Opened Radical Cation (74).

Neutral Substrate	Transfer Observed		Product Ion (m/z) (intensity[a])	Reaction
CH_2O	$CH_2^{+\cdot}$	b	44 (s)	10.15
CH_3CHO	$CH_2^{+\cdot}$	b,c	58 (m)	10.16
$CH_3\overset{O}{\overset{\|}{C}}CH_3$	$CH_2^{+\cdot}$	b,c	72 (m)	10.17
CH_3COOH	$CH_2^{+\cdot}$		74 (vs)	10.18
$HCOOCH_3$	No reaction			
CH_3COOCH_3	No reaction			
CH_3CONH_2	No reaction			
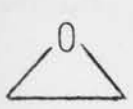	$CH_2^{+\cdot}$	b	58 (vs)	10.19
	$CH_2^{+\cdot} - H^{\cdot}$	b	57 (m)	10.20
	No reaction			
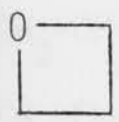	$CH_2^{+\cdot}$	b,c	72 (vs)	10.21
	$CH_2^{+\cdot} - H^{\cdot}$	b,c	71 (m)	10.22
	No reaction			
	$CH_2^{+\cdot}$	d	88 (m)	10.23
	$CH_2^{+\cdot} - H^{\cdot}$	d	87 (s)	10.24
	$CH_2^{+\cdot} - CH_2O$	d	58 (m)	10.25

Table 10.3 (Cont'd)

Neutral Substrate	Transfer Observed		Product Ion ($^{m}/_{z}$) (intensity[a])	Reaction
	No reaction			
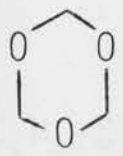	$CH_2^{+\cdot}$ - CH_2O - $H^{\cdot}$	d	73 (m)	10.26
CH_3-C≡N	$CH_2^{+\cdot}$	b,c	55 (1)	10.27
CH_2=CH-C≡N	$CH_2^{+\cdot}$	b,c	67 (1)	10.28
C_6H_5-C≡N	$CH_2^{+\cdot}$		117 (1)	10.29
CH≡CH	$CH_2^{+\cdot}$		40 (vs)	10.30
	$CH_2^{+\cdot}$ - $H^{\cdot}$		39 (s)	10.31
CH≡C-CH_2OH	$CH_2^{+\cdot}$ - $H^{\cdot}$	b,c	69 (m)	10.32
CH≡C-CH_2Br	$CH_2^{+\cdot}$ - $Br^{\cdot}$	b,c	53 (m)	10.33
CH≡C-C_6H_5	$CH_2^{+\cdot}$	b	116 (s)	10.34
	$CH_2^{+\cdot}$ - $H^{\cdot}$	b	115 (m)	10.35
CH_2=CH-CH_3	No reaction			
CH_2=CH-CH_2OH	$CH_2^{+\cdot}$ - $H^{\cdot}$		71 (s)	10.36
CH_2=CH-CH_2Br	$CH_2^{+\cdot}$ - $Br^{\cdot}$		55 (m)	10.37
CH_2=CBr-CH_3	$CH_2^{+\cdot}$ - $Br^{\cdot}$		55 (m)	10.38
CH_2=CH-CH_2Cl	$CH_2^{+\cdot}$ - $Cl^{\cdot}$		55 (m)	10.39
CH_2=CH-CH_2-C_6H_5	$CH_2^{+\cdot}$ - $H^{\cdot}$		131 (s)	10.40
$CH_3(CH_2)_4Br$	No reaction			
$CH_3CH_2NO_2$	$CH_2^{+\cdot}$ - CH_2O	e	59 (m)	10.41
$CH_3\overset{O}{\overset{\|}{S}}CH_3$	No reaction			

Table 10.3 (Cont'd)

Neutral Substrate	Transfer Observed	Product Ion ($^{m}/_{z}$) (intensity[a])	Reaction
C_6H_6	$CH_2^{+\cdot}$ b,c	92 (s)	10.42
	$CH_2^{+\cdot}$ - $H^{\cdot}$ b,c	91 (vs)	10.43
C_6H_5-CH_3	$CH_2^{+\cdot}$	106 (s)	10.44
	$CH_2^{+\cdot}$ - H	105 (vs)	10.45
C_6H_5-Cl	$CH_2^{+\cdot}$ - $Cl^{\cdot}$	91 (m)	10.46
C_6H_5-Br	$CH_2^{+\cdot}$ - $Br^{\cdot}$	91 (m)	10.47
C_6H_5-NO_2	$CH_2^{+\cdot}$ - CH_2O b,c,e	107 (m)	10.48
C_6H_5-OCH_3	$CH_2^{+\cdot}$ b	122 (s)	10.49
	$CH_2^{+\cdot}$ - $H^{\cdot}$ b	121 (m)	10.50
C_6H_5-NH_2	$CH_2^{+\cdot}$ - $H^{\cdot}$ b,c	106 (m)	10.51
	$CH_2^{+\cdot}$	93 (l)	10.52

[a] Intensity: vs = very small; s = small; m = medium; l = large.

[b] Transfer confirmed by deuterium labelling.

[c] Experiment was also carried out with $C_2H_4O^{+\cdot}$ from 1,3-dioxolane.

[d] Deuterium labelling shows that, in part, the $C_2H_4O^{+\cdot}$ is incorporated, see text.

[e] Oxygen abstraction by (74).

determine whether this transfer was occurring *via* ion (74) or (75), 4,4,5,5-d_4-1,3-dioxolane (106a) was prepared. The ICR and mass spectra of (106a) showed that the $^{m}/_{z}$ 44 ion had moved exclusively to $^{m}/_{z}$ 46 (74a), thus eliminating the possibility of (75a) as the reacting species (Scheme 10.3).

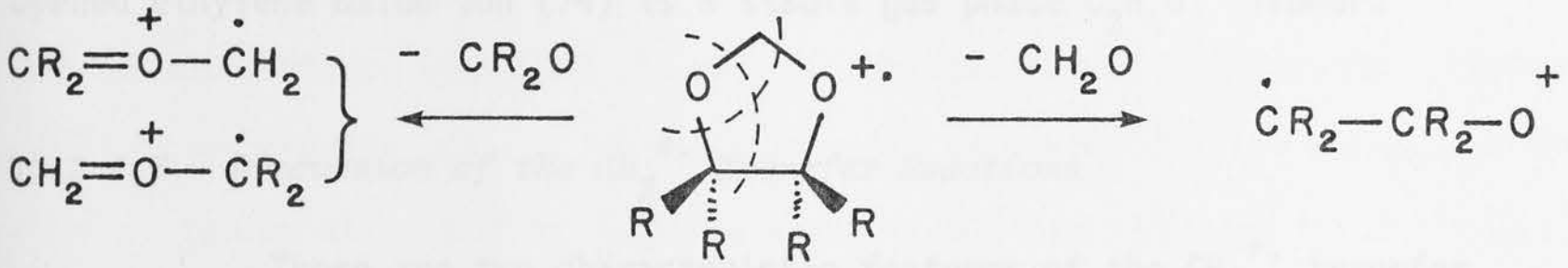

(74) $^{m}/_{z}$ 44 (106) R = H (75) $^{m}/_{z}$ 44

(74 a) $^{m}/_{z}$ 46 (106a) R = D (75 a) $^{m}/_{z}$ 48

SCHEME 10.3

When (106a) and acrylonitrile were examined in the ICR spectrometer, the $^{m}/_{z}$ 46 ion (74a) from (106a) transferred both $CH_2^{+\cdot}$ and $CD_2^{+\cdot}$ to the nitrile to give ions at $^{m}/_{z}$ 67 and $^{m}/_{z}$ 69 in the ratio 0.7 : 1.0. The identity of the $^{m}/_{z}$ 44 ion produced from 1,3-dioxolane was confirmed in yet another way by examination of the ICR spectrum of 4-methyl-1,3-dioxolane (107). The molecular ion of (107) can fragment with loss of formaldehyde to give $^{m}/_{z}$ 58 or with loss

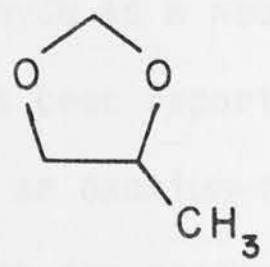

(107)

of acetaldehyde to give $^{m}/_{z}$ 44. If the latter process occurs, the ion formed will be of structure (74). Indeed, the ICR spectrum of (107) shows two prominent signals at $^{m}/_{z}$ 44 and 58. In a mixture of (107) and acetonitrile, a $CH_2^{+\cdot}$ transfer from $^{m}/_{z}$ 44 (reaction 10.27) is observed.

Thus evidence has been presented showing that the C---C ring-opened ethylene oxide ion (74) is a stable gas phase $C_2H_4O^{+\cdot}$ isomer.

10.2.4.3 Discussion of the $CH_2^{+\cdot}$ Transfer Reactions

There are two characteristic features of the $CH_2^{+\cdot}$ transfer reactions. Firstly, the transfer is mainly to substrates with electron rich functional groups and secondly, the product ion is often stabilized by loss of a hydrogen or halide radical to yield in general a more stable even-electron ion species. Clearly the loss of formaldehyde from (74) during the $CH_2^{+\cdot}$ transfer is the main driving force in the reaction. A similar $CH_2^{+\cdot}$ transfer has been observed[267,268] for the $C_3H_6^{+\cdot}$ ion produced by electron impact from cyclopropane, tetrahydrofuran and cyclohexanone. This ion was found to transfer a $CH_2^{+\cdot}$ moiety to ammonia, the neutral fragment lost being ethylene. The initial product ion $CH_2\text{-}NH_3^{+\cdot}$ can easily lose a hydrogen radical to produce the main product ion of m/z 30 ($CH_2{=}\overset{+}{N}H_2$). Another reaction related to the $CH_2^{+\cdot}$ transfer from (74) is the methyl cation transfer to suitable substrates found for the methyoxymethyl cation[269] ($CH_3\text{-}\overset{+}{O}{=}CH_2$), where the driving force is also likely to be the loss of formaldehyde as a neutral fragment. Yet another related ion/molecule reaction which has been reported[270] is a reaction in which a $C_2H_4^{+\cdot}$ moiety is transferred from an oxonium-type radical cation (108) to nitriles (reaction 10.53), again with the concomitant elimination of a small, stable neutral molecule.

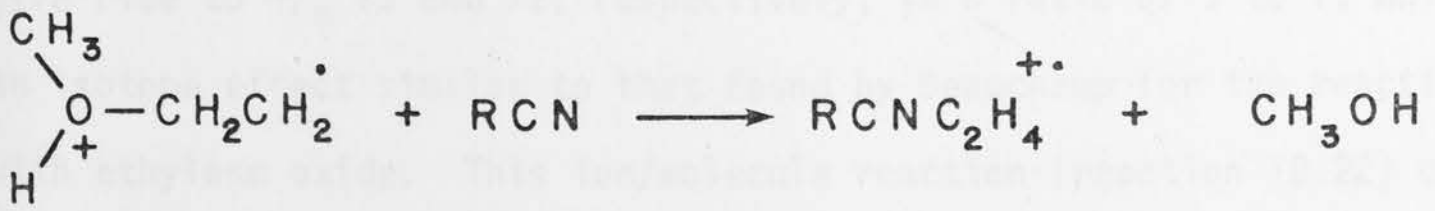

10.53

(108)

Reactions of (74) with compounds containing a carbonyl functional group. The intensity of the product ion for the $CH_2^{+\cdot}$ transfer to formaldehyde, acetaldehyde and acetone (reactions 10.15 - 10.17) increases in that order. Reaction 10.15 is degenerate but can be shown to exist by using ethylene oxide-d_4. The product ion in the reaction with acetaldehyde has been studied theoretically, and is found to be best represented by $CH_3\text{-}CH{=}\overset{+}{O}\text{-}\dot{C}H_2$ (Chapter 11). Similarly, the product ion of the reaction with acetone is expected to have the structure $(CH_3)_2C{=}\overset{+}{O}\text{-}\dot{C}H_2$. This is probably the same ion as the one reported to be produced[271] by an ion/molecule reaction of the acetone radical cation with ketene, in which a $CH_2^{+\cdot}$ abstraction by the acetone radical cation leads to a product ion of m/z 72. Experiments involving acetic acid, methyl formate, methyl acetate and acetamide showed no transfer reaction or only a trace of a product ion in the case of acetic acid (reaction 10.18).

Reactions of (74) with oxocyclic compounds. The reaction of (74) with ethylene oxide has previously been studied by Beauchamp[187], and the same results are found here. It is worth noting that a small signal is observed at m/z 58, which corresponds to the intermediate trimethylene oxide cation proposed by Beauchamp (reaction 7.13). Three of the oxocyclic compounds studied did not react with (74): propylene oxide, tetrahydrofuran and 1,4-dioxane. Trimethylene oxide, however, did react in much the same way as ethylene oxide, the principal product ion arising from $CH_2^{+\cdot}$ transfer with loss of a hydrogen radical ($H^{\cdot}$). Use of ethylene oxide-d_4 showed that upon $CD_2^{+\cdot}$ transfer, both $H^{\cdot}$ and $D^{\cdot}$ are lost to give rise to m/z 73 and 72, respectively, in a ratio of 3 to 1, which constitutes an isotope effect similar to that found by Beauchamp for the reaction of (74) with ethylene oxide. This ion/molecule reaction (reaction 10.22) can therefore be proposed to proceed *via* a mechanism similar to reaction 7.13.

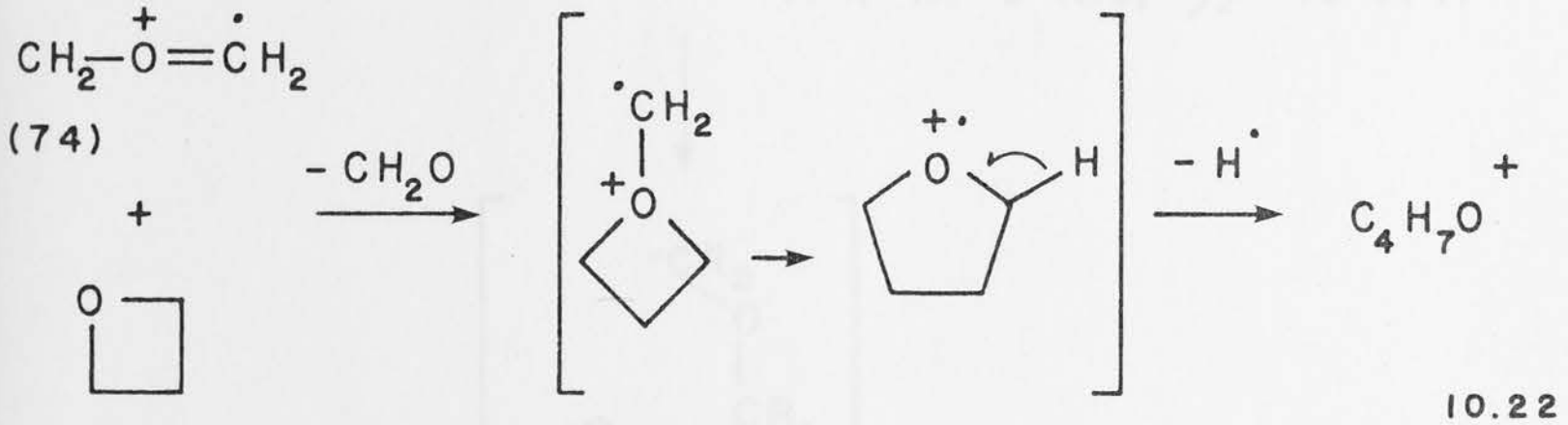

10.22

1,3-Dioxolane shows a $CH_2^{+\cdot}$ adduct ion at $^m/_z$ 88 (reaction 10.23), as well as ions for subsequent losses of H$^\cdot$ ($^m/_z$ 87, reaction 10.24) and CH_2O ($^m/_z$ 58, reaction 10.25). A labelling experiment using $CD_2{=}\overset{+}{O}{-}\dot{C}D_2$ from ethylene oxide-d_4 showed product ions at $^m/_z$ 58, 60, 62, 90 and 92, which by double resonance were shown to be due to reactions of $^m/_z$ 48. The presence of the ion at $^m/_z$ 92 indicates the incorporation of all four deuterium atoms of the reactant ion and must arise from loss of CH_2O from the initial adduct of ion (74) with 1,3-dioxolane. A reaction scheme to rationalize the observed product ions is shown in Scheme 10.4. With trioxane only one product ion is observed, at $^m/_z$ 73 (reaction 10.26). This ion is found, surprisingly, to shift mainly to $^m/_z$ 76 when ethylene oxide-d_4 is used, with minor signals for $^m/_z$ 77, 75, and 74. Thus the formation of the product ion is not a simple $CH_2^{+\cdot}$ transfer followed by loss of CH_2O and H$^\cdot$, which would lead to $^m/_z$ 74 or 75 in the labelled study. A plausible mechanism is shown in Scheme 10.5, where the ion (74) is added to the trioxane molecule, with concomitant loss of two CH_2O units from the ring, leading to the formation of a 1,3-dioxolane ion, which subsequently loses D$^\cdot$ (H$^\cdot$).

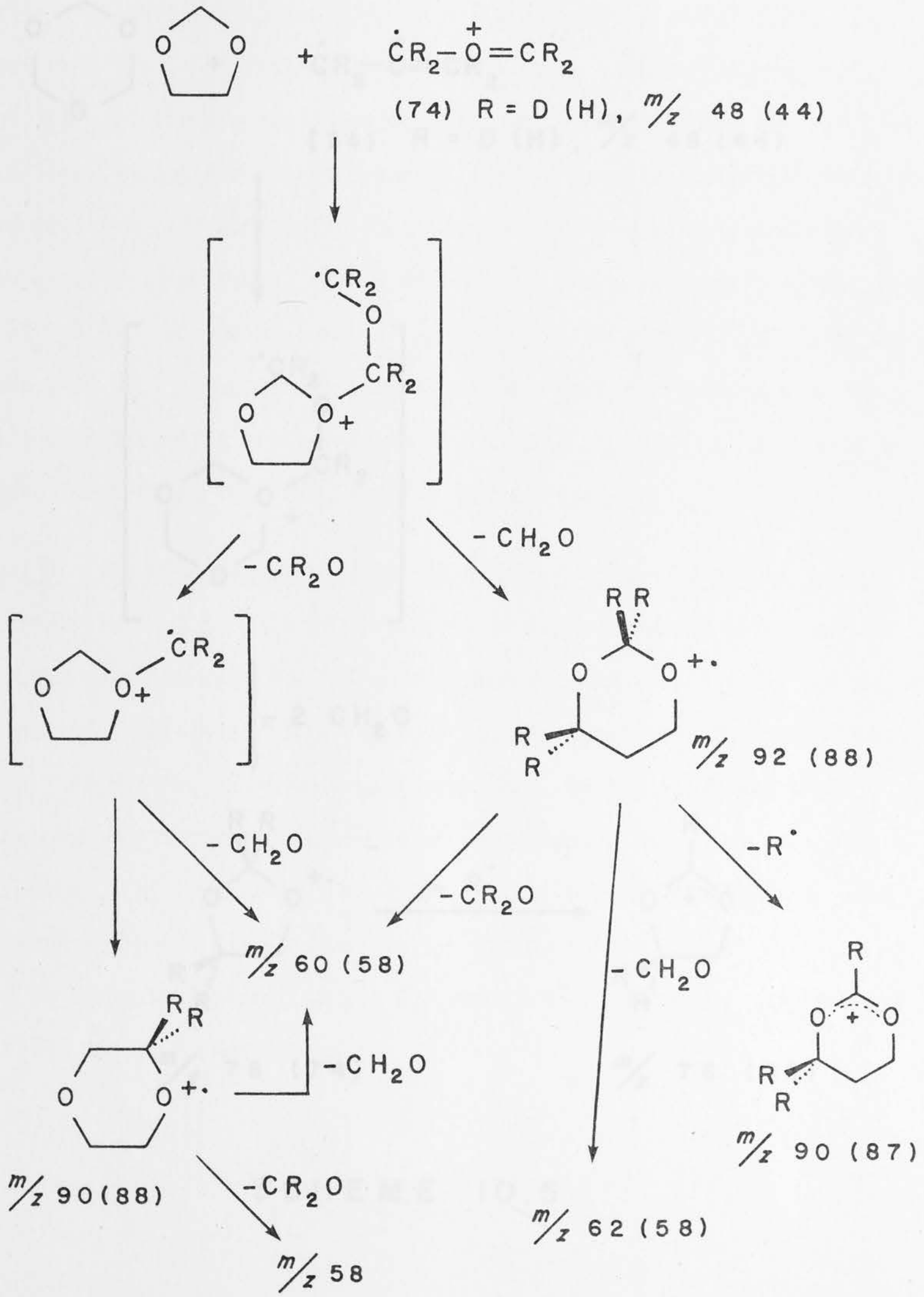
+
$\dot{C}R_2-\overset{+}{O}=CR_2$
(74) R = D (H), m/z 48 (44)
$\cdot CR_2$
O
CR_2
O
O^+
$-CR_2O$
$-CH_2O$
CR_2
O^+
R R
$O^{+\cdot}$
R
R
m/z 92 (88)
$-CH_2O$
$-CR_2O$
$-R^\cdot$
m/z 60 (58)
R R
$O^{+\cdot}$
$-CH_2O$
$-CR_2O$
m/z 90(88)
m/z 58
$-CH_2O$
R
O^+
R
R
m/z 90 (87)
m/z 62 (58)

SCHEME 10.4

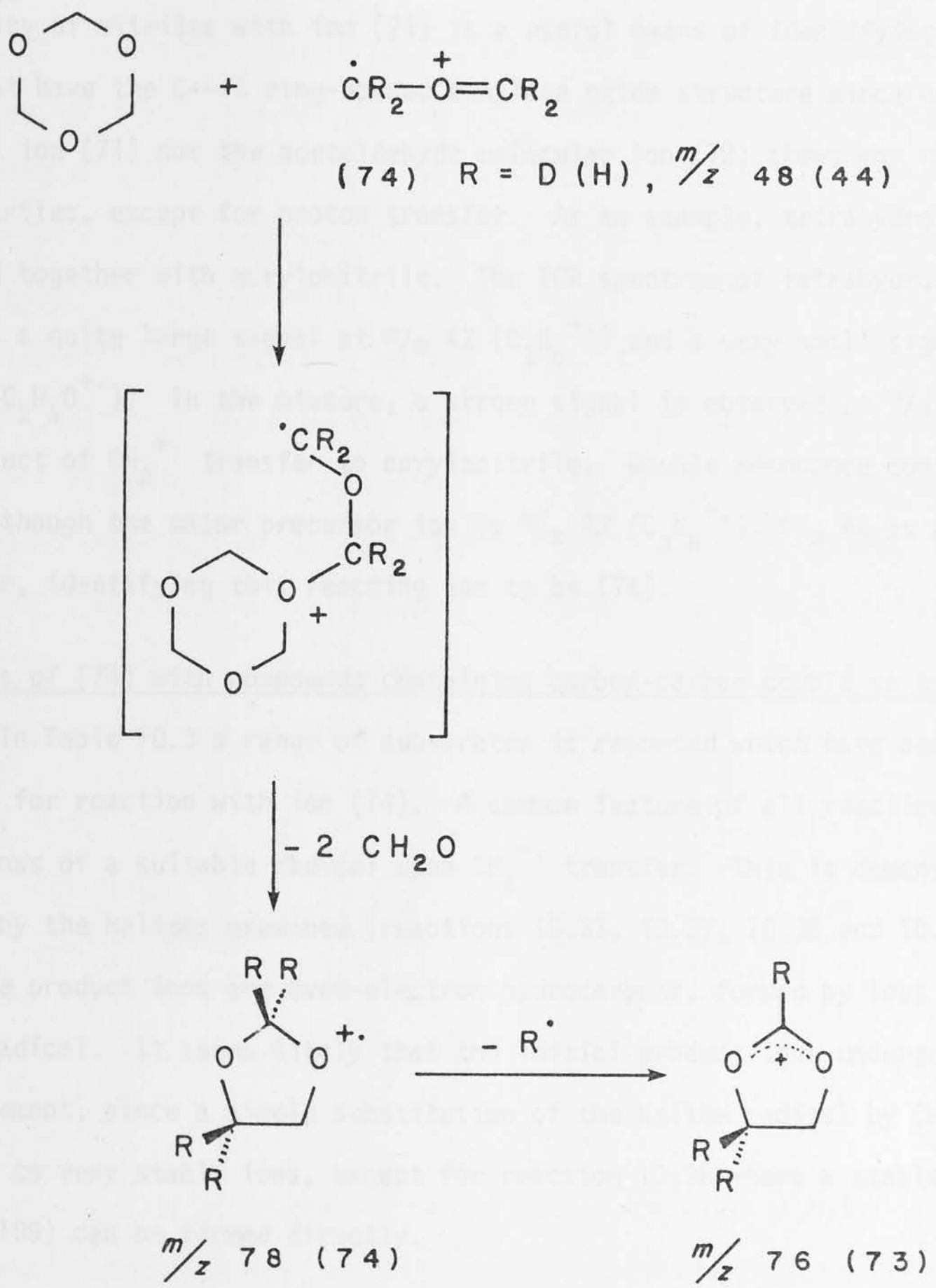

SCHEME 10.5

Reactions of (74) with nitriles. Nitriles are found to be very efficient as substrates for the $CH_2^{+\cdot}$ transfer reactions. The product ion might be expected to have a structure similar in character to the reacting ion (74)

e.g. $R\text{-}C{\equiv}\overset{+}{N}\text{-}\dot{C}H_2$[†]. Because of the high cross-section for this reaction, the reactivity of nitriles with ion (74) is a useful means of identifying $C_2H_4O^{+\cdot}$ ions that have the C---C ring-opened ethylene oxide structure since neither the enol ion (71) nor the acetaldehyde molecular ion (72) shows any reaction with nitriles, except for proton transfer. As an example, tetrahydrofuran was examined together with acrylonitrile. The ICR spectrum of tetrahydrofuran contains a quite large signal at $^{m}/_{z}$ 42 ($C_3H_6^{+\cdot}$) and a very small signal at $^{m}/_{z}$ 44 ($C_2H_4O^{+\cdot}$). In the mixture, a strong signal is observed at $^{m}/_{z}$ 67 for the product of $CH_2^{+\cdot}$ transfer to acrylonitrile. Double resonance confirms that, although the major precursor ion is $^{m}/_{z}$ 42 ($C_3H_6^{+\cdot}$), $^{m}/_{z}$ 44 is also a precursor, identifying this reacting ion to be (74).

Reactions of (74) with compounds containing carbon-carbon double or triple bonds. In Table 10.3 a range of substrates is reported which have been examined for reaction with ion (74). A common feature of all reactions found is the loss of a suitable radical upon $CH_2^{+\cdot}$ transfer. This is demonstrated clearly by the halides examined (reactions 10.33, 10.37, 10.38 and 10.39), where the product ions are even-electron hydrocarbons, formed by loss of the halide radical. It seems likely that the initial product ions undergo some rearrangement, since a simple substitution of the halide radical by $CH_2^{+\cdot}$ would not lead to very stable ions, except for reaction 10.38 where a stable allyl cation (109) can be formed directly.

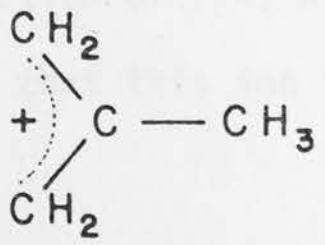

(109)

† Confirmed by *ab initio* calculations for $H\text{-}C{\equiv}N\text{-}CH_2^{+\cdot}$ and $CH_3\text{-}C{\equiv}N\text{-}CH_2^{+\cdot}$.

The fact that acetylene reacts only to a minor extent and that propene does not react at all illustrates that a $CH_2^{+\cdot}$ transfer occurs only if the accompanying loss of a radical species can lead to a reasonably stable product ion. On the other hand, the necessity for a double or triple bond to be present in the molecule is shown by the result that 1-bromopentane does not react at all with (74). Propargyl alcohol reacts with (74) *via* ($CH_2^{+\cdot}$ - $H^{\cdot}$) transfer (reaction 10.32). When ethylene oxide-d_4 is used a $CD_2^{+\cdot}$ transfer occurs, but still with loss of $H^{\cdot}$, not $D^{\cdot}$. Exchange of the hydroxylic hydrogen with D_2O in the inlet system afforded propargyl alcohol-O-*d*, which in reaction with unlabelled (74) shows retention of the deuterium in the product ion. These results indicate that the $H^{\cdot}$ loss must involve either the acetylenic hydrogen or the methylene group of the substrate. If it is assumed that the latter occurs, to lead to extended conjugation, a reaction *via* (110) to give (111) is possible.

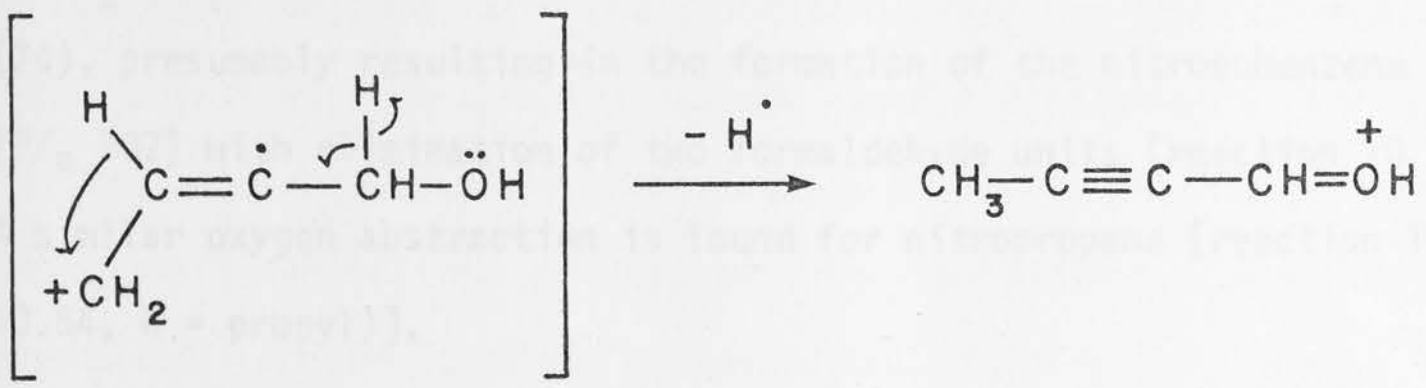

(110) (111)

The reaction with allyl alcohol (reaction 10.36) might be expected to proceed in a similar fashion to that discussed for propargyl alcohol. A consideration of the pathway for the reaction of (74) with phenyl acetylene and allyl benzene is complicated by the fact that this ion is also found to react with aromatic compounds (see below).

Reactions of (74) with aromatic compounds. Surprisingly, a $CH_2^{+\cdot}$ transfer is found for the reaction of (74) with benzene (reaction 10.42). The product ion

of $^{m}/_{z}$ 92 would be expected to have the toluene or cycloheptatriene structure. Also present is an ion at $^{m}/_{z}$ 91, only a fraction of which shows $^{m}/_{z}$ 44 as a precursor, indicating that the major process occurring from (74) is $CH_2^{+\cdot}$ transfer, not ($CH_2^{+\cdot}$ - H$^{\cdot}$) transfer. In a similar way, the principal reaction of (74) with toluene is $CH_2^{+\cdot}$ transfer, resulting in a product ion at $^{m}/_{z}$ 106 (reaction 10.44). For chlorobenzene and bromobenzene a $CH_2^{+\cdot}$ transfer coupled with Cl$^{\cdot}$ or Br$^{\cdot}$ loss is found. Here a stable even-electron ion is formed which can either have the benzyl cation or tropylium ion structure, with the latter being more likely since it is lower in energy[272]. The reaction with nitrobenzene is interesting (reaction 10.48). With ethylene oxide, a product ion is observed at $^{m}/_{z}$ 107, originating from $^{m}/_{z}$ 44. This corresponds to a $CH_2^{+\cdot}$ transfer, followed by loss of 30, which could be either NO or CH_2O. Using ethylene oxide-d_4, the observed product ion remains at $^{m}/_{z}$ 107, confirming that the fragment lost is CH_2O. Thus an oxygen atom is abstracted from the neutral substrate by ion (74), presumably resulting in the formation of the nitrosobenzene radical cation ($^{m}/_{z}$ 107) with elimination of two formaldehyde units (reaction 10.54, R = phenyl). A similar oxygen abstraction is found for nitropropane [reaction 10.41 (reaction 10.54, R = propyl)].

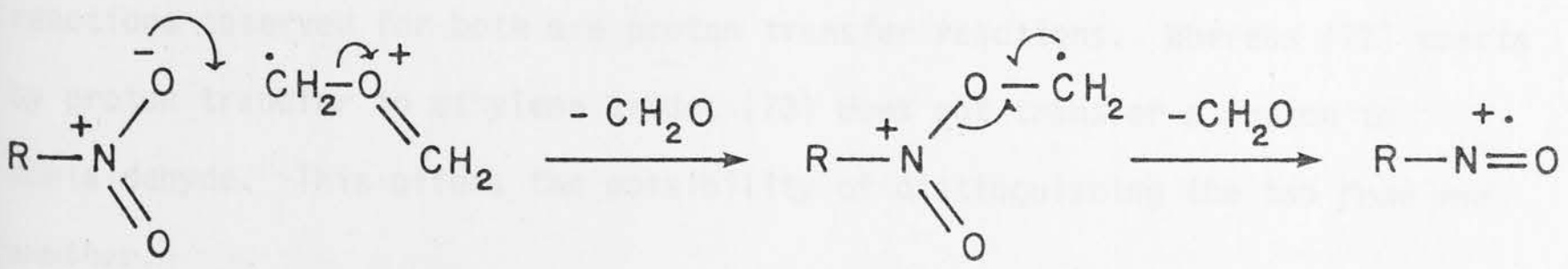

10.54

The ion/molecule reactions of (74) with anisole (reactions 10.49 and 10.50) and aniline (reaction 10.51) seem to take place at the functional group. Deuterium labelling shows that the H$^{\cdot}$ which is lost upon $CH_2^{+\cdot}$ transfer does not come from the $CH_2^{+\cdot}$ moiety. Thus for reaction 10.51 a likely structure of the product ion at $^{m}/_{z}$ 106 is (112).

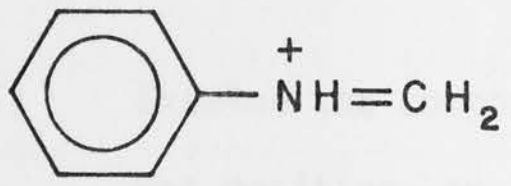

(112)

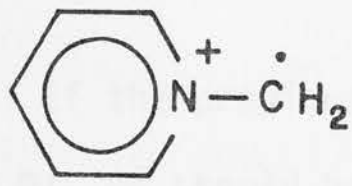

(113)

Finally, a very efficient $CH_2^{+\cdot}$ transfer is found for the reaction of (74) with pyridine (reaction 10.52, see Fig. 9.5). By analogy with the ion/molecule reactions of (74) with nitriles, it seems likely that the transfer is to the nitrogen, leading to a product ion at $^m/_z$ 93 of structure (113).

10.2.5 EVALUATION OF THE RESULTS

So far, four $C_2H_4O^{+\cdot}$ isomers have been examined by ICR spectroscopy with the aim of identifying specific ion/molecule reactions that can distinguish each isomer. Two isomers, the vinyl alcohol radical cation (71) and the C---C ring-opened ethylene oxide radical cation (74), show distinct ion/molecule reactions, the former reacting mainly *via* 2 + 2 addition of the double bond to olefins and acetylenes and the latter by $CH_2^{+\cdot}$ transfer to a variety of polarizable substrates. Of the remaining two isomers, the acetaldehyde radical cation (72) and the ethylene oxide radical cation (73), the only ion/molecule reactions observed for both are proton transfer reactions. Whereas (72) reacts by proton transfer to ethylene oxide, (73) does not transfer a proton to acetaldehyde. This offers the possibility of distinguishing the two *from one another*.

A general approach for assigning a structure to an $^m/_z$ 44 ion of composition C_2H_4O by ICR spectrometry would be:

(i) Examine the compound which gives rise to the $^m/_z$ 44 ion with a nitrile or pyridine. A prominent signal for $CH_2^{+\cdot}$ transfer from $^m/_z$ 44 to either substrate will indicate the presence of isomer (74).

(ii) Examine the compound with trioxane. If the previous test was positive, an ion at $^{m}/_{z}$ 73 from $^{m}/_{z}$ 44 should be observed. If, however, an ion at $^{m}/_{z}$ 74 with $^{m}/_{z}$ 44 as precursor is found, the presence of the enol isomer (71) is suggested. This can be confirmed by other ion/molecule reactions listed in Table 10.1.

(iii) If the previous tests were negative, the ion under study is likely to be the acetaldehyde radical cation (72) or, less likely, the ethylene oxide radical cation (73). The compound under investigation can then be examined with acetaldehyde-d_4. If double resonance shows that $^{m}/_{z}$ 44 (the ion to be identified) reacts by proton transfer to acetaldehyde-d_4, then it has structure (72) rather than (73).

Since ionized ethylene oxide reacts as the C---C ring-opened species (74), it is difficult to determine if only (74) or a mixture of (74) and (73) is present. When produced from 1,3-dioxolane, the ion (74) does not show proton transfer to ethylene oxide-d_4, whereas in a mixture of ethylene oxide and ethylene oxide-d_4 a weak proton transfer from $^{m}/_{z}$ 44 to give $^{m}/_{z}$ 49 is observed. The latter transfer presumably is from the ring-closed ethylene oxide radical cation (73), but could also be due to differences in the internal energy of the two ions.

A rather remarkable aspect of the ion/molecule reactions which have been studied here is the stability of some of the odd-electron ions produced in the reactions. The ions produced in the reactions of the vinyl alcohol ion [(71), reactions 10.1 and 10.2] can be trapped in the ICR cell, at pressures of $\sim 10^{-5}$ torr, for times up to 1 second, during which they must undergo collisions

with neutral molecules. Likewise, some of the odd-electron species produced by $CH_2^{+\cdot}$ transfer from the C---C ring-opened ethylene oxide ion [(74), reaction 10.17] show by trapping experiments that they have lifetimes > 500 ms. These results are in contrast to the general belief that odd-electron species are much less stable than even-electron ions and tend to fragment readily to give an even-electron ion and a radical fragment.

10.3 THE EXISTENCE OF OTHER STABLE $C_2H_4O^{+\cdot}$ ISOMERS

In Chapter 8, a number of low energy $C_2H_4O^{+\cdot}$ isomers were identified which are not yet known as existing species, but have reasonable prospects for being observable. The fact that one such isomer, the C---C ring-opened ethylene oxide ion (74), was calculated to be of lower energy than the ethylene oxide ion (73), and subsequently was identified experimentally as a stable $C_2H_4O^{+\cdot}$ isomer, lends confidence to our predictions.

The three isomers most likely to be observable are $CH_3COH^{+\cdot}$ (76), $CH_3OCH^{+\cdot}$ (77) and $CHCHOH_2^{+\cdot}$ (78). In order to generate these ions, either suitable precursors need to be found which might produce these isomers upon electron impact, or ion/molecule reactions have to be designed which might lead to such a species.

Pyruvic acid had been reported to have a fragment ion of $^m/_z$ 44 in its mass spectrum[186], for which ion structure (76) had been proposed. When examined in the ICR spectrometer at low temperatures, no significant signal at $^m/_z$ 44 could be detected and therefore no further investigation was possible. It seems probable that the reported $^m/_z$ 44 ions arose from thermal decarboxylation of the pyruvic acid to acetaldehyde.

An experiment in which a mixture of acetylene and water was studied in order to probe for the occurrence of reaction 10.55 and possible

formation of (78), was unsuccessful. A similar reaction between $H_2S^{+\cdot}$ and acetylene has been reported[273], however, in which a H_2S---$HC{\equiv}CH^{+\cdot}$ complex was proposed as a transient species which subsequently lost $H^{\cdot}$ to give the observed $C_2H_3S^+$ species.

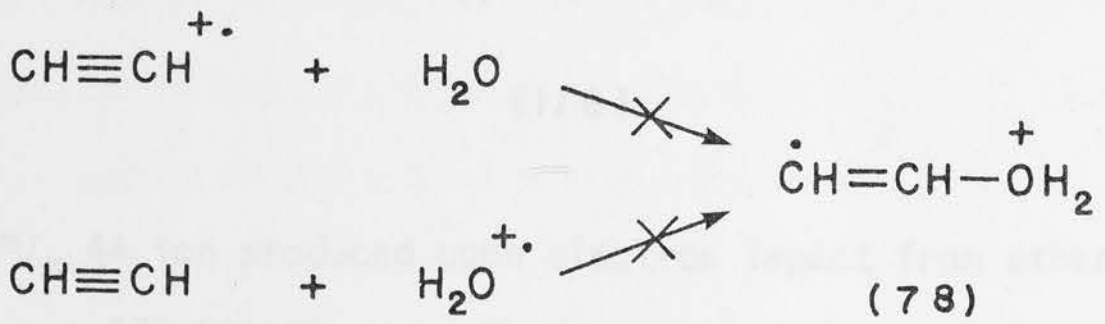

10.55

(78)

No other approaches to generation of new $C_2H_4O^{+\cdot}$ species were carried out during this study. Possible precursor molecules for other as yet unobserved but energetically plausible $C_2H_4O^{+\cdot}$ ions include (dimethoxymethyl)-trimethoxy silane (114), which is known to produce methoxymethylene ($CH_3O\ddot{C}H$) upon heating[274].

$$(CH_3O)_3Si{-}CH(OCH_3)_2$$

(114)

This might be a way of generating the corresponding ion, $CH_3OCH^{+\cdot}$ (77). Another possible precursor for the ion (77) is methoxymethyl acetate (115) which was shown to produce $CH_3O\ddot{C}H$ upon thermolysis[275].

$$CH_3\overset{\overset{O}{\|}}{C}{-}O{-}CH_2OCH_3$$

(115)

Another way of generating (77) or (76) could be from a suitably substituted, but as yet unknown, diazirine[276,277] (116), which for R_1 = H, R_2 = OCH_3 might

produce $CH_3O\ddot{C}H$ by elimination of nitrogen, and for R_1 = OH, R_2 = CH_3 could lead to $CH_3\ddot{C}OH$.

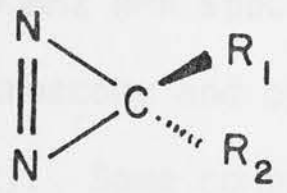

(116)

The $^{m}/_{z}$ 44 ion produced upon electron impact from ethane-1,2-diol cyclic carbonate[278] [(117), X = C] and the thiocarbonate [(117), X = S], which might have the CH_2-CH_2-$O^{+\cdot}$ structure (75), or be a rearranged species [(72), (73) or (74)], is also worth investigating.

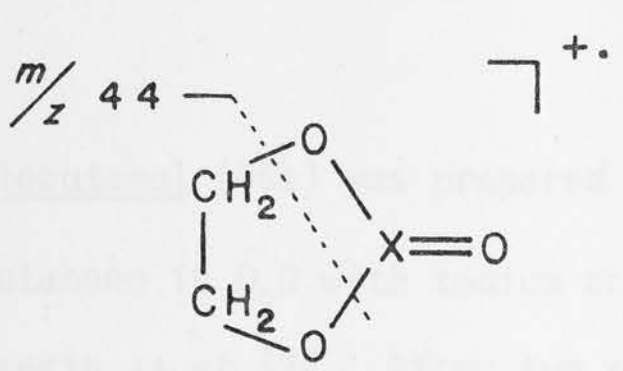

(117)

Two major problems in extending these experimental studies are that not only does a suitable way of generating a new isomer need to be found, but also that specific ion/molecule reactions which will unequivocally identify the new isomer need to be discovered.

10.4 EXPERIMENTAL

Unless otherwise stated the reagents used for the experiments were commercially available and of reagent grade. When necessary they were distilled before use. Formaldehyde was generated in the inlet system by thermolysis of paraformaldehyde. Ethylene oxide-d_4 and acetaldehyde-d_4 were obtained from

Merck, Sharp and Dohme, Canada, Ltd. A number of compounds, that were not readily available, were synthesized. Their identity and purity were checked by n.m.r. (Jeol Minimar 100 MHz NMR spectrometer) and infrared (Perkin-Elmer 257 spectrophotometer) spectroscopy and by mass spectrometry (at 70 and 20 eV on an AEI MS-902 instrument). Some compounds were purified by preparative gas liquid chromatography (g.l.c.). Analytical g.l.c. analysis and preparative g.l.c. were carried out on Varian aerograph 1400 and Varian aerograph 90-P instruments, respectively, using 20% OV-17 columns.

2,2,2-d_3-Acetaldehyde was prepared according to Baldwin and Pudussery[279] by exchanging the methyl protons of acetaldehyde in D_2O with pyridine as base. Three exchanges resulted in CD_3CHO with 99% deuterium incorporation in the methyl group.

2,2,4,4,-d_4-Cyclobutanol (95b) was prepared by exchanging the α-hydrogen atoms in cyclobutanone in D_2O with sodium acetate as base, in a sealed tube, according to Caserio *et al.*[280]. After two exchanges, the 2,2,4,4-d_4-cyclobutanone was reduced with $LiAlH_4$ to give 2,2,4,4-d_4-cyclobutanol which was purified by preparative g.l.c. Mass spectral analysis showed ∿ 80% deuterium incorporation.

1,2,2,4,4-d_5-Cyclobutanol (95c). 2,2,4,4-d_4-cyclobutanone was prepared from cyclobutanone as above[280], and reduced with $LiAlD_4$ to give 1,2,2,4,4-d_5-cyclobutanol which was purified by preparative g.l.c. Mass spectral analysis showed ∿ 90% deuterium incorporation.

1-Methylcyclobutanol was prepared from cyclobutanone and methyl iodide according to Semenow *et al.*[281], and purified by preparative g.l.c.

1,3-Dioxolane (106). This compound was prepared by the method of Brikenshtein *et al.*[282] from condensation of 1,2-ethanediol (ethylene glycol) and formaldehyde (using paraformaldehyde) with concentrated H_2SO_4 as catalyst. Water formed was removed by adding CaH_2 to the reaction mixture. Distillation afforded 1,3-dioxolane.

4,4,5,5-d_4-1,3-Dioxolane (106a) was prepared as for 1,3-dioxolane, using 1,1,2,2-d_4-ethylene glycol which had been obtained by $LiAlD_4$ reduction of diethyl oxalate. Deuterium incorporation was > 97%.

4-Methyl-1,3-dioxolane (107) was prepared as described for 1,3-dioxolane, using 1,2-propanediol instead of ethylene glycol.

CHAPTER 11

A THEORETICAL STUDY OF $C_3H_6O^{+\cdot}$ ISOMERS

11.1 INTRODUCTION

In this thesis, theoretical and some experimental studies have been described of small ion species for which a number of isomers are possible, for example, the $CH_2O^{+\cdot}$ and $C_2H_4O^{+\cdot}$ systems (Chapters 6, 8 and 10). The next higher homologue in this series, the $C_3H_6O^{+\cdot}$ system, has received considerable attention from experimentalists[187,210,263-266,283-290]. As was the case for the $C_2H_4O^{+\cdot}$ isomers, no theoretical study of the $C_3H_6O^{+\cdot}$ isomers has been reported to date. In this chapter, theoretical results for a substantial number of $C_3H_6O^{+\cdot}$ isomers are reported. The study includes seven species [(121) - (124), (130), (132) and (133)] which correspond to the molecular ions of known neutral C_3H_6O isomers, and ten additional $C_3H_6O^{+\cdot}$ isomers [(118) - (120), (125) - (129), (131) and (134)] which might also be observable species. The experimental studies of the $C_3H_6O^{+\cdot}$ system have been concerned with identification of and distinguishing between various isomers. Ion cyclotron resonance studies[263,283,284] established that the acetone radical cation (121) and its enol isomer (118) generated from suitable precursors, are distinct, non-interconverting species, but found no evidence for the symmetric oxonium ion (126), which had been proposed to result from a double McLafferty rearrangement in alkanones. ICR studies[264-266] of the methyl vinyl ether radical cation (122) identified ion/molecule reactions characteristic of this ion (cf. reaction 10.12), and in an ICR study of cyclopropanol[290] the molecular ion (133) was assumed to retain the cyclopropanol structure. The problem of whether (118) and (121) are distinct species was also examined by labelling and metastable ion studies[285,287], which confirmed the ICR result. Metastable analysis of the decomposition of the molecular ions of propylene oxide (132), propanal (123) and trimethylene oxide (130) showed that they were distinct species.[210] It must be noted that metastable ion studies are of short-lived decomposing ions (10^{-5} - 10^{-6} sec), whereas ICR

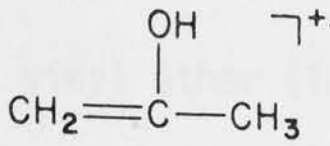

(118)

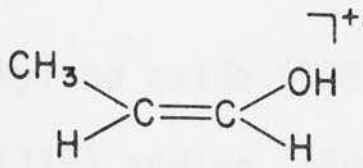

(119)

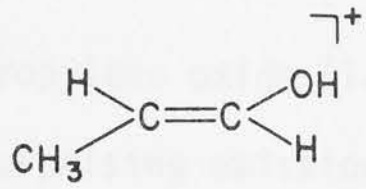

(120)

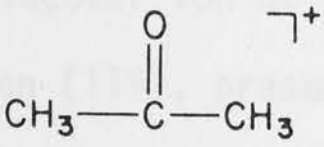

(121)

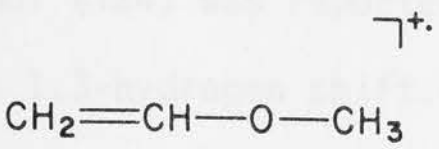

(122)

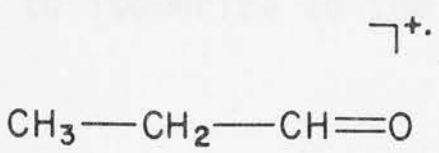

(123)

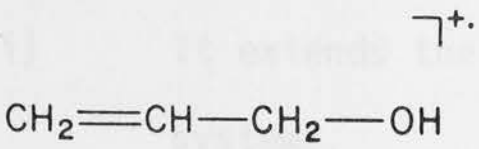

(124)

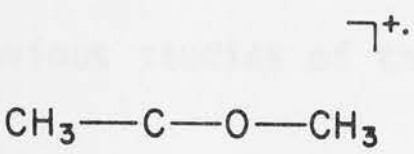

(125)

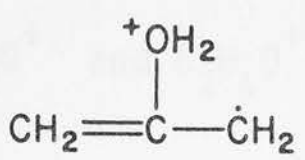

(126)

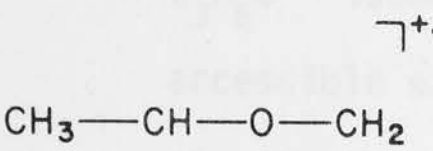

(127)

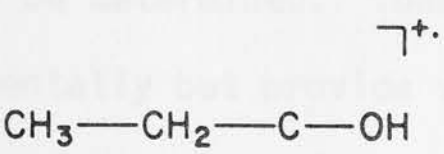

(128)

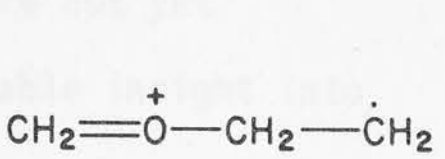

(129)

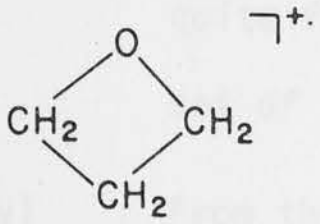

(130)

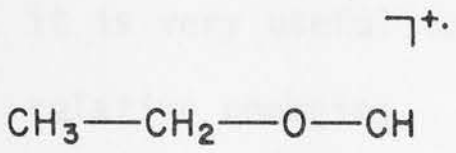

(131)

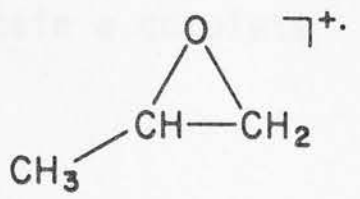

(132)

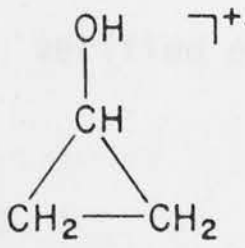

(133)

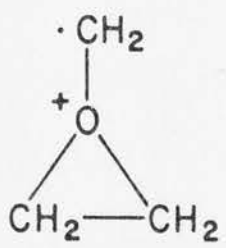

(134)

experiments involve stable ions of relatively long lifetimes (> 10^{-3} sec). Another method of distinguishing stable gas-phase isomeric ion species is by their collisional activation (CA) spectra. With this technique, seven $C_3H_6O^{+\cdot}$ isomers were identified[286,289] as distinct species formed from a number of precursors. They were the molecular ions of acetone (121), propanal (123),

methyl vinyl ether (122), trimethylene oxide (130) and propylene oxide (132), plus the enol isomers (118) and (119) and/or (120). A surprising omission from this CA study[289] was the cyclopropanol molecular ion (133). In this study, the molecular ion of allyl alcohol (124) was reported[289] to isomerize to the enol ion (119), presumably *via* a 1,3-hydrogen shift.

There are several reasons for undertaking this theoretical study of the $C_3H_6O^{+\cdot}$ system.

(i) It extends the previous studies of the $CH_2O^{+\cdot}$ and $C_2H_4O^{+\cdot}$ systems.

(ii) It enables the detailed structural parameters of the various $C_3H_6O^{+\cdot}$ isomers to be determined. These are not yet accessible experimentally but provide valuable insight into the properties of the ions.

(iii) Since thermochemical information for the $C_3H_6O^{+\cdot}$ system is quite fragmentary, it is very useful to obtain a complete set of theoretical relative energies.

(iv) From these energy calculations, low energy isomers can be identified, whose structures have not hitherto been verified experimentally.

11.2 METHOD

The *ab initio* molecular orbital calculations described here were carried out at the RHF/4-31G//RHF/STO-3G level, which was described earlier (see Chapter 10). All geometries were optimized subject to specified symmetry constraints, and are displayed within the text. The resulting total and relative energies are listed in Table 11.1.

11.3 STRUCTURES, ENERGIES AND RELATIVE STABILITIES OF THE $C_3H_6O^{+\cdot}$ ISOMERS

$\underline{CH_2{=}C(OH){-}CH_3}^{+\cdot}$ (118). For the optimization of the 1-propen-2-ol radical cation, an initial structure based on the optimized geometry of the vinyl alcohol radical cation (71) was chosen. The structure of (118) was optimized in the conformation shown, imposing C_s symmetry only. This isomer, which is the enol tautomer of the acetone radical cation, is found to be the most stable $C_3H_6O^{+\cdot}$ isomer. This is consistent with experimental[79] and theoretical (Chapter 8) results for the $C_2H_4O^{+\cdot}$ isomers, where the enol isomer was also found to be the most stable radical cation.

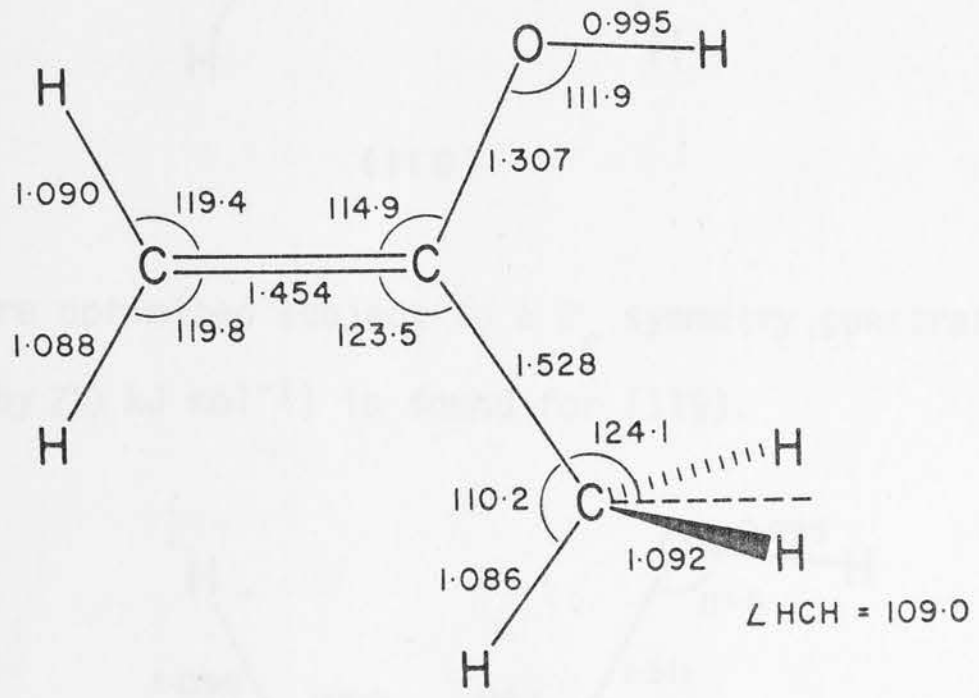

(118)

The results indicate that in (118) an electron has been removed from the π-electron system of 1-propen-2-ol resulting in elongation of the C=C double bond and a shortening of the C-O bond, similar to that found for vinyl alcohol. The parent neutral compound, 1-propen-2-ol is not a particularly stable C_3H_6O isomer, but it has been identified as a transient species by CIDNP PMR and C^{13} NMR spectroscopy[291,292].

$\underline{CH_3{-}CH{=}CH{-}OH}^{+\cdot}$ [(119) and (120)]. For 1-propen-1-ol, geometric isomers corresponding to the methyl group being *cis* (119) or *trans* (120) to

the hydroxyl group are possible and both have been examined. As for (118), the hydroxylic hydrogen was chosen *anti* to the double bond, by analogy with the structure of the vinyl alcohol radical cation (71).

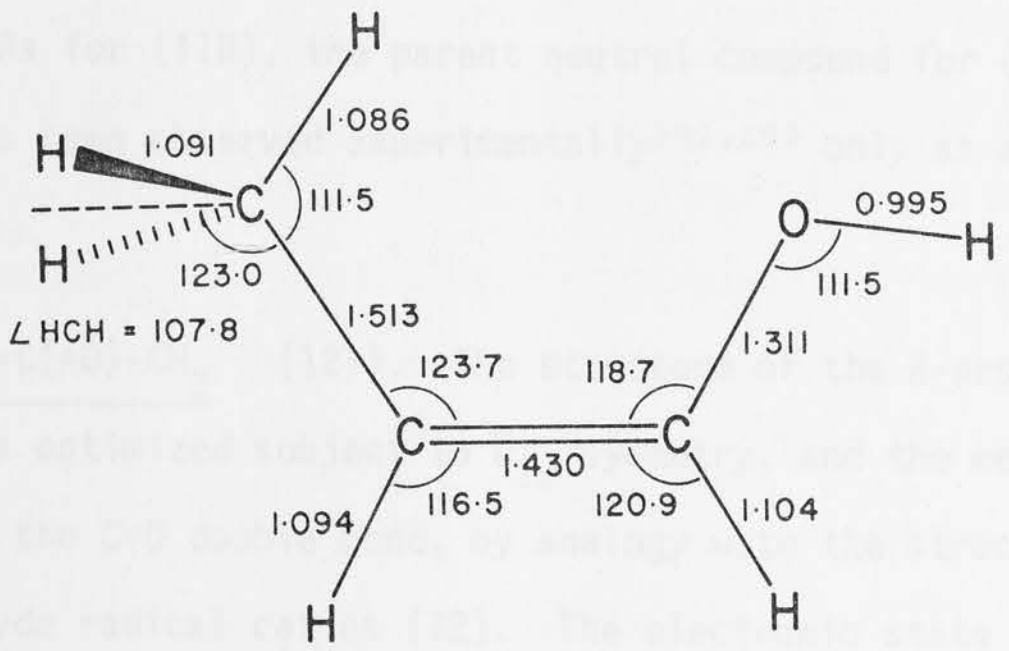

(119)

Both (119) and (120) were optimized subject to a C_s symmetry constraint. A slightly lower energy (by 2.0 kJ mol^{-1}) is found for (119).

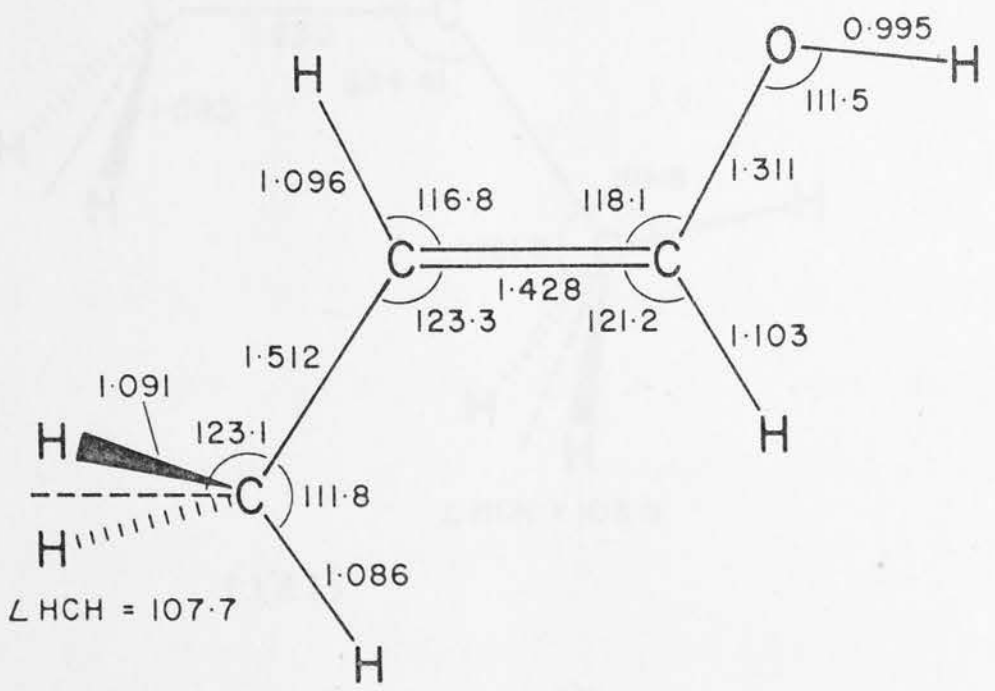

(120)

Isomers (119) and (120) have the same electronic state as (118), with one electron being removed from the π-electron system of the neutral parent. The geometries of the enol moiety in [(118) -(120)] and the vinyl alcohol radical

cation (71) are very similar. The energy of (119) relative to (118) is only 13 kJ mol^{-1} (Table 11.1), reflecting the difference between substitution of a methyl group in the 1- or 2-position of the vinyl alcohol ion. Thus substitution of a methyl in the 1-position is favoured over substitution in the 2-position. As for (118), the parent neutral compound for (119) or (120), 1-propen-1-ol, has been observed experimentally[292,293] only as a transient species.

$\underline{CH_3\text{-}C(=O)\text{-}CH_3}^{+\cdot}$ (121). The structure of the 2-propanone (acetone) radical cation was optimized subject to C_{2v} symmetry, and the methyl groups were chosen to eclipse the C=O double bond, by analogy with the structure determined for the acetaldehyde radical cation (72). The electronic state for (121) is $^2A'$, with the odd electron residing in a σ-molecular orbital, mainly on oxygen.

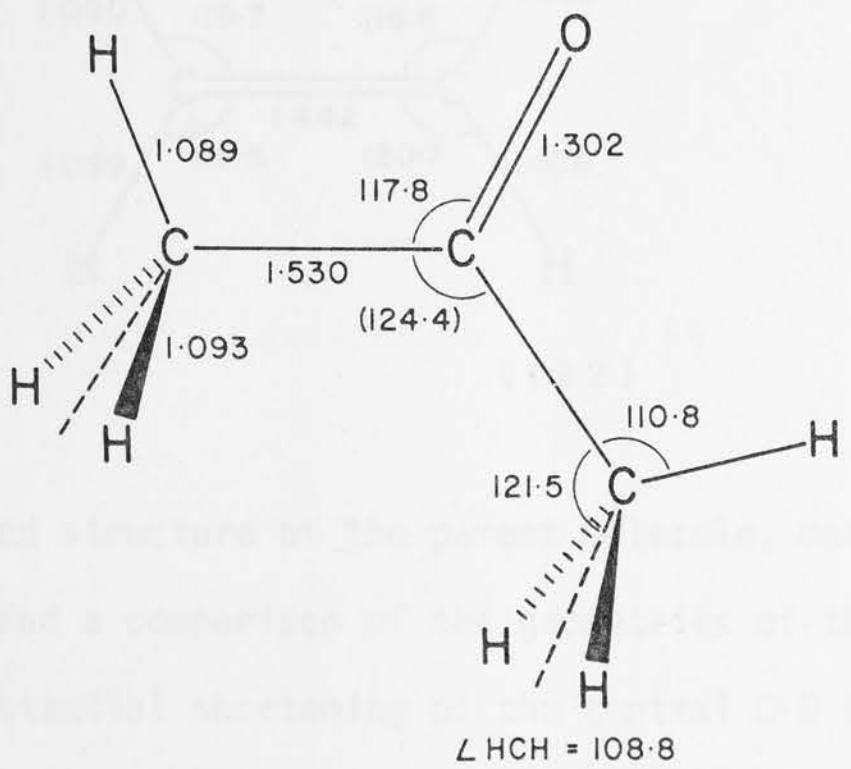

(121)

The relative energy for (121) with respect to its enol isomer (118) is found to be 20 kJ mol^{-1}. This is less than the energy difference of 42 kJ mol^{-1} which was calculated at a similar level of theory for the corresponding $C_2H_4O^{+\cdot}$ isomers, the acetaldehyde and vinyl alcohol cations (Table 8.1), and shows that a methyl

substituent in the 1-position *stabilizes* the keto isomer relative to the enol isomer. Experimentally, the heat of formation of (121) is known[76], and will be used in discussions of other $C_3H_6O^{+\cdot}$ radical cations with known ΔH_f values.

CH_2=CH-O-$CH_3^{+\cdot}$ (122). The starting point for the optimization of the methoxyethene (methyl vinyl ether) radical cation (122) was the structure of the vinyl alcohol radical cation (71), with a methyl group substituted for the hydroxylic hydrogen, and located *anti* with respect to the double bond. This geometry was optimized constraining C_s symmetry.

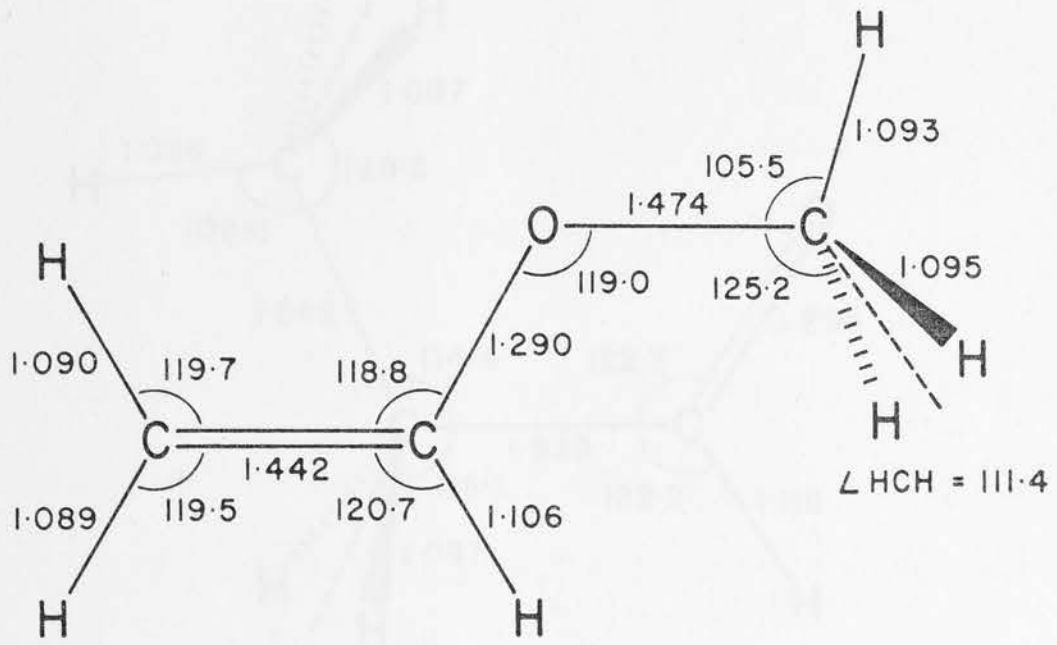

(122)

An STO-3G optimized structure of the parent molecule, methyl vinyl ether, has been reported[75], and a comparison of the geometries of the neutral and the ion (122) shows a substantial shortening of the central C-O bond (1.290 vs. 1.400 Å), and a lengthening of the C=C double bond (1.442 vs. 1.312 Å). This result parallels the effect of removal of an electron from the lower homologue, vinyl alcohol. Isomer (122) has an electron removed from a π-type orbital which is bonding for the C=C double bond and antibonding for the central C-O bond, consistent with the observed structural changes. The methyl vinyl ether radical cation is quite low in energy, being only 54 kJ mol^{-1} higher in energy than (118).

$\underline{CH_3\text{-}CH_2\text{-}CH{=}O^{+\cdot}}$ (123). For the optimization of the radical cation of propanal, the structure of the acetaldehyde radical cation (72), with a methyl group substituted on the α-carbon and eclipsing the C=O bond, was taken as a starting geometry. The optimized structure of (123) (C_s symmetry) resembles closely the acetaldehyde radical cation, and the electronic ground state is the same, the odd electron residing in a σ-molecular orbital located mainly on the oxygen.

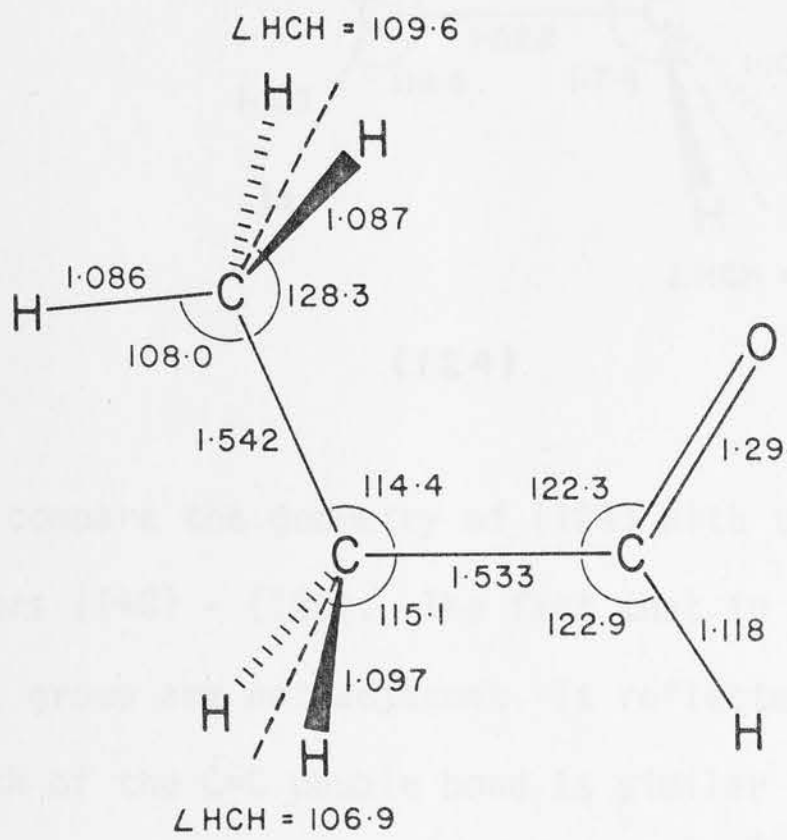

(123)

The relative energy calculated for the propanal radical cation with respect to the acetone radical cation (121) is 73 kJ mol^{-1}, and can be compared with the experimental energy difference of 51 kJ mol^{-1} derived from thermochemical measurements (Table 11.1). The energy difference between (123) and its enol isomer (119) is calculated to be 80 kJ mol^{-1}, a value which is higher than the keto-enol energy difference of 42 kJ mol^{-1} calculated for the $C_2H_4O^{+\cdot}$ isomers. This implies that a methyl substituent in the 2-position *destabilizes* the acetaldehyde radical cation relative to the vinyl alcohol radical cation, a result similar to that found for α-methyl substitution in the corresponding neutral C_2H_4O isomers (Chapter 3).

$\underline{CH_2{=}CH{-}CH_2{-}OH^{+\cdot}}$ (124). The 2-propen-1-ol (allyl alcohol) radical cation was optimized in the conformation shown, subject to C_s symmetry only.

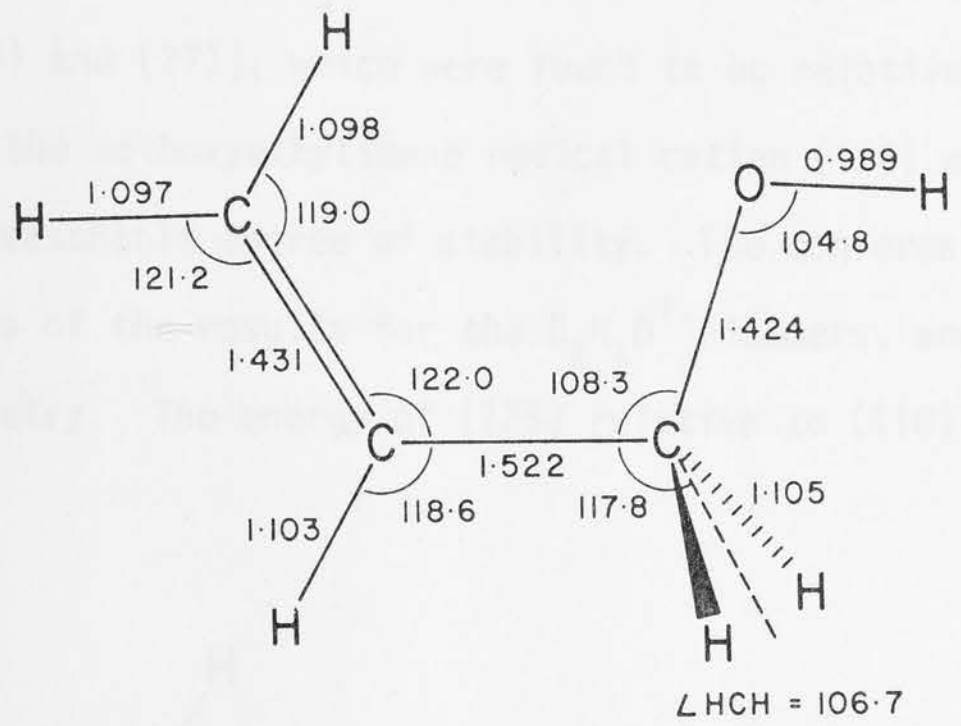

(124)

It is interesting to compare the geometry of (124) with the geometries of the closely related isomers (118) - (120). The fact that in (124) the double bond and the hydroxyl group are not adjacent is reflected in the bond lengths concerned. The length of the C=C double bond is similar to the values obtained for (118) and (119) (1.431 vs 1.454 and 1.430 Å), but the C-O bond length is longer than the corresponding C-O bond lengths in (118) and (119) (1.424 vs 1.307 and 1.311 Å). In fact, the C-O bond length and the COH angle have not changed significantly upon ionization of (124); this is seen clearly by comparison of these values with the corresponding STO-3G values for neutral methanol[70] (1.424 vs 1.433 Å and 104.8 vs 103.8°, respectively). The electronic structure of (124) is consistent with the calculated geometrical parameters in that an electron has been removed from a π-type orbital which is bonding across the C=C double bond. Unlike the $C_3H_6O^{+\cdot}$ isomers (118) - (123), (124) has not yet been established as a stable, identifiable isomer, even though the parent molecule is stable. It has been proposed[289] that the molecular ion of allyl

alcohol undergoes a facile 1,3-hydrogen shift to the enol ion (119) or (120).

$\underline{CH_3\text{-}C\text{-}O\text{-}CH_3}^{+\cdot}$ (125). By analogy with the two carbenoid $C_2H_4O^{+\cdot}$ isomers, the hydroxyethylidene (CH_3-C-OH) and methoxymethylene (CH_3-O-CH) radical cations [(76) and (77)], which were found to be relatively low in energy (Chapter 8), the methoxyethylidene radical cation (125) was also expected to show a reasonable degree of stability. The conformation shown was selected on the basis of the results for the $C_2H_4O^{+\cdot}$ isomers, and was optimized constraining C_s symmetry. The energy of (125) relative to (118) was found to be 110 kJ mol^{-1}.

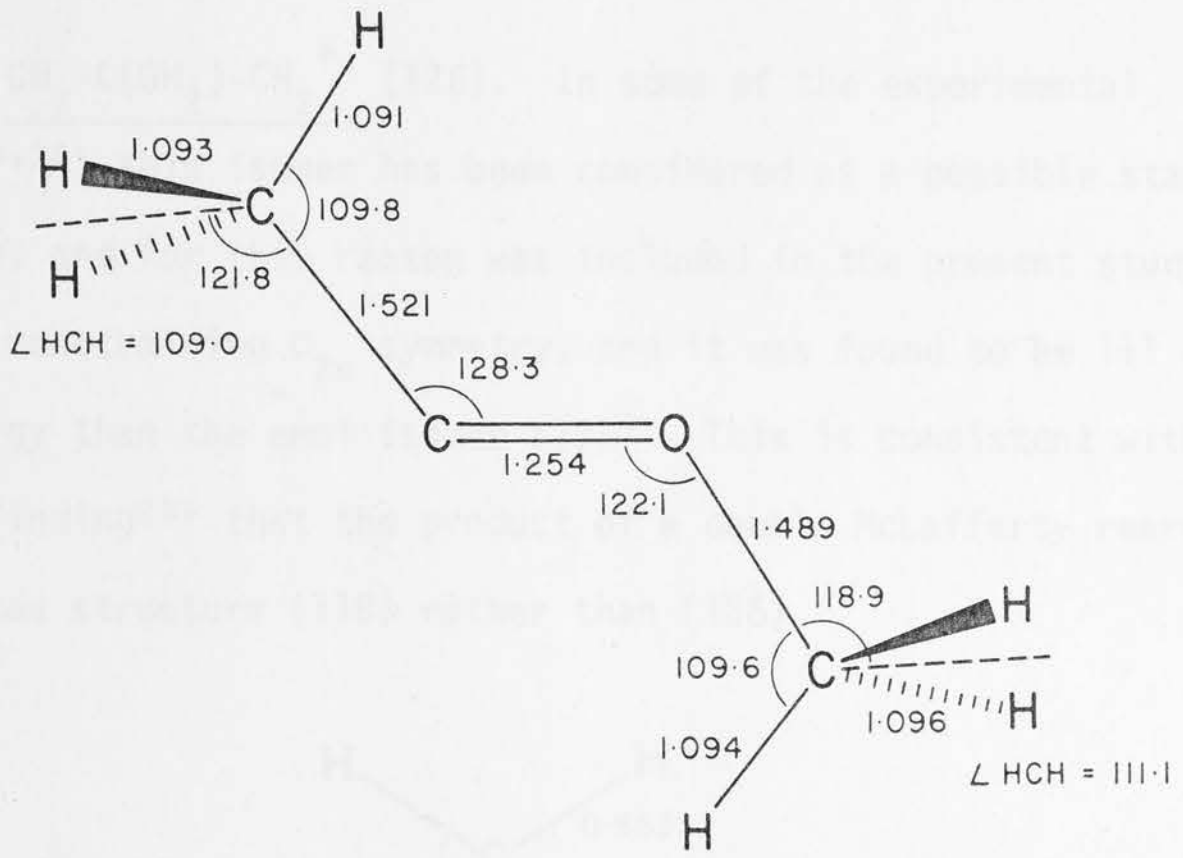

(125)

The central C-O bond is depicted as a double bond, and the calculated bond length substantiates this; it is, for example, shorter than the C=O bonds in (121) and (123) (1.254 vs 1.302 and 1.294 Å, respectively). The stability of (125) will in part depend on the barrier for the 1,2-hydrogen shift in the ethylidene moiety [which would lead to the more stable isomer (122)]. In the study of the $C_2H_4O^{+\cdot}$ isomers (Chapter 8), it was found that such barriers are substantial, and on the basis of that result the barrier for a 1,2-hydrogen

shift in (125) is expected to be also large. Finally, the possibility of (125) dissociating into $CH_3C{=}O^+$ and $CH_3^{\cdot}$ should be considered. The total heat of formation [$\Delta H_f^{\circ}(298^{\circ})$] for these fragments[76] is 772 kJ mol^{-1}. Examination of Table 11.1 shows that the heat of formation of (125), estimated from calculated relative energies and known heats of formation for (121), (123), (130) and (132), is 785 - 810 kJ mol^{-1}. Thus the dissociation of (125) into $CH_3C{=}O^+$ and $CH_3^{\cdot}$ might be an exothermic process. Finally, it is noted that the electronic structure of (125) is similar to the electronic structures found for the two related $C_2H_4O^{+\cdot}$ isomers [(76) and (77)], the odd electron residing in a σ-orbital.

$\underline{CH_2\text{-}C(OH_2)\text{-}CH_2}^{+\cdot}$ (126). In some of the experimental studies[263,283,284] this isomer has been considered as a possible stable $C_3H_6O^{+\cdot}$ isomer, and for this reason was included in the present study. (126) was optimized, constraining C_{2v} symmetry, and it was found to be 111 kJ mol^{-1} higher in energy than the enol isomer (118). This is consistent with the experimental finding[284] that the product of a double McLafferty rearrangement in alkanones has structure (118) rather than (126).

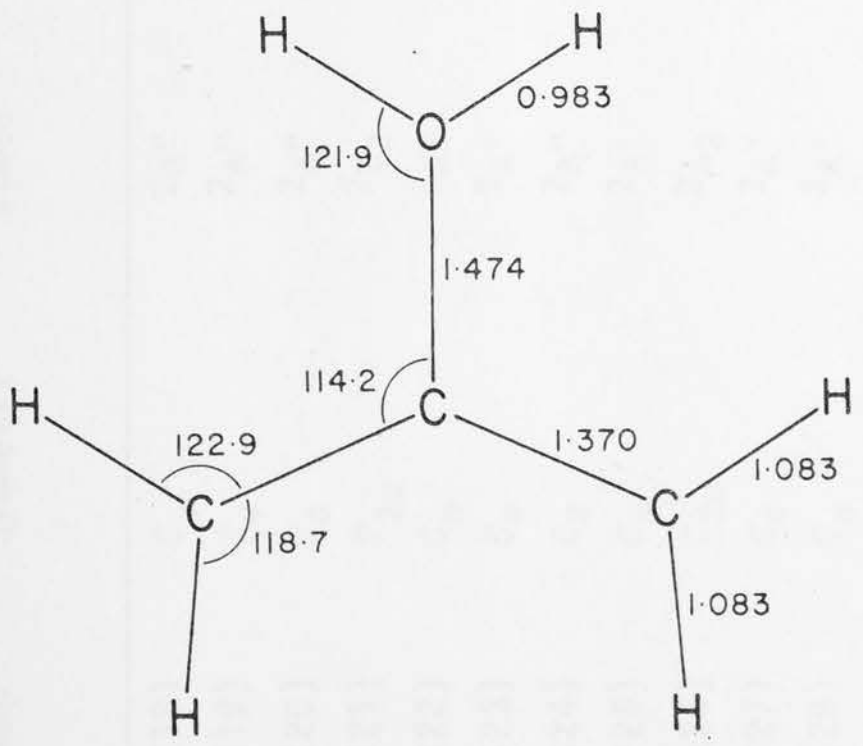

(126)

Table 11.1 Calculated Total Energies and Relative Energies for the $C_3H_6O^{+\cdot}$ Isomers[a].

Isomer[b]	Symmetry	State	RHF/STO-3G//RHF/STO-3G Energy		RHF/4-31G//RHF/STO-3G Energy		Experimental[c] ΔH_f° (298°)
			Total	Rel.	Total	Rel.	
(118)	C_s	$^2A''$	-189.29615	0	-191.37488	0	d
(119)	C_s	$^2A''$	-189.28951	17.4	-191.36991	13.0	d
(120)	C_s	$^2A''$	-189.28951	17.4	-191.36915	15.0	d
(121)	C_{2v}	$^2B_2$	-189.32383	-72.7	-191.36715	20.3	719
(122)	C_s	$^2A''$	-189.28472	30.0	-191.35451	53.5	d
(123)	C_s	$^2A'$	-189.29594	0.6	-191.33949	92.9	770
(124)	C_s	$^2A''$	-189.23405	163.0	-191.33394	107.5	d
(125)	C_s	$^2A'$	-189.28047	41.2	-191.33296	110.1	d
(126)	C_{2v}	$^2A_2$	-189.23046	172.5	-191.33254	111.2	d
(127)	C_s	$^2A'$	-189.27314	60.4	-191.33226	111.9	d
(128)	C_s	$^2A'$	-189.26885	71.7	-191.32802	123.0	d
(129)	C_s	$^2A'$	-189.25088	118.9	-191.31870	147.5	d
(130)	$C_s \rightarrow C_{2v}$	$^2B_1$	-189.31790	-57.1	-191.31495	157.3	852
(131)	C_s	$^2A'$	-189.25401	110.6	-191.30869	173.8	d
(132)	C_1	^2A	-189.28311	34.2	-191.29618	206.6	893
(133)	C_s	$^2A''$	-189.25176	116.5	-191.28750	229.4	d
(134)	$C_1 \rightarrow C_s$	$^2A'$	-189.24925	123.1	-191.28099	246.5	d

a Experimental heats of formation are listed for comparison.
b For geometries, see text.
c From ref. 76.
d Not available.

$\underline{CH_3\text{-}CH\text{-}O\text{-}CH_2}^{+\cdot}$ (127). The theoretical and experimental studies reported in Chapters 8 and 10 had shown that there is a low energy isomer of the ethylene oxide ion (73), the C---C ring-opened ethylene oxide ion (74). It is possible that for the propylene oxide radical cation (132), such a C---C ring-opened isomer might exist as well.

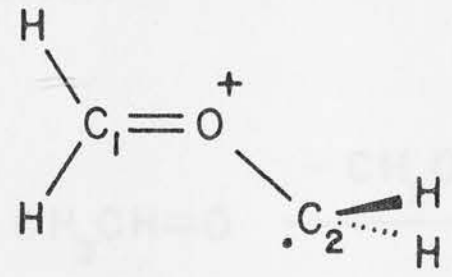

(74)

A preliminary calculation involving the substitution of a methyl group in (74) at C_1 or C_2 showed a preference for substitution on the planar carbon (i.e. C_1). Optimization of this geometry (C_s symmetry) resulted in (127), which has a quite low relative energy, being 112 kJ mol^{-1} higher than (118).

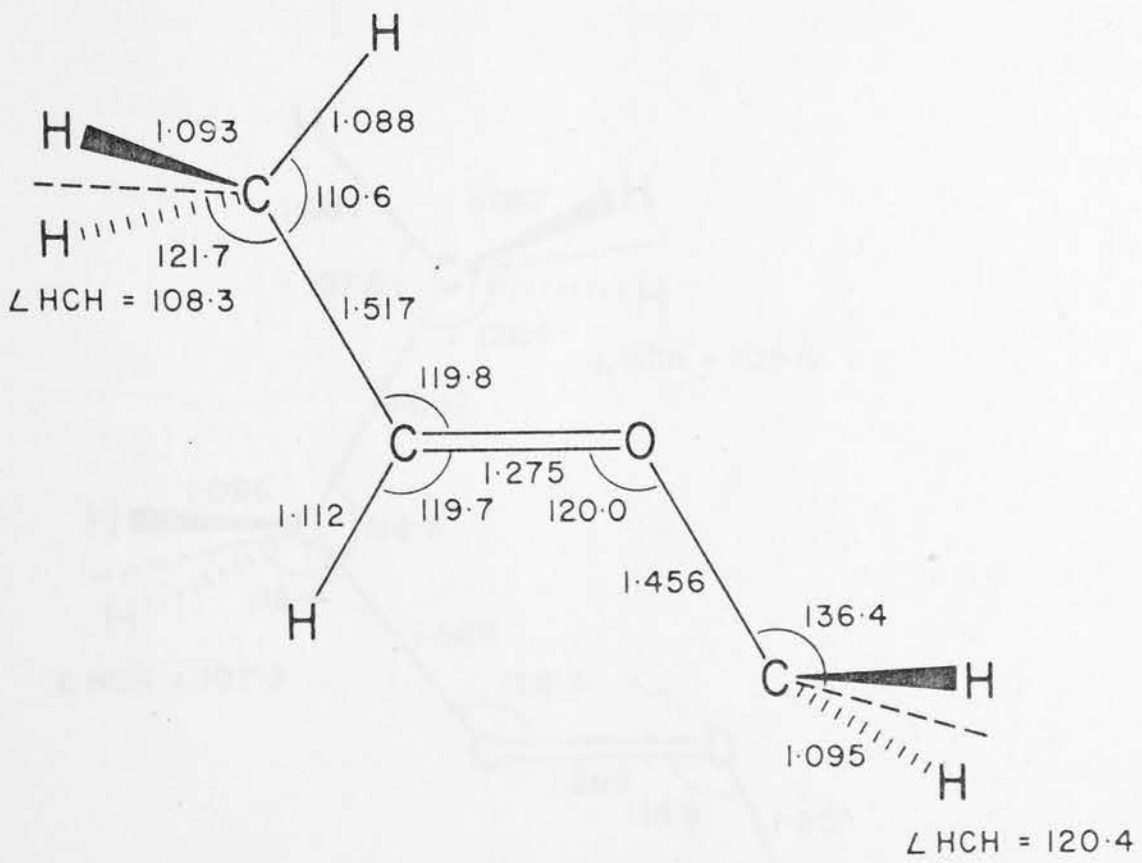

(127)

As for the $C_2H_4O^{+\cdot}$ isomer (74), (127) has an odd electron in a σ-type molecular

orbital, and has one C-O bond considerably longer than the other. This allows the possibility of $CH_2^{+\cdot}$ transfer reactions, as was found for (74). Some experimental results which relate to this ion are described in Section 11.4. In addition, it is noted that (127) is likely to be the product of the observed $CH_2^{+\cdot}$ transfer from the C---C ring-opened ethylene oxide radical cation to acetaldehyde (reaction 10.16).

$$\underset{(74)\ m/z\ 44}{CH_2{=}\overset{+}{O}{-}\dot{C}H_2} + CH_3CH{=}O \xrightarrow{-CH_2O} \underset{(127)\ m/z\ 58}{CH_3CH{=}\overset{+}{O}{-}\dot{C}H_2} \qquad (10.16)$$

$\underline{CH_3\text{-}CH_2\text{-}C\text{-}OH^{+\cdot}}$ (128). As the hydroxypropylidene radical cation (128) is closely related to its $C_2H_4O^{+\cdot}$ homologue (76), optimization was started from the geometry of the hydroxyethylidene radical cation [(76), $CH_3\text{-}C\text{-}OH^{+\cdot}$], with a methyl substituent added (C_s symmetry).

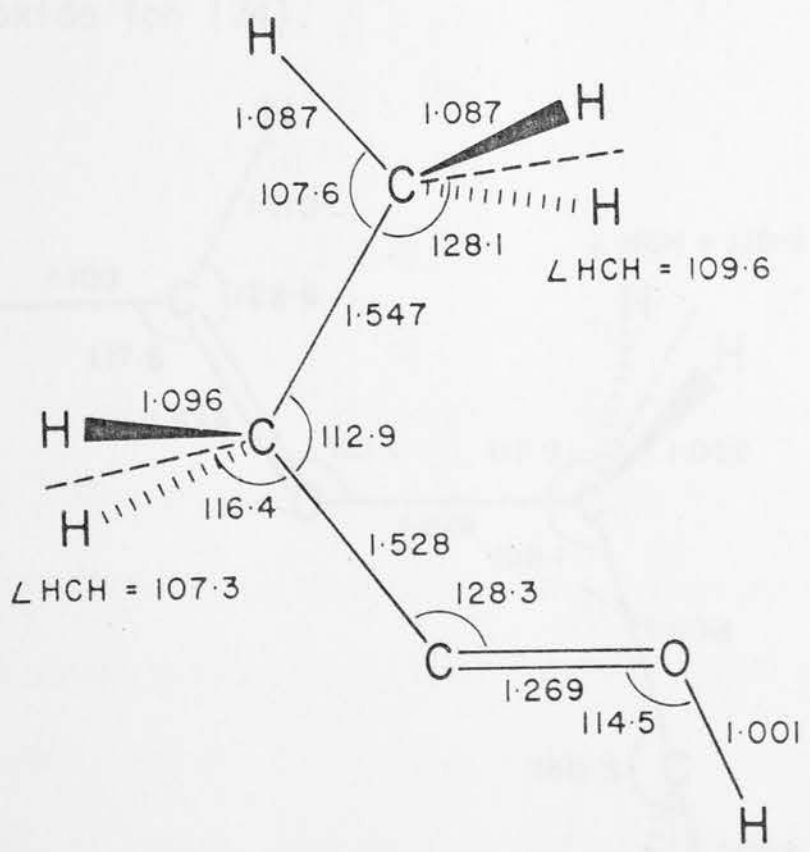

(128)

The resulting structure is very similar to (76), and is 123 kJ mol^{-1} higher than (118). The electronic state of (128) is the same as for (125) ($^2A'$). Isomerization of (128) to (119), (120) or (123) by way of a 1,2-hydrogen shift is unlikely, based on studies of similar situations in the $CH_2O^{+\cdot}$ and $C_2H_4O^{+\cdot}$ systems (Chapters 6 and 8). Dissociation of (128) to give $CH_3CH_2C{\equiv}O^+$ and $H^\cdot$ should be considered in order to assess its stability. The combined heat of formation[76] of $CH_3CH_2C{\equiv}O^+$ and $H^\cdot$ is 820 kJ mol^{-1}, a value marginally higher than the heat of formation of (128) (795 - 820 kJ mol^{-1}) estimated from Table 11.1. Thus (128), although higher in energy than (125), has a better chance of being observed, due to the absence of an exothermic dissociative pathway.

$\underline{CH_2{=}O\text{-}CH_2\text{-}CH_2}^{+\cdot}$ (129). This isomer, which formally is a C---C ring-opened isomer of the trimethylene oxide radical cation (130), was optimized in the conformation shown, constraining C_s symmetry, and is found to be 10 kJ mol^{-1} lower in energy than (130). The most interesting feature of (129) is that it can be considered to be a higher homologue of the C---C ring-opened ethylene oxide ion (74).

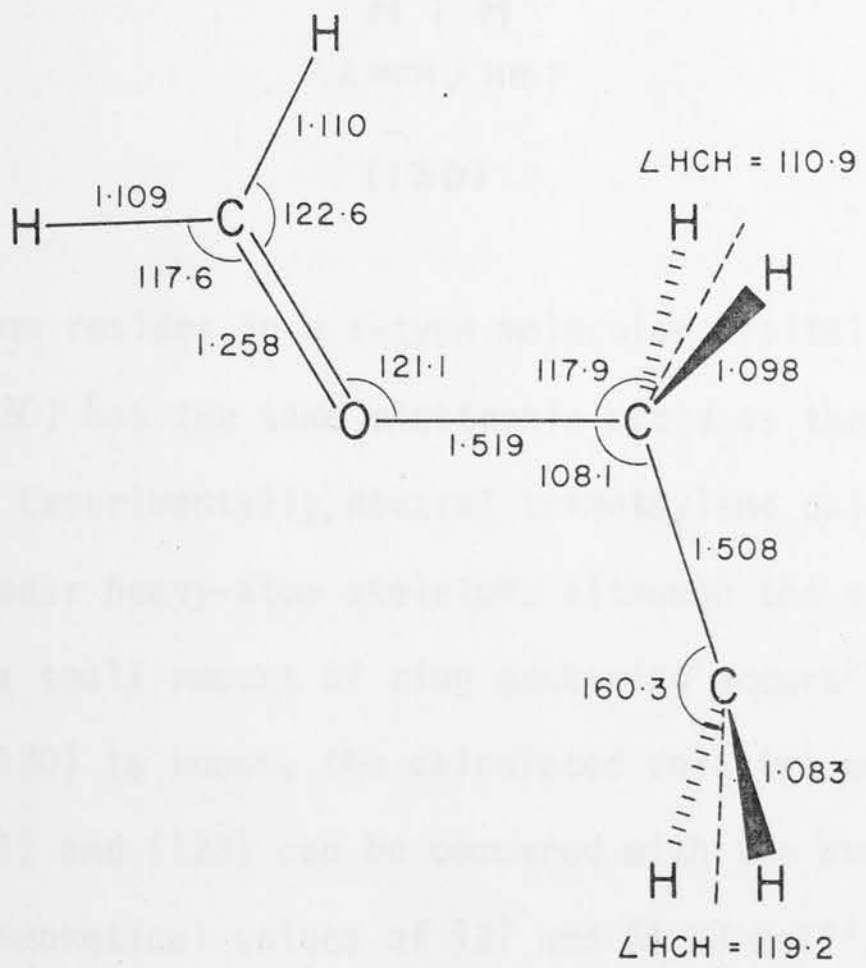

(129)

Whereas ICR experiments show that (74) transfers $CH_2^{+\cdot}$ to suitable substrates such as nitriles (Chapter 10), (129) might be expected, under similar conditions, to show a $C_2H_4^{+\cdot}$ transfer. In both cases the driving force in the ion/molecule reaction would be mainly due to the loss of formaldehyde as a small stable neutral fragment. Some experimental results concerning the possible existence of (129) are given in Section 11.4.

$\underline{\lceil CH_2\text{-}CH_2\text{-}CH_2\text{-}O \rceil^{+\cdot}}$ (130). For the oxetane (trimethylene oxide) radical cation, C_s distorted structures were allowed in the optimization process, but the fully optimized structure has C_{2v} symmetry.

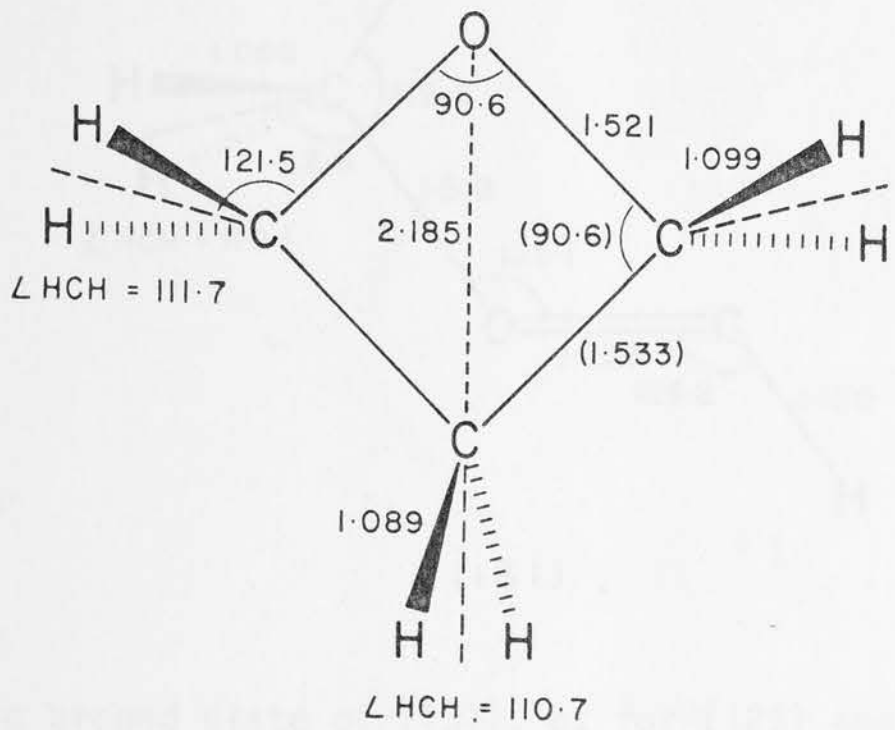

(130)

The odd electron resides in a π-type molecular orbital, centred mainly on oxygen, and (130) has the same electronic state as the ethylene oxide radical cation ($^2B_1$). Experimentally, neutral trimethylene oxide is found to have an essentially planar heavy-atom skeleton, although the microwave spectrum suggests that a small amount of ring puckering occurs[294]. Since the heat of formation of (130) is known, the calculated relative energies of (130) with respect to (121) and (123) can be compared with the available experimental values. The theoretical values of 137 and 64 kJ mol^{-1}, respectively, compare

reasonably well with the experimental values of 133 and 82 kJ mol^{-1}.

$\underline{CH_3\text{-}CH_2\text{-}O\text{-}CH^{+\cdot}}$ (131). The ethyoxymethylene radical cation (131) is closely related to its $C_2H_4O^{+\cdot}$ homologue, the methyoxymethylene radical cation [(77), $CH_3\text{-}O\text{-}CH^{+\cdot}$], the structure of which was substituted with a methyl group and fully optimized with C_s symmetry.

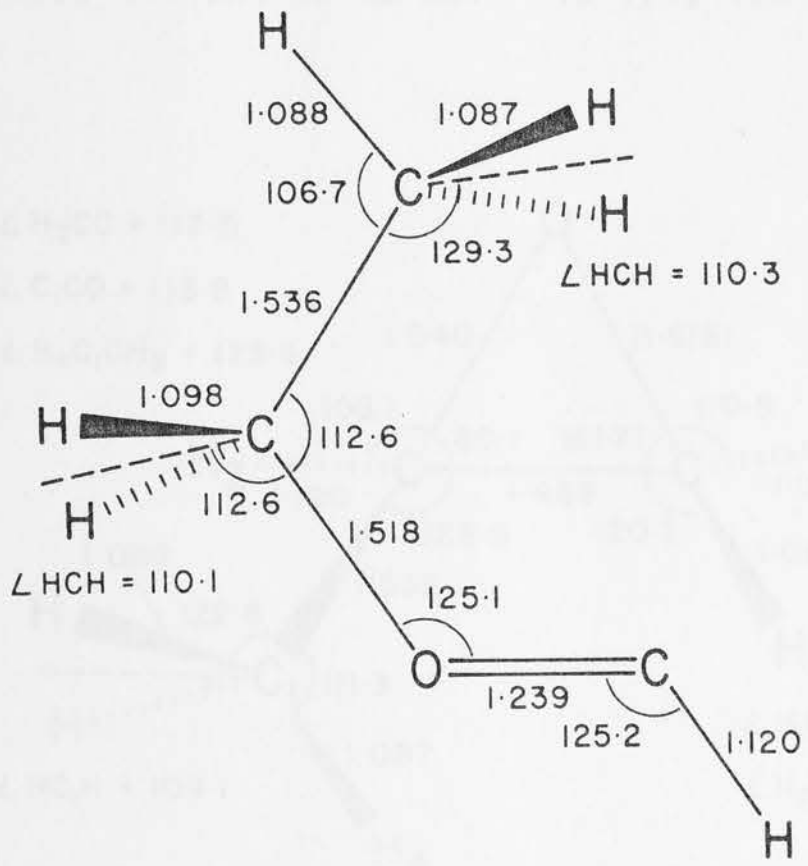

(131)

The electronic ground state of (131), as for (125) and (128), is $^2A'$. The stability of (131) with respect to dissociation into $CH_3CH_2O{=}C^+$ and $H^\cdot$ cannot be assessed in the same manner as for (125) and (128), since no experimental heat of formation is available for $CH_3CH_2O{=}C^+$. Calculations at the 4-31G level show (see Chapter 7) that $HO{=}C^+$ is 91 kJ mol^{-1} (4-31G//4-31G) higher in energy than $HC{\equiv}O^+$. If this is taken as an estimate for the energy difference of $CH_3CH_2O{=}C^+$ and $CH_3CH_2C{\equiv}O^+$, this will give a total heat of formation of about 910 kJ mol^{-1} for $CH_3CH_2O{=}C^+$ and $H^\cdot$. This is higher than the heat of formation of (845 - 870 kJ mol^{-1}) estimated from Table 11.1. Thus dissociation of (131) into $CH_3CH_2O{=}C^+$ and $H^\cdot$ is likely to be an endothermic process.

$\underline{CH_3\text{-}\overset{\frown}{CH}\text{-}CH_2\text{-}O^{+\cdot}}$ (132). The methyloxirane (propylene oxide) radical cation (132) is asymmetric, and was optimized as such, constraining local C_s symmetry for the methyl group only. Experimentally (132) is known as a stable isomer, and its heat of formation is available. Comparison of the calculated and experimentally determined energy differences between (132) and the stable isomers (121), (123) and (130) shows that good agreement exists between theory and experiment (186, 114 and 49 kJ mol^{-1} vs 174, 123 and 41 kJ mol^{-1}, respectively).

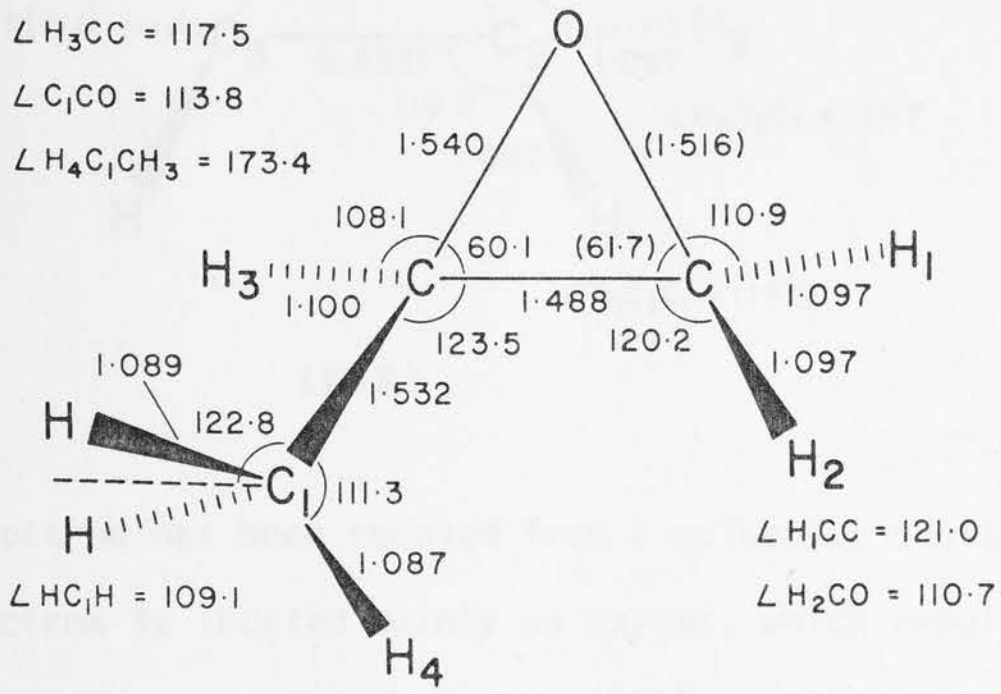

(132)

By analogy with the situation for the ethylene oxide radical cation (73), the propylene oxide radical cation (132) could undergo C-C bond cleavage to give the more stable C---C ring-opened isomer (127), which is lower in energy than (132) by 95 kJ mol^{-1}. This indicates that, if under experimental conditions the isomerization of (132) to (127) does occur, it should be possible to detect (127) by an ion/molecule reaction showing $CH_2^{+\cdot}$ transfer to a suitable substrate, as was found for the C---C ring-opened ethylene oxide ion (74).

$\overline{CH_2\text{-}CH_2\text{-}CH\text{-}OH}^{+\cdot}$ (133). The cyclopropanol radical cation has been examined in the conformation with C_s symmetry, as shown.

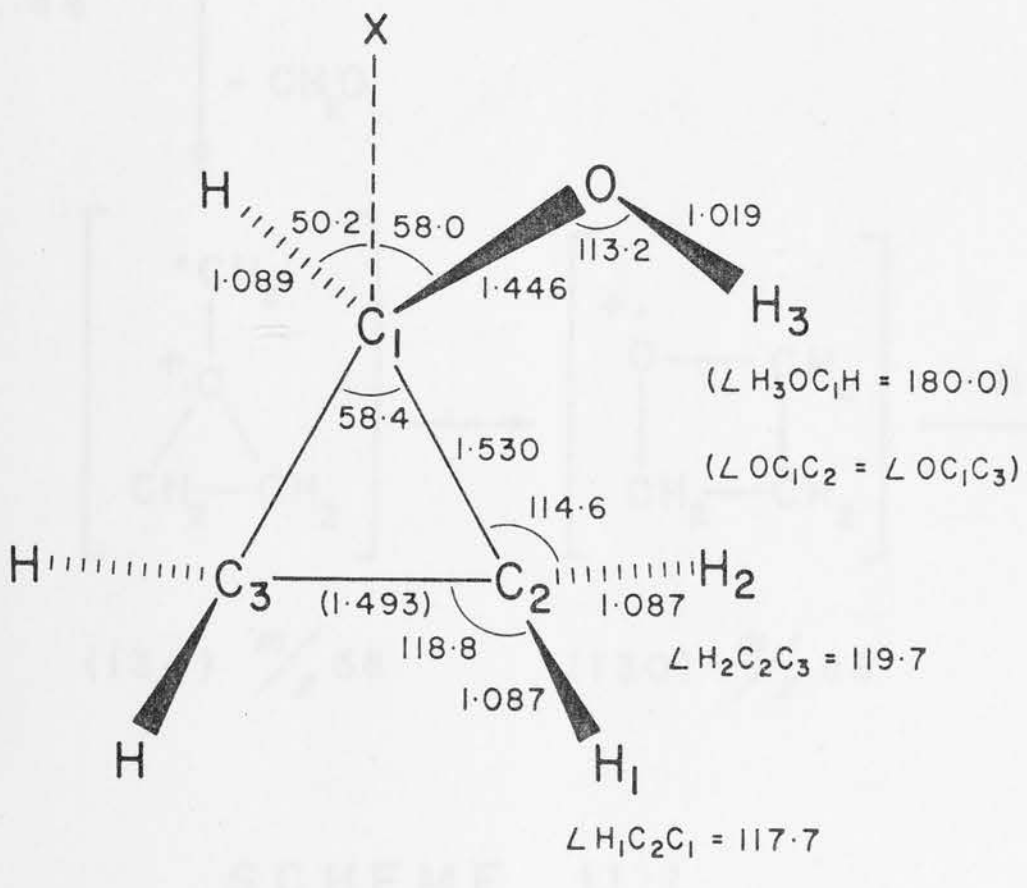

(133)

In (133), one electron has been removed from a molecular orbital with A" symmetry, and the odd electron is located mainly on oxygen, which results in a large COH angle, as was found for the COH angles in (118) and (119). Experimentally (133) has been studied[290], but has not as yet been uniquely characterized as an identifiable $C_3H_6O^{+\cdot}$ isomer.

$\overline{CH_2\text{-}CH_2\text{-}O\text{-}CH_2}^{+\cdot}$ (134). This isomer is of special interest since it has been proposed[187] as an intermediate in the reaction of the C---C ring-opened ethylene oxide ion (74) with ethylene oxide, in which the ion (74) transfers a $CH_2^{+\cdot}$ moiety to the neutral ethylene oxide molecule (reaction 7.13). The proposed reaction mechanism, based on deuterium labelling experiments, includes a rearrangement of the intermediate (134) to the trimethylene oxide ion (130), which subsequently has to lose a hydrogen radical to explain the product ion at m/z 57 (Scheme 11.1).

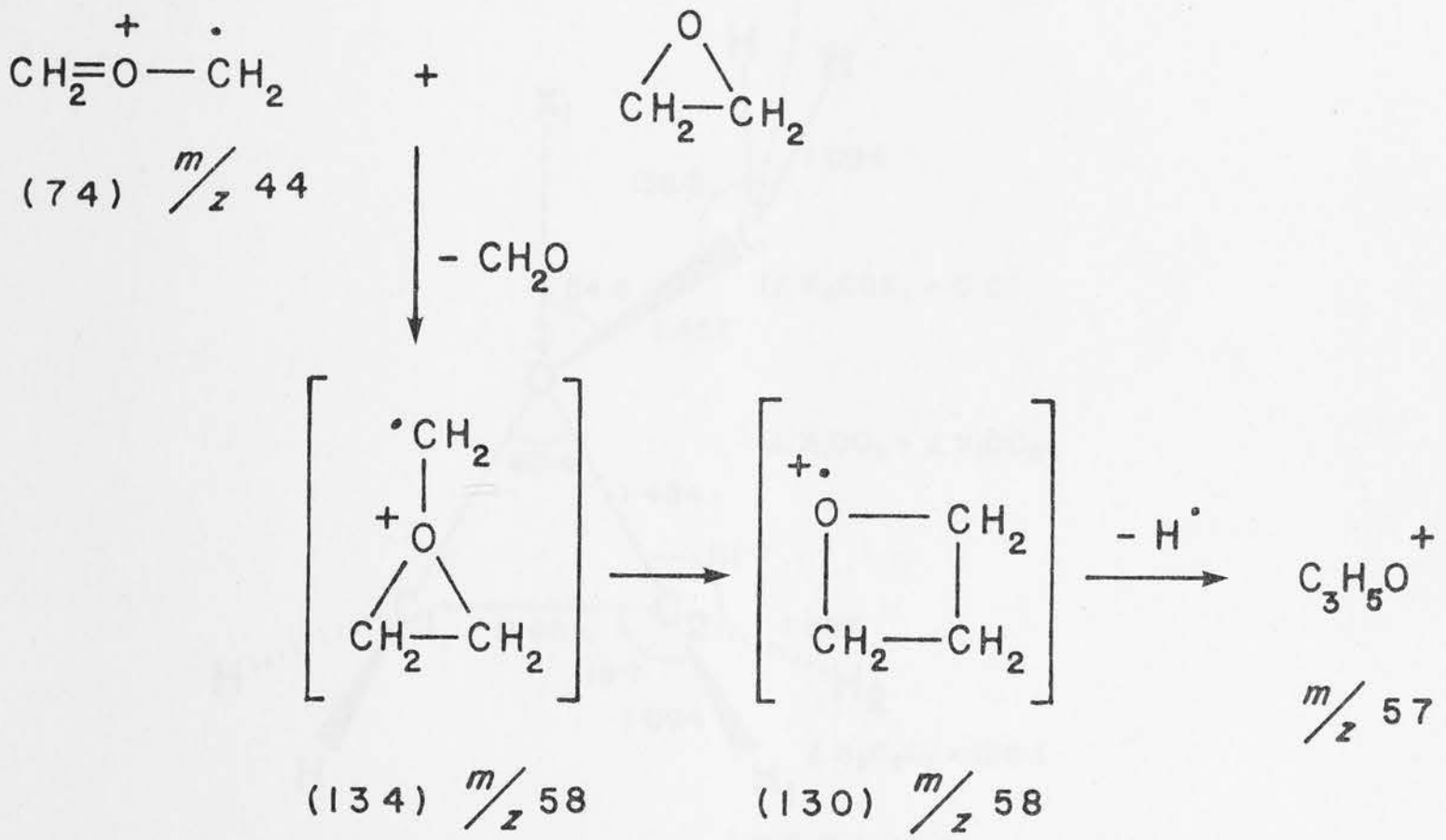

SCHEME 11.1

Initial optimizations of (134) indicated that the CH_2 moiety preferred to be out of the plane of the ring, in an *anti* arrangement with respect to the ring about the C-O bond. This structure was fully optimized, and the odd electron is found to be centred on the free methylene group. The total energy of (134) is quite high, but not substantially higher than the experimentally known $C_3H_6O^{+\cdot}$ isomers (132) and (133). The energy changes for the reactions of Scheme 11.1 can be obtained using 4-31G//STO-3G total energies[†]. The initial step is found to be exothermic by 71 kJ mol^{-1}, and the subsequent rearrangement (134) → (130) is exothermic by 89 kJ mol^{-1}. Thus the calculations confirm the exothermicity of the important reaction steps shown in Scheme 11.1.

[†] The RHF/4-31G//RHF/STO-3G energies are: $CH_2=\overset{+}{O}-\dot{C}H_2$ -152.32124 (Table 8.1); $CH_2=O$ -113.69171[70]; $\overline{CH_2CH_2-O}$ -152.62444 (Table 2.7).

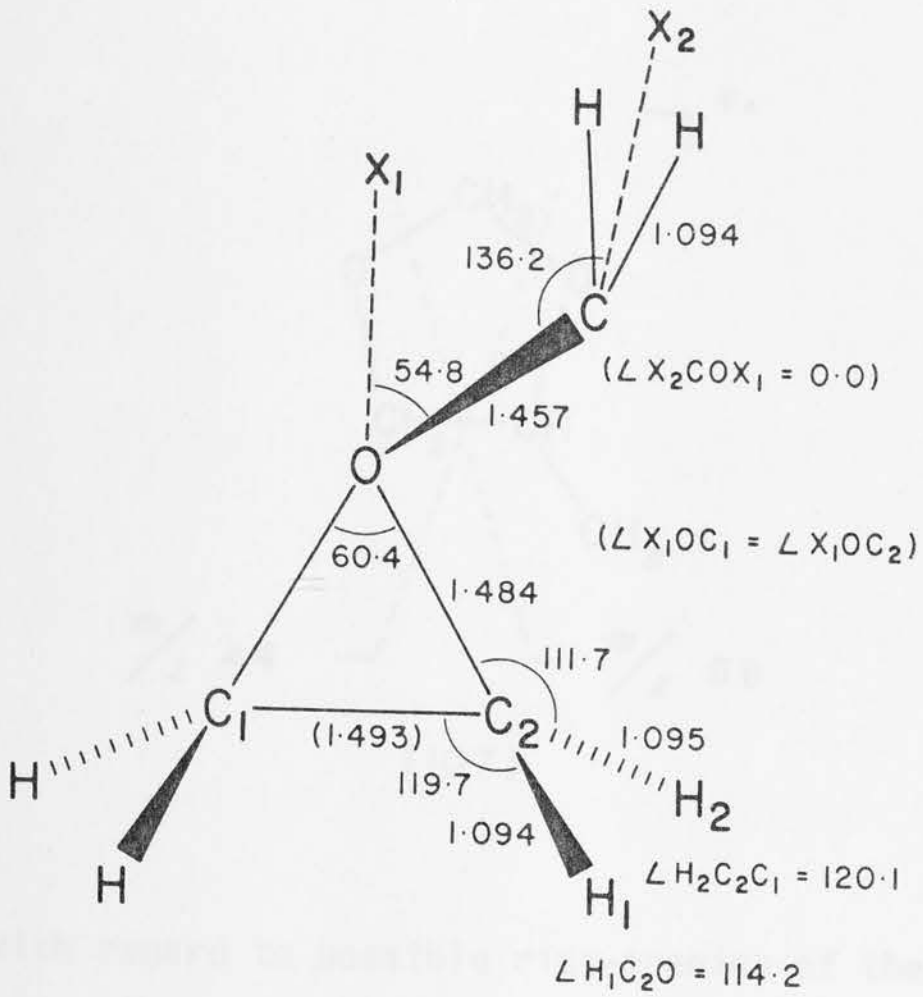

(134)

11.4 EXPERIMENTAL RESULTS CONCERNING TWO PREVIOUSLY UNOBSERVED $C_3H_6O^{+\cdot}$ ISOMERS

In the course of the ICR experimental investigation on the $C_2H_4O^{+\cdot}$ isomers, described in Chapter 10, some experiments were performed which involved $C_3H_6O^{+\cdot}$ ions, and the results supported the existence of the previously undetected ions (127) and (129). When 4-methyl-1,3-dioxolane (107) was examined in the ICR spectrometer, together with acetonitrile, not only was a $CH_2^{+\cdot}$ transfer observed from $^m/_z$ 44 (discussed in Section 10.2.4), but also a small double resonance signal was obtained from $^m/_z$ 58. This suggests that the molecular ion of (107) can fragment in two ways to give $^m/_z$ 44 (74) and $^m/_z$ 58 (127) as shown. The fact that a more efficient $CH_2^{+\cdot}$ transfer is found for (74) than for (127) can be explained by examination of the energetics of reaction 10.16. At the RHF/4-31G//RHF/STO-3G level the reaction is calculated to be exothermic by 47 kJ mol^{-1}, clearly indicating that (74) should be a better $CH_2^{+\cdot}$ transfer agent.

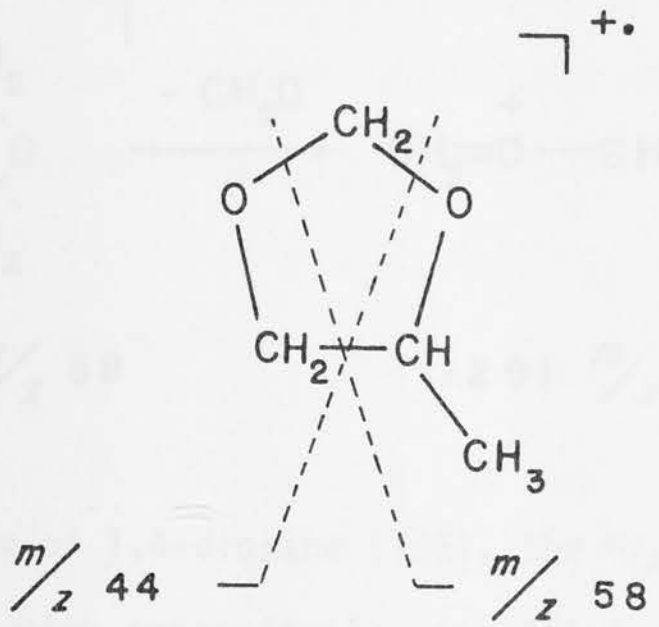

(107)

With regard to possible ring-opening of the propylene oxide ion (130) to give (127), the ICR experiments have so far not shown a definitive $CH_2^{+\cdot}$ transfer from $^m/_z$ 58 in mixtures of propylene oxide and nitriles, indicating that the isomerization (130) → (127) does not occur to any reasonable extent.

When a mixture of trimethylene oxide and acetonitrile was examined in the ICR spectrometer, a $C_2H_4^{+\cdot}$ transfer reaction (reaction 11.1) was observed, but only to a very minor extent.

$$CH_2{=}\overset{+}{O}{-}CH_2{-}\dot{C}H_2 \quad + \quad CH_3CN \xrightarrow{-\,CH_2O} CH_3CN\,C_2H_4^{+\cdot} \qquad 11.1$$

(129) $^m/_z$ 58 $\qquad\qquad$ $^m/_z$ 69

A reaction of this type is related to a recently reported[270] ion/molecule reaction in which $CH_3\text{-}\overset{+}{O}H\text{-}CH_2\dot{C}H_2$ transfers a $C_2H_4^{+\cdot}$ moiety to various nitriles (reaction 10.53). In order to look for another possible source of ion (129) it was decided to examine 1,4-dioxane (135) which has a prominent fragment ion at $^m/_z$ 58 ($C_3H_6O^{+\cdot}$) in its mass spectrum arising from the loss of formaldehyde, presumably of structure (129) (reaction 11.2).

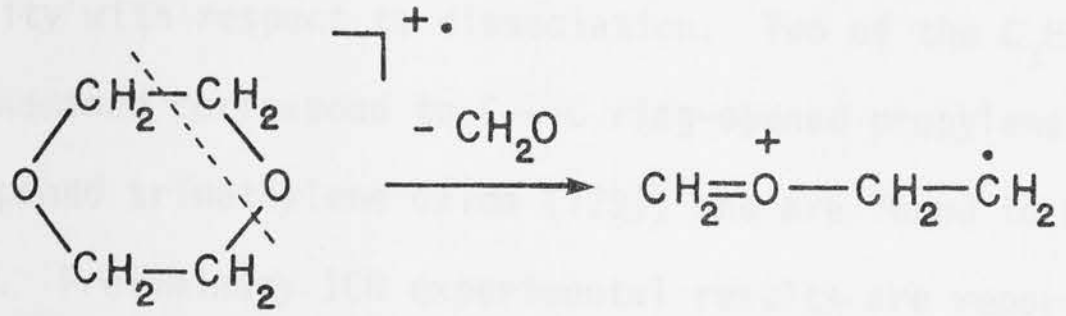

(135) $^{m}/_{z}$ 88 (129) $^{m}/_{z}$ 58 11.2

In the ICR spectrum of 1,4-dioxane (135), the $^{m}/_{z}$ 58 ion is present, and when (135) was examined with acetonitrile, an efficient $C_2H_4^{+\cdot}$ transfer from $^{m}/_{z}$ 58 (reaction 11.1) was observed, supporting the existence of (129) as an observable $C_3H_6O^{+\cdot}$ isomer.

Thus experimental evidence is available, suggesting that the hitherto unknown $C_3H_6O^{+\cdot}$ isomers (127) and (129) might be identifiable species. A more detailed investigation of the ion/molecule reactions of these ions will be necessary to provide conclusive evidence for their structures.

11.5 CONCLUSIONS

The study of the $C_3H_6O^{+\cdot}$ radical cations described here has resulted in the ranking of known, and as yet unknown, $C_3H_6O^{+\cdot}$ isomers according to their relative energies. For those isomers for which experimental heats of formation are available, a reasonable agreement with the theoretical results is found. The theoretical study has shown a total of 15 isomers of $C_3H_6O^{+\cdot}$ that have an energy less than, or equal to, the experimentally characterized propylene oxide cation. Consistent with theoretical and experimental results for the $C_2H_4O^{+\cdot}$ isomers, the enol isomers CH_2=C(OH)-$CH_3^{+\cdot}$ (118) and CH_3-CH=CH-$OH^{+\cdot}$ [(119) and (120)] are found to be the lowest energy $C_3H_6O^{+\cdot}$ isomers. The three carbenoid radical cations (125), (128) and (131) that have been examined are relatively low in energy, and might be observable $C_3H_6O^{+\cdot}$ isomers, depending on their

stability with respect to dissociation. Two of the $C_3H_6O^{+\cdot}$ isomers that have been examined correspond to C---C ring-opened propylene oxide (127) and C---C ring-opened trimethylene oxide (129), and are found to be relatively low in energy. Preliminary ICR experimental results are reported which indicate that (127) and (129) are observable species.

Finally, it is noted that the energetics of the reaction of the open ethylene oxide ion (74) with ethylene oxide involving the $C_3H_6O^{+\cdot}$ isomer (134), as proposed by Beauchamp (reaction 7.13, Scheme 11.1), have been calculated, and confirm that the overall process is exothermic.

REFERENCES

1. Hückel, E., *Z. Physik*, 1931, 70, 204; *ibid.*, 1932, 76, 628.

2. Hoffmann, R., *J. Chem. Phys.*, 1963, 39, 1397.

3. Pople, J.A., and Beveridge, D.L., "Approximate Molecular Orbital Theory", McGraw Hill, New York, N.Y., 1970.

4. Pople, J.A., Santry, D.P., and Segal, G.A., *J. Chem. Phys.*, 1965, 43, S129.

5. Pople, J.A., and Segal, G.A., *J. Chem. Phys.*, 1966, 44, 3289.

6. Pople, J.A., Beveridge, D.L., and Dobosh, P.A., *J.Chem. Phys.*, 1967, 47, 2026.

7. Baird, N.C., and Dewar, M.J.S., *J. Chem. Phys.*, 1969, 50, 1262.

8. Dewar, M.J.S., and Haselbach, E., *J. Am. Chem. Soc.*, 1970, 92, 590.

9. Bingham, R.C., Dewar, M.J.S., and Lo, D.H., *J. Am. Chem. Soc.*, 1975, 97, 1285.

10. Richards, W.G. and Horsley, J.A., "*Ab Initio* Molecular Orbital Calculations for Chemists", Clarendon Press, Oxford, 1970.

11. Pople, J.A., *Acc. Chem. Res.*, 1970, 3, 217.

12. Radom, L., and Pople, J.A., *MTP Int. Rev. Sci., Phys. Chem., Ser. One*, 1972, 1, 71.

13. Hehre, W.J., *Acc. Chem. Res.*, 1976, 9, 399.

14. Pople, J.A., Hehre, W.J., Radom, L., and Schleyer, P.v.R., "A Chemist's Guide to *Ab Initio* Molecular Orbital Calculations", Academic Press, New York, N.Y., in press.

15. Schrödinger, E., *Phys. Rev.*, 1926, 28, 1049.

16. Born, M., and Oppenheimer, J.R., *Ann. Physik*, 1927, 84, 457.

17. Hartree, D.R., *Proc. Cam. Phil. Soc.*, 1928, 24, 89; *ibid.*, 1928, 24, 111; *ibid.*, 1928, 24, 426.

18. Slater, J.C., *Phys. Rev.*, 1930, 35, 509.

19. Fock, V., *Z. Physik*, 1930, 61, 126.

20. Roothaan, C.C.J., *Rev. Mod. Phys.*, 1951, 23, 161; *ibid.*, 1960, 32, 179.

21. Slater, J.C., *Phys. Rev.*, 1930, 36, 57.

22. Boys, S.F., *Proc. Roy. Soc.*, 1950, *A200*, 542.

23. Binkley, J.S., Pople, J.A., and Dobosh, P.A., *Mol. Phys.*, 1974, 28, 1423.

24. Hehre, W.J., Lathan, W.A., Ditchfield, R., Newton, M.D., and Pople, J.A., program No. 326, Q.C.P.E., University of Indiana, Bloomington, Ind., 1973.

25. Poppinger, D., Vincent, M.A., Hinde, A.L., and Radom, L., unpublished.

26. Vincent, M.A., Ph.D. Thesis, Australian National University, Canberra, 1978.

27. Pople, J.A., and Nesbet, R.K., *J. Chem. Phys.*, 1954, 22, 571.

28. Hehre, W.J., Stewart, R.F., and Pople, J.A., *J. Chem. Phys.*, 1969, 51, 2657.

29. Ditchfield, R., Hehre, W.J., and Pople, J.A., *J. Chem. Phys.*, 1971, 54, 724.

30. Dill, J.D., and Pople, J.A., *J. Chem. Phys.*, 1975, 62, 2921.

31. Hehre, W.J., Ditchfield, R., and Pople, J.A., *J. Chem. Phys.*, 1972, 56, 2257.

32. Hariharan, P.C., and Pople, J.A., *Theor. Chim. Acta*, 1973, 28, 213.

33. Pople, J.A., and Gordon, M., *J. Am. Chem. Soc.*, 1967, 89, 4253.

34. Hehre, W.J., Ditchfield, R., Stewart, R.F., and Pople, J.A., *J. Chem. Phys.*, 1970, 52, 2769.

35. Dill, J.D., Schleyer, P.v.R., and Pople, J.A., *J. Am. Chem. Soc.*, 1975, 97, 3402.

36. Dill, J.D., Schleyer, P.v.R., and Pople, J.A., *J. Am. Chem. Soc.*, 1976, 98, 1663.

37. Dill, J.D., Schleyer, P.v.R., Binkley, S., and Pople, J.A., *J. Am. Chem. Soc.*, 1977, 99, 6159.

38. Poppinger, D., *Chem. Phys. Lett.*, 1975, 34, 332.

39. Poppinger, D., *Chem. Phys. Lett.*, 1975, 35, 550.

40. Mulliken, R.S., *J. Chem. Phys.*, 1955, 23, 1833.

41. Salem, L., and Rowland, C., *Angew. Chem., Int. Ed. Engl.*, 1972, 11, 92.

42. Townshend, R.E., Ramunni, G., Segal, G., Hehre, W.J., and Salem, L., *J. Am. Chem. Soc.*, 1976, 98, 2190.

43. Jorgensen, W.L., and Salem, L., "The Organic Chemists's Book of Orbitals", Academic Press, New York, N.Y., 1973.

44. Dewar, M.J.S., and Dougherty, R.C., "The PMO Theory of Organic Chemistry", Plenum Press, New York, N.Y., 1975.

45. Hehre, W.J., Ditchfield, R., Radom, L., and Pople, J.A., *J. Am. Chem. Soc.*, 1970, 92, 4796.

46. Radom, L., Hehre, W.J., and Pople, J.A., *J. Am. Chem. Soc.*, 1971, 93, 289.

47. Radom, L., and Pople, J.A., *J. Am. Chem. Soc.*, 1970, 92, 4786.

48. Radom, L., Hehre, W.J., and Pople, J.A., *J. Am. Chem. Soc.*, 1972, 94, 2371.

49. Levine, I.N., "Quantum Chemistry", 2nd Edition, Allyn and Bacon, Boston, Mass., 1974.

50. Radom, L., Hehre, W.J., and Pople, J.A., *J. Chem. Soc., (A)*, 1971, 2299.

51. Radom, L., Lathan, W.A., Hehre, W.J., and Pople, J.A., *Aust. J. Chem.*, 1972, 25, 1601.

52. Hehre, W.J., Pople, J.A., and Devaquet, A.J.P., *J. Am. Chem. Soc.*, 1976, 98, 664.

53. Mezey, P.G., Kresge, A.J., and Csizmadia, I.G., *Can. J. Chem.*, 1976, 54, 2526.

54. Samdal, S., and Seip, H.M., *J. Mol. Struct.*, 1975, 28, 193.

55. Basch, H., Robin, M.B., Kuebler, N.A., Baker, C., and Turner, D.W., *J. Chem. Phys.*, 1969, 51, 52.

56. Bonaccorsi, R., Petrongolo, C., Scrocco, E.S., and Tomasi, J., *Quantum Aspects Heterocycl. Compounds Chem. Biochem., Proc. Int. Symp.*, Vol. II, 1969, 181.

57. Eisenstein, O., Lefour, J.M., and Minot, C., *Tetrahedron Lett.*, 1976, 1681.

58. Mollere, P.D., and Honk, K.N.; *J. Am. Chem. Soc.*, 1977, 99, 3226.

59. Lathan, W.A., Radom, L., Hariharan, P.C., Hehre, W.J., and Pople, J.A., *Fortschr. Chem. Forsch.*, 1973, 40, 1.

60. Hopkinson, A.C., Lien, M.H., Csizmadia, I.G., and Yates, K., *Theor. Chim. Acta*, 1978, 47, 97.

61. Kilb, R.W., Lin, C.C., and Wilson, E.B., *J. Chem. Phys.*, 1957, 26, 1695.

62. Erlenmeyer, E., *Chem. Ber.*, 1881, 14, 320.

63. Blank, B., and Fischer, H., *Helv. Chim. Acta*, 1973, 56, 506.

64. Saito, S., *Chem. Phys. Lett.*, 1976, 42, 399.

65. Owen, N.L., and Sheppard, N., *Trans. Faraday Soc.*, 1964, 60, 634.

66. Hirose, C., *Bull. Chem. Soc. Jpn.*, 1974, 47, 1311.

67. Lathan, W.A., Hehre, W.J., Curtiss, L.A., and Pople, J.A., *J. Am. Chem. Soc.*, 1971, 93, 6377.

68. Herzberg, G., "Molecular Spectra and Molecular Structure", Vol. 2, D. van Nostrand Company, Princeton, N.J., 1966.

69. Gordy, W., and Cook, R.L., "Microwave Molecular Spectra", Interscience, New York, N.Y., 1970.

70. Lathan, W.A., Curtiss, L.A., Hehre, W.J., Lisle, J.B., and Pople, J.A., *Progr. Phys. Org. Chem.*, 1974, 11, 175.

71. Duncan, J.L., Wright, I.J., and van Lerberghe, D., *J. Mol. Spectrosc.*, 1972, 42, 463.

72. Radom, L., Lathan, W.A., Hehre, W.J., and Pople, J.A., *J. Am. Chem. Soc.*, 1971, 93, 5339.

73. Blom, C.E., Slingerland, P.J., and Altona, C., *Mol. Phys.*, 1976, 31, 1359.

74. Carlos, J.L., Karl, R.R., and Bauer, S.H., *J. Chem. Soc., Faraday Trans. 2*, 1970, 70, 177.

75. John, I.G., and Radom, L., *J. Mol. Struct.*, 1977, 36, 133.

76. Rosenstock, H.M., Draxl, K., Steiner, B.W., and Herron, J.T., *J. Phys. Chem. Ref. Data*, 1977, 6, suppl. 1.

77. Hollenstein, H., and Günthard, H.H., *Spectrochim. Acta, Part A*, 1971, 27A, 2027.

78. Cant, N.W., and Armstead, W.J., *Spectrochim. Acta, Part A*, 1975, 31A, 839.

79. Holmes, J.L., Terlouw, J.K., and Lossing, F.P., *J. Phys. Chem.*, 1976, 80, 2860.

80. Pollack, S.K., and Hehre, W.J., *J. Am. Chem. Soc.*, 1977, 99, 4845.

81. Bouma, W.J., Radom, L., and Rodwell, W.R., unpublished.

82. Rodwell, W.R., Bouma, W.J., and Radom, L., unpublished.

83. Forsén, S., and Nilsson, M., "The Chemistry of the Carbonyl Group", Zabicky, J., Ed., Vol. 2, p.157, Interscience, New York, N.Y., 1970.

84. Hehre, W.J., and Lathan, W.A., *J. Chem. Soc., Chem. Commun.*, 1972, 771.

85. Vishveshwara, S., and Pople, J.A., *J. Am. Chem. Soc.*, 1977, 99, 2422.

86. Newton, M.D., and Jeffrey, G.A., *J. Am. Chem. Soc.*, 1977, 99, 2413.

87. Hehre, W.J., and Salem, L., *J. Chem. Soc., Chem. Commun.*, 1973, 754.

88. Hehre, W.J., and Pople, J.A., *J. Am. Chem. Soc.*, 1975, 97, 6941.

89. Allinger, N.L., and Hickey, M.J., *J. Mol. Struct.*, 1973, 17, 233.

90. Butcher, S.S., and Wilson, E.B., *J. Chem. Phys.*, 1964, 40, 1671.

91. Abraham, R.J., and Pople, J.A., *Mol. Phys.*, 1960, 3, 609.

92. Radom, L., and Stiles, P.J., *Tetrahedron Lett.*, 1975, 789.

93. Radom, L., Pople, J.A., and Schleyer, P.v.R., *J. Am. Chem. Soc.*, 1972, 94, 5935.

94. Saegebarth, E., and Krisher, L.C., *J. Chem. Phys.*, 1970, 52, 3555.

95. Ford, R.G., *J. Chem. Phys.*, 1976, 65, 354.

96. Saegebarth, E., and Wilson, E.B., *J. Chem. Phys.*, 1967, 46, 3088.

97. Marstokk, K.M., and Møllendal, H., *J. Mol. Struct.*, 1973, 16, 259.

98. Radom, L., Stiles, P.J., and Vincent, M.A., *J. Mol. Struct.*, 1978, 48, 259.

99. Schuster, P., *Chem. Phys. Lett.*, 1969, 3, 433.

100. Marsh, F.J., Thomas, B.G., and Gordon, M.S., *J. Mol. Struct.*, 1975, 25, 101.

101. Karlström, G., Wennerström, H., Jönsson, B., Forsén, S., Almlöf, J., and Roos, B., *J. Am. Chem. Soc.*, 1975, 97, 4188.

102. Isaacson, A.D., and Morokuma, K., *J. Am. Chem. Soc.*, 1975, 97, 4453.

103. Del Bene, J.E., and Kochenour, W.L., *J. Am. Chem. Soc.*, 1976, 98, 2041.

104. Karlström, G., Jönsson, B., Roos, B., and Wennerström, H., *J. Am. Chem. Soc.*, 1976, 98, 6851.

105. Fluder, E.M., and De la Vega, J.R., *J. Am. Chem. Soc.*, 1978, 100, 5265.

106. Catalán, J., Yáñez, M., Fernández-Alonso, J.I., *J. Am. Chem. Soc.*, 1978, 100, 6917.

107. Seliskar, C.J., and Hoffman, R.E., *Chem. Phys. Lett.*, 1976, 43, 481.

108. Rowe, W.F., Duerst, R.W., and Wilson, E.B., *J. Am. Chem. Soc.*, 1976, 98, 4021.

109. Brown, R.S., *J. Am. Chem. Soc.*, 1977, 99, 5497.

110. Bravo, P., Gaudiano, G., Quilico, A., and Ricca, A., *Gazz. Chim. Ital.*, 1961, 91, 47.

111. Raulin, F., and Toupance, G., *Bull. Soc. Chim. Fr.*, 1975, 188.

112. Ferris, J.P., Sanchez, R.A., and Orgel, L.E., *J. Mol. Biol.*, 1968, 33, 693.

113. Boileau, J., *Bull. Soc. Chim. Fr.*, 1954, 761.

114. Smidt, J., and Sieber, R., *Angew. Chem.*, 1959, 71, 626.

115. Taylor, E.C., Perlman, K.L., Kim, Y.H., Sword, I.P., and Jacobi, P.A., *J. Am. Chem. Soc.*, 1973, 95, 6413.

116. Vincent, M.A., and Radom, L., *J. Am. Chem. Soc.*, 1978, 100, 3306.

117. Niemeyer, H.M., *Helv. Chim. Acta*, 1977, 60, 1487.

118. Woodward, R.B., and Hoffmann, R., *Angew. Chem., Int. Ed. Engl.*, 1969, 8, 781.

119. Dewar, M.J.S., *Angew. Chem., Int. Ed. Engl.*, 1971, 10, 761.

120. Fukui, K., *Acc. Chem. Res.*, 1971, 4, 57.

121. Zimmerman, H.E., *Acc. Chem. Res.*, 1972, 5, 393.

122. Berson, J.A., *Acc. Chem. Res.*, 1972, 5, 406.

123. Epiotis, N.D., *Angew. Chem., Int. Ed. Engl.*, 1974, 13, 751.

124. Bingham, R.C., and Dewar, M.J.S., *J. Am. Chem. Soc.*, 1972, 94, 9107.

125. De Dobbelaere, J.R., van Dijk, J.M.F., de Haan, J.W., and Buck, H.M., *J. Am. Chem. Soc.*, 1977, 99, 392.

126. Kato, S., Kato, H., and Fukui, K., *J. Am. Chem. Soc.*, 1977, 99, 684.

127. Carlsen, L., and Duus, F., *J. Am. Chem. Soc.*, 1978, 100, 281.

128. Grima, J.P., Choplin, F., and Kaufman, G., *J. Organomet. Chem.*, 1977, 124, 315.

129. Peyerimhoff, S.D., and Buenker, R.J., *J. Chem. Phys.*, 1969, 50, 1846.

130. Koller, J., Hadzi, D., and Azman, A., *J. Mol. Struct.*, 1973, 17, 157.

131. Meyer, R., Ha, T.K., Frei, H., and Günthard, H.H., *Chem. Phys.*, 1975, 9, 393.

132. Berson, J.A., and Salem, L., *J. Am. Chem. Soc.*, 1972, 94, 8917.

133. Kwei, G.H., and Curl, R.F., *J. Chem. Phys.*, 1960, 32, 1592.

134. Hammond, G.S., *J. Am. Chem. Soc.*, 1955, 77, 334.

135. Bamberger, E., and Seligman, R., *Chem. Ber.*, 1903, 36, 685.

136. Coe, C.S., and Doumani, T.F., *J. Am. Chem. Soc.*, 1948, 70, 1516.

137. Gowenlock, B.G., and Trotman, J., *J. Chem. Soc.*, 1955, 4190.

138. Gowenlock, B.G., and Trotman, J., *J. Chem. Soc.*, 1956, 1670.

139. Batt, L., Gowenlock, B.G., and Trotman, J., *J. Chem. Soc.*, 1960, 2222.

140. Turner, P.T., and Cox, A.P., *J. Chem. Soc., Faraday Trans. 2*, 1978, 74, 533.

141. Levine, I.N., *J. Mol. Spectrosc.*, 1962, 8, 276.

142. Levine, I.N., *J. Chem. Phys.*, 1963, 38, 2326.

143. Robb, M.A., and Csizmadia, I.G., *J. Chem. Phys.*, 1969, 50, 1819.

144. Kollman, P.A., and Allen, L.C., *Chem. Phys. Lett.*, 1970, 5, 75.

145. Mochel, A.R., Griffin, L.L., Kramling, R.W., and Boggs, J.E., *J. Chem. Phys.*, 1973, 58, 4040.

146. Talberg, H.J., and Ottersen, T., *J. Mol. Struct.*, 1975, 29, 225.

147. Flood, E., Pulay, P., and Boggs, J.E., *J. Am. Chem. Soc.*, 1977, 99, 5570.

148. Liotard, D., Dargelos, A., and Chaillet, M., *Theor. Chim. Acta* , 1973, 31, 325.

149. Dargelos, A., Liotard, D., and Chaillet, M., *Theor. Chim. Acta* , 1975, 38, 79.

150. Pouchan, C., Liotard, D., Dargelos, A., and Chaillet, M., *J. Chim. Phys.*, 1976, 73, 1046.

151. Hwang, W.F., and Kuska, H.A.; *J. Mol. Struct.*, 1978, 48, 239.

152. Ochiai, M., Obayashi, M., and Morita, K., *Tetrahedron*, 1967, 23, 2641.

153. Dobashi, T.S., Goodrow, M.H., and Grubbs, E.J., *J. Org. Chem.*, 1973, 38, 4440.

154. Bjørgo, J., Boyd, D.R., and Neill, D.C., *J. Chem. Soc., Chem. Commun.*, 1974, 478.

155. Houk, K.N., Caramella, P., Munchhausen, L.L., Chang, Y.-M., Battaglia, A., Sims, J., and Kaufman, D.C., *J. Electron Spectrosc. Rel. Phenom.*, 1977, 10, 441.

156. Folting, K., and Lipscomb, W.N., *Acta Cryst.*, 1964, 17, 1263.

157. Azman, A., Hadzi, D., Kidric, J., and Orel, B., *Spectrochim. Acta, Part A*, 1971, 27A, 2499.

158. See for example: Pople, J.A., in "Modern Theoretical Chemistry", Vol. IV, Schaefer, H.F., Ed., Plenum, New York, N.Y., 1977, Chapter 1.

159. Calleri, M., Ferraris, G., and Vitterbo, D., *Acta Cryst.*, 1966, 20, 73.

160. Rogowski, R.S., and Schwendeman, R.H., *J. Chem. Phys.*, 1969, 50, 397.

161. Ohashi, O., Ishihara, R., Murakami, K., Sakaizumi, T., Onda, M., and Yamaguchi, I., *Bull. Chem. Soc. Jpn.*, 1976, 49, 891.

162. Ohashi, O., Hara, H., Noji, K., Sakaizumi, T., Onda, M., and Yamaguchi, I., *Bull. Chem. Soc. Jpn.*, 1977, 50, 834.

163. Smith, P.A., "The Chemistry of Open-Chain Organic Nitrogen Compounds", Vol. 1, Benjamin, New York, N.Y., 1965.

164. See for example: Beynon, J.H., and Cooks, R.G., *Adv. Mass Spectrom.* 1974, 6, 835.

165. See for example: Richards, W.G., Walker, T.E.H., and Hinkley, R.K., "A Bibliography of *ab initio* Molecular Wave Functions", Oxford University Press, London, 1971; and Richards, W.G., Walker, T.E.H., Farnell, L., and Scott, P.R., *ibid*, "Supplement for 1970-1973", 1974.

166. Ditchfield, R., Del Bene, J.E., and Pople, J.A., *J. Am. Chem. Soc.*, 1972, 94, 4806.

167. Altmann, J.A., Csizmadia, I.G., Yates, K., and Yates, P., *J. Chem. Phys.*, 1977, 66, 298.

168. Altmann, J.A., Csizmadia, I.G., Robb, M.A., Yates, K., and Yates, P., *J. Am. Chem. Soc.*, 1978, 100, 1653.

169. Lucchese, R.R., and Schaefer, H.F., *J. Am. Chem. Soc.*, 1978, 100, 298.

170. Kemper, M.J.H., Van Dijk, J.M.F., and Buck, H.M., *J. Am. Chem. Soc.*, 1978, 100, 7841.

171. Goddard, J.D., and Schaefer, H.F., to be published.

172. Pople, J.A., Krishnan, R., Schlegel, H.B., and Binkley, J.S., *Int. J. Quant. Chem.*, 1978, 14, 545.

173. Davis, T.D., Maggiora, G.M., and Christoffersen, R.E., *J. Am. Chem. Soc.*, 1974, 96, 7878.

174. Guyon, P.M., Chupka, W.A., and Berkowitz, J., *J. Chem. Phys.*, 1976, 64, 1419.

175. Mishra, S.P., and Symonds, M.C.R., *J. Chem. Soc., Chem. Commun.*, 1975, 909.

176. Karpas, Z., and Klein, F.S., *Int. J. Mass Spectrom. Ion Phys.*, 1975, 16, 289.

177. Huntress, W.T., *Chem. Soc. Rev.*, 1977, 6, 295.

178. Herzberg, G., *Quart. Rev.*, 1971, 25, 201.

179. Levsen, K., *Prog. Mass Spectrom.*, 1978, 4.

180. Beynon, J.H., *Adv. Mass Spectrom*, 1959, 328.

181. Gilpin, J.A., and McLafferty, F.W., *Anal. Chem.*, 1957, 29, 990.

182. Audier, H.E., *Org. Mass Spectrom.*, 1969, 2, 283.

183. McLafferty, F.W., *Anal. Chem.*, 1959, 31, 2072.

184. Katoh, M., Jaeger, D.A., and Djerassi, C., *J. Am. Chem. Soc.*, 1972, 94, 3107.

185. Holmes, J.L., and Rye, R.T.B., *Can. J. Chem.*, 1973, 51, 2342.

186. Turro, N.J., Weiss, D.S., Haddon, W.F., and McLafferty, F.W., *J. Am. Chem. Soc.*, 1967, 89, 3370.

187. Corderman, R.R., LeBreton, P.R., Buttrill, S.E., Williamson, A.D., and Beauchamp, J.L., *J. Chem. Phys.*, 1976, 65, 4929.

188. Holmes, J.L., and Terlouw, J.K., *Can. J. Chem.*, 1975, 53, 2076.

189. Kumakura, M., Arakawa, K., and Sugiura, T., *Int. J. Mass Spectrom. Ion Phys.*, 1978, 26, 303.

190. Kumakura, M., Arakawa, K., and Sugiura, T., *Bull. Chem. Soc. Jpn.*, 1978, 51, 54.

191. Herzberg, G., "Spectra of Diatomic Molecules", Van Nostrand Reinhold, New York, N.Y., 1950.

192. Herzberg, G., "Electronic Spectra of Polyatomic Molecules", Van Nostrand Reinhold, New York, N.Y., 1966.

193. Watanabe, K., Marmo, F.F., and Inn, E.C.Y., *Phys. Rev.*, 1953, 91, 1155.

194. Watanabe, K., *J. Chem. Phys.*; 1957, 26, 542.

195. Turner, D.W., and May, D.P., *J. Chem. Phys.*, 1966, 45, 471.

196. Cocksey, B.J., Eland, J.H.D., and Danby, C.J., *J. Chem. Soc. (B)*, 1971, 790.

197. Turner, D.W., Baker, C., Baker, A.D., and Brundle, C.R., "Molecular Photoelectron Spectroscopy", Wiley-Interscience, London, 1970.

198. Morrison, J.D., *Revs. Pure and Appl. Chem.*, 1955, 5, 22.

199. Hurzeler, H., Inghram, M.G., and Morrison, J.D., *J. Chem. Phys.*, 1958, 28, 76.

200. Collin, J.E., and Conde-Caprace, G., *Int. J. Mass Spectrom. Ion Phys.*, 1968, 1, 213.

201. Krässig, R., Reinke, D., and Baumgartel, H., *Ber. Bunsenges. Phys. Chem.*, 1974, 78, 425.

202. Shannon, T.W., and McLafferty, F.W., *J. Am. Chem. Soc.*, 1966, 88, 5021.

203. Cooks, R.G., Beynon, J.H., Caprioli, R.M., and Lester, G.R., "Metastable Ions", Elsevier, Amsterdam, 1973.

204. Beynon, J.H., and Cooks, R.G., *Res. Dev.*, 1971, 22, 26.

205. Schlunegger, U.P., *Angew. Chem., Int. Ed. Engl.*, 1975, 14, 679.

206. Barber, M., and Elliott, R.M., 12th Annual Conference on Mass Spectrometry and Applied Topics, ASTM Committee E-14, Montreal, 1964.

207. Bruins, A.P., Jennings, K.R., and Evans, S., *Int. J. Mass Spectrom. Ion Phys.*, 1978, 26, 395.

208. Beynon, J.H., Saunders, R.A., and Williams, A.E., *Z. Naturforsch.*, 1965, 20a, 180.

209. Beynon, J.H., and Fontaine, A.E., *Z. Naturforsch.*, 1967, 22a, 334.

210. Pritchard, J.G., *Org. Mass Spectrom.*, 1974, 8, 103.

211. Jennings, K.R., *Int. J. Mass Spectrom. Ion Phys.*, 1968, 1, 227.

212. Haddon, W.F., and McLafferty, F.W., *J. Am. Chem. Soc.*, 1968, 90, 4745.

213. Levsen, K., and Schwarz, H., *Angew. Chem., Int. Ed. Engl.*, 1976, 15, 509.

214. Giardini-Guidoni, A., Platania, R., and Zocchi, F., *Int. J. Mass Spectrom. Ion Phys.*, 1974, 13, 453.

215. Van de Sande, C.C., and McLafferty, F.W., *J. Am. Chem. Soc.*, 1975, 97, 4613.

216. McDaniel, E.W., Cermak, V., Dalgarno, A., Ferguson, E.E., and Friedman, L., "Ion-Molecule Reactions", Wiley-Interscience, New York, N.Y., 1970.

217. See the various contributions in "Ion-Molecule Reactions", Franklin, J.L., Ed., Plenum Press, New York, N.Y., 1972, Vol. 1 and 2.

218. Baldeschwieler, J.D., *Science*, 1968, 159, 263.

219. Tal'roze, V.L., *Pure Appl. Chem.*, 1962, 5, 455.

220. Herod, A.A., and Harrison, A.G., *Int. J. Mass Spectrom. Ion Phys.*, 1970, 4, 415.

221. Ferguson, E.E., Fehsenfeld, F.C., and Schmeltekopf, A.L., *Adv. At. Mol. Phys.*, 1969, 5, 1.

222. Kumakura, M., and Sugiura, T., in "Recent Developments in Mass Spectroscopy", Ogata, K., and Hayakawa, T., Ed., University Park Press, Baltimore, Md., 1970, 988.

223. Munson, M.S.B., *J. Am. Chem. Soc.*, 1965, 87, 5313.

224. Giardini-Guidoni, A., Mele, A., Platania, R., and Zocchi, F., *J. Chem. Soc., Faraday Trans. 1*, 1975, 71, 351.

225. Pritchard, H., and Harrison, A.G., *J. Chem. Phys.*, 1968, 48, 5623.

226. Blair, A.S., and Harrison, A.G., *Can. J. Chem.*, 1973, 51, 703.

227. Beauchamp, J.L., and Dunbar, R.C., *J. Am. Chem. Soc.*, 1970, 92, 1477.

228. Staley, R.H., Corderman, R.R., Foster, M.S., and Beauchamp, J.L., *J. Am. Chem. Soc.*, 1974, 96, 1260.

229. Kumakura, M., Ito, A., and Sugiura, T., *Mass Spectroscopy*, 1974, 22, 16.

230. Kumakura, M., and Sugiura, T., *Bull. Chem. Soc. Jpn.*, 1977, 50, 2046.

231. Kumakura, M., Arakawa, K., and Sugiura, T., *Bull. Chem. Soc. Jpn.*, 1978, 51, 49.

232. Kumakura, M., Arakawa, K., and Sugiura, T., *J. Chem. Soc., Faraday Trans. 1*, 1978, 74, 1953.

233. Kumakura, M., Arakawa, K., and Sugiura, T., *Can. J. Chem.*, 1978, 56, 533.

234. Kumakura, M., Arakawa, K., and Sugiura, T., *Int. J. Mass Spectrom. Ion Phys.*, 1979, 29, 21.

235. Turner, D.W., Baker, C., Baker, A.D., and Brundle, C.R., "Molecular Photoelectron Spectroscopy", Wiley-Interscience, London, 1970.

236. Hoffmann, R., Radom, L., Pople, J.A., Schleyer, P.v.R., Hehre, W.J., and Salem, L., *J. Am. Chem. Soc.*, 1972, 94, 6221.

237. Golding, B.T., and Radom, L., *J. Am. Chem. Soc.*, 1976, 98, 6331.

238. Hipple, J.A., Sommer, H., and Thomas, H.A., *Phys. Rev.*, 1949, 76, 1877.

239. Wobschall, D., Graham, J.R., and Malone, D.P., *Phys. Rev.*, 1963, 131, 1565.

240. *Chem. Eng. News*, 1965, 43 (25), 55.

241. Goode, G.C., O'Malley, R.M., Ferrer-Correia, A.J., and Jennings, K.R., *Nature*, 1970, 227, 1093.

242. Baldeschwieler, J.D., and Woodgate, S.S., *Acc. Chem. Res.*, 1971, 4, 114.

243. Gray, G.A., *Adv. Chem. Phys.*, 1971, 19, 141.

244. Beauchamp, J.L., *Ann. Rev. Phys. Chem.*, 1971, 22, 527.

245. Goode, G.C., O'Malley, R.M., Ferrer-Correia, A.J., and Jennings, K.R., *Chem. Brit.*, 1971, 7, 12.

246. Henis, J.M.S., in "Ion-Molecule Reactions", Vol. 2, Franklin, J.L., Ed., Plenum Press, New York, N.Y., 1972.

247. Hartmann, H., Lebert, K.H., and Wanczek, K.P., *Fortschr. Chem. Forsch.*, 1973, 43, 57.

248. Lehman, T.A., and Bursey, M.M., "Ion Cyclotron Resonance Spectrometry", Wiley-Interscience, New York, N.Y., 1976.

249. O'Haver, T.C., *J. Chem. Educ.*, 1971, 49, A131; *ibid.*, 1971, 49, A211.

250. McMahon, T.B. and Beauchamp, J.L., *Rev. Sci. Instrum.*, 1971, 42, 1632.

251. Henis, J.M.S., and Frasure, W., *Rev. Sci. Instrum.*, 1968, 39, 1772.

252. McIver, R.T., *Rev. Sci. Instrum.*, 1970, 41, 126.

253. Anders, L.R., Beauchamp, J.L., Dunbar, R.C., and Baldeschwieler, J.D., *J. Chem. Phys.*, 1966, 45, 1062.

254. Beauchamp, J.L., Anders, L.R., and Baldeschwieler, J.D., *J. Am. Chem. Soc.*, 1967, 89, 4569.

255. Goode, G.C., Ferrer-Correia, A.J., and Jennings, K.R., *Int. J. Mass Spectrom. Ion Phys.*, 1970, 5, 229.

256. McIver, R.T., *Rev. Sci. Instrum.*, 1970, 41, 555; *ibid.*, 1978, 49, 111.

257. McIver, R.T., and Dunbar, R.C., *Int. J. Mass Spectrom. Ion Phys.*, 1971, 7, 471.

258. McMahon, T.B., and Beauchamp, J.L., *Rev. Sci. Instrum.*, 1972, 43, 509.

259. Comisarow, M.B., and Marshall, A.G., *Chem. Phys. Lett.*, 1974, 25, 282; *ibid.*, 1974, 26, 489.

260. Comisarow, M.B., in "Transfer Techniques in Chemistry", Griffiths, P.R., Ed., Plenum Press, New York, N.Y., 1978.

261. Wilkins, C.L., *Anal. Chem.*, 1978, 50, 493A.

262. Hunter, R.L., and McIver, R.T., *American Laboratory*, 1977, (November), 13.

263. Diekman, J., MacLeod, J.K., Djerassi, C., and Baldeschwieler, J.D., *J. Am. Chem. Soc.*, 1969, 91, 2069.

264. Ferrer-Correia, A.J.V., Jennings, K.R., and Sen Sharma, D.K., *J. Chem. Soc., Chem. Commun.*, 1975, 973.

265. Drewery, C.J., and Jennings, K.R., *Int. J. Mass Spectrom. Ion Phys.*, 1976, 19, 287.

266. Ferrier-Correia, A.J.V., Jennings, K.R., and Sen Sharma, D.K., *Org. Mass Spectrom.*, 1976, 11, 867.

267. Gross, M.L., and McLafferty, F.W., *J. Am. Chem. Soc.*, 1971, 93, 1267.

268. Gross, M.L., *J. Am. Chem. Soc.*, 1972, 94, 3744.

269. Beauchamp, J.L., and Dunbar, R.C., *J. Am. Chem. Soc.*, 1970, 92, 1477.

270. Busch, K.L., Nixon, W.B., and Bursey, M.M., *J. Am. Chem. Soc.*, 1978, 100, 1621.

271. Vogt, J., Williamson, A.D., and Beauchamp, J.L., *J. Am. Chem. Soc.*, 1978, 100, 3478.

272. Jackson, J.-A.,A., Lias, S.G., and Ausloos, P., *J. Am. Chem. Soc.*, 1977, 99, 7515.

273. Buttrill, S.E., *J. Am. Chem. Soc.*, 1970, 92, 3560.

274. Attwell, W.H., Weyenberg, D.R., and Uhlmann, J.G., *J. Am. Chem. Soc.*, 1969, 91, 2025.

275. Oele, P.C., and Louw, R., *Tetrahedron Lett.*, 1972, 4941.

276. Schmitz, E., *Angew. Chem., Int. Ed. Engl.*, 1964, 5, 333.

277. Moss, R.A., and Munjal, R.C., *J. Chem. Soc., Chem. Commun.*, 1978, 775.

278. Brown, P., and Djerassi, C., *Tetrahedron*, 1968, 24, 2949.

279. Baldwin, J.E., and Pudussery, R.G., *J. Chem. Soc., Chem. Commun.*, 1968, 408.

280. Caserio, M.C., Graham, W.H., and Roberts, J.D., *Tetrahedron*, 1960, 171.

281. Semenow, D.A., Cox, E.F., and Roberts, J.D., *J. Am. Chem. Soc.*, 1956, 78, 3221.

282. Brikenshtein, A.A., Volkov, V.P., and Abrosimov, A.F., *Khim. Prom.*, 1966, 42, 500. (*Chem. Abstr.*, 1966, 65, 15359g.).

283. Eadon, G., Diekman, J., and Djerassi, C., *J. Am. Chem. Soc.*, 1969, 91, 3986.

284. Eadon, G., Diekman, J., and Djerassi, C., *J. Am. Chem. Soc.*, 1970, 92, 6205.

285. McLafferty, F.W., McAdoo, D.J., Smith, J.S., and Kornfeld, R., *J. Am. Chem. Soc.*, 1971, 93, 3720.

286. McLafferty, F.W., Kornfeld, R., Haddon, W.F., Levsen, K., Sakai, I., Bente, P.F., Tsai, S.-C., and Schuddemagge, H.D.R., *J. Am. Chem. Soc.*, 1973, 95, 3886.

287. Beynon, J.H., Caprioli, R.M., and Cooks, R.G., *Org. Mass Spectrom.*, 1974, 9, 1.

288. Conrath, K., Van de Sande, C., and Vandewalle, M., *Org. Mass Spectrom.*, 1974, 9, 585.

289. Van de Sande, C.C., and McLafferty, F.W., *J. Am. Chem. Soc.*, 1975, 97, 4617.

290. Luippold, D.A., and Beauchamp, J.L., *J. Phys. Chem.*, 1976, 80, 795.

291. Laroff, G.P., and Fisher, H., *Helv. Chim. Acta*, 1973, 56, 2011.

292. Sojka, S.A., Poranski, C.F., and Moniz, W.B., *J. Magn. Reson.*, 1976, 23, 417.

293. Blank, B., Henne, A., Laroff, G.P., and Fischer, H., *Pure Appl. Chem.*, 1975, 41, 475.

294. Creswell, R.A., *Mol. Phys.*, 1975, 30, 217.